2020

Impact of polycystic ovary syndrome on methyl group metabolism

Amanda Bries
Iowa State University

Impact of polycystic ovary syndrome on methyl group metabolism

by

Amanda Elizabeth Bries

A dissertation submitted to the graduate faculty

in partial fulfillment of the requirements for the degree of

DOCTOR OF PHILOSOPHY

Major: Nutritional Sciences

Program of Study Committee:
Kevin Schalinske, Major Professor
Aileen Keating
Matthew Rowling
Manju Reddy
Elizabeth McNeill
Rachel Derscheid

The student author, whose presentation of the scholarship herein was approved by the program of study committee, is solely responsible for the content of this dissertation. The Graduate College will ensure this dissertation is globally accessible and will not permit alterations after a degree is conferred.

Iowa State University

Ames, Iowa

2020

TABLE OF CONTENTS

LIST OF FIGURES

Page

LIST OF TABLES

Page

NOMENCLATURE

TS%	transferrin saturation
AgRP	agouti related protein
Akrc1	aldo-keto reductase family
ALT	alanine aminotransferase
AST	aspartate aminotransferase
AUC	area under the curve
BHMT	betaine homocysteine S-methyltransferase
BMI	body mass index
BUN	blood urea nitrogen
BW	body weight
CAS	casein
CBS	cystathionine β-synthase
cDNA	complementary DNA
CRP	C-reactive protein
CVD	cardiovascular disease
Cyp	cytochrome P450
CYP19A1	aromatase
Cyp51	Lanosterol 14α demethylase
DAI	Disease activity index
DAVID	Database for Annotation, Visualization, Integrated Discovery
DEGs	differentially expressed genes
DHEA	dihydroepiandrosterone

DHF	dihydrofolate
DHT	dihydrotestosterone
DMBA	7,12-dimethylbenz[a]anthracene
DMT	N,N-dimethyltryptamine
DSS	dextran sulfate sodium
E2	estradiol
eGFR	glomerular filtration rate
FDR	FALSE discovery rate
Fe	iron
$FeSO_4$	ferrous sulfate
Frs2	fibroblast growth factor receptor substrate-2
FSH	follicle stimulating hormone
GCs	granulosa cells
GISQ	gastrointestinal side effects questionnaire
GnRH	gonadotropin release hormone
GO	gene ontology
GST	glutathione S-transferase
Gstm1	glutathione S-transferase mu-1
Gstm2	glutathione s-transferase mu-2
Gstp1	glutathione S-transferase pi-1
Gsts	glutathione s-transferases
Gstt3	glutathione S-transferase, theta 3
Gstz1	glutathione S-transferase zeta 1

H&E	hematoxylin and eosin
Hamp	hepcidin
Hb	hemoglobin
Hcy	homocsyteine
HDL	high-density lipoprotein
HHcy	hyperhomocysteinemia
HOMA-IR	homeostatic assessment of insulin resistance
HPG	hypothalamus pituitary gonadal axis
HPO	hypothalamus pituitary ovarian axis
HRE	hemoglobin regeneration efficiency
IBD	inflammatory bowel disease
IDA	iron deficiency anemia
IL	interleukin
INMT	indolethylamine N-methyltransferase
IPGTT	intraperitoneal glucose tolerance test
IR	insulin resistance
IRB	Institutional Review Board
IRS	insulin receptor substrate
ISU	Iowa State University
KEGG	Kyoto Encyclopedia of Genes and Genomes
KNN	K-nearest-neighbor
LDL	low density lipoprotein
LEPR	leptin receptor

LH	luteinizing hormone
MAPK	mitogen-activated protein kinase
MC3R/MC4R	melanocortin 3 receptor/melanocortin 4 receptor
MDA	malondialdehyde
mRNA	messenger RNA
MS	methinine synthase
MTHFR	methylene tetrahydrofolate reductase
NFe	no Fe
NTBI	non-transferrin bound iron
OCM	one-carbon metabolism
PCA	Principal Component Analysis
PCOS	polycystic ovary syndrome
PCOs	protein carbonyls
PEMT	phosphatidylethanolamine N-methyltransferase
PFC	prefrontal cortex
PI3K	phosphoinositol 3 kinase
PNA	prenatal androgenization
POMC	pro-opiomelanocortin
PPARϒ	peroxisome proliferator-activated receptors
Prlr	prolactin receptor
REV3L	reversionless like 3-like protein
RIN	rna integrity number
SAH	*S*-adenosyl-homocysteine

SAM	*S*-adenosyl-methionine
SD	Sprague Dawley
SF	serum ferritin
SHBG	sex hormone binding globulin
SHMT	serine hydroxymethyltransferase
SI	serum iron
Sqle	squalene epoxidase
StAR	steroidogenic acute regulatory protein
sTFR	soluble transferrin receptor
T1D	type 1 diabetes
T2D	type 2 diabetes
T2DM	type 2 diabetes mellitus
TBARS	thiobarbituric acid reactive substances
THF	tetrahydrofolate
TIBC	total iron binding capacity
TMM	trimmed mean of M
TZDS	thiazolidinediones
ULT	Ultimine® Koji Iron
WE	whole egg
ZDF	Zucker Diabetic Fatty
α-MSH	alpha-melanocyte stimulating hormone

ACKNOWLEDGMENTS

I want to extend a sincere thank you to my Major Professor, Dr. Kevin Schalinske, for your continued support, guidance, and encouragement throughout my undergraduate and graduate careers. Not only was your mentorship essential in the completion of this dissertation, but you provided me with an invaluable experience that focused on fostering growth, independence, and scientific exploration. Your encouragement is what helps students like me perform to the highest of our abilities, and I am forever grateful for your respectful mentorship.

Additionally, I would like to thank the members of my Program of Study Committee, all of whom I have had the privilege of working alongside. Dr. Matthew Rowling, Dr. Manju Reddy, Dr. Aileen Keating, Dr. Elizabeth McNeill, and Dr. Rachel Derscheid, thank you for challenging me and guiding me through the unknowns of my graduate research by providing your time and expertise. Special thanks to Dr. Manju Reddy, who oversaw the research studies in this dissertation examining iron supplementation, and providing me with unique opportunities to collaborate across the University. Furthermore, thank you to Dr. Matthew Rowling for your technical expertise on the inflammatory bowel disease and sequencing studies, in addition to the life lessons you have shared along the way to help me muster through the challenges. I thank Dr. Aileen Keating and her students, Bailey McGuire and Dr. Kendra Clark, who trained me on the reproduction-related techniques used in this dissertation's central chapters. Sincere thanks to Dr. Elizabeth McNeill for having confidence in me carrying out new experiments and pushing me intellectually through new concepts. I would also like to acknowledge both Dr. Derscheid and Jennifer Groeltz-Thrush for their scientific expertise in histopathology and for the diagnostic work presented in the inflammatory bowel disease study. It was a joy to have the experience of working with you both.

Additionally, I would like to thank my labmates, Dr. Cassondra Saande, Dr. Samantha Pritchard, Dr. Isaac Agbemafle, Laura Walter, Claudia Carrillo, Brooke Vogel, and the dozens of hardworking undergraduate research assistants that have become wonderful friends over the years. To my incredible friends that I have made along the way, you have sweetened this journey with the abundance of memories made: Ella Bauer, Spencer Bauer, MaryKate Horak, Nate Garton, Hyeyoon Eo, Remy Wyatt, Ross Wyatt, Norin Chaudhry, Nicole Sun-McClanahan, Alicia Taylor, Simon Moe, Alyssa Hohman, and Carter Reed. A special thank you to Dr. Joe Webb, my great friend, confidant, and lab partner whom I have worked alongside for the past three years to complete a lot of the work presented in this dissertation. Thank you for your unwavering support, the many laughs, the many hours, and helping bring several instruments back to life so we could complete our research!

Lastly, I would like to thank my family. To my sister and best friend, Kayla, for your support, optimism, and invitations to the needed live music getaways! To my parents, Ron and Angie, for your encouragement, inquisitiveness, and understanding of the sacrifices made to tend to my research projects. To my brothers, sisters-in-law, and many nieces and nephews. Thank you for your love and for cheering me on in my journey.

ABSTRACT

It is estimated that polycystic ovary syndrome (PCOS) affects one in ten women, making it the most common endocrine disorder among reproductive-aged women. PCOS displays diverse clinical manifestations, such as anovulation, infertility, and hyperandrogenism. Moreover, patients diagnosed with PCOS are at risk of developing comorbidities like obesity, cardiovascular disease, and type 2 diabetes. Due to the wide array of metabolic consequences, PCOS remains one of the most challenging conditions to diagnose and treat. Recently, evidence has suggested that individuals with PCOS exhibit nutritional deficits in serum folate and vitamin B_{12} concentrations. Emerging evidence also indicates that PCOS, similar to other metabolic conditions, leads to the imbalance of methyl groups. These nutritional deficiencies may lead to compensatory hyperhomocysteinemia, a medical condition that has been deemed significant in patients with PCOS. Methyl group metabolism is an essential biological system, whereby three interrelated pathways work in concert to maintain homocysteine concentrations and methyl group supply. The comprehensive system utilizes substrates and cofactors, such as choline, methionine, folate, B_{12}, B_6, and B_2, to support homocysteine homeostasis. The etiology of PCOS remains inconclusive, but evidence supports the idea of perturbed methyl group metabolism. The objective of the studies described in the central part of this dissertation is to characterize methyl group metabolism as a function of the progression of polycystic ovary syndrome in 1) letrozole-induced PCOS Sprague Dawley rats and 2) genetic mouse model of PCOS.

The first study described in this dissertation examined the impact of letrozole, a chemical aromatase inhibitor, treatment on the development of PCOS-related downstream effects of ovarian methyl group metabolism outcomes. Female Sprague Dawley rats (n = 36) were randomly assigned to letrozole or vehicle carboxymethylcellulose via a surgically implanted

subcutaneous slow-release bead every 30 days. All animals were randomized to be euthanized at the time of proestrus at either 8, 16, or 24 wk of age. Letrozole-induced rats exhibited elevated body weight gain immediately upon letrozole exposure and throughout the study ($P<0.0001$). Moreover, letrozole exposure perturbed estrous cyclicity, with decreased time spent in proestrus ($P<0.0001$) accompanied by elevated serum testosterone concentrations. Interestingly, inhibition of aromatase led to diminished ovarian cystathionine β-synthase (*Cbs*) transcript abundance by 59% at 16 wk of age ($P<0.05$) and 77% by 24 wk of age ($P<0.01$). Additionally, CBS protein abundance was 32% lower in the ovary of letrozole-induced rats at 8 wk of age ($P = 0.02$). When testing as a function of age, betaine-homocysteine *S*-methyltransferase (*Bhmt*) transcript abundance increased exclusively in letrozole-induced rats ($P = 0.03$). These data support the idea that the transsulfuration pathway, involving CBS enzymatic activity in the ovary, is perturbed as a function of time in a chemically-induced model of PCOS.

The second study's objective was to determine the effects of a metabolically compromised mouse model of PCOS, using the agouti lethal yellow mouse. Canonically, agouti mice display early adult-onset of obesity, type 2 diabetes, and infertility. Five wk old female lethal yellow agouti mice (KK.CG-A^y/J; agouti; $n = 18$), and their wild type (WT) controls (a/a; $n = 18$), were aged out to 8, 16, or 24 wk, then euthanized at the time of proestrus. All acyclic mice (24 wk old agouti mice) were euthanized in the diestrus stage. PCOS was confirmed by elevated serum testosterone concentrations, which were significantly higher at 16 and 24 wk of age ($P<0.05$). A 4.6-fold increase in ovarian *Bhmt* transcript abundance was observed in 8 wk old agouti mice; whereas, a 27% decrease in hepatic *Bhmt* transcript abundance. No differences in *Bhmt* was observed at any other experimental time point. There was a trend for decreased hepatic BHMT protein abundance in 8 wk old agouti mice. By 16 wk of age, we observed a 44%

reduction in ovarian glycine N-methyltransferase (*Gnmt*) transcript abundance, along with a 33% reduction in hepatic *Gnmt* at 24 wk old agouti mice was detected. This was not a supported finding at any other stage of PCOS.

Collectively, the studies described in this dissertation demonstrate that potential mechanisms involved in the pathogenesis of PCOS may be due to the transient response in BHMT and CBS-mediated methyl group metabolism pathways. Furthermore, decreased expression of these two enzymes indicates increased demand for methyl groups in the ovary, potentially revealing shifts in methyl group/one-carbon metabolism contributing to the pathogenesis of PCOS. Future nutrition intervention studies are being employed to determine whether dietary methyl groups support the aberrations in methyl group metabolism observed in the early onset of PCOS in both the chemically-induced and genetic rodent PCOS models.

CHAPTER 1. GENERAL INTRODUCTION

Introduction

Polycystic ovary syndrome (PCOS) is an endocrine disorder that commonly occurs among women of childbearing age (1). The name stems from the presence of small cysts around the ovary, but the complexity of this disorder is far more comprehensive than the exclusive appearance of ovarian cysts. The metabolic anomalies of PCOS are vast, including hyperandrogenism, anovulation, infertility, abnormal hair growth, insulin resistance, and compensatory hyperinsulinemia (2). Long-term consequences of PCOS include the significant risk for developing cardiovascular disease, type 2 diabetes, and metabolic syndrome. Patients with PCOS often seek reproductive assistance; however, there are subsequent risks involved during gestation that may impair fetal outcomes, such as gestational diabetes and pre-eclampsia (3,4). It is challenging to diagnose the early onset of PCOS, as the diagnostic criteria for PCOS is variable due to the complexity of this disorder (5). However, it is well established that the pathophysiology of PCOS includes the dysfunction of the hypothalamus-pituitary-ovarian (HPO) axis – a central regulator of reproductive processes (1). Although the etiology of PCOS is unknown, research has postulated that PCOS is a combination of genetic, epigenetic, and environmental factors that play a role in the dysfunction of the HPO axis, ultimately leading to impaired ovarian androgen production and the aforementioned complications (6).

Methyl group metabolism is a biological system that regulates the provision of methyl groups for the regulation of gene expression by the methylation of DNA and histone proteins (7). This methylation process is considered an epigenetic regulatory process, whereby methylation of CpG sites on DNA and histone proteins generally represses gene transcription. An inadequate supply of methyl groups may compromise the regulatory mechanisms of critical HPO axis-

related genes involved in the progression of PCOS (8). Moreover, methyl group metabolism governs the methyl group supply, but it is also critical for homocysteine homeostasis (9). This is important to note because homocysteine concentrations are positively associated with various diseases, including PCOS (10). Given the associations between epigenetics in conjunction with homocysteine-associated risk factors of PCOS, the imbalance of methyl group metabolism may underlie the mechanisms involved in the etiology and progression of PCOS.

The central research's overall objectives in this dissertation are to characterize methyl group metabolism in both the liver and ovary in PCOS as a function of disease onset and progression. More specifically, the studies were employed to examine two distinct rodent models of PCOS 1) the chemical aromatase-inhibitor model of PCOS and 2) a genetic model of PCOS. Findings from this research will be used to identify dietary intervention strategies to support the imbalances observed in the methyl group cycle during PCOS progression.

Dissertation Organization

This dissertation consists of five chapters with a general introduction (Chapter 1), literature review (Chapter 2), two research manuscripts (Chapter 3 and 4), an overall conclusion (Chapter 5), and appendices containing four first-author manuscripts (Appendix A, B, C, and D). The first manuscript, "Letrozole-induced polycystic ovary syndrome reduces cystathionine-β synthase mRNA and protein abundance in the ovaries of female Sprague Dawley rats," has been submitted to the *Journal of Nutrition*. This manuscript characterized ovarian one-carbon metabolism under the conditions of a chemically-induced polycystic ovary syndrome rat model. This study aimed to characterize the one-carbon/methyl group metabolism as a result of aromatase inhibition on both the ovary and liver, in addition to examining the phenotypic outcomes that coincide with this model at three different developmental stages. The experiments and data presented in the second manuscript in chapter 4 of this dissertation titled, “Polycystic

ovary syndrome modulates betaine homocysteine *S*-methyltransferase in 8 week old female lethal yellow agouti mice," has been prepared for submission to the *Journal of Nutrition*. The final main chapter of this dissertation includes an overall discussion of the results and future directions for the next research phase. All literature cited throughout this dissertation is based on the format of *Journal of Nutrition* and listed at the end of each respective chapter.

References

1. Goodarzi MO, Dumesic DA, Chazenbalk G, Azziz R. Polycystic ovary syndrome: Etiology, pathogenesis and diagnosis. Nature Reviews Endocrinology. *Nature Publishing Group*. 2011. p. 219–31.

2. Teede H, Deeks A, Moran L. Polycystic ovary syndrome: A complex condition with psychological, reproductive and metabolic manifestations that impacts on health across the lifespan. *BMC Medicine.* 2010. p. 1–10.

3. Lo JC, Feigenbaum SL, Escobar GJ, Yang J, Crites YM, Ferrara A. Increased prevalence of gestational diabetes mellitus among women with diagnosed polycystic ovary syndrome: A population-based study. *Diabetes Care*. 2006; 29:1915–7.

4. Yu HF, Chen HS, Rao DP, Gong J. Association between polycystic ovary syndrome and the risk of pregnancy complications A PRISMA-compliant systematic review and meta-analysis. *Medicine*. 2016. p. e4863.

5. Ibáñez L, Oberfield SE, Witchel S, Auchus RJ, Chang RJ, Codner E, Dabadghao P, Darendeliler F, Elbarbary NS, Gambineri A, et al. An International Consortium Update: Pathophysiology, Diagnosis, and Treatment of Polycystic Ovarian Syndrome in Adolescence. *Horm Res Paediatr*. 2017. p. 371–95.

6. Rosenfield RL, Ehrmann DA. The Pathogenesis of Polycystic Ovary Syndrome (PCOS): The Hypothesis of PCOS as Functional Ovarian Hyperandrogenism Revisited. *Endocr Rev*. 2016; 37:467–520.

7. Friso S, Udali S, De Santis D, Choi SW. One-carbon metabolism and epigenetics. *Mol Aspects Med*. 2017. p. 28–36.

8. Ducker GS, Rabinowitz JD. One-Carbon Metabolism in Health and Disease. *Cell Metab*. 2017; 25:27–42.

9. Schalinske KL, Smazal AL. Homocysteine Imbalance: a Pathological Metabolic Marker. *Adv Nutr*. 2012; 3:755–62.

10. Li D, Liu HX, Fang YY, Huo JN, Wu QJ, Wang TR, Zhou YM, Wang XX, Ma XX. Hyperhomocysteinemia in polycystic ovary syndrome: decreased betaine-homocysteine methyltransferase and cystathionine β-synthase-mediated homocysteine metabolism. *Reprod Biomed Online*. 2018; 37:234–41.

CHAPTER 2. LITERATURE REVIEW

Polycystic Ovary Syndrome

Polycystic ovary syndrome (PCOS) is estimated to affect up to 10% of reproductive-aged women in the United States, depending on the diagnostic criteria used (1). A vast array of symptoms commonly occur during PCOS, such as ovarian cysts, anovulation, infertility, and hyperandrogenism (2). Moreover, an imbalance of androgen production imposes a significant risk of developing morbidities like type 2 diabetes, metabolic syndrome, and cardiovascular disease (CVD) later in life (3). PCOS remains one of the most challenging conditions to diagnose and treat, especially amongst adolescent females, in part because PCOS is not limited to adult reproductive years (4). There is a high degree of variability in metabolic and phenotypic characteristics, making a PCOS diagnosis challenging. Due to this variability, many women may be living with undiagnosed PCOS or receive a delayed diagnosis because of this disorder's multifactorial characteristics. In order to understand both the metabolic and reproductive consequences of PCOS, it is important to understand the intersection between the endocrine system and metabolism. The purpose of this literature review is to describe the main dysfunctional characteristics, while postulating new ideas from the current research in the field.

Hypothalamic Pituitary Ovarian Axis

The hypothalamic-pituitary-ovarian axis (HPO), otherwise referred to as the hypothalamic-pituitary-gonadal (HPG) axis, is dependent upon the synchrony and feedback mechanisms among these three organs: hypothalamus, anterior pituitary, and the ovaries (Figure 2-1) (5). The hormonal cascade begins with the hypothalamic pulse of the master hormonal regulator, gonadotropin-releasing hormone (GnRH), whereby it travels to the anterior pituitary to stimulate the release of gonadotropins, follicle-stimulating hormone (FSH) and luteinizing

hormone (LH) (6). These two hormones work in concert to govern folliculogenesis and ovulation.

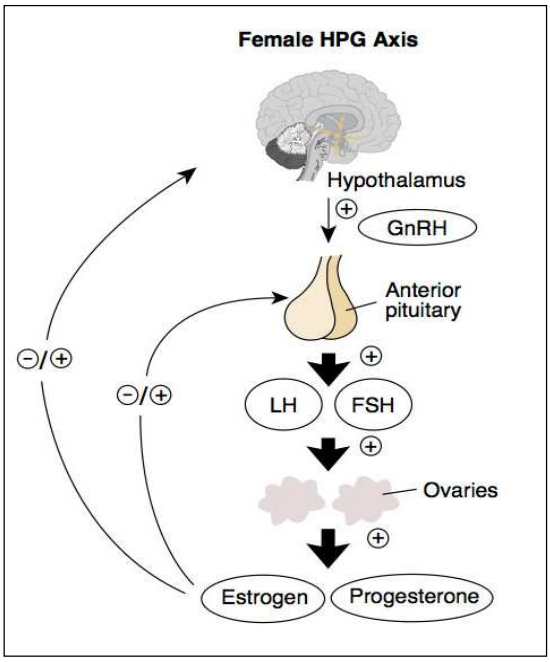

Figure 2-1. Hypothalamic-pituitary-gonadal (HPG) axis. Adapted from Kong et al (5). Abbreviations: FSH, follicle stimulating hormone; GnRH, gonadotropin releasing hormone; HPG, hypothalamic pituitary gonadal axis; and LH, luteinizing hormone.

The ovaries contain follicles that, through their maturation, consist of both the theca and granulosa cells (GCs). Both cell types are required for estrogen production in what is referred to as the "two-cell theory" (7). Theca cells exclusively respond to a rise in LH to increase circulating cholesterol absorption into theca cells via the rate-limiting enzyme, steroidogenic acute regulatory (StAR) protein. Cholesterol is then synthesized into androstenedione by several critical cytochrome p450 enzymes (Cyp) presented in Figure 2-2 (8)**.** Androstenedione can then be converted into testosterone via the catalytic action of 17-*β*-hydroxyl steroid dehydrogenase or diffuse across the basement membrane into the adjacent GCs (9). FSH acts on the GCs to convert thecal androstenedione into estradiol (E2) via aromatization.

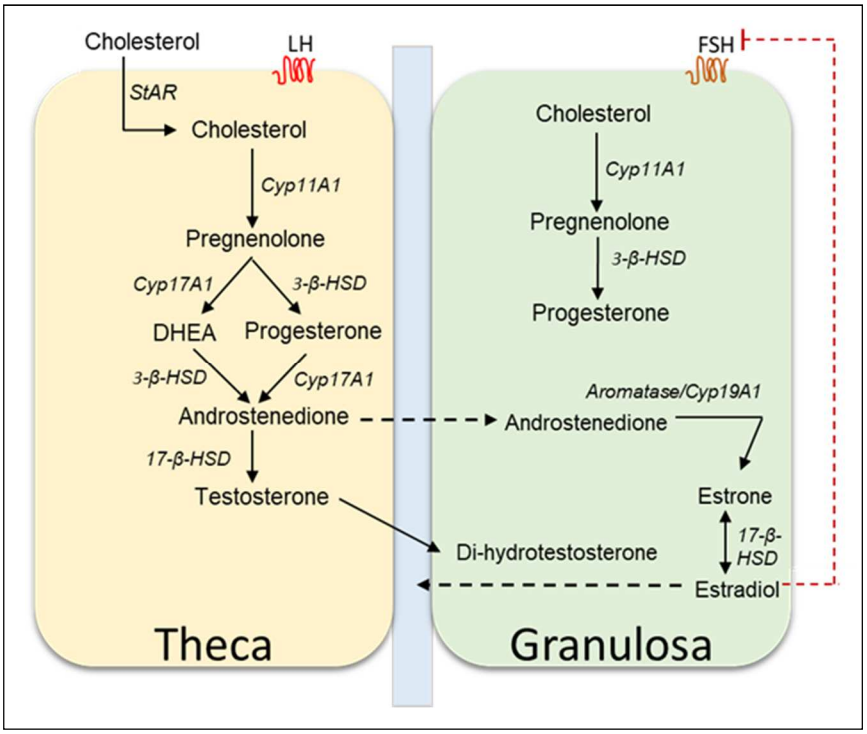

Figure 2-2. Two-cell theory of theca and granulosa cell production of androgen and estradiol under healthy conditions. Adapted from Rosenfield et al (8) Abbreviations: LH, luteinizing hormone; FSH, follicle-stimulating hormone; StAR, steroidogenic acute regulatory protein; Cyp, cytochrome p450; and HSD, hydroxyl steroid dehydrogenase.

Therefore, the ablation of aromatase prevents the GCs from synthesizing E2. This coordination between the ovaries, anterior pituitary, and hypothalamus is orchestrated via the canonical feedback inhibition pathway, whereby E2 production partakes in both positive and negative feedback inhibition (9). During the follicular phase, E2 functions as a negative feedback signal and switches to a positive inducer during the luteal phase. This positive feedback then exerts its action on the anterior pituitary gland to stimulate LH and FSH production, resulting in the classic LH surge responsible for inducing ovulation (9).

Disruption of this HPO axis, such as in PCOS, derails the negative feedback loop, resulting in abnormal GnRH pulsatility and hyperandrogenism (6). Under healthy conditions, LH and FSH fluctuate intermittently during various phases of the menstrual cycle. For instance, the ratio of LH to FSH favors FSH during the early follicular and luteal phases, whereas during the

late events of folliculogenesis and ovulation, LH is favored (6). Under PCOS conditions, this oscillation between LH and FSH is disrupted, resulting in the chronic elevation of LH and compensatory hyperandrogenism (10). Ultimately, the consequences of elevated LH and testosterone concentrations impair menstrual cyclicity, ovulation, and reproduction (8).

Pathogenesis

Despite the large prevalence of PCOS, the underlying etiology remains elusive. The developmental origins of PCOS are thought to be a complex interaction of both genetic and epigenetic factors. Increasing evidence suggests a genetic basis for the pathogenesis of PCOS, although studies have not identified one specific gene target (8). Reports from a twin-study point to PCOS as an X-linked polygenic disorder, highlighting the complicated gene networks involved in its progression (11). Candidate genes potentially implicated in the pathophysiology of PCOS are involved in steroidogenesis, folliculogenesis, androgen transport, and signaling, as well as insulin signaling (12). The primary perturbations that contribute to the pathogenesis of PCOS are 1) hyperandrogenism and 2) insulin resistance. Hypothalamic GnRH pulsatility and amplitude play a central role in the mechanisms that stimulate androgen production (13). Persistent marked elevation of GnRH and LH concentrations underlie the reproductive complications in women with PCOS, in part, due to the compensatory suppression of FSH-mediated folliculogenesis (14). Defective folliculogenesis leads to anovulation, and ultimately, infertility - the main symptom in PCOS patients (15).

There are several animal studies that explain a potential heritable basis for PCOS. In prenatally androgenized (PNA) mice, an increase in neuronal GnRH pulsatility is observed, but interestingly the inverse was reported in prepubescent female PNA mice (16). Association-based studies have reported implications of the decreased sensitivity of GnRH receptors in adolescents, and research suggests that this desensitization delays the onset of menarche, manifesting in

adolescent PCOS (17). Another developmental hypothesis for PCOS is *in utero* neuroendocrine dysfunction from exposure to maternal hyperandrogenism (18). Consequences of fetal exposure to high testosterone concentrations during gestation have demonstrated fetal outcomes such as low birth weight and peripubertal metabolic characteristics that reflect PCOS (19). For instance, the female offspring of dams with chemical-hyperandrogenism encountered delayed puberty, elevated serum FSH, and impaired estrous cyclicity (20). Similarly, rhesus monkeys exposed to maternal hyperandrogenism exhibited an increase in unbound circulating testosterone and serum LH concentrations in the prepubescent years (21). Therefore, maternal exposures may play a more vital role in the pathogenesis of PCOS, partially explaining the clustering of familial PCOS that is predominantly reported (12).

Insulin resistance (IR) is clinically present in approximately 70% of the PCOS population (22), and it is widely reported that IR is closely associated with PCOS due to the consequences of concomitant hyperinsulinemia on androgen biosynthesis (23,24). Insulin is classically recognized for its function in glucose regulation and uptake in the liver, muscle, and adipose tissue (25); however, several lines of evidence report the critical role of insulin as a driver of ovarian function and oocyte quality (26–28). Ovaries contain insulin receptors, whereby insulin exerts its action through two insulin receptor substrate (IRS)-mediated signal transduction pathways, 1) phosphatidylinositol 3-kinase (PI3K)/Akt pathway and 2) the mitogen-activated protein kinase (MAPK) pathway. The former is conventionally involved in glucose transport, and the latter is mechanistically coupled with the PI3K pathway to regulate cellular proliferation and differentiation (29). When examining mouse oocytes, the *in vivo* loss of the subunit responsible for PI3K/Akt activation resulted in follicular atresia and even infertility (30). Similar findings were also found in a high-fat diet-induced obesity model (31). Results from this study

observed reduced mRNA and protein levels of the IRS-1, further explained by the induction of the PI3K pathway, which has been previously reported as a critical signaling pathway for primordial follicle activation (32,33).

Hyperinsulinemia is also disruptive to the HPO axis. Numerous research studies have determined a high correlation between insulin and sex hormone-binding globulin (SHBG), which functions to acquire and transport unbound circulating hormones, such as testosterone (24,34). The inverse association between hyperinsulinemia-mediated PCOS and SHBG is prominent (35). Moreover, this inverse association has also been reported in type 2 diabetes and metabolic syndrome, demonstrating its close relationship with IR (36,37). Furthermore, seminal work by Nestler et al., demonstrated that PCOS patients treated with an insulin inhibitory drug, diazoxide, exhibited decreased fasting insulin levels and markedly reduced free testosterone concentrations (38,39). The direct mechanistic role of insulin in attenuating SHBG production is unknown, but SHBG is clinically used as a biomarker for diagnostic purposes of PCOS, suggesting hyperinsulinemia as a basis for the derangements in androgen synthesis and signaling (40).

Diagnostic Criteria

Due to the heterogeneity of PCOS, there is no globally adopted set of criteria. Diagnostic criteria are a combination of gynecologic, dermatologic, and metabolic symptoms (2,41,42). More robust descriptions of these general fields are presented below**.** Diagnosis of PCOS is not limited to one specialty and requires a thorough medical history with an investigation on a per-patient basis. The Rotterdam diagnostic criteria (10) is commonly used in the United States and requires the presence of at least two of the following: 1) biochemical hyperandrogenism evidenced by a total testosterone concentration >70 ng/dL; androstenedione >245 ng/dL, and dehydroepiandrosterone >248 µg/dL; 2) ovulatory dysfunction assessed by oligomenorrhea (>35

d menstrual cycle) or anovulation (< 9 menses/year); 3) polycystic ovaries determined by ≥ 12 follicles (2-9 mm diameter) in each ovary (43).

Although PCOS is predominantly detected among adult women, it has been estimated that roughly every 1 in 200 adolescent females has PCOS (4). Detecting PCOS among individuals in the pediatric population is less common; however, there are slightly different guidelines for adolescents given the regular presence of acne and menstrual irregularities in the peripubertal stages. The diagnostic criteria for adolescents are similar to that of adults, with the additional specification of oligo- or amenorrhea two years post-menarche and hyperinsulinemia accompanied by abdominal obesity, nigricans, and glucose intolerance (44). Despite these guidelines, definitive diagnosis is not mandatory before initiating the treatment strategies that are discussed in the next section.

Lifestyle Modifications and Therapeutic Treatments

The therapeutic management of PCOS utilizes both pharmacologic and nonpharmacologic strategies, depending on the patient's primary symptom of concern. First-line therapy for women with PCOS includes lifestyle modifications, primarily directed towards weight loss through dietary or physical activity regimens. Several studies have demonstrated the effects of weight loss on the metabolic anomalies of PCOS (45–47), and most dietary intervention strategies mimic those recommended for type 2 diabetes and metabolic syndrome (48,49).

Research implementing a restricted low-carbohydrate diet coupled with a minimum of 90 min of physical activity assessed primary outcomes of body weight, fertility, and abundance of critical endometrial genes and proteins in PCOS women classified as obese (50). Findings from Ujvari et al., reported that following the 3-month intervention, 80% of the patients that achieved just a 5% reduction in weight was significant enough to restore ovulation in 35% of the cohort, in

addition to demonstrating improvements in endometrial IRS-1 mRNA and protein abundance (50). Most dietary approaches are directed towards the metabolic derangements of PCOS, with primary indicators of IR, fasting blood glucose, and testosterone concentrations. In a meta-analysis of eight randomized controlled trials examining the effects of low carbohydrate diets on PCOS, reported a marked reduction in body mass index and homeostatic model assessment of IR (HOMA-IR) (51). Positive correction of SHBG and testosterone levels was only observed in the randomized control trials employing interventions longer than one-month; however, no diet outcomes on fertility and reproductive management were reported. A prospective study compared the long-term effects (two-year) of a hypocaloric diet vs. treatment with the insulin-sensitizing drug, metformin, on clinical and reproductive outcomes (52). Following the two-year intervention, obese women with PCOS demonstrated a significant reduction in LH and androgen concentrations, alongside improvements in body mass index irrespective of the treatment group. The efficacy of exclusive long-term lifestyle modifications on the amelioration of PCOS outcomes has not been determined; therefore, lifestyle modifications, alone, may not be suitable to reverse the effects of PCOS.

The complexity of PCOS makes lifestyle approaches towards treating the disorder challenging, especially in the prepubescent years. Depending on the patient's needs, various treatments will be recommended to address 1) anovulation/infertility, 2) insulin resistance and obesity, or 3) hirsutism through the pharmacological approaches, as indicated in Figure 2-3. In general, the pharmaceuticals that mechanistically target glucose metabolism, androgen production, or ovulation are commonly prescribed (10).

The mode of action for metformin is to decrease intestinal glucose absorption and mobilize glucose uptake into the cells (53). It has been long used as a second-line treatment for

PCOS, as it functions to address IR, obesity, anovulation, and may reduce hirsutism, owing to normalized testosterone concentrations (54). Thiazolidinediones (TZDs) are sometimes used in place of metformin. TZDs are agonists of the peroxisome proliferator-activated receptor-gamma ($PPAR_{\Upsilon}$) that function by increasing the transcription of critical energy-sensing transporters involved in glucose uptake, such as adipocyte and muscular glucose transporter type-4 (55).

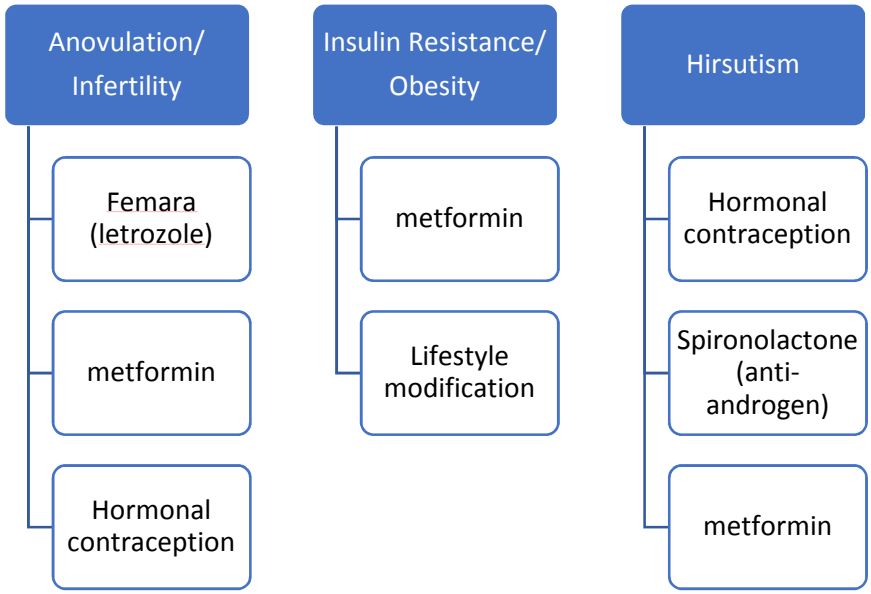

Figure 2-3. Therapeutic strategies for PCOS management. Adapted from Williams et al (10).

Both metformin and TZDs have demonstrated their efficacy in inducing ovulation and promoting fertility (56,57). Like many pharmacologic compounds, there are associated risks with their use. Nutrition deficits, such as serum vitamin B_{12} and folate deficiency, are commonly reported in women using metformin long-term, increasing the risk for hyperhomocysteinemia (HHcy), an associated risk factor for cardiovascular disease (58,59). Furthermore, TZDs are considered potentially teratogenic and impose serious risks to fetal outcomes and hence, are not suitable therapies during the conception, gestation, and breastfeeding periods (60). Therefore, both therapeutic strategies are only used in combination if their perceived benefits outweigh the risks.

Oral contraceptives are typically used in women with PCOS that are not seeking pregnancy as a means to treat concurrent symptoms of acne, menstrual irregularity, and hirsutism (61). There are conflicting results in whether birth control can address dyslipidemia, IR, and hyperinsulinemia; therefore, alternative therapies are recommended for PCOS's joint metabolic aberrations (62). Spironolactone is a mild antagonist of the androgen receptor, which blocks testosterone and dihydrotestosterone's signaling power, reducing excessive hair growth and acne (63). A combinatorial approach of prescribing both spironolactone and metformin has been used for over two decades and shows to be efficacious in addressing the physical anomalies of PCOS (64). The American Association of Clinical Endocrinologists (AACE) submitted recent guidelines for the effective use of letrozole (Femara®), a competitive inhibitor of granulosa cell aromatase, and climophene citrate, an FSH and LH-inducer, both of which are considered as ovulatory stimulants (15). Taken together, there is currently no one-size-fits-all approach, and due to the inconclusive pathogenesis of PCOS, often times several intervention strategies are prescribed throughout the lifetime of a woman with PCOS.

Animal Models of PCOS

Animal models, particularly the use of rodents, are used in laboratory settings to explore the mechanisms involved in the pathogenesis of PCOS. Rodent models of PCOS are beneficial due to the ability to investigate tissue-specific alterations that cannot be routinely conducted using human populations. Their high reproductive capacity, small size, and shorter lifespan make rodent models a suitable candidate in better understanding the pathophysiology of PCOS. Careful considerations are to be made when employing animal models, as there is a spectrum of phenotypic and metabolic outcomes between the chemically-induced and genetic animal models employed in studies. The various models of PCOS are discussed in further detail in the following sections.

Chemically-induced

Chemical induction of PCOS can be achieved through multiple modalities to recapitulate specific characteristics of this disorder. Conventional approaches include androgen- and estrogen-induction, PNA, and enzymatic aromatase inhibition (65). Chemically-induced models help identify the transient effects of acute PCOS, as restoration of estrous cyclicity occurs upon chemical cessation. Dehydroepiandrosterone (DHEA) is an androgenic hormone, with negligible biological effects (66). Rather, DHEA is a substrate for androstenedione, whereby it is metabolized into the potent androgens, testosterone, and dihydrotestosterone (DHT), via 3-β-HSD and 17-β-HSD enzymes. Chemical induction of PCOS with DHEA in an emulsion of sesame oil is often used in rat and mouse models for 20-30 days in the prepubertal period (67–69). Li et al., reported that following daily subcutaneous injections of DHEA for 20 days, mice exhibited immature follicles, anovulatory infertility, and a significant reduction in zygote quantity (68). These observations have also been corroborated in a rat model, whereby atretic, cystic follicles were detected following DHEA-induction (69). The effects of DHEA also led to diminished GC and thickened thecal layers, providing evidence for perturbed folliculogenesis. DHEA-induction augments concentrations of FSH, LH, testosterone, E2, and the LH/FSH ratio. One major differentiator between the DHEA model and human PCOS is the elevation in circulating E2 and FSH, as the inverse is characteristic of women with PCOS (70).

Depending on the primary outcome of interest, other chemically-induced rodent models may be considered to recapitulate PCOS. Alternative hormonal agents to DHEA include DHT and letrozole. Mechanistically DHT is similar to that of DHEA, except that DHT is a non-aromatazible androgen that has potent effects on phenotypic features exhibited in women with PCOS, such as impaired glucose tolerance, adipocyte hypertrophy, and anovulation (71). Research studies employing DHT can either acutely induce impaired folliculogenesis and

metabolic dysfunction or continuously administer DHT for 3 months to achieve aberrations in ovarian morphology (72,73). The downsides of this model is that acute and long-term administration of DHT manifests in lower serum testosterone and 4-fold higher E2 concentrations, which does not commonly occur in women with PCOS (73,74). One of the main differences between DHEA and DHT is that the former results in hypertrophy of the ovary, whereas long-term DHT exposure will result in ovarian atrophy (75).

Aromatase is an enzyme that catalytically converts androstenedione to E2 via aromatization. It is primarily localized in the ovarian theca cells, although its abundance can also be found in extragonadal tissues, such as adipose and bone (76). Letrozole-induced PCOS is an exceptional model to utilize when characterizing the pathophysiology of PCOS that is independent of metabolic alterations is of interest. A study by Caldwell et al., compared the three chemicals, DHEA, DHT, and letrozole, for 90 consecutive days via subcutaneous implantation in female Wistar rats (74). Aromatase inhibition was the only treatment that closely recapitulated the hallmarks of PCOS, such as acyclicity, increased body weight, oligo-ovulation, elevated LH, and testosterone with concomitantly suppressed E2. Letrozole is not a strong model for metabolic anomalies commonly reported in PCOS, as letrozole treatment results in unchanged body fat, total cholesterol, insulin and blood glucose concentrations (77). In comparison, treatment with DHT more closely reflects the metabolic perturbations common in humans, such as increased body fat coupled with hypercholesterolemia and hyperinsulinemia (74). On the contrary, DHT does not significantly alter circulating testosterone or LH concentrations, limiting its scope on some of the morphological alterations classically observed in PCOS.

Lastly, PNA is another frequently used PCOS model, allowing researchers to examine the transgenerational effects of high *in utero* androgen exposure on offspring outcomes. Studies

determining the influence of maternal hyperandrogenism on fetal birth and developmental outcomes were discussed earlier in this chapter (16,17,19); however, a more recent study reported the effects of female DHEA exposure on two generations of offspring (78). Findings from Zhang et al., indicated that DHEA exposure in first generation dams led to reproductive and metabolic characteristics similar to that of PCOS, such as disrupted cyclicity, decreased glucose tolerance, and elevated serum testosterone concentrations in offspring for two generations following (78). This basic study exploring the implications of maternal hyperandrogenism revealed its significant transgenerational effects. Taken together, there are several chemical models that may be deemed appropriate when exploring the pathogenesis of PCOS; however, it is critical to identify the primary outcome of interest prior to selecting a chemical to induce PCOS in rodent models.

Genetic Models

In general, the genetic strains that reflect PCOS or lead to the development of polycystic ovaries and irregular estrous cycles are those that exhibit dysregulated metabolic characteristics, such as obesity, dyslipidemia, and insulin resistance (79). In addition to hyperinsulinemia, many women with PCOS present leptin resistance with concomitant hyperleptinemia (80). Leptin receptor (LEPR) deficient animal models, in theory, may be a suitable representation of PCOS due to leptin's indirect effects on GnRH neurons and its functional role in the metabolic outcomes. The melanocortin system contains crucial neuronal circuitry that functions in governing body weight and appetite control, but it is also recognized for its vital off-target effects on reproduction (81). Two melanocortins regulate appetite, the alpha-melanocyte-stimulating hormone (α–MSH) secreted by the proopiomelanocortin (POMC) suppressing appetite, and the agouti-related protein (AgRP) released from the AgRP neuron, stimulating appetite (82). The hormone leptin functions by activating the POMC and inhibiting the AgRP

neurons. Therefore, LEPR deficient rodents, such as the Zucker Diabetic Fatty (ZDF) rats, become hyperphagic and exhibit progressive obesity and impaired glucose tolerance by 14 wk of age (83,84). Leptin resistance or LEPR deficiency reduces the POMC-activated α–MSH production, perturbing reproductive processes, as α–MSH stimulates GnRH neuronal firing (85).

Concerning the LEPR deficient female ZDF rats that harbor the (LEPR(*fa)*) mutation (86), the parameters of androgen production are lesser-known. However, few studies have reported follicular atresia, perturbed ovarian morphology, and infertility in ZDF rats, resulting from inadequate stimulation of the GnRH neurons (79,87). Deghestani et al., demonstrated the positive association between polymorphisms in the human LEPR gene and incidence of PCOS-mediated infertility (88). Moreover, an *in vitro* model culturing porcine follicles in high leptin media observed elevated testosterone production accompanied by the induced expression of *Cyp11A1* and *17-β-HSD* (89). Other models of altered leptin metabolism, examining the outcomes of ovarian folliculogenesis and infertility are more comprehensively characterized, such as the *ob/ob* (90,91), *db/db* (92), and *IR/LEPR*^{POMC} (93) models.

Another well-established genetic model for PCOS is the agouti lethal yellow mouse (KK.Cg-Ay/J) with a mutation in the agouti (Ay) locus, resulting in overexpression of the agouti gene. The Ay mutation is pleiotropic, leading to ectopic agouti protein expression that manifests in phaeomelanin (hair yellowing), obesity, IR, infertility, and a propensity for reproductive failure (94–96). Interestingly, the degree of methylation inversely correlates with AgRP (97); therefore, hypomethylation leads to overexpression and production of AgRP, an antagonist of the melanocortin-3 and -4 receptors (MC3R and MC4R) (98). With respect to Ay and reproduction, a study in MC4R-deficient mice identified reduced reproductive capacity, owing to anovulation (99); hence, mice homozygous for the Ay mutation leads to complete infertility due to AgRP-

inhibition of the MC3R/MC4R. Research by Nteeba et al., determined the impact of progressive obesity on ovarian folliculogenesis using the agouti mouse model (94). Their findings indicated that decreased primary follicles accompanied by elevated NF-kappaB-mediated inflammatory pathways were observed beginning at 12 wk of age when high fasting blood glucose and obesity were apparent in the agouti mice (94).

Methyl Group Metabolism

Methyl group metabolism is comprised of both homocysteine (Hcy) and folate metabolism, and is central for the transfer of one-carbon units to aid in cellular function, purine and thymidine synthesis, DNA methylation, and the remethylation of Hcy (100). It is also a key biochemical process for the provision of methyl groups, which mediate environmental influencers on gene expression, in a field known as epigenetics (101). Methionine is an essential amino acid that is derived from dietary sources, and serves as a substrate for the synthesis of cysteine, taurine, SAM, and glutathione. In the central step of methyl group metabolism, methionine adenosyltransferase catalyzes the formation of S-adenosylmethionine (SAM) from methionine as shown in Figure 2-4 (100,102). SAM is a ubiquitous compound that acts as a methyl donor in transmethylation reactions, and is converted to S-adenosylhomocysteine (SAH). Both SAM and SAH serve as intermediates between methionine and Hcy by the catalytic activity of SAH hydrolase. To complete the active methionine pathway, Hcy is enzymatically converted to methionine, generating tetrahydrofolate (THF). Under conditions of sufficient methionine and THF supply, Hcy is subsequently irreversibly catabolized into cysteine via the transsulfuration pathway (Figure 2-4). In the folate-dependent remethylation of Hcy, 5-methyltetrahydrofolate donates a methyl group to Hcy via B12-dependent methionine-synthase (MS).

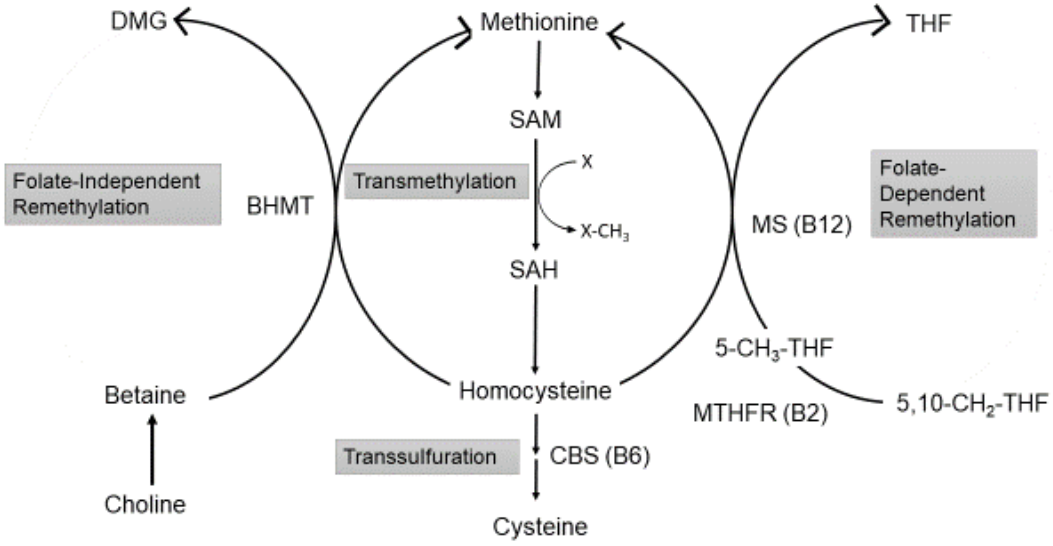

Figure 2-4. Methyl group and homocysteine metabolism pathway.Adapted from Williams et al (102). BHMT, betaine homocysteine *S*-methyltransferase; CBS, cystathinine *B*-synthase; DMG, dimethylglycine; MS, methionine synthase; MTHFR, methylenetetrahydrofolate reductase; SAH, *S*-adenosylhomocysteine; SAM, *S*-adenosylmethionine; THF, tetrahydrofolate; 5-CH_3-THF, 5-methyltetrahydrofolate; and X, methyl group acceptor.

The folate-independent remethylation of Hcy requires dietary choline, an essential nutrient that is oxidized to betaine and is acted on by betaine-homocysteine *S*-methyltransferase (BHMT) to regenerate methionine from Hcy, and produce the by-product, dimethylglycine. Alternatively, Hcy enters the transsulfuration pathway. In this pathway, Hcy is irreversibly catabolized to cysteine through the intermediate, cystathionine, via the pyridoxal phosphate (B_6)-dependent cystathionine *β*-synthase (CBS). Other sulfur metabolites, such as glutathione and hydrogen sulfide, are key downstream products of the transsulfuration pathway. Moreover, taurine is an amino acid that is also a product of the transsulfuration pathway, whereby it is critical for bile salt production through conjugation. Importantly, DNA methylatransferases (DNMTs) are a conserved family of enzymes that are critical for epigenetic mechanisms, as they are responsible for the covalent transfer of methyl groups from SAM for methylation of the

carbon-5 (C5) position of cytosine (5-methylcytosine; 5mC), in the promoter region of genes, resulting in downregulation of gene expression (103). Although this completes a large portion of methyl group metabolism, the key components of this regulatory process are the cofactors and substrates required for efficient enzymatic activity.

Nutrients and Methyl Group Metabolism

Several indispensable nutrients function as coenzymes and methyl donors within the methyl group metabolism pathways aforementioned. Folate is a nutrient derived from dietary sources that are essential for DNA and RNA production. Folate is enzymatically reduced into dihydrofolate (DHF) or further into tetrahydrofolate (THF) via the enzyme dihydrofolate reductase. Dietary folate deficiency is of concern, especially during the periconceptional years, as deficiency increases the risk for neural tube defects (NTDs) (104). Due to this severe birth defect, folic acid fortification was deemed mandatory in the United States by the Food and Drug Administration in 1998 as a means for preventing NTDs (105). The recommended daily amount of folate consumption is 400 mcg for adults and 800 mcg for pregnant women. Folic acid is the precursor to THF, which is acted on via serine hydroxymethyltransferase (SHMT), whereby serine is converted into glycine (106). This enzymatic conversion requires the cofactor, vitamin B_6. Another critical step in the folate metabolism pathway is recycling THF back into DHF carried out by dihyrdofolate reductase, whereby the enzyme thymidylate synthase converts dUMP to dTMP, a precursor for DNA synthesis, and requires the cofactor, $FADH_2$ – a metabolic product of riboflavin (B_2). Numerous cancer-targeting therapeutics, such as methotrexate, block the activity of dihydrofolate reductase to prevent the synthesis of thymidine triphosphate, and subsequent tumor progression (107,108).

Additional vitamins and minerals that are necessary for methyl group metabolism include B_{12}, B_6, and zinc. Methylenetetrahydrofolate reductase (MTHFR) requires the cofactor vitamin

B_2 to generate 5-CH3-THF from the intermediate, 5,10-methylenetetrahydrofolate. Polymorphisms in the MTHFR gene or vitamin B_2 deficiency could lead to an insufficient supply of 5-CH3-THF, compromising the remethylation of Hcy to methionine. Vitamin B_{12} is exclusively present in animal sources and requires the carrier protein, intrinsic factor when its free circulating form allows for its absorption and activity. It is also a cofactor for MS; therefore, B_{12} deficiency impairs the remethylation from Hcy to methionine, resulting in a "methyl trap" as 5-CH3-THF. Susceptibility to B_{12} deficiency exists in two significant populations: vegans and those greater than 65 years of age (109,110). Intrinsic factor-mediated B_{12} absorption is related to age, as its production declines with age (100). Moreover, patients with neurological complications are at the highest risk of vitamin B_{12} deficiency, a condition explaining 90% of the B_{12} deficient population (110,111). Pyridoxal 5'-phosphate (B_6)-dependent enzymes include CBS and SHMT. While B_6 deficiencies are rare, their implications on methyl group metabolism can have deleterious effects. Vitamin B_6 is critically essential in the irreversible catabolism, not only for Hcy balance. B_6-dependent CBS activity contributes to approximately 50% of the required cysteine for glutathione production (112). Adequate B_6 supply is critical for regulating inflammation due to cytokine and antibody production, lymphocyte maturation, and natural killer cell activity (112–114).

Homeostasis of the methyl group metabolism pathway not only relies on a sufficient supply of folic acid, b-vitamins and choline, but zinc is critically important for the provision of methyl groups, as MS and BHMT are zinc metalloenzymes. Several studies have examined the implications of zinc-deficiency on methyl group metabolism. Wallwork et al., determined the rate of metabolic turnover of methyl groups, as assessed by the SAM concentrations, is drastically lower in a zinc-deficient rat model than normal controls (115), resulting in diminished

SAM production downstream methylation of DNA and histone proteins. Zinc is also required for the activity of BHMT (116); therefore, zinc deficiency leads to an increase in Hcy concentrations, a decrease in SAM, and consequently an increase in the potent methyltransferase inhibitor, SAH. Since all of the enzymes required for SAM biosynthesis are present in oocytes (117), there is evidence in the literature reporting the adverse effects of zinc-deficiency on reproductive outcomes, particularly in examination of oocyte quality (118). Furthermore, the ratio of SAM/SAH, and in turn, follicular Hcy concentrations, may be robust biomarkers for infertility and oocyte quality for those seeking assisted reproduction (117–119).

Estrogen and Methyl Group Metabolism

In addition to nutritional aspects, hormonal factors like estrogen may diminish or enhance methyl group metabolism. For instance, researchers examined women with and without hypertension and identified a significant inverse association between circulating Hcy concentrations and E2 (120). This association was corroborated by the work of Shah et al., who observed that postmenopausal women given hormonal replacement therapies exhibited a reduction in circulating Hcy concentrations (121). The exact mechanisms underlying the association between estradiol and Hcy are unknown. However, one study using human umbilical endothelial cells reported a possible mediating effect of estrogen on hydrogen sulfide production (120). After subjecting the endothelial cells to high E2 concentrations, CBS expression was induced with a concomitant reduction in intracellular Hcy.

One of the most well-known links between estrogen and methyl group metabolism is the estrogenic effect of hepatic phosphatidylethanolamine *N*-methyltransferase (PEMT), which is required for *de novo* synthesis of phosphatidylcholine (122). Pregnancy and lactation are periods of increased demand for choline in order to support fetal cognitive development. A study examining *PEMT* knockout dams identified that all pups were aborted *in utero*; whereas, dams

administered exogenous choline restored their pregnancies, despite the *PEMT* mutation (123). While the association between *PEMT* mutations and PCOS has not been studied, there may be a mediating link between the observed aberrations in PCOS and global methylation status as a result of choline deficiency. For instance, middle-aged women consuming dietary choline below the recommended amounts exhibited leukocyte DNA hypomethylation (124,125). Conversely, a study comparing the methylation status of males vs. females reported lower methylation levels due to increased estrogen concentrations (126). This is also reported in a mouse study, whereby they injected mice with estrogen and examined the uterine methylation status of DNA cytosine bases; they observed a dose-dependent effect of estrogen on attenuated 5mC (127). Whether the functional roles of estrogen on methylation status are mediated via the canonical methyl group metabolism pathway through the provision of *de novo* choline biosynthesis is yet to be examined. However, numerous studies have reported perturbed methylation patterns across various tissues during the progression of PCOS (128–131).

PCOS and Methyl Group Metabolism

Methyl group metabolism is critical for the provision of methyl groups from dietary components like choline, B-vitamins, and folate (132). Dietary derived methyl donors are critical for DNA methylation, and epigenetic modifications. Epigenetics is a field that studies heritable and, environmental factors that influence gene expression but do not alter the underlying DNA sequence (101,133). Rather, epigenetic modifications comprise 2 mechanisms: 1) DNA methylation and 2) posttranslational modification of histones. DNA methylation has been long studied in reproductive science, as DNA methylation is a critical epigenetic modifier functioning in ovary development, maturation, and overall reproduction (134,135). DNA methylation (5mC) generally functions by methylating the cytosine in the CpG dinucleotide region, thereby inhibiting gene expression (136). Interestingly, several genome-wide association studies have

identified the potential role of DNA methylation in the pathogenesis of PCOS (130,131,137). Limited studies have examined how PCOS disrupts methyl group metabolism and/or how deprivation of critical methyl group suppliers (i.e., folate, B_{12}, B_6, and B_2) impact ovarian methyl group metabolism (138–140). Several studies exemplify certain aspects of methyl group or one-carbon metabolism, such as primary outcomes of methylation status, Hcy concentrations, and mRNA or protein abundance of critical enzymes (141–147). Animal models are frequently studied to assess the epigenetic and methylation drivers of oogenesis (148,149), whereas human studies have explored some of the metabolic perturbations in nutrient and methylation status in patients with PCOS (Table 2-1). By piecing together some of these related events, we may ascertain new knowledge between methyl group metabolism and its potential role in the pathogenesis of PCOS. Several *in vivo, in vitro*, and human studies have reported alterations in methyl group related enzymes either through a robust model of PCOS or through androgen excess models. These studies are represented in Table 2-1.

Hyperhomocysteinemia

Homocysteine is a sulfur-containing non-essential amino acid that is the by-product of the metabolism of methionine in the broader process of methyl group metabolism, as aforementioned. The concentrations of Hcy are tightly regulated by two pathways 1) remethylation and 2) transsulfuration (Figure 2-4). Augmented synthesis of intracellular Hcy concentrations may be attributed to acquired dietary deficiencies (155), genetic factors (156,157), and several underlying health conditions that will be discussed in more detail. In humans, the normal levels of serum Hcy are classified in a range of 5 – 15 µmol/L (158). Therefore, HHcy is subclassified into three categories, mild/moderate (15-30 µmol/L), intermediate (30-100 µmol/L), and severe (> 100 µmol/L) (159,160). Since humans contain both the reduced and oxidized forms of Hcy, the diagnosis must account for these variants.

Table 2-1. Key studies linking aspects of polycystic ovary syndrome with methyl group metabolism.

Model	Reference	Model Description	Intervention	Methyl group metabolism indicators	Other key outcomes
In vitro	Jia et al., 2019 (141)	Primary culturing of gilt oocytes, artificial *in vitro* maturation	Control, cumulus-oocyte complexes and HHcy exposed oocytes (200 μM).	- ↑ *DNMT1, BHMT,* and *GNMT* mRNA abundance - ↑ *BHMT,* and *GNMT* protein abundance	- ↓ oocyte survival and polar body extrusion rates - ↓ oocyte differentiation
	Bhattacharyya et al., 2013 (143)	Female athymic nude mice	Primary epithelial ovarian cancer cells	- ↑ CBS mRNA and protein expression	- N/A
In vivo	Jia et al., 2016 (142)	Prepubertal gilt, normal and polycystic ovaries	*In vitro* oocyte maturation	- ↑ *DNMT1, BHMT,* and *GNMT* mRNA and protein abundance - ↑ methylation of mtDNA; - ↑ follicular Hcy.	- ↓ cellular blastocysts
	Lei et al., 2017 (150)	Female, ICR/HaJ mice	PNA with 350 μg of DHT in 70 μL sesame oil	- ↓ granulosa cell MTR mRNA expression in PNA mice - ↓ ovarian MTR protein at 3 wk and 3 mo of age - ↓ serum SAM	- Absence of proestrus - ↑ ovarian weight - ↑ antral follicles - ↓ primordial follicles

Table 2-1. Continued

Model	Reference	Model Description	Intervention	Methyl group metabolism indicators	Other key outcomes
In vivo					
	Tian and Diaz, 2013 (118)	Female, CD1 mice	Acute dietary zinc deficiency	- ↓ global DNA methylation - ↓ histone methylation	- ↓ mature eggs following IVF - ↓ blastocysts - ↓ oocytes
	Cui et al., 2018 (146)	Female wistar rats	Diet-induced obesity (DIO), 5α-dihydrotestosterone-induced PCOS	- ↑ 5-methylated cytosine DNA in PCOS and DIO models - ↓ 5-hydroxymethyl cytosine DNA in PCOS and DIO models - ↑ *Dnmt3a* mRNA expression in PCOS - ↑ *Dnmt3b* mRNA expression in PCOS	- Ovarian atrophy - ↑ diestrus stages - DIO did not alter ovarian morphology or estrous cyclicity - ↑ body weight - ↑ glucose intolerance
	Li et al., 2018 (151)	Female rats	DHEA-induced PCOS or DHEA + HFD-induced PCOS	- ↑ serum homocysteine - ↓ hepatic *Bhmt* and *Cbs* - ↓ methylation of the promoter regions of hepatic *Bhmt* and *Cbs*	N/A
Human					
	Sinclair et al., 2007 (152)	Ewes, 5-6 yr old Scottish Blackface	Specialty diet to meet caloric need; control group (standard diet); vs. B12-deficient group	- ↓ methylation of CpG regions of the offspring (male and female) from B-12 deficient ewes - ↑ Hcy - ↓ methionine, folate - ↓ granulosa cell SAM	- ↑ body weight in 22 mo old male sheep from B12-deficient ewes - ↑ glucose intolerance in male

Table 2-1. Continued

Model	Reference	Model Description	Intervention	Methyl group metabolism indicators	Other key outcomes
Human	Sinclair et al., 2007 (152)	Ewes, 5-6 yr old Scottish Blackface	administered elemental cobalt and sulfur to reduce microbial B12 synthesis.	- ↓ granulosa cell SAM:SAH ratio ↑ granulosa cell Hcy	- sheep from B12-deficient ewes
	Lei et al., 2017 (150)	Hyperandrogenic PCOS patients and controls undergoing IVF.	GnRH injections at midluteal phase, human chorionic gonadotropin (hCG) injection at follicle, 16 mm prior to oocyte retrieval.	- ↓ granulosa cell MTR mRNA and protein expression - ↓ serum SAM	- ↑ BMI - ↑ Mean arterial pressure - ↑ Ovarian volume - ↑ Serum LH, testosterone, and LH/FSH
	Bhattacharyya et al., 2013 (143)	210 tissue microarrays	Ovarian cancer cell lines	- ↑ CBS mRNA and protein expression	N/A
	Pan et al., 2018 (128)	110 PCOS, 119 healthy women undergoing IVF	RNA-sequencing of critical genes in granulosa cells	- ↓ 25% DNA methylation - ↓ methylation of gene promoters involved in steroidogenesis	- ↑ HOMA-IR - ↑ LH/FSH ratio - ↑ testosterone - ↓ SHBG and oocyte quantity

Table 2-1. Continued

Model	Reference	Model Description	Intervention	Methyl group metabolism indicators	Other key outcomes
Human	Sagvekar et al. 2019 (129)	20 healthy women and 20 women with PCOS undergoing IVF	DNA extracted from cumulus granulose cells. RNA-seq and bisulfite-seq	- ↓ methylation in pathways w/ inflammation, chemokine, and cytokine - ↑ methylation in androgen production, leading to androgen excess	- N/A
	Jiao et al., 2019 (153)	PCOS women with and without regular menstruation	DNA methylation, and RT-PCR	- ↓ DNA methylation in PCOS + irregular menstruation - ↑ in cancer-related genes in PCOS + irregular menstruation	- N/A
	Sang et al., 2014 (154)	PCOS patients (n = 81) and health controls (n = 99) with anovulation; biochemical hyperandrogenism; and polycystic ovaries	Fasting blood samples for genomic DNA and mass-array methylation analysis.	- ↓ methylation of *EPHX1* (steroidogenesis) in CpG clusters: 13-14, 15-16, 19-24, 55-57 in women with PCOS	- ↑ LH - ↑ E2 - ↓ FSH - ↑ testosterone
	Xu et al., 2016 (139)	PCOS patients (n = 40) and healthy controls (n = 40); 25-35 years of age; and on GnRH agonists	Oocyte retrieval and follicular fluid obtained, granulosa cells DNA bisulfite seq.	- ↑ DNA methylation in PCOS vs. control - ↑ DNA methylation in PCOS-obesity vs. control - ↑ granulosa cell global hypermethylation in PCOS vs. control	- ↑ LH - ↑ testosterone

Table 2-1. Continued

Model	Reference	Model Description	Intervention	Methyl group metabolism indicators	Other key outcomes
Human	Yu et al., 2015 (137)	Case-control, matched for age and BMI. PCOS women (n = 10) and healthy (n = 10).	Ovarian drilling-induced ovulation for oocyte extraction. Genome-wide DNA methylation assessment.	- ↑ DNA methylation in PCOS vs. control in CpG island shores (outside of promoter regions) - ↓ methylation in gene bodies of PCOS women vs controls.	- N/A

BHMT, betaine homocysteine *S*-methyltransferase; BMI, body mass index; CBS, cystationine *B*-synthase; DHT, dihydrotestosterone; DIO, diet-induced obesity; DNMT1, DNA methyltransferase-1; E2, estradiol; FSH, follicular stimulating hormone; GNMT, glycine *N*-methyltransferase; HOMA-IR homeostatic model assessment of insulin resistance; HHcy, hyperhomocystienemia; IVF, *in vitro* fertilization; LH, luteinizing hormone; MTR, methionine synthase; PCOS, polycystic ovary syndrome; PNA, prenatally androgenized; SAM, *S*-adenosylhomocysteine; and SHBG, sex hormone binding globulin.

Four forms constitute the total plasma Hcy concentrations (161). For instance, the reduced, sulfhydryl form (Hcy) and oxidized, disulfide forms make up 1% and 5-10%, respectively. Mixed disulfides include the albumin-bound Hcy, which accounts for 80-90% of the total Hcy in circulation; and lastly, the other 5-10% of remaining Hcy is in the cysteine-Hcy form. Upwards of 99% of the total circulating Hcy concentrations are in the oxidized, "free," and albumin-bound forms, whereby healthy individuals have a total Hcy concentration of around 2-3 μmol/L (161). Kidneys can only filter out trace amounts of Hcy (162); therefore, HHcy is a cause of concern for multiple diseases, hence, why it is frequently used as a biomarker or indicator of disease risk.

Pathogenesis of Hyperhomocysteinemia

It is well established that HHcy is an independent risk factor for cardiovascular disease – an association first proposed by McCully in 1969 (163). This association's origins were identified from the observation of an inborn error in metabolism, termed homocystinuria, which is a condition that results in elevated Hcy in the urine. Homocystinuria is a heritable condition that manifests from the inability to regulate Hcy metabolism, owing to a genetic defect in CBS and/or γ-cystathionase (164). This reduced enzymatic activity impairs the ability to metabolize Hcy into cysteine via the transsulfuration pathway. A second inborn error in metabolism leading to HHcy is a polymorphism in the gene encoding MTHFR, such as the C677T mutation, which substitutes thymine for a cytosine nucleotide 677 (165). Moreover, MS can also be subjected to single nucleotide polymorphisms (MTR, A2756G), whereby the base substitution of glycine for aspartic acid (166) interferes with MS enzymatic activity, manifesting in a ‘methyl folate trap,’ and ultimately, HHcy (167).

Apart from genetic and nutritional anomalies, the pathogenesis of HHcy is also implicated in numerous chronic diseases. Hyperhomocysteinemia is reported in up to 85% of

patients with renal failure (168), as research suggests that microalbuminuria (protein-bound Hcy) impedes renal glomerular filtration rate (169). Subsequent disease states that alter Hcy metabolism, leading to HHcy include hypothyroidism, hypertension, liver disease, among others (102,158). Collectively, these diseases either directly affect the methyl group metabolism or result in deficiencies of nutritional cofactors (i.e., vitamins and zinc) that aid in the remethylation and transsulfuration of Hcy.

Association with PCOS

Several research studies have examined the implications of concomitant hyperandrogenism, hyperinsulinemia, and obesity on the increased prevalence of cardiovascular disease indicators. Early research by Talbott et al., reported that women with PCOS exhibited significantly higher total cholesterol, fasting low-density lipoprotein (LDL) levels, insulin, and BMI, combined with decreased total high-density lipoprotein (HDL) (170). While the cause-and-effect between HHcy and cardiovascular disease has not been elucidated (171), it is widely respected for its robustness as a risk factor for cardiovascular disease (172,173). Given the comorbidities in patients with PCOS, foundational research by Talbott and others (170) has led to the emergence of association-based clinical studies examining the link between PCOS and HHcy (174–177).

Upwards of 80% of women with PCOS present clinical hyperinsulinemia (178), and it is not exclusive to patients with obesity (179). Given this high prevalence of hyperinsulinemia, several research studies have reported increased risk of HHcy (179–181). These results have been corroborated by Sen et al., wherein they determined IR was a strong predictor of elevated homocysteine concentrations in adolescents with PCOS (182). Similar findings have been reported on numerous occasions among varying demographics (175,176). Interestingly, these results may be a consequence of the multifactorial conditions of PCOS, rather than

hyperandrogenism alone. A study examining the relationship between HHcy and disease, assessed patients with PCOS and women with congenital adrenal hyperplasia (183). Results from this observational study reported elevated Hcy concentrations in PCOS patients, but not in patients with congenital adrenal hyperplasia; additionally, this association with HHcy was positively explained by the presence of IR in 70% of the PCOS cohort (183). Chakraborty et al., did a study examining the hypothesis of HHcy and IR-mediated frequent pregnancy loss. Their retrospective study examining 126 women with PCOS, determined that the frequency of miscarriages was markedly higher among the HHcy-PCOS study population (71%) than those with normal Hcy levels (29%) (184). Additional studies have corroborated these findings, as a study examining the Hcy concentrations in follicular fluid of 52 women with PCOS seeking reproductive assistance, determined a negative correlation between both follicular Hcy and B_{12} concentrations with rate of successful fertilization (185).

In contrast to these studies presenting the positive correlation between IR and HHcy in cases of PCOS, a more recent meta-analysis collating results from 34 studies determined no significant effect between HHcy and IR (175). This unmarked relationship was also reported in a study enrolling young women with and without PCOS, whereby multiple regression analysis concluded that IR was not a predictor of Hcy concentrations (186). These conflicting results may be indication of the duration of diagnosis, or population-specific responses to IR and concomitant hyperinsulinemia. Regardless, mechanistic studies suggest that insulin directly mediates CBS enzymatic activity, thereby inhibiting the transsulfuration of Hcy, which may, in part, explain the link between IR and HHcy in PCOS (187–189). In a study exposing hepatocytes to high extracellular insulin concentrations, a 50% reduction in CBS enzymatic activity was reported (188). Research by Ratnam et al., examined the effects of an insulin-dependent animal

model of type 1 diabetes mellitus (T1DM) on primary outcomes of CBS activity and Hcy concentrations (187,190). Results from their study demonstrated that T1DM directly elevated hepatic CBS activity and subsequent, hypomethylation. Upon insulin administration in their T1DM model, these effects were reversed. It is possible that in women with PCOS, the metabolic consequences of hyperinsulinemia (independent of diabetes) results in this diminished CBS activity, manifesting in HHcy. To date, no mechanistic studies have reported a molecular basis for HHcy in lean and obese women with PCOS.

Nutrition, Homocysteine, and PCOS

The literature employing nutrition-based strategies to support methyl group metabolism in PCOS are scant, but observational studies examining the impact of nutrient supplementation or deprivation on HHcy in PCOS do exist in the literature. The compilation of these studies are important to take note of when proposing nutrient interventions based on the PCOS animal models described in Table 2-1. Most studies that yielded positive correction of serum total Hcy concentrations, were studies implementing a high dose of folic acid (1-5 mg/d) for greater than 8 consecutive weeks (191–193). This is even exemplified when patients are co-treated with subsequent medications. For instance, a randomized double-blind trial in PCOS patients on metformin treatment, were either supplemented with (n = 25) or without (n = 25) folic acid for 6 months (194). Findings from Palomba et al., reported a significant improvement in Hcy concentrations as a result from folic acid supplementation when compared to the placebo group (194). Albeit few, there are studies examining the effects of micronutrients that support methyl group metabolism in clinical populations of middle-aged women with PCOS. Moreover, it is evident from this literature search that nutrition-based strategies to address PCOS, particular in the United States, are limited. The main studies employed include supplementation with folic acid. Results from these trials in women with PCOS are presented in Table 2-2.

Table 2-2. Human studies identifying the clinical implications of polycystic ovary syndrome on circulating homocysteine concentrations and the role of diet and supplementation of methyl group-donors on clinical outcomes.

Reference	Population	Study Design	Dose	Impact of PCOS on methyl group metabolism	Subsequent Major Outcomes
Kazerooni et al., 2008 (Iran) (191)	Women w/ PCOS (n = 210); PCOS + HHcy (n = 70); and PCOS + HHcy + IR (n = 32).	PCOS + HHcy +IR (n = 32); PCOS + HHcy (n = 38). Parallel design for 3 months. Baseline Hcy and insulin measured	1 mg folic acid / day	- ↓ 11% in Hcy in PCOS + HHcy + IR - ↓ 37% in Hcy in PCOS + HHcy	- N/A
Asemi et al., 2014 (Iran) (192) and Bahmani et al., 2014 (Iran) (193)	Women w/ PCOS (18-40 yr of age; n = 81).	RCT, double-blind placebo controlled; low folate (n = 27); high folate (n = 27); placebo (n = 27). 8 wk intervention.	Low folic acid (1 mg/day); high folic acid (5 mg/day); and placebo.	- High folic acid vs. low folic acid and placebo = ↓ plasma Hcy	- High folic acid vs. low folic acid and placebo = ↓ HOMA-IR, ↓ total cholesterol,↓ CRP, ↓ MDA, and ↑ GSH.
Gaskins et al., 2012 (United States) (195)	Women (n = 259) 18-44 years of age; PCOS	Cross-sectional observational study to examine folate intake on PCOS-related anomalies	N/A	- High folate intake associated with ↑ progesterone, ↓ anovulation.	- N/A
Schiuma et al., 2020 (Italy) (196)	PCOS women 18+ years of age	Parallel, open label control vs. treatment group.	Treatment = 2:1 ratio of treatment with micronutrient supplementation (Impryl)	- ↓ AMH - ↓ SHBG - ↑ Testosterone - ↑ Hcy	- N/A

Table 2-2. Continued.

Reference	Population	Study Design	Dose	Impact of PCOS on methyl group metabolism	Subsequent Major Outcomes
Esmaeilzadeh et al., 2017 (Iran) (197)	PCOS women (n = 18).	Intervention study, with metformin treatment 2x daily, 6 months.	Metformin (500 mg, 2x/day).	- ↓ serum vitamin B12 - - no change in serum folic acid - ↑ Hcy in PCOS + IR, obesity group	- N/A
Guler et al., 2014 (Turkey) (198)	Women with PCOS (n = 53); healthy controls (n = 33)	Cross-sectional study; evaluating markers of zinc and Hcy status	No treatment	- ↓ serum zinc in PCOS - Zinc significant predictor of PCOS	- ↑ BMI in PCOS - ↑ TG/HDL-cholesterol in PCOS - ↑ Hcy
Stracquadanio et al., 2017 (Italy) (199)	Women with PCOS (n = 100); age 20-35; and 6 month parallel intervention.	PCOS + myo-inositol, gymnemic acid and l-methylfolate (n = 50); or PCOS + myo-insositol + folic acid (n = 50)	Myo-inositol (2 g); gymnemic acid (75 mg); and folic acid (400 µg).	- ↓ Hcy	- ↓ BMI - ↑ cyclicity - ↓ testosterone - ↑ SHBG - ↓ total cholesterol - ↑ HDL - ↓ basal insulin
Carlsen et al., 2007 (Norway) (200)	Women with PCOS; PCOS + infertile (n = 63); and PCOS + pregnant (n = 38).	RCT with intervention for 16 wk. High or medium dose metformin or placebo control	PCOS + infertile = metformin (1,000 mg); PCOS + pregnant (850 mg). All women had multivitamin folic acid and vitamin B12 supplementation	- ↓ serum vitamin B12 with metformin, both groups - ↓ serum folate with metformin, both groups - ↑ Hcy, in infertile women	- N/A

Table 2-2. Continued.

Reference	Population	Study Design	Dose	Impact of PCOS on methyl group metabolism	Subsequent Major Outcomes
Palomba et al., 2010 (Italy) (194)	Women with PCOS (n = 50), absent of metabolic or cardiovascular disease.	Prospective, nonrandomized, double-blind study. Metformin + folic acid (n = 25) or metformin + placebo (n = 25).	Metformin (1,700 mg); folic acid (400 µg) consumed daily for 6 months.	- ↑ Hcy, in metformin + placebo group - ↓ Hcy, in folic acid treatment group	- ↓ LDL cholesterol, both groups - ↓ testosterone, both groups - ↑ SHBG, both groups - ↓ fasting insulin, both groups
Kilicdag et al., 2005 (Turkey) (201)	PCOS patients (n = 60).	RCT with 3 treatment groups: 1) metformin 2x daily; 2) metformin + B-vitamins 2x daily; and 3) metformin + folic acid	Metformin (850 mg), B-vitamins (thiamin, 250 mg; B6, 250 mg; and B12, 1 mg), and folic acid (174 µg).	- ↑ 27% Hcy, in metformin only - ↓ 21% Hcy, metformin + B-vitamins - ↓ 8% Hcy, metformin + folic acid	↑ 2-fold serum B12, in metformin + B-vitamins

AMH, ; BMI, body mass index; CRP, c-reactive protein; GSH, glutathione; IR, insulin resistance; Hcy, homocysteine; HDL, high density lipoprotein; HOMA-IR, homeostatic model assessment of insulin resistance; HHcy, hyperhomocysteinemia; MDA, malondialdehyde; PCOS, polycystic ovary syndrome; RCT, randomized control trial; SHBG, sex hormone binding globulin; and TG, triglycerides.

Summary

Polycystic ovary syndrome is a complex condition with many underlying complications that affect both metabolic and reproductive outcomes. Many researchers mark PCOS as the metabolic syndrome of reproductive-aged women, but this review highlights the lines of evidence that propose a wide array of alternative complications and exposures. Despite the hallmarks of PCOS, (i.e., hyperandrogenism, hirsutism, infertility), this review provides insight into some of the observed associations that may be critical for elucidating the mechanisms involved in the pathogenesis of disease. Several animal models of PCOS exist, however research is scant in examining the outcomes of methyl group metabolism during progressive PCOS. Therefore, the premise of the studies described in the central chapters of my dissertation aim to discern these methyl group metabolism anomalies in a non-metabolically perturbed model of PCOS, and a more classic PCOS model accompanied by obesity and IR. Our studies were hypothesized on the basis of this gap in research identifying the relationship between dysfunctional methyl group metabolism and PCOS. These findings have not been reported elsewhere, and they lay the foundation for extensive research employing nutrition-based strategies that address the potential methyl group imbalance. This literature review exposes the lack of knowledge identifying the impact of methyl group-related micronutrients on reproductive, metabolic, or a combination of these outcomes in prepubescent and middle-aged models of PCOS.

References

1. Wolf WM, Wattick RA, Kinkade ON, Olfert MD. Geographical Prevalence of Polycystic Ovary Syndrome as Determined by Region and Race/Ethnicity. *Int J Environ Res Public Health*. 2018; 15.

2. Ibáñez L, Oberfield SE, Witchel S, Auchus RJ, Chang RJ, Codner E, Dabadghao P, Darendeliler F, Elbarbary NS, Gambineri A, et al. An International Consortium Update: Pathophysiology, Diagnosis, and Treatment of Polycystic Ovarian Syndrome in Adolescence. *Horm Res Paediatr*. 2017; 88:371–95.

3. Caldwell ASL, Middleton LJ, Jimenez M, Desai R, McMahon AC, Allan CM, Handelsman DJ, Walters KA. Characterization of reproductive, metabolic, and endocrine features of polycystic ovary syndrome in female hyperandrogenic mouse models. *Endocrinology*. 2014; .

4. Christensen SB, Black MH, Smith N, Martinez MM, Jacobsen SJ, Porter AH, Koebnick C. Prevalence of polycystic ovary syndrome in adolescents. *Fertil Steril*. 2013; 100:470–7.

5. Kong L, Tang M, Zhang T, Wang D, Hu K, Lu W, Wei C, Liang G, Pu Y. Nickel Nanoparticles Exposure and Reproductive Toxicity in Healthy Adult Rats. *Int J Mol Sci*. 2014; 15:21253–69.

6. Baskind NE, Balen AH. Hypothalamic–pituitary, ovarian and adrenal contributions to polycystic ovary syndrome. *Best Pract Res Clin Obstet Gynaecol*. 2016; 37:80–97.

7. Barnes RB, Rosenfield RL, Namnoum A, Layman LC. Effect of follicle-stimulating hormone on ovarian androgen production in a woman with isolated follicle-stimulating hormone deficiency. *N Engl J Med*. 2000; 1197–8.

8. Rosenfield RL, Ehrmann DA. The Pathogenesis of Polycystic Ovary Syndrome (PCOS): The Hypothesis of PCOS as Functional Ovarian Hyperandrogenism Revisited. *Endocr Rev*. 2016; 37:467–520.

9. Messinisi IE. Ovarian feedback, mechanism of action and possible clinical implications. *Hum Reprod Update*. 2006; 12:557–71.

10. Williams T. Diagnosis and Treatment of Polycystic Ovary Syndrome. *Am Fam Physician.* 2016.

11. Jahanfar S, Eden JA, Nguyen T, Wang XL, Wilcken DEL. A twin study of polycystic ovary syndrome and lipids. *Gynecol Endocrinol*. 1997; 11:111–7.

12. Prapas N, Karkanaki A, Prapas I, Kalogiannidis I, Katsikis I, Panidis D. Genetics of polycystic ovary syndrome. *Hippokratia*. 2009; 216–23.

13. Tsutsumi R, Webster NJG. GnRH pulsatility, the pituitary response and reproductive dysfunction. *Endocr J.* 2009; 729–37.

14. Dewailly D, Robin G, Peigne M, Decanter C, Pigny P, Catteau-Jonard S. Interactions between androgens, FSH, anti-Mullerian hormone and estradiol during folliculogenesis in the human normal and polycystic ovary. *Hum Reprod Update*. 2016; 22:709–24.

15. Goodman NF, Cobin RH, Futterweit W, Glueck JS, Legro RS, Carmina E. American association of clinical endocrinologists, American college of endocrinology, and androgen excess and pcos society disease state clinical review: Guide to the best practices in the evaluation and treatment of polycystic ovary syndrome - Part 1. Endocrine Practice. *Am Assoc Clin Endocrinol*. 2015. p. 1291–300.

16. Dulka EA, Burger LL, Moenter SM. Ovarian androgens maintain high GnRH neuron firing rate in adult prenatally-androgenized female mice. *Endocrinol.* 2020; 161.

17. Pastor CL, Griffin-Korf ML, Aloi JA, Evans WS, Marshall JC. Polycystic Ovary Syndrome: Evidence for Reduced Sensitivity of the Gonadotropin-Releasing Hormone Pulse Generator to Inhibition by Estradiol and Progesterone [1]. *J Clin Endocrinol Metab*. 1998; 83:582–90.

18. Zhou Y, Zhang A, Gong M, Lu Y, Zhao C, Shen X, Zhang X, Wang L, Chen J, Ju R. Maternal Testosterone Excess Contributes to Reproductive System Dysfunction of Female Offspring Mice. *Endocrinol*. 2020; 161.

19. Carlsen SM, Jacobsen G, Romundstad P. Maternal testosterone levels during pregnancy are associated with offspring size at birth. *Eur J Endocrinol*. 2006; 155:365–70.

20. Wang Z, Shen M, Xue P, Divall SA, Segars J, Wu S. Female Offspring from Chronic Hyperandrogenemic Dams Exhibit Delayed Puberty and Impaired Ovarian Reserve. *Endocrinol.* 2018; 159:1242–52.

21. Abbott DH, Barnett DK, Levine JE, Padmanabhan V, Dumesic DA, Jacoris S, Tarantal AF. Endocrine antecedents of polycystic ovary syndrome in fetal and infant prenatally androgenized female rhesus monkeys. *Biol Reprod*. 2008; 79:154–63.

22. Belani M, Deo A, Shah P, Banker M, Singal P, Gupta S. Differential insulin and steroidogenic signaling in insulin resistant and non-insulin resistant human luteinized granulosa cells—A study in PCOS patients. *J Steroid Biochem Mol Biol*. 2018; 178:283-292.

23. Nestler JE. Insulin regulation of human ovarian androgens. *Hum Reprod*. 1997; 53–62.

24. Baptiste CG, Battista MC, Trottier A, Baillargeon JP. Insulin and hyperandrogenism in women with polycystic ovary syndrome. *J Steroid Biochem Mol Bio*. 2010; 42–52.

25. Petersen MC, Shulman GI. Mechanisms of insulin action and insulin resistance. *Physiol Rev*. 2018; 2133–223.

26. Wang F, Wang S, Zhang Z, Lin Q, Liu Y, Xiao Y, Xiao K, Wang Z. Defective insulin signaling and the protective effects of dimethyldiguanide during follicular development in the ovaries of polycystic ovary syndrome. *Mol Med Rep*. 2017; 16:8164–70.

27. Dupont J, Scaramuzzi RJ. Insulin signalling and glucose transport in the ovary and ovarian function during the ovarian cycle . *Biochem J.* 2016; 1483–501.

28. Poretsky L, Cataldo NA, Rosenwaks Z, Giudice LC. The insulin-related ovarian regulatory system in health and disease. *Endocrin Rev.*1999; 535–82.

29. Teng JA, Wu SG, Chen JX, Li Q, Peng F, Zhu Z, Qin J, He ZY. The activation of ERK1/2 and JNK MAPK signaling by Insulin/IGF-1 is responsible for the development of colon cancer with type 2 diabetes mellitus. *PLoS One*. *Public Library of Science*. 2016; 11.

30. Liang QX, Wang ZB, Lin F, Zhang CH, Sun HM, Zhou L, Zhou Q, Schatten H, Odile FC, Brigitte B, et al. Ablation of beta subunit of protein kinase CK2 in mouse oocytes causes follicle atresia and premature ovarian failure article. *Cell Death Dis*. 2018; 9.

31. Nteeba J, Ross JW, Perfield II JW, Keating AF. High fat diet induced obesity alters ovarian phosphatidylinositol-3 kinase signaling gene expression. *Reprod Toxicol*. 2013; 42:68–77.

32. Zheng W, Nagaraju G, Liu Z, Liu K. Functional roles of the phosphatidylinositol 3-kinases (PI3Ks) signaling in the mammalian ovary. *Mol Cell Endocrinol*. 2012; 24–30.

33. Liu K, Rajareddy S, Liu L, Jagarlamudi K, Boman K, Selstam G, Reddy P. Control of mammalian oocyte growth and early follicular development by the oocyte PI3 kinase pathway: New roles for an old timer. *Dev Biol.* 2006; 1–11.

34. Kajaia N, Binder H, Dittrich R, Oppelt PG, Flor B, Cupisti S, Beckmann MW, Mueller A. Low sex hormone-binding globulin as a predictive marker for insulin resistance in women with hyperandrogenic syndrome. *Eur J Endocrinol*. *2*007; 157:499–507.

35. Daka B, Rosen T, Jansson PA, Råstam L, Larsson CA, Lindblad U. Inverse association between serum insulin and sex hormone-binding globulin in a population survey in Sweden. *Endocr Connect*. 2012; 2:18–22.

36. Le TN, Nestler JE, Strauss JF, Wickham EP. Sex hormone-binding globulin and type 2 diabetes mellitus. *Trends Endocrinol Metab*. 2012; 32–40.

37. Alinezhad A, Jafari F. The relationship between Components of Metabolic Syndrome and Plasma Level of Sex Hormone-Binding Globulin. *Eur J Transl Myol*. 2019; 29:143–50.

38. Nestler Je, Barlascini Co, Matt Dw, Steingold Ka, Plymate Sr, Clore Jn, Blackard Wg. Suppression of Serum Insulin by Diazoxide Reduces Serum Testosterone Levels in Obese Women with Polycystic Ovary Syndrome*. *J Clin Endocrinol Metab*. 1989; 68:1027–32.

39. Nestler JE, Jakubowicz DJ. Lean Women with Polycystic Ovary Syndrome Respond to Insulin Reduction with Decreases in Ovarian P450c17α Activity and Serum Androgens [1]. *J Clin Endocrinol Metab*. 1997; 82:4075–9.

40. Deswal R, Yadav A, Dang AS. Sex hormone binding globulin - an important biomarker for predicting PCOS risk: A systematic review and meta-analysis. *Syst Biol Reprod Med*. 2018; 64:12–24.

41. Teede H, Deeks A, Moran L. Polycystic ovary syndrome: A complex condition with psychological, reproductive and metabolic manifestations that impacts on health across the lifespan. *BMC Med*. 2010; 1–10.

42. Goodarzi MO, Dumesic DA, Chazenbalk G, Azziz R. Polycystic ovary syndrome: Etiology, pathogenesis and diagnosis. *Nature Rev Endocrinol*. 2011; 219–31.

43. Petraglia F, Fauser BC, editors. Female Reproductive Dysfunction. *Cham* 2020.

44. Bremer AA. Polycystic ovary syndrome in the pediatric population . Metabolic Syndrome and Related Disorders. *Mary Ann Liebert, Inc.* 2010; 375–94.

45. Douglas CC, Gower BA, Darnell BE, Ovalle F, Oster RA, Azziz R. Role of diet in the treatment of polycystic ovary syndrome. *Fertil Steril*. 2006; 85:679–88.

46. Barrea L, Arnone A, Annunziata G, Muscogiuri G, Laudisio D, Salzano C, Pugliese G, Colao A, Savastano S. Adherence to the mediterranean diet, dietary patterns and body composition in women with polycystic ovary syndrome (PCOS). *Nutrients*. 2019; 11.

47. Soares NP, Santos ACS Dos, Costa EC, Azevedo GD, Damasceno DC, Fayh APT, Lemos TMAM. Diet-Induced Weight Loss Reduces DNA Damage and Cardiometabolic Risk Factors in Overweight/Obese Women with Polycystic Ovary Syndrome. *Ann Nutr Metab*. 2016; 68:220–7.

48. Zubrzycki A, Cierpka-Kmiec K, Kmiec Z, Wronska A. The role of low-calorie diets and intermittent fasting in the treatment of obesity and type-2 diabetes . Journal of Physiology and Pharmacology. *Polish Physiological Society*. 2018; 663–83.

49. Mirabelli M, Chiefari E, Arcidiacono B, Corigliano DM, Brunetti FS, Maggisano V, Russo D, Foti DP, Brunetti A. Mediterranean diet nutrients to turn the tide against insulin resistance and related diseases. *Nutrients*. 2020.

50. Ujvari D, Hulchiy M, Calaby A, Nybacka A, Byström B, Hirschberg AL. Lifestyle intervention up-regulates gene and protein levels of molecules involved in insulin signaling in the endometrium of overweight/obese women with polycystic ovary syndrome. *Hum Reprod*. 2014; 29:1526–35.

51. Zhang X, Zheng Y, Guo Y, Lai Z. The Effect of Low Carbohydrate Diet on Polycystic Ovary Syndrome: A Meta-Analysis of Randomized Controlled Trials. *Int J Endocrinol*. 2019; 4386401.

52. Qublan H, Yannakoula EK, Al-Qudah MA, El-Uri FI. Dietary intervention versus metformin to improve the reproductive outcome in women with polycystic ovary syndrome. A prospective comparative study. *Saudi Med J.* 2007; 11:1694-9.

53. Pernicova I, Korbonits M. Metformin—mode of action and clinical implications for diabetes and cancer. *Nat Rev Endocrinol*. 2014; 10:143–56.

54. Fleming R. The use of insulin sensitising agents in ovulation induction in women with polycystic ovary syndrome. *Hormones (Athens)*. 2006; 171–8.

55. Froment P, Touraine P. Thiazolidinediones and fertility in polycystic ovary syndrome (PCOS). *PPAR Res*. 2006; 73986.

56. Azziz R, Ehrmann D, Legro RS, Whitcomb RW, Hanley R, Fereshetian AG, O'Keefe M, Ghazzi MN. Troglitazone Improves Ovulation and Hirsutism in the Polycystic Ovary Syndrome: A Multicenter, Double Blind, Placebo-Controlled Trial 1 . *J Clin Endocrinol Metab*. 2001; 86:1626–32.

57. Tso LO, Costello MF, Albuquerque LET, Andriolo RB, Macedo CR. Metformin treatment before and during IVF or ICSI in women with polycystic ovary syndrome. *Cochrane Database Syst Rev*. 2014.

58. Esmaeilzadeh S, Gholinezhad-Chari M, Ghadimi R. The effect of metformin treatment on the serum levels of homocysteine, folic acid, and vitamin B12 in patients with polycystic ovary syndrome. *J Hum Reprod Sci*. 2017; 10:95.

59. De Jager J, Kooy A, Lehert P, Wulffelé MG, Van Der Kolk J, Bets D, Verburg J, Donker AJM, Stehouwer CDA. Long term treatment with metformin in patients with type 2 diabetes and risk of vitamin B-12 deficiency: Randomised placebo controlled trial. *BMJ*. 2010; 340:1177.

60. Bailey CJ. Thiazolidinediones. *Elsevier Inc.* 2007; 1–2.

61. Orio F, Muscogiuri G, Giallauria F, Savastano S, Bottiglieri P, Tafuri D, Predotti P, Colarieti G, Colao A, Palomba S. Oral contraceptives *versus* physical exercise on cardiovascular and metabolic risk factors in women with polycystic ovary syndrome: a randomized controlled trial. *Clin Endocrinol (Oxf)*. 2016; 85:764–71.

62. Manzoor S, Ganie MA, Amin S, Shah ZA, Bhat IA, Yousuf SD, Jeelani H, Kawa IA, Fatima Q, Rashid F. Oral contraceptive use increases risk of inflammatory and coagulatory disorders in women with Polycystic Ovarian Syndrome: An observational study. *Sci Rep*. 2019; 9:1–8.

63. Corvol P, Michaud A, Menard J, Freifeld M, Mahoudeau J. Antiandrogenic effect of spirolactones: mechanism of action. *Endocrinology*. 1975; 97:52–8.

64. Ganie MA, Khurana ML, Eunice M, Gulati M, Dwivedi SN, Ammini AC. Comparison of Efficacy of Spironolactone with Metformin in the Management of Polycystic Ovary Syndrome: An Open-Labeled Study. *J Clin Endocrinol Metab*. 2004; 89:2756–62.

65. Osuka S, Nakanishi N, Murase T, Nakamura T, Goto M, Iwase A, Kikkawa F. Animal models of polycystic ovary syndrome: A review of hormone□induced rodent models focused on hypothalamus□pituitary□ovary axis and neuropeptides. *Reprod Med Biol*. 2019; 18:151–60.

66. Webb SJ, Geoghegan TE, Prough RA, Miller KKM. The biological actions of dehydroepiandrosterone involves multiple receptors. *Drug Metabol Rev.* 2006; 89–116.

67. Zhang F, Ma T, Cui P, Tamadon A, He S, Huo C, Yierfulati G, Xu X, Hu W, Li X, et al. Diversity of the gut microbiota in dihydrotestosterone-induced PCOS rats and the pharmacologic effects of diane-35, probiotics, and berberine. *Front Microbiol*. 2019; 10.

68. Li SY, Song Z, Song MJ, Qin JW, Zhao ML, Yang ZM. Impaired receptivity and decidualization in DHEA-induced PCOS mice. *Sci Rep*. 2016; 6.

69. Çelik LS, Kuyucu Y, Yenilmez ED, Tuli A, Dağlıoğlu K, Mete UÖ. Effects of vitamin D on ovary in DHEA-treated PCOS rat model: A light and electron microscopic study. *Ultrastruct Pathol*. 2018; 42:55–64.

70. Hunter MH, Sterrett JJ. Polycystic Ovarian Syndrome: It's Not Just Infertility. *Am Fam Physician*. 2000; 62:1079–88.

71. Benrick A, Chanclón B, Micallef P, Wu Y, Hadi L, Shelton JM, Stener-Victorin E, Asterholm IW. Adiponectin protects against development of metabolic disturbances in a PCOS mouse model. *Proc Natl Acad* Sci. 2017; 114:E7187–96.

72. Leonie E, Van Houten AF, Kramer P, McLuskey A, Karels B, Themmen APN, Visser JA. Reproductive and metabolic phenotype of a mouse model of PCOS. *Endocrinology*. 2012; 153:2861–9.

73. Mannerås L, Cajander S, Holmäng A, Seleskovic Z, Lystig T, Lönn M, Stener-Victorin E. A new rat model exhibiting both ovarian and metabolic characteristics of polycystic ovary syndrome. *Endocrinology*. 2007; 148:3781–91.

74. Caldwell ASL, Middleton LJ, Jimenez M, Desai R, McMahon AC, Allan CM, Handelsman DJ, Walters KA. Characterization of reproductive, metabolic, and endocrine features of polycystic ovary syndrome in female hyperandrogenic mouse models. *Endocrinology*. 2014; 155:3146–59.

75. Shi D, Vine DF. Animal models of polycystic ovary syndrome: a focused review of rodent models in relationship to clinical phenotypes and cardiometabolic risk. *Fertil Steril*. 2012; 98:185-193.e2.

76. Stocco C. Tissue physiology and pathology of aromatase. *Steroids*. 2012; 27–35.

77. Torres PJ, Skarra D V., Ho BS, Sau L, Anvar AR, Kelley ST, Thackray VG. Letrozole treatment of adult female mice results in a similar reproductive phenotype but distinct changes in metabolism and the gut microbiome compared to pubertal mice. *BMC Microbiol*. 2019; 19:57.

78. Zhang HL, Yi M, Li D, Li R, Zhao Y, Qiao J. Transgenerational Inheritance of Reproductive and Metabolic Phenotypes in PCOS Rats. *Front* Endocrinol. 2020; 11:144.

79. Ryu Y, Kim SW, Kim YY, Ku SY. Animal models for human polycystic ovary syndrome (PCOS) focused on the use of indirect hormonal perturbations: A review of the literature. *Intern J Mol Sci*. 2019.

80. Li MG, Ding GL, Chen XJ, Lu XP, Dong LJ, Dong MY, Yang XF, Lu XE, Huang HF. Association of serum and follicular fluid leptin concentrations with granulosa cell phosphorylated signal transducer and activator of transcription 3 expression in fertile patients with polycystic ovarian syndrome. *J Clin Endocrinol Metab*. 2007; 92:4771–6.

81. Cone RD. Anatomy and regulation of the central melanocortin system. *Nat Neurosci*. 2005; 571–8.

82. Sohn JW. Network of hypothalamic neurons that control appetite. *BMB Reports*. 2015; 229–33.

83. Saande CJ, Webb JL, Curry PE, Rowling MJ, Schalinske KL. Dietary Whole Egg Reduces Body Weight Gain in a Dose-Dependent Manner in Zucker Diabetic Fatty Rats. *J Nutr*. 2019; 149:1766–75.

84. Saande CJ, Jones SK, Hahn KE, Reed CH, Rowling MJ, Schalinske KL. Dietary Whole Egg Consumption Attenuates Body Weight Gain and Is More Effective than Supplemental Cholecalciferol in Maintaining Vitamin D Balance in Type 2 Diabetic Rats. *J Nutr*. 2017; 147:jn254193.

85. Roa J, Herbison AE. Direct regulation of GnRH neuron excitability by arcuate nucleus POMC and NPY neuron neuropeptides in female mice. *Endocrinology*. 2012; 153:5587–99.

86. Yokoi N, Hoshino M, Hidaka S, Yoshida E, Beppu M, Hoshikawa R, Sudo K, Kawada A, Takagi S, Seino S. A novel rat model of type 2 diabetes: The zucker fatty diabetes mellitus ZFDM rat. *J Diabetes Res*. 2013.

87. Honnma H, Endo T, Kiya T, Shimizu A, Nagasawa K, Baba T, Fujimoto T, Henmi H, Kitajima Y, Manase K, et al. Remarkable features of ovarian morphology and reproductive hormones in insulin-resistant Zucker fatty (fa/fa) rats. *Reprod Biol Endocrinol*. 2010; 8:73.

88. Daghestani MH, Daghestani MH, Daghistani MH, Bjørklund G, Chirumbolo S, Warsy A. The influence of the rs1137101 genotypes of leptin receptor gene on the demographic and metabolic profile of normal Saudi females and those suffering from polycystic ovarian syndrome. *BMC Womens Health*. 2019; 19.

89. Gregoraszczuk EL, Rak-Mardyla A. Supraphysiological leptin levels shift the profile of steroidogenesis in porcine ovarian follicles toward progesterone and testosterone secretion through increased expressions of CYP11A1 and 17β-HSD: A tissue culture approach. *Reproduction*. 2013; 145:311–7.

90. Barash IA, Cheung CC, Weigle DS, Ren H, Kabigting EB, Kuijper JL, Clifton DK, Steiner RA. Leptin is a metabolic signal to the reproductive system. *Endocrinology*. 1996; 137:3144–7.

91. Hamm ML, Bhat GK, Thompson WE, Mann DR. Folliculogenesis is impaired and granulosa cell apoptosis is increased in leptin-deficient mice. *Biol Reprod*. 2004; 71:66–72.

92. Garris DR, Williams SK, West L. Morphometric evaluation of diabetes□associated ovarian atrophy in the C57BL/KsJ mouse: Relationship to age and ovarian function. *Anat Rec*. 1985; 211:434–43.

93. Hill JW, Elias CF, Fukuda M, Williams KW, Berglund ED, Holland WL, Cho YR, Chuang JC, Xu Y, Choi M, et al. Direct Insulin and Leptin Action on Pro-opiomelanocortin Neurons Is Required for Normal Glucose Homeostasis and Fertility. *Cell Metab*. 2010; 11:286–97.

94. Nteeba J, Ganesan S, Keating AF. Progressive Obesity Alters Ovarian Folliculogenesis with Impacts on Pro-Inflammatory and Steroidogenic Signaling in Female Mice1. *Biol Reprod*. 2014; 91:86.

95. Brannian JD, Eyster KM, Weaber M, Diggins M. Pioglitazone administration alters ovarian gene expression in aging obese lethal yellow mice. *Reprod Biol Endocrinol*. 2008; 6.

96. Granholm NH, Dickens GA. Effects of reciprocal ovary transplantation on reproductive performance of lethal yellow mice (A(y)/a; C57BL/6J). *J Reprod Fertil*. 1986; 78:749–53.

97. Dolinoy DC. The agouti mouse model: An epigenetic biosensor for nutritional and environmental alterations on the fetal epigenome. *NIH Public Access*. 2008; S7.

98. Roa J. Role of GnRH neurons and their neuronal afferents as key integrators between food intake regulatory signals and the control of reproduction. *Int J Endocrinol*. 2013.

99. Sandrock M, Schulz A, Merkwitz C, Schöneberg T, Spanel-Borowski K, Ricken A. Reduction in corpora lutea number in obese melanocortin-4-receptor-deficient mice. *Reprod Biol Endocrinol*. 2009; 7.

100. Finkelstein JD. Pathways and regulation of homocysteine metabolism in mammals. *Semin Thromb Hemost.* 2000; 219–25.

101. Friso S, Udali S, De Santis D, Choi SW. One-carbon metabolism and epigenetics. *Mol Aspects Med*. 2017; 28–36.

102. Williams KT, Schalinske KL. New insights into the regulation of methyl group and homocysteine metabolism. *J Nutr*. 2007; 137:311–4.

103. Jin B, Li Y, Robertson KD. DNA methylation: Superior or subordinate in the epigenetic hierarchy? *Genes and Cancer*. 2011; 607–17.

104. Das JK, Salam RA, Kumar R, Bhutta ZA. Micronutrient fortification of food and its impact on woman and child health: a systematic review. *Syst Rev*. 2013; 2:67.

105. Updated Estimates of Neural Tube Defects Prevented by Mandatory Folic Acid Fortification — United States, 1995–2011 .

106. MacFarlane AJ, Liu X, Perry CA, Flodby P, Allen RH, Stabler SP, Stover PJ. Cytoplasmic serine hydroxymethyltransferase regulates the metabolic partitioning of methylenetetrahydrofolate but is not essential in mice. *J Biol Chem*. 2008; 283:25846–53.

107. Rose MG, Farrell MP, Schmitz JC. Thymidylate synthase: A critical target for cancer chemotherapy. *Clin Colorec Cancer*. 2002; 220–9.

108. Takemura Y, Jackman AL. Folate-based thymidylate synthase inhibitors in cancer chemotherapy. *Anticancer Drugs*. 1997; 3–16.

109. Pawlak R, Lester SE, Babatunde T. The prevalence of cobalamin deficiency among vegetarians assessed by serum vitamin B12: A review of literature. *Euro J Clin Nutr*. 2014; 541–8.

110. Stover PJ. Vitamin B12 and older adults. *Curr Opin Clin Nutr Metab Care*. 2010; 24–7.

111. Carmel R. Nutritional Anemias and the Elderly. *Semin Hematol*. 2008; 45:225–34.

112. Maggini S, Pierre A, Calder PC. Immune function and micronutrient requirements change over the life course. *Nutrients*. 2018.

113. Qian B, Shen S, Zhang J, Jing P. Effects of Vitamin B6 Deficiency on the Composition and Functional Potential of T Cell Populations. *J Immunol Res*. 2017.

114. Saeed F, Nadeem M, Ahmed RS, Tahir Nadeem M, Arshad MS, Ullah A. Studying the impact of nutritional immunology underlying the modulation of immune responses by nutritional compounds – a review. *Food Agric Immunol*. 2016; 27:205–29.

115. Wallwork JC, Duerre JA. Effect of zinc deficiency on methionine metabolism, methylation reactions and protein synthesis in isolated perfused rat liver. *J Nutr*. 1985; 115:252–62.

116. Millian NS, Garrow TA. Human betaine-homocysteine methyltransferase is a zinc metalloenzyme. *Arch Biochem Biophys*. 1998; 356:93–8.

117. Benkhalifa M, Montjean D, Cohen-Bacrie P, Ménézo Y. Imprinting: RNA expression for homocysteine recycling in the human oocyte. *Fertil Steril*. 2010; 93:1585–90.

118. Tian X, Diaz FJ. Acute dietary zinc deficiency before conception compromises oocyte epigenetic programming and disrupts embryonic development. *Dev Biol*. 2013; 376:51–61.

119. Ebisch IMW, Peters WHM, Thomas CMG, Wetzels AMM, Peer PGM, Steegers-Theunissen RPM. Homocysteine, glutathione and related thiols affect fertility parameters in the (sub)fertile couple. *Hum Reprod*. 2006; 21:1725–33.

120. Zhang D, Hong X, Wang J, Jiang Y, Zhang Y, Chen J, Niu X. Estradiol□17β inhibits homocysteine mediated damage by promoting H_2S production via upregulating CBS and CSE expression in human umbilical vein endothelial cells. *J Cell Biochem*. 2019; :jcb.29527.

121. Shah S, Bell RJ, Davis SR. Homocysteine, estrogen and cognitive decline. *Climacteric*. 2006; 77–87.

122. Resseguie ME, Da Costa KA, Galanko JA, Patel M, Davis IJ, Zeisel SH. Aberrant estrogen regulation of PEMT results in choline deficiency-associated liver dysfunction. *J Biol Chem*. 2011; 286:1649–58.

123. Zhu X, Song J, Mar MH, Edwards LJ, Zeisel SH. Phosphatidylethanolamine N-methyltransferase (PEMT) knockout mice have hepatic steatosis and abnormal hepatic choline metabolite concentrations despite ingesting a recommended dietary intake of choline. *Biochem J*. 2003; 370:987–93.

124. Anderson OS, Sant KE, Dolinoy DC. Nutrition and epigenetics: An interplay of dietary methyl donors, one-carbon metabolism and DNA methylation. *J Nutr Biochem*. 2012; 853–9.

125. Shelnutt KP, Kauwell GPA, Gregory JF, Maneval DR, Quinlivan EP, Theriaque DW, Henderson GN, Bailey LB. Methylenetetrahydrofolate reductase 677C→T polymorphism affects DNA methylation in response to controlled folate intake in young women. *J Nutr Biochem*. 2004; 15:554–60.

126. El-Maarri O, Walier M, Behne F, van Üüm J, Singer H, Diaz-Lacava A, Nüsgen N, Niemann B, Watzka M, Reinsberg J, et al. Methylation at global LINE-1 repeats in human blood are affected by gender but not by age or natural hormone cycles. *PLoS One*. 2011; 6.

127. Newbold RR, Jefferson WN, Padilla-Banks E, Haseman J. Developmental exposure to diethylstilbestrol (DES) alters uterine response to estrogens in prepubescent mice: Low versus high dose effects. *Reprod Toxicol*. 2004; 18:399–406.

128. Pan J-X, Tan Y-J, Wang F-F, Hou N-N, Xiang Y-Q, Zhang J-Y, Liu Y, Qu F, Meng Q, Xu J, et al. Aberrant expression and DNA methylation of lipid metabolism genes in PCOS: a new insight into its pathogenesis. *Clin Epigenetics*. 2018; 10:6.

129. Sagvekar P, Kumar P, Mangoli V, Desai S, Mukherjee S. DNA methylome profiling of granulosa cells reveals altered methylation in genes regulating vital ovarian functions in polycystic ovary syndrome. *Clin Epigenetics*. 2019; 11:61.

130. Li S, Zhu D, Duan H, Ren A, Glintborg D, Andersen M, Skov V, Thomassen M, Kruse T, Tan Q. Differential DNA methylation patterns of polycystic ovarian syndrome in whole blood of Chinese women. *Oncotarget*. 2017; 8:20656–66.

131. Vázquez-Martínez ER, Gómez-Viais YI, García-Gómez E, Reyes-Mayoral C, Reyes-Muñoz E, Camacho-Arroyo I, Cerbón M. DNA methylation in the pathogenesis of polycystic ovary syndrome. *Reprod.* 2019; R27–40.

132. Zeisel SH. Choline, other methyl-donors and epigenetics. *Nutrients*. 2017.

133. Choi S-W, Claycombe KJ, Martinez JA, Friso S, Schalinske KL. Nutritional Epigenomics: A Portal to Disease Prevention. *Adv Nutr*. 2013; 4:530–2.

134. Sendžikaitė G, Kelsey G. The role and mechanisms of DNA methylation in the oocyte. *Essays Biochem.* 2019; 691–705.

135. Tomizawa SI, Nowacka-Woszuk J, Kelsey G. DNA methylation establishment during oocyte growth: Mechanisms and significance. *Int J Dev Biol*. 2012; 56:867–75.

136. Moore LD, Le T, Fan G. DNA methylation and its basic function. *Neuropsychopharm*. 2013; 23–38.

137. Yu YY, Sun CX, Liu YK, Li Y, Wang L, Zhang W. Genome-wide screen of ovary-specific DNA methylation in polycystic ovary syndrome. *Fertil Steril*. 2015; 104:145-153.e6.

138. Xu N, Azziz R, Goodarzi MO. Epigenetics in polycystic ovary syndrome: a pilot study of global DNA methylation. *Fertil Steril*. 2010; 94:781.

139. Xu J, Bao X, Peng Z, Wang L, Du L, Niu W, Sun Y. Comprehensive analysis of genome-wide DNA methylation across human polycystic ovary syndrome ovary granulosa cell. *Oncotarget*. 2016; 7:27899–909.

140. Echiburú B, Milagro F, Crisosto N, Pérez-Bravo F, Flores C, Arpón A, Salas-Pérez F, Recabarren SE, Sir-Petermann T, Maliqueo M. DNA methylation in promoter regions of genes involved in the reproductive and metabolic function of children born to women with PCOS. *Epigenetics*. 2020; 1-17.

141. Jia L, Zeng Y, Hu Y, Liu J, Yin C, Niu Y, Wang C, Li J, Jia Y, Hong J, et al. Homocysteine impairs porcine oocyte quality via deregulation of one-carbon metabolism and hypermethylation of mitochondrial DNA. *Biol Reprod*. 2019; 100:907–16.

142. Jia L, Li J, He B, Jia Y, Niu Y, Wang C, Zhao R. Abnormally activated one-carbon metabolic pathway is associated with mtDNA hypermethylation and mitochondrial malfunction in the oocytes of polycystic gilt ovaries. *Sci Rep*. 2016; 6.

143. Bhattacharyya S, Saha S, Giri K, Lanza IR, Nair KS, Jennings NB, Rodriguez-Aguayo C, Lopez-Berestein G, Basal E, Weaver AL, et al. Cystathionine Beta-Synthase (CBS) Contributes to Advanced Ovarian Cancer Progression and Drug Resistance. *PLoS One*. 2013; 8.

144. Lei L, Ding L, Su J, Liu M, Shi Q, Zhou J, Sun H, Yan G. Attenuated expression of MTR in both prenatally androgenized mice and women with the hyperandrogenic phenotype of PCOS. *PLoS One*. 2017; 12:e0187427.

145. Tian X, Diaz FJ. Acute dietary zinc deficiency before conception compromises oocyte epigenetic programming and disrupts embryonic development. *Dev Biol*. 2013; 376:51–61.

146. Cui P, Ma T, Tamadon A, Han S, Li B, Chen Z, An X, Shao LR, Wang Y, Feng Y. Hypothalamic DNA methylation in rats with dihydrotestosterone-induced polycystic ovary syndrome: effects of low-frequency electro-acupuncture. *Exp Physiol*. 2018; 103:1618–32.

147. Xu J, Sinclair KD. One-carbon metabolism and epigenetic regulation of embryo development. *Reprod Fertil Dev*. 2015; 667–76.

148. Ge ZJ, Schatten H, Zhang CL, Sun QY. Oocyte ageing and epigenetics. Reprod. 2015; 149:R103–14.

149. Rivera RM, Ross JW. Epigenetics in fertilization and preimplantation embryo development. *Prog Biophys Mol Biol*. 2013; 113:423–32.

150. Lei L, Ding L, Su J, Liu M, Shi Q, Zhou J, Sun H, Yan G. Attenuated expression of MTR in both prenatally androgenized mice and women with the hyperandrogenic phenotype of PCOS. *PLoS One*. 2017; 12.

151. Li D, Liu HX, Fang YY, Huo JN, Wu QJ, Wang TR, Zhou YM, Wang XX, Ma XX. Hyperhomocysteinemia in polycystic ovary syndrome: decreased betaine-homocysteine methyltransferase and cystathionine β-synthase-mediated homocysteine metabolism. *Reprod Biomed Online*. 2018; 37:234–41.

152. Sinclair KD, Allegrucci C, Singh R, Gardner DS, Sebastian S, Bispham J, Thurston A, Huntley JF, Rees WD, Maloney CA, et al. DNA methylation, insulin resistance, and blood pressure in offspring determined by maternal periconceptional B vitamin and methionine status. *Proc Natl Acad Sci U S A*. 2007; 104:19351–6.

153. Jiao J, Sagnelli M, Shi B, Fang Y, Shen Z, Tang T, Dong B, Li D, Wang X. Genetic and epigenetic characteristics in ovarian tissues from polycystic ovary syndrome patients with irregular menstruation resemble those of ovarian cancer. *BMC Endocr Disord*. 2019; 19.

154. Sang Q, Li X, Wang H, Wang H, Zhang S, Feng R, Xu Y, Li Q, Zhao X, Xing Q, et al. Quantitative methylation level of the EPHX1 promoter in peripheral blood DNA is associated with polycystic ovary syndrome. *PLoS One*. 2014; 9.

155. Verhoef P, De Groot LCPGM. Dietary determinants of plasma homocysteine concentrations. *Semin Vasc Med*. 2005; 110–23.

156. Rozen R., Molecular genetic aspects of hyperhomocysteinemia and its relation to folic acid. *Clin Invest Med.* 1996; 3:171-8.

157. Schalinske KL, Smazal AL. Homocysteine Imbalance: A pathological metabolic marker. *Adv Nutr.* 2012; 755–62.

158. Kumar A, Palfrey HA, Pathak R, Kadowitz PJ, Gettys TW, Murthy SN. The metabolism and significance of homocysteine in nutrition and health. *Nutr Metab*. 2017.

159. Total homocysteine in plasma or serum: methods and clinical applications - PubMed .

160. Maron BA, Loscalzo J. The treatment of hyperhomocysteinemia . Annual Review of Medicine. *NIH Public Access*. 2009; 39–54.

161. Homocysteine species as components of plasma redox thiol status - PubMed .

162. Hultberg B, Andersson A, Sterner G. Plasma homocysteine in renal failure. *Clin Nephrol*. 1993; 40:230–5.

163. McCully KS. Vascular pathology of homocysteinemia: implications for the pathogenesis of arteriosclerosis. *Am J Pathol*. 1969; 56:111–28.

164. Casique L, Kabil O, Banerjee R, Martinez JC, De Lucca M. Characterization of two pathogenic mutations in cystathionine beta-synthase: Different intracellular locations for wild-type and mutant proteins. *Gene*. 2013; 531:117–24.

165. Liew SC, Gupta E Das. Methylenetetrahydrofolate reductase (MTHFR) C677T polymorphism: Epidemiology, metabolism and the associated diseases. *Europ J Med Genetic*. 2015; 1–10.

166. Li WX, Dai SX, Zheng JJ, Liu JQ, Huang JF. Homocysteine metabolism gene polymorphisms (MTHFR C677T, MTHFR A1298C, MTR A2756G and MTRR A66G) jointly elevate the risk of folate deficiency. *Nutrients*. 2015; 7:6670–87.

167. Olteanu H, Munson T, Banerjee R. Differences in the efficiency of reductive activation of methionine synthase and exogenous electron acceptors between the common polymorphic variants of human methionine synthase reductase. *Biochemistry*. 2002; 41:13378–85.

168. Cianciolo G, De Pascalis A, Di Lullo L, Ronco C, Zannini C, La Manna G. Folic Acid and Homocysteine in Chronic Kidney Disease and Cardiovascular Disease Progression: Which Comes First? *Cardiorenal Med*. 2017; 7:255–66.

169. Xie D, Yuan Y, Guo J, Yang S, Xu X, Wang Q, Li Y, Qin X, Tang G, Huo Y, et al. Hyperhomocysteinemia predicts renal function decline: A prospective study in hypertensive adults. *Sci Rep*. 2015; 5:16268.

170. Talbott E, Guzick D, Clerici A, Berga S, Detre K, Weimer K, Kuller L. Coronary heart disease risk factors in women with polycystic ovary syndrome. *Arterioscler Thromb Vasc Biol*. 1995; 15:821–6.

171. Marcus J, Sarnak MJ, Menon V. Homocysteine lowering and cardiovascular disease risk: Lost in translation. *Can J Cardiol*. 2007; 23:707–10.

172. Ganguly P, Alam SF. Role of homocysteine in the development of cardiovascular disease. *Nutr J*. 2015.

173. Obradovic M, Zaric BL, Haidara MA, Isenovic ER. Link between Homocysteine and Cardiovascular Diseases. *Curr Pharmacol Rep*. 2018; 1–9.

174. Maleedhu P, Vijayabhaskar M, Sharma SSB, Kodumuri PK, Vasundhara Devi D. Status of homocysteine in polycystic ovary syndrome. *J Clin Diagnostic Res*. 2014; 8:31–3.

175. Meng Y, Chen X, Peng Z, Liu X, Sun Y, Dai S. Association between high serum homocysteine levels and biochemical characteristics in women with polycystic ovarian syndrome: A systematic review and meta-analysis. *PLoS One*. 2016; 11.

176. Yilmaz N, Pektas M, Tonguc E, Kilic S, Gulerman C, Gungor T, Mollamahmutoglu L. The correlation of plasma homocysteine with insulin resistance in polycystic ovary syndrome. *J Obstet Gynaecol Res*. 2008; 34:384–91.

177. Diwaker A, and Kishore D. Evaluation of Plasma Homocysteine Levels in Patients of PCOS. *J Assoc Physicians India*. 2018; 10:17-20.

178. Marshall JC, Dunaif A. Should all women with PCOS be treated for insulin resistance? *Fertil Steril*. 2012; 97:18–22.

179. Li D, Liu HX, Fang YY, Huo JN, Wu QJ, Wang TR, Zhou YM, Wang XX, Ma XX. Hyperhomocysteinemia in polycystic ovary syndrome: decreased betaine-homocysteine methyltransferase and cystathionine β-synthase-mediated homocysteine metabolism. *Reprod Biomed Online*. 2018; 37:234–41.

180. Chang H, Xie L, Ge H, Wu Q, Wen Y, Zhang D, Zhang Y, Ma H, Gao J, Wang CC, et al. Effects of hyperhomocysteinaemia and metabolic syndrome on reproduction in women with polycystic ovary syndrome: a secondary analysis. *Reprod Biomed Online*. 2019; 38:990–8.

181. Grodnitskaya EE, Kurtser MA. Homocysteine metabolism in polycystic ovary syndrome. *Gynecol Endocrinol*. 2012; 28:186–9.

182. Altuğ Şen T, Köken R, Narci A, Yilmazer M. Homocysteine and Ghrelin Link with Polcystic Ovary Syndrome in Relation to Obesity. *J Pediatr Adolesc Gynecol*. 2011; 24:211–7.

183. Bayraktar F, Dereli D, Özgen AG, Yilmaz C. Plasma homocysteine levels in polycystic ovary syndrome and congenital adrenal hyperplasia. *Endocr J*. 2004; 51:601–8.

184. Chakraborty P, Goswami SK, Rajani S, Sharma S, Kabir SN, Chakravarty B, Jana K. Recurrent Pregnancy Loss in Polycystic Ovary Syndrome: Role of Hyperhomocysteinemia and Insulin Resistance. Franks S, editor. *PLoS One*. 2013; 8:e64446.

185. Berker B, Kaya C, Aytac R, Satiroglu H. Homocysteine concentrations in follicular fluid are associated with poor oocyte and embryo qualities in polycystic ovary syndrome patients undergoing assisted reproduction. *Hum Reprod*. 2009; 24:2293–302.

186. Kilic-Okman T, Guldiken S, Kucuk M. Relationship between homocysteine and insulin resistance in women with polycystic ovary syndrome. *Endocr J*. 2004; 51:505–8.

187. Ratnam S, Maclean KN, Jacobs RL, Brosnan ME, Kraus JP, Brosnan JT. Hormonal regulation of cystathionine β-synthase expression in liver. *J Biol Chem*. 2002; 277:42912–8.

188. Dicker-Brown A, Fonseca VA, Fink LM, Kern PA. The effect of glucose and insulin on the activity of methylene tetrahydrofolate reductase and cystathionine-β-synthase: Studies in hepatocytes. *Atherosclerosis*. 2001; 158:297–301.

189. Schalinske, K.L. Interrelationship between Diabetes and Homocysteine Metabolism: Hormonal Regulation of Cystathionine-Synthase. *Nutr Rev.* 2003; 61:4.

190. Jacobs RL, House JD, Brosnan ME, Brosnan JT. Effects of streptozotocin-induced diabetes and of insulin treatment on homocysteine metabolism in the rat. *Diabetes*. 1998; 47:1967–70.

191. Kazerooni T, Asadi N, Dehbashi S, Zolghadri J. Effect of folic acid in women with and without insulin resistance who have hyperhomocysteinemic polycystic ovary syndrome. *Int J Gynecol Obstet*. 2008; 101:156–60.

192. Asemi Z, Karamali M, Esmaillzadeh A. Metabolic response to folate supplementation in overweight women with polycystic ovary syndrome: A randomized double□blind placebo□controlled clinical trial. *Mol Nutr Food Res*. 2014; 58:1465–73.

193. Bahmani F, Karamali M, Shakeri H, Asemi Z. The effects of folate supplementation on inflammatory factors and biomarkers of oxidative stress in overweight and obese women with polycystic ovary syndrome: a randomized, double-blind, *placebo* -controlled clinical trial. *Clin Endocrinol.* 2014; 81:582–7.

194. Palomba S, Falbo A, Giallauria F, Russo T, Tolino A, Zullo F, Colao A, Orio F. Effects of metformin with or without supplementation with folate on homocysteine levels and vascular endothelium of women with polycystic ovary syndrome. *Diabetes Care*. 2010; 33:246–51.

195. Gaskins AJ, Mumford SL, Chavarro JE, Zhang C, Pollack AZ, Wactawski-Wende J, Perkins NJ, Schisterman EF. The impact of dietary folate intake on reproductive function in premenopausal women: a prospective cohort study. *PLoS One*. 2012; 7:e46276.

196. Schiuma N, Costantino A, Bartolotti T, Dattilo M, Bini V, Aglietti MC, Renga M, Favilli A, Falorni A, Gerli S. Micronutrients in support to the one carbon cycle for the modulation of blood fasting homocysteine in PCOS women. *J Endocrinol Invest*. 2020; 43:779–86.

197. Esmaeilzadeh S, Gholinezhad-Chari M, Ghadimi R. The effect of metformin treatment on the serum levels of homocysteine, folic acid, and vitamin B12 in patients with polycystic ovary syndrome. *J Hum Reprod Sci*. 2017; 10:95–101.

198. Guler I, Himmetoglu O, Turp A, Erdem A, Erdem M, Onan MA, Taskiran C, Taslipinar MY, Guner H. Zinc and homocysteine levels in polycystic ovarian syndrome patients with insulin resistance. *Biol Trace Elem Res*. 2014; 158:297–304.

199. Stracquadanio M, Ciotta L, Palumbo MA. Effects of myo-inositol, gymnemic acid, and L-methylfolate in polycystic ovary syndrome patients. *Gynecol Endocrinol*. 2018; 34:495–501.

200. Carlsen SM, Kjøtrød S, Vanky E, Romundstad P. Homocysteine levels are unaffected by metformin treatment in both nonpregnant and pregnant women with polycystic ovary syndrome. *Acta Obstet Gynecol Scand*. 2007; 86:145–50.

201. Kilicdag EB, Bagis T, Tarim E, Aslan E, Erkanli S, Simsek E, Haydardedeoglu B, Kuscu E. Administration of B-group vitamins reduces circulating homocysteine in polycystic ovarian syndrome patients treated with metformin: A randomized trial. *Hum Reprod*. 2005; 20:1521–8.

CHAPTER 3. LETROZOLE-INDUCED POLYCYSTIC OVARY SYNDROME ATTENUATES CYSTHATIONINE β-SYNTHASE MRNA AND PROTEIN ABUNDANCE IN THE OVARIES OF FEMALE SPRAGUE DAWLEY RATS

A manuscript submitted to the *Journal of Nutrition*

Amanda E. Bries, Joseph L. Webb, Brooke Vogel, Claudia Carrillo, Samantha Pritchard, Aileen F. Keating, and Kevin L. Schalinske

Abstract

Background: Polycystic ovary syndrome (PCOS) is an endocrine disorder that affects 10% of reproductive-aged women and leads to hyperandrogenism, polycystic ovaries, and infertility. Moreover, PCOS has been associated with elevated serum homocysteine; however, characterization of one-carbon metabolism (OCM) in PCOS remains incomplete.

Objective: The aim of our research was to characterize OCM in a letrozole-induced Sprague Dawley (SD) rat model of PCOS.

Methods: Five wk old female SD rats (n = 36) were acclimated for one wk and then were randomly assigned to letrozole (1g/kg body weight; BW) treatment or vehicle (carboxymethylcellulose) control that were administered via a subcutaneously implanted slow-release pellets every 30-d. For both treatment groups, 12 rats were randomly assigned to be euthanized during proestrus at one of the following timepoints: 8, 16 or 24 wk of age. Daily BW was measured and estrous cyclicity was monitored during the last 30-d of the experimental period. Ovaries were collected to assess gene expression and protein abundance of OCM enzymes. These data were analyzed using a t-test and linear mixed model for repeated measures at a significance level of $P < 0.05$.

Results: Letrozole-induced rats had increased cumulative BW gain compared to control rats across all age groups ($P < 0.0001$). Letrozole reduced the time spent at the proestrus and estrus

stages ($P = 0.0001$ and $P = 0.006$, respectively) of the estrous cycle. Cystathionine β-synthase (*Cbs*) mRNA abundance was reduced in the letrozole vs. control rats at 16 (59%; $P < 0.05$) and 24 (77%; $P < 0.01$) wk of age. Additionally, CBS protein abundance was 32% lower in the letrozole-induced rats at 8 wk of age ($P = 0.02$). Interestingly, betaine-homocysteine *S*-methyltransferase (*Bhmt*) mRNA abundance increased as a function of age in letrozole-induced rats ($P = 0.03$).

Conclusion: These data demonstrate that letrozole-induced PCOS temporally decreases the ovarian abundance of *Cbs* mRNA and protein in the early stages of PCOS.

Introduction

Polycystic ovary syndrome (PCOS) is the most common endocrine disorder in reproductive-aged women, affecting one in ten females (1). Clinical manifestations include anovulation, infertility, and hyperandrogenism. A hallmark of PCOS is the rapid hypothalamic pulsatility of gonadotropin release hormone (GnRH) (2), which stimulates the anterior pituitary hormones luteinizing hormone (LH) and follicle stimulating hormone (FSH). Hypersecretion of LH is the central pathophysiological driver of PCOS, which in turn, leads to elevated circulating testosterone concentrations. Together, these imbalances lead to follicular arrest, amenorrhea, and infertility. Furthermore, a large concern for women with PCOS is the diminution in oocytes (3), as well as alterations to folliculogenesis (4).

A persistent imbalance of androgen production and the duration of PCOS diagnosis increases the risk for developing co-morbidities, such as diabetes and cardiovascular disease (5). Aberrant methyl group metabolism and concomitant hyperhomocysteinemia is an independent risk factor for cardiovascular disease, as well as other chronic conditions (6). It is well established that women with PCOS have elevated blood and follicular homocysteine concentrations (7,8), but the exact reason and its implications on ovarian function remain elusive.

Furthermore, diabetic conditions compromise methyl group and homocysteine metabolism (9,10). Given the common comorbidity of PCOS and diabetes (11), it is important to characterize ovarian one carbon metabolism (OCM) and determine its relationship in the pathogenesis of PCOS.

One carbon metabolism is a ubiquitous system, comprised of several essential nutrients functioning as coenzymes and methyl donors (12). Physiological processes, such as maintaining serine and glycine homeostasis, DNA synthesis, and providing sufficient methyl groups for S-adenoyslmethioine (SAM)-dependent transmethylation reaction, including gene expression, are reliant on a tightly regulated OCM system. Three central pathways are involved in the metabolism and balance of methyl groups and homocysteine: 1) folate-dependent remethylation of homocysteine to methionine; 2) folate-independent remethylation of homocysteine to methionine; and 3) irreversible catabolism of homocysteine via transsulfuration **(Figure 3-1).** The consequences of both hypo- and hypermethylation results in impaired gene expression, which has been closely linked to a myriad of metabolic diseases (13). The deleterious effects of hypermethylation on oocyte quality have been previously reported (14). Jia et al. identified compromised mitochondrial DNA copy numbers and elevated follicular homocysteine concentrations in progressive polycystic gilt ovaries. Nevertheless, characterization of the key enzymes in the OCM pathway has not been examined. Therefore, the main objective of the present study was to induce the PCOS phenotype and characterize the OCM cycle as a function of disease progression. To achieve this objective, animals were maintained on a chemical treatment until either 8, 16, or 24 wk of age and differential mRNA, protein abundance, and enzyme activity between the letrozole-induced or placebo control rats was measured.

Materials and Methods

Rats and Diets. All animal studies were approved by the Institutional Animal Care and Use Committee at Iowa State University (IACUC # 18-294) and were performed according to the Iowa State University Laboratory Animal Resources Guidelines. Female Sprague Dawley (SD) rats (n = 36) were purchased at 5 wk of age (Envigo, Madison, WI) and were dually housed according to treatment group in a temperature-controlled room with a 12-h light-dark cycle. All rats were acclimated on a modified semi-purified diet (AIN-93G) for one wk. Following acclimation, rats were randomly assigned to cage, experimental treatment, and age (8, 16, or 24 wk of age) of sacrifice. At the beginning of the experimental period, animals were divided into two groups: placebo (n = 18; n = 6/age) and letrozole (n = 18; n = 6/age) and subcutaneously implanted with a 30-d continuous, slow-release pellet (Innovative Research of American, Sarasota, FL) containing a 1 mg/kg body weight (BW) dose of letrozole (Sigma-Aldrich; no. 112809-51-5) or a 1 mg/kg BW dose of the vehicle control, carboxymethylcellulose. Each 30-d dose was pre-determined based on the average predicted change in BW as a function of age to maintain a dosage of 1mg/1kg BW. Rats were fed *ad libitum* a modified standard AIN93G diet containing 50.4% carbohydrate; 17.3% protein, and 32.3% fat from kcals. For the last 30 d of the experimental period, vaginal cytology was monitored to determine the stage of the estrous cycle, as previously described (15). Additionally, daily BW was recorded throughout the entire study. Animals were randomly assigned to be euthanized at proestrus in 1 of 3 groups (n = 12): 8, 16, and 24 wk of age. Letrozole-induced rats were euthanized in diestrus, because they failed to cycle into proestrus. Rats were anesthetized via a single intraperitoneal injection of ketamine:xylazine (90:10 mg/kg BW) and whole blood was collected via cardiac puncture for serum separation. Euthanasia was carried out via vital tissue harvest, whereby the epididymal fat pad, liver, kidneys, and ovaries were removed and weighed. Confirmation of euthanasia was

performed by bilateral thoracotomy. One ovary was stored in *RNA*later solution. Liver, kidney and adipose samples were either snap frozen in liquid nitrogen or stored in *RNA*later. All tissues were stored at -80°C until subsequent analysis.

Intraperitoneal glucose tolerance test. One wk before euthanasia, rats underwent an intraperitoneal glucose tolerance test (IPGTT). Following a 14 h overnight fast with *ab libitum* water, animals were injected with a 1g/kg BW dose of D-glucose in sterile 1X PBS after obtaining baseline blood glucose measurements via the lateral tail vein. Subsequent blood glucose measurements were obtained at 30, 60, 90, and 120 min post-injection using a standard glucometer (Bayer Healthcare). Data are reported as a change in blood glucose from baseline values.

Assessment of estrous cyclicity. During the last 30 d of the experimental period, vaginal smears were obtained daily from all rats between 8-9 am. Smears were collected via a vaginal lavage of 15 µL using sterile PBS solution. Samples were mounted and stained with methylene blue, as previously described (16,17). The stage of the estrous cycle (i.e. proestrus, estrus, metestrus, and diestrus) was determined and classified by the relative proportion of leukocytes, epithelial, and cornified cells by light microscopy, as detailed previously (18).

Testosterone. Serum testosterone concentrations were determined using a commercially available enzyme linked-immunosorbent assay (Crystal Chem; Elk Grove Village, IL).

Quantitative real-time polymerase chain reaction. Total ovarian RNA was extracted from half of one ovary using a Qiagen RNAeasy Mini kit (no. 74134; Germantown, MD). RNA quantity and the λ= 260:280 nm absorption for determination of quality was measured via spectrophotometry using a Nanodrop 2000 (Thermo Fisher Scientific). Using the Agilent High Capacity cDNA kit (Thermo-Fisher Scientific), mRNA was converted to complementary DNA and 1.9 µg/20 µL reaction was used. Primers (**Table 3-1**) were designed and obtained from Integrated DNA Technologies (Coralville, IA). Reverse transcription PCR reactions were performed on each sample in triplicate and inter variation was controlled by analyzing all of the genes of a given animal on the same 96-well reaction plate using LightCycler FastStart Master SYBR Green 1 (no. 03003230001; Roche) on a LightCyler 96-well Real-time PCR System (Roche) according to manufacturer's instructions. CT values were normalized to 18S ribosomal mRNA and presented as relative-fold change. Amplification efficiencies of target and reference gene assays were verified and data were analyzed using the Livak, delta delta CT method for relative mRNA expression (19).

Western blotting. One ovary (5 mg) was homogenized in 200 µL lysis buffer [Tris-HCl (50 mM, pH 7.4), EDTA (1 mM), EGTA (1 mM), DTT (1 mM), glycerol (10%, w/v), and Triton-X (1%, w/v)] with halt protease inhibitor cocktail (Thermo Fisher Scientific, no. 78439). Protein concentrations were determined using a Pierce Coomassie Bradford assay (ThermoFisher Scientific, no. 23236) according to the manufacturer's instructions. Ovarian lysates were diluted to 1.7 µg/µL in Laemmli loading buffer and a total of 40 µg protein was loaded onto a 15% sodium dodecyl sulfate polyacrylamide gel for separation of proteins via electrophoresis (80 min; 200V) in 1X Tris-Glycine SDS buffer. After separation, proteins were transferred to a

nitrocellulose membrane via a fully-wet transfer in 25 mM Tris, 192 mM glycine, 20% v/v methanol, pH 8.3 buffer via electrophoresis (120 min; 100V). All membranes were stained with Ponceau S to verify equal loading and transfer efficiency. Membranes were washed with PBS and incubated with CBS (1:750 dilution) and α-tubulin (1:400 dilution) primary antibodies (CBS, cat. no MA517273; α-tubulin, cat. no sc-5286; ThermoFisher Scientific) in 5% non-fat dry milk in PBS-tween buffer, overnight at 4°C. After 3 washes with PBS, membranes were incubated with a secondary antibody (IRDye 800CW Goat anti-Mouse cat no. 926-32210 and 600CW Goat anti-rabbit cat. no 926-68021) at a dilution of 1:5,000 for 1 h at room temperature. Membranes were washed 4 times, 10 min each, in PBS before imaging via digital fluorescence detection using an Odyssey CLx imaging system (Li-Cor). The net intensity of each band was determined using Empiria Studio Software (Li-Cor) and normalized to α-tubulin

Cystathionine beta synthase activity. Ovarian CBS enzyme activity was determined using a commercially available assay by Abcam (cat. no ab241043; Cambridge, MA). Briefly, one ovary per rat (5.5 mg) was homogenized in CBS assay buffer using a mechanical homogenizer on ice at speed 3.5 for 5 sec. Tissue lysates were then centrifuged at 10,000 x g for 15 min at 4°C. The remaining preparation of the assay was performed per the manufacturer's instructions using the Synergy H1 Hybrid Microplate Reader (BioTek Instruments, Winooski, VT). CBS activity was determined by analyzing the assay in kinetic mode with the gain setting on auto for 50 minutes, at 1-min intervals, resulting in a total of 50 reads. CBS enzyme activity is presented as nmol/min/mL.

Statistical Analysis. All data were analyzed with SAS 9.4 Statistic Software (Cary, NC). Means were assessed for normality using Pearson residuals. Normally distributed data are presented as means ± SEMs and analyzed using unpaired t-tests between treatment groups within each age as determined previously (20). When data were assessed as an overall effect across age and treatment groups, a linear mixed model with analysis of main effects of treatment and age in addition to simple effects of within age and treatment groups was reported. Repeated measure analysis of IPGTT and BW were assessed via a mixed-model analysis and Satterthwaite approximations were used to estimate degrees of freedom for post-hoc tests to compare pairwise treatment means within each age level for all indicators. Statistical significance was determined at a level of $P < 0.05$.

Results

Letrozole-induced rats had higher body weight. A main effect of letrozole treatment was observed for growth, resulting in higher cumulative BW gain as a function of time across all three age groups ($P < 0.001$; **Figure 3-2**). At 8 wk of age, letrozole-induced rats had ~2-fold higher cumulative BW gain compared to their placebo counterparts ($P < 0.01$) and by 24 wk of age, letrozole-induced rats gained ~1.8-fold more weight than the placebo group ($P < 0.0001$). There was a significant interaction between treatment and age ($P < 0.0001$). Moreover, pairwise comparisons determined differences in BW gain as a function of age in both the letrozole-induced and placebo rats ($P < 0.0001$).

Letrozole did not impair glucose tolerance. There were no main effects of letrozole treatment on impaired glucose tolerance ($P = 0.80$) as measured by the change in blood glucose concentrations from baseline up to 120 minutes, indicating that the growth rate of the letrozole-induced rats was not concomitant with blood glucose intolerance **(Figure 3-3)**. A main effect of

age on a greater change in blood glucose concentrations was detected ($P = 0.034$), but there was no interaction between treatment and age ($P = 0.13$).

Letrozole attenuated the frequency of proestrus occurrence. There are four stages of the estrous cycle: proestrus, estrus, metestrus and diestrus; however, due to the effects of letrozole, a number of vaginal smears were unclassifiable potentially as a result of letrozole-induced acyclicity. The impact of letrozole exposure on the time spent at each stage of the estrous cycle was determined **(Figure 3-4).** Samples that only presented leukocytes and not able to be classified into one of the 4 estrous stages, were termed pseudodiestrus and have been described in previous studies (21,22). These samples were maintained in the analyses, and indicated as pseudodiestrus (U). There was a main effect of treatment ($P = 0.01$) and age ($P < 0.0001$) on the percentage of samples that were in pseudodiestrus. Moreover, there was a main interaction between treatment and age on percent in pseudodiestrus ($P < 0.01$). When simple effects were examined by extrapolating to treatment effects within age groups, there was higher prevalence of animals in pseudodiestrus ($P = 0.0002$) in letrozole-treated (22.7 ± 2.0%) vs. placebo-treated (12.7 ± 2.0 %) rats. A shorter time ($P < 0.0001$) spent at proestrus was observed in the letrozole-induced rats compared to their placebo counterparts. This effect was not observed as a function of age ($P = 0.71$) and differed as animals aged (16 wk, $P = 0.003$; 24 wk, $P < 0.001$). There were no main effects of treatment or age on the time spent in estrus or diestrus, but a prolonged occurrence of metestrus was observed in the letrozole-induced rats ($P < 0.0001$) and as a function of age ($P = 0.03$). Metestrus was more prevalent in the letrozole-induced rats compared to controls at 8 ($P <0.001$), 16 ($P <0.001$), and 24 ($P <0.001$) wk of age.

Relative uterine horn weights were atrophic as a result of letrozole exposure. A main effect of letrozole treatment for a marked reduction in relative uterine horn weight ($P < 0.0001$) was observed, but there was no effect of age or the interaction of the two on relative uterine horn weight (**Table 3-2**). At 8 wk of age, letrozole-induced rats had a 53% decrease in relative uterine horn weight compared to the placebo group ($P = 0.003$), an 80% decrease at 16 wk ($P = 0.0003$), and a decrease of 81% by 24 wk ($P = 0.003$). Interestingly, there was a trend ($P = 0.085$) for higher relative ovarian weight as a result of letrozole-exposure. There was a main effect of age ($P < 0.0001$) and the interaction of treatment and age ($P = 0.017$) on relative ovarian weight. When we examined the simple effects of letrozole treatment on relative ovarian weight within an age group, a difference was only observed at 8 wk of age ($P = 0.003$).

Letrozole-induced rats had elevated circulating testosterone concentrations. To confirm the PCOS phenotype, circulating testosterone concentrations were measured in the rats. Letrozole-induced rats had higher circulating serum testosterone concentrations at 8 ($P = 0.009$), 16 ($P = 0.005$), and 24 ($P = 0.02$) wk of age (**Figure 3-5**). Concentrations in the letrozole-induced rats were elevated as much as 2.8-fold higher when compared to the placebo rats.

Letrozole modulates the gene expression of two key enzymes in the OCM pathway. Out of the five OCM enzymes examined with respect to transcript level, only two were altered ($P < 0.05$) in the letrozole-induced rats **(Figure 3-6)**. An analysis within age groups determined a reduction in ovarian cystathionine β-synthase *(Cbs)* mRNA abundance in letrozole-treated rats of 59% ($P = 0.05$; Fig 3-6B), and 77% ($P = 0.008$; Fig 3-6C) at 16 and 24 wk of age, respectively. There was a trend for a 39% reduction of *Cbs* mRNA abundance in rats at 8 wk of age ($P = 0.06$; Fig 3-6A).

In contrast, there was a trend for 85% higher *Cbs* transcript abundance in letrozole-induced rats compared to the placebo controls at 16 ($P = 0.06$) wk of age (*data not shown*). When testing across both treatment and age, there was an overall effect of treatment as a function of age as evidenced by increased *Bhmt* mRNA abundance ($P = 0.034$) in the letrozole-treated rats (Figure 3-6). No differences in *Bhmt* mRNA level were identified between treatment groups ($P = 0.32$). The abundance of mRNA encoding *Cyp19a1* was significantly reduced by 75% in rats at 8 wk of age.

Cystathionine β-synthase protein abundance is diminished in the early onset of PCOS. We measured the protein abundance and enzyme activity of CBS in rats with and without PCOS across 3 age groups. Protein abundance decreased 32% in the letrozole-induced rats at 8 wk of age ($P = 0.02$), but there was no significant change at 16 or 24 wk of age **(Figure 3-6E)**. Furthermore, there was no significant variation in the level of ovarian CBS enzymatic activity at any age **(Figure 3-6F).**

Discussion

Our previous work determined aberrations in methyl group and homocysteine metabolism, resulting in global hypermethylation (23) in an obese model of type 2 diabetes (T2D), suggesting potential alterations in the OCM pathway during the pathophysiological progression of PCOS. Therefore, the objective in this study was to characterize OCM in an animal model of chemically-induced PCOS, and potentially one that displays an obese phenotype. In addition, similar to our studies in a hyperphagia-induced mouse model of obesity (20), the experimental paradigm included analysis of tissues at three ages in order to examine mechanisms involved in the progression of a PCOS phenotype.

Letrozole is an inhibitor of CYP19A1, which is the key enzyme involved in the ovarian conversion of testosterone to 17β-estradiol. Compromised CYP19A1 activity is one of the underlying conditions in the pathogenesis of PCOS, resulting in concomitant elevations in testosterone concentrations, thus making circulating testosterone an excellent biomarker for PCOS (24). Although polycystic ovaries are a consistent result from letrozole treatment (25), there are inconsistencies in the reported metabolic and phenotypic characteristics of letrozole exposure. For instance, several studies have reported almost full recapitulation of insulin-resistant PCOS that is observed in humans, as evidenced by observations of insulin sensitivity, increased adiposity, and obesity in the letrozole-induced rodents (25–27). In contrast, the letrozole-treated rats in this study had no indication of glucose intolerance when compared to their control counterparts at any age. There were no differences in fasting blood glucose concentrations or glucose tolerance tests between treatment groups. There was a robust difference in absolute BW and cumulative BW gain across all age groups, but this was not concomitant with increased adiposity. The findings in our study are consistent with other studies reporting a lack of glucose intolerance (28), insulin sensitivity (29,30), and adiposity (27) in adult letrozole-induced rodents.

We are one of the first groups to report using a slow, time-release pellet method for delivering letrozole, as compared to the more common practice of daily intramuscular injections, a clearly stressful mode of delivery. Thus, it is evident that the phenotypic outcomes of letrozole treatment are variable and could be species, dose, and/or developmental stage dependent (31–33). Furthermore, the letrozole treated rats in this study were affected by the intervention, albeit to a more moderate level. We chose the three age groups of 8, 16, and 24 wk of age because they reflect earlier reproductive periods of approximately 12, 20, and 28 years of human age,

respectively (34). Creating a model of PCOS that eliminates many of the confounding factors, such as insulin resistance and glucose intolerance is important, as the model in this current study is therefore more suitable for elucidating the mechanisms that are involved in the pathogenesis of PCOS.

We observed significantly perturbed estrous cyclicity in our letrozole-induced rats. During metestrus, cornified epithelial cells along with leukocytes are present in the vaginal smears, whereas predominant presence of leukocytes indicates diestrus. Other studies employing letrozole treated rodents have confirmed to be almost entirely acyclic, as assessed by exclusive presence of leukocytes, otherwise classified as pseudodiestrus (21,22,35). For the purpose of our model, acyclicity allows us to reduce the variability within the letrozole treated group and examine differences in ovarian metabolism that is indicative of human PCOS conditions. Additionally, we determined greater evidence of perturbations to ovarian function due to the observed uterine horn atrophy in the letrozole-induced rats across all stages. Uterine growth is responsive to circulating estrogen levels, and previous studies have reported dose-dependent suppression of the uterine weight upon letrozole exposure (32). Taken together, these observations provide us with evidence of a strong and robust model of PCOS.

A hallmark of the PCOS phenotype is elevated circulating testosterone concentrations, leading to disruption of the hypothalamic pituitary ovarian axis. It was important for us to examine the influence of letrozole on circulating testosterone concentrations, because research has reported sex differences on OCM, but it has not been investigated whether conditions of PCOS affect OCM (36). Our letrozole-induced PCOS model resulted in an overall mean of 3.5 ng/mL of serum testosterone, which is comparable to the circulating testosterone concentrations of 5.5 ng/mL and 3.2 ng/mL that have been reported in 12-wk old male SD rats (37,38). The

effects of testosterone on OCM have predominantly been reported in prostate cancer models. For instance, high testosterone concentrations post-transcriptionally decreased *Cbs* gene expression specifically in a prostate cancer cell line (39). Furthermore, high testosterone exposure resulted in a compensatory decrease in the transsulfuration flux and glutathione production, partially explained by reduced CBS activity in the cell line. These findings are also corroborated by research examining the effects of estrogen-replacement therapies on postmenopausal women. Estrogen has been reported to have a dose-dependent effect on the transsulfuration of homocysteine to cysthathionine, whereby oral estradiol has been reported to result in an increase in plasma glutathione concentrations and a reduction in circulating homocysteine (40,41).

Cystathionine-β synthase is an enzyme encoded by the *Cbs* gene that is critical in the transsulfuration pathway by catalyzing the irreversible conversion of homocysteine to cystathionine (42). The primary role of CBS is its involvement in the canonical transsulfuration pathway that results in maintaining homocysteine concentrations, as well as the downstream production of cysteine and glutathione, the latter representing a major antioxidant (43). To date, when it comes to the female reproductive systems, altered *Cbs* expression has been almost exclusively studied in ovarian cancer as indicated by enhanced cellular proliferation, tumorigenic overexpression, and enhanced antioxidative capacity in cancer cells (42). Though it remains largely uncharacterized, due to the presence of increased circulating homocysteine concentrations (7) and elevated inflammatory stress (44) in the ovaries in women with PCOS, the OCM pathway is a logical candidate for involvement in PCOS pathogenesis.

We demonstrated a temporal decrease in ovarian *Cbs* mRNA abundance during the progression of PCOS. Moreover, we reported a significant reduction in CBS protein abundance, but this was not a progressional response as it was only observed at 8 wk of age. Due to the role

of CBS in the transsulfuration pathway, this finding suggests reduced catabolism of homocysteine which, in part, may explain the elevated follicular homocysteine concentrations that have been previously reported (7,8). Although we did not report fasting blood insulin levels, previous research by Ratnam *et al*. demonstrated the effects of insulin on decreasing CBS enzymatic activity (45). In their diabetic animal model, insulin treatment restored the elevated CBS activity back to baseline. We previously established that diabetic rats exhibit elevated hepatic CBS activity (23), and interestingly, we observed a trend in increased *Cbs* gene expression in the liver (*data not shown*). It is possible, that our markedly lower ovarian *Cbs* expression and trend for elevated hepatic *Cbs* mRNA abundance is influenced by circulating insulin concentrations; however, we were not able to confirm this finding, since we did not observe a significant reduction in CBS activity.

Although letrozole treatment did not affect the abundance of *Bhmt* significantly within each time point, we did observe increased transcript abundance in *Bhmt* as a function of age, exclusively in our letrozole-treated rats. To our knowledge, there is only one report indicating altered *Bhmt* expression in a model of PCOS. A study by Jia and colleagues (14) reported increased *Bhmt* gene expression in the ovaries of gilts with PCOS. Their findings were accompanied by hyperhomocysteinemia; therefore, elevated circulating levels of homocysteine resulted in perturbed ovarian OCM, particularly disrupting *Bhmt* and *Gnmt* activation in the oocytes of gilts. BHMT is the enzyme that functions in the transmethylation of homocysteine back to the amino acid, methionine via the donation of one methyl group from betaine. Upregulation of *Bhmt* suggests prevention of hyperhomocysteinemia conditions, as previous research has reported elevated BHMT activity at the expense of elevated homocysteine concentrations in models of progressive folic-acid deficiency (46) and diabetes (47).

In conclusion, our results demonstrate that progressive PCOS via letrozole treatment perturbs the enzymatic mRNA abundance and protein level of CBS at the early stage of PCOS (8 wk of age). The data and results provide a novel representation of the mechanistic OCM consequences in the ovaries during the progression of PCOS, one that is absent of metabolic characteristics such as increased adiposity and insulin resistance. Additionally, the importance of determining the alterations in OCM enzymes allows us to apply our findings to understand how nutrition in the early stages of development may help mitigate alterations to the canonical OCM pathway and thereby limit the severity of PCOS. Future dietary intervention studies, such as intervening with a high dietary methyl diet, are warranted to examine the therapeutic role of nutrition in supporting OCM during progressive PCOS.

Acknowledgments

We thank Dr. Kathleen Mullin and her veterinary interns, Clara Kiepe and James Chung for their technical assistance in the initial surgical procedures. The author's responsibilities were as follows - A.E.B drafted the original version of this manuscript. A.E.B performed all aspects of animal maintenance, surgical procedures, and laboratory experiments. J.L.W and B.V. assisted in surgical procedures. B.V. and C.C. assisted in animal maintenance. A.E.B., S.P., A.K., and K.L.S. assisted in the study design and revising the manuscript. All authors read and approved the final version of the manuscript.

References

1. Wolf WM, Wattick RA, Kinkade ON, Olfert MD. Geographical prevalence of polycystic ovary syndrome as determined by region and race/ethnicity. *Int J Environ Res Public Health*. 2018; 15.

2. Ibáñez L, Oberfield SE, Witchel S, Auchus RJ, Chang RJ, Codner E, Dabadghao P, Darendeliler F, Elbarbary NS, Gambineri A, et al. An international consortium update: pathophysiology, diagnosis, and treatment of polycystic ovarian syndrome in adolescence. hormone research in paediatrics. *S. Karger AG*. 2017. p. 371–95.

3. Wu LLY, Norman RJ, Robker RL. The impact of obesity on oocytes: Evidence for lipotoxicity mechanisms. *Reprod, Fertil, and Dev*. 2012. p. 29–34.

4. Sander VA, Hapon MB, Sícaro L, Lombardi EP, Jahn GA, Motta AB. Alterations of folliculogenesis in women with polycystic ovary syndrome. *J Steroid Biochem Mol Biol*. 2011; 124:58–64.

5. Rosenfield RL, Ehrmann DA. The pathogenesis of polycystic ovary syndrome (PCOS): the hypothesis of PCOS as functional ovarian hyperandrogenism revisited. *Endocr Rev*. 2016; 37:467–520.

6. Schalinske KL, Smazal AL. Homocysteine imbalance: a pathological metabolic marker. *Adv Nutr*. 2012; 3:755–62.

7. Eskandari Z, Sadrkhanlou RA, Nejati V, Tizro G. PCOS women show significantly higher homocysteine level, independent to glucose and E2 level. *Int J Reprod Biomed*. 2016; 14:495–500.

8. Berker B, Kaya C, Aytac R, Satiroglu H. Homocysteine concentrations in follicular fluid are associated with poor oocyte and embryo qualities in polycystic ovary syndrome patients undergoing assisted reproduction. *Hum Reprod*. 2009; 24:2293–302.

9. Nieman KM, Hartz CS, Szegedi SS, Garrow TA, Sparks JD, Schalinske KL. Folate status modulates the induction of hepatic glycine *N* -methyltransferase and homocysteine metabolism in diabetic rats. *Am J Physiol Metab*. 2006; 291:E1235–42.

10. Williams KT, Garrow TA, Schalinske KL. Type I diabetes leads to tissue-specific dna hypomethylation in male rats. *J Nutr Biochem Mol Genet Mech J Nutr*. 2008; 138:2064–9.

11. Rubin KH, Glintborg D, Nybo M, Abrahamsen B, Andersen M. Development and risk factors of type 2 diabetes in a nationwide population of women with polycystic ovary syndrome. *J Clin Endocrinol Metab*. 2017; 102:3848–57.

12. Ducker GS, Rabinowitz JD. One-carbon metabolism in health and disease. *Cell Metab*. 2017; 25:27–42.

13. Choi S-W, Claycombe KJ, Martinez JA, Friso S, Schalinske KL. Nutritional epigenomics: a portal to disease prevention. *Adv Nutr*. 2013; 4:530–2.

14. Jia L, Li J, He B, Jia Y, Niu Y, Wang C, Zhao R. Abnormally activated one-carbon metabolic pathway is associated with mtDNA hypermethylation and mitochondrial malfunction in the oocytes of polycystic gilt ovaries. *Sci Rep*. 2016; 6.

15. Ganesan S, Nteeba J, Keating AF. Impact of obesity on 7,12-dimethylbenz[a]anthracene-induced altered ovarian connexin gap junction proteins in female mice. *Toxicol Appl Pharmacol*. 2015; 282:1–8.

16. Nteeba J, Ortinau LC, Perfield JW, Keating AF. Diet-induced obesity alters immune cell infiltration and expression of inflammatory cytokine genes in mouse ovarian and peri-ovarian adipose depot tissues. *Mol Reprod Dev*. 2013; 80:948–58.

17. Yener T, Turkkani Tunc A, Aslan H, Aytan H, Caliskan AC. Determination of oestrous cycle of the rats by direct examination: How reliable? *J Vet Med Ser C Anat Histol Embryol*. 2007; 36:75–7.

18. Byers SL, Wiles M V., Dunn SL, Taft RA. Mouse estrous cycle identification tool and images. *PLoS One*. 2012; 7:e35538.

19. Livak KJ, Schmittgen TD. Analysis of relative gene expression data using real-time quantitative pcr and the 2−ΔΔCT method. *Methods*. 2001; 25:402–8.

20. Nteeba J, Ganesan S, Keating AF. Progressive obesity alters ovarian folliculogenesis with impacts on pro-inflammatory and steroidogenic signaling in female mice. *Biol Reprod*. 2014; 91:86.

21. Ortega I, Sokalska A, Villanueva JA, Cress AB, Wong DH, Stener-Victorin E, Stanley SD, Duleba AJ. Letrozole increases ovarian growth and Cyp17a1 gene expression in the rat ovary. *Fertil Steril*. 2013; 99:889–96.

22. Maliqueo M, Sun M, Johansson J, Benrick A, Labrie F, Svensson H, Loïn M, Duleba AJ, Stener-Victorin E. Continuous administration of a P450 aromatase inhibitor induces polycystic ovary syndrome with a metabolic and endocrine phenotype in female rats at adult age. *Endocrinology*. 2013; 154:434–45.

23. Williams KT, Schalinske KL. Tissue-specific alterations of methyl group metabolism with DNA hypermethylation in the Zucker (type 2) diabetic fatty rat. *Diabetes Metab Res Rev*. 2012; 28:123–31.

24. Mannerås L, Cajander S, Holmäng A, Seleskovic Z, Lystig T, Lönn M, Stener-Victorin E. A new rat model exhibiting both ovarian and metabolic characteristics of polycystic ovary syndrome. *Endocrinology*. 2007; 148:3781–91.

25. Shi D, Vine DF. Animal models of polycystic ovary syndrome: A focused review of rodent models in relationship to clinical phenotypes and cardiometabolic risk. *Fertil Steril*. 2012; 98:185-93.

26. Kauffman AS, Thackray VG, Ryan GE, Tolson KP, Glidewell-Kenney CA, Semaan SJ, Poling MC, Iwata N, Breen KM, Duleba AJ, et al. A novel letrozole model recapitulates both the reproductive and metabolic phenotypes of polycystic ovary syndrome in female mice. *Biol Reprod*. 2015; 93:69.

27. Adeyanju OA, Falodun TO, Fabunmi OA, Olatunji LA, Soladoye AO. Very low dose spironolactone protects experimentally-induced polycystic ovarian syndrome from insulin-resistant metabolic disturbances by suppressing elevated circulating testosterone. *Chem Biol Interact*. 2019; 310:108742.

28. Arroyo P, Ho BS, Sau L, Kelley ST, Thackray VG. Letrozole treatment of pubertal female mice results in activational effects on reproduction, metabolism and the gut microbiome. *PLoS One*. 2019; 14.

29. Torres PJ, Skarra D V., Ho BS, Sau L, Anvar AR, Kelley ST, Thackray VG. Letrozole treatment of adult female mice results in a similar reproductive phenotype but distinct changes in metabolism and the gut microbiome compared to pubertal mice. *BMC Microbiol*. 2019; 19:57.

30. Shi D, Vine DF. Animal models of polycystic ovary syndrome: a focused review of rodent models in relationship to clinical phenotypes and cardiometabolic risk. *Fertil Steril*. 2012; 98:185-193.e2.

31. Osuka S, Nakanishi N, Murase T, Nakamura T, Goto M, Iwase A, Kikkawa F. Animal models of polycystic ovary syndrome: A review of hormone□induced rodent models focused on hypothalamus□pituitary□ovary axis and neuropeptides. *Reprod Med Biol*. 2019; 18:151–60.

32. Kafali H, Iriadam M, Ozardali I, Demir N. Letrozole-induced polycystic ovaries in the rat: A new model for cystic ovarian disease. *Arch Med Res*. 2004; 35:103–8.

33. Torres PJ, Skarra D V., Ho BS, Sau L, Anvar AR, Kelley ST, Thackray VG. Letrozole treatment of adult female mice results in a similar reproductive phenotype but distinct changes in metabolism and the gut microbiome compared to pubertal mice. *BMC Microbiol*. 2019; 19:1–15.

34. Pallav Sengupta. The laboratory rat : Relating its age with human's. *Int J Prev Med*. 2013; 4:624–30.

35. Caldwell ASL, Middleton LJ, Jimenez M, Desai R, McMahon AC, Allan CM, Handelsman DJ, Walters KA. Characterization of reproductive, metabolic, and endocrine features of polycystic ovary syndrome in female hyperandrogenic mouse models. *Endocrinology*. 2014; 155:3146–59.

36. Sadre-Marandi F, Dahdoul T, Reed MC, Nijhout HF. Sex differences in hepatic one-carbon metabolism. *BMC Syst Biol*. 2018; 12.

37. Wu D, Lin G, Gore AC. Age-related changes in hypothalamic androgen receptor and estrogen receptor α in male rats. *J Comp Neurol*. 2009; 512:688–701.

38. Chin KY, Ima-Nirwana S. The effects of testosterone deficiency and its replacement on inflammatory markers in rats: A pilot study. *Int J Endocrinol Metab*. 2017; 15.

39. Vitvitsky V, Prudova A, Stabler S, Dayal S, Lentz SR, Banerjee R. Testosterone regulation of renal cystathionine β-synthase: Implications for sex-dependent differences in plasma homocysteine levels. *Am J Physiol - Ren Physiol*. 2007; 293:F594-600.

40. Dimitrova KR, DeGroot K, Myers AK, Kim YD. Estrogen and homocysteine. *Cardiovasc Res*. 2002. p. 577–88.

41. Smolders RGV, De Meer K, Kenemans P, Jakobs C, Kulik W, Van Der Mooren MJ. Oral estradiol decreases plasma homocysteine, vitamin B6, and albumin in postmenopausal women but does not change the whole-body homocysteine remethylation and transmethylation flux. *J Clin Endocrinol Metab*. 2005; 90:2218–24.

42. Zhu H, Blake S, Chan KT, Pearson RB, Kang J. Cystathionine β-synthase in physiology and cancer. *Biomed Res Int*. 2018; 2018:3205125.

43. Jhee KH, Kruger WD. The role of cystathionine β-synthase in homocysteine metabolism. *Antioxid Redox Signal*. 2005. p. 813–22.

44. Kalhori Z, Mehranjani MS, Azadbakht M, Shariatzadeh MA. L -Carnitine improves endocrine function and folliculogenesis by reducing inflammation, oxidative stress and apoptosis in mice following induction of polycystic ovary syndrome. *Reprod Fertil Dev*. 2019; 31:282–93.

45. Ratnam S, Maclean KN, Jacobs RL, Brosnan ME, Kraus JP, Brosnan JT. Hormonal regulation of cystathionine β-synthase expression in liver. *J Biol Chem*. 2002; 277:42912–8.

46. Saande CJ, Pritchard SK, Worrall DM, Snavely SE, Nass CA, Neuman JC, Luchtel RA, Dobiszewski S, Miller JW, Vailati-Riboni M, et al. Dietary egg protein prevents hyperhomocysteinemia via upregulation of hepatic betaine-homocysteine s-methyltransferase activity in folate-restricted rats. *J Nutr*. 2019; 149:1369–76.

47. Nieman KM, Hartz CS, Szegedi SS, Garrow TA, Sparks JD, Schalinske KL, Schalinske Folate KL. Folate status modulates the induction of hepatic glycine N-methyltransferase and homocysteine metabolism in diabetic rats. *Am J Physiol Endo-crinol Metab*. 2006; 291:1235–42.

Tables and Figures

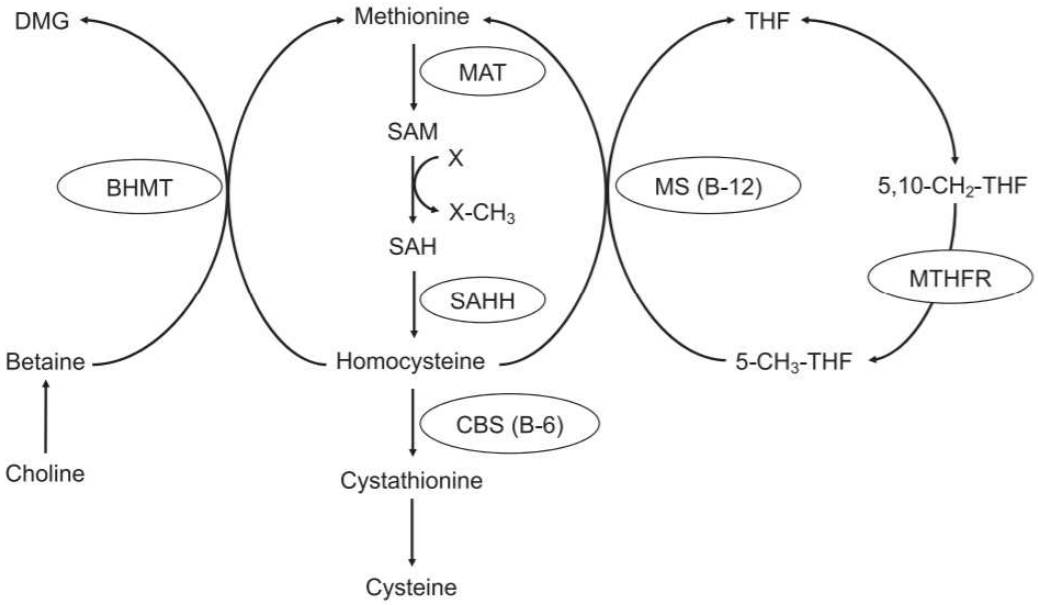

Figure 3-1. Schematic of the one-carbon and methyl group metabolism pathwayAbbreviations used: BHMT, betaine homocysteine S-methyltransferase; CBS, cystathionine β-synthase; DMG, dimethylglycine; MAT, methionine adenosyltransferase; MS, methionine synthase; MTHFR, methylenetetrahydrofolate reductase; SAH, S-adenosylhomocysteine; SAHH, S-adenosylhomocysteine hydrolase; SAM, S-adenosylmethionine; THF, tetrahydrofolate; X, methyl group acceptor; 5-CH3-THF, 5-methyltetrahydrofolate.

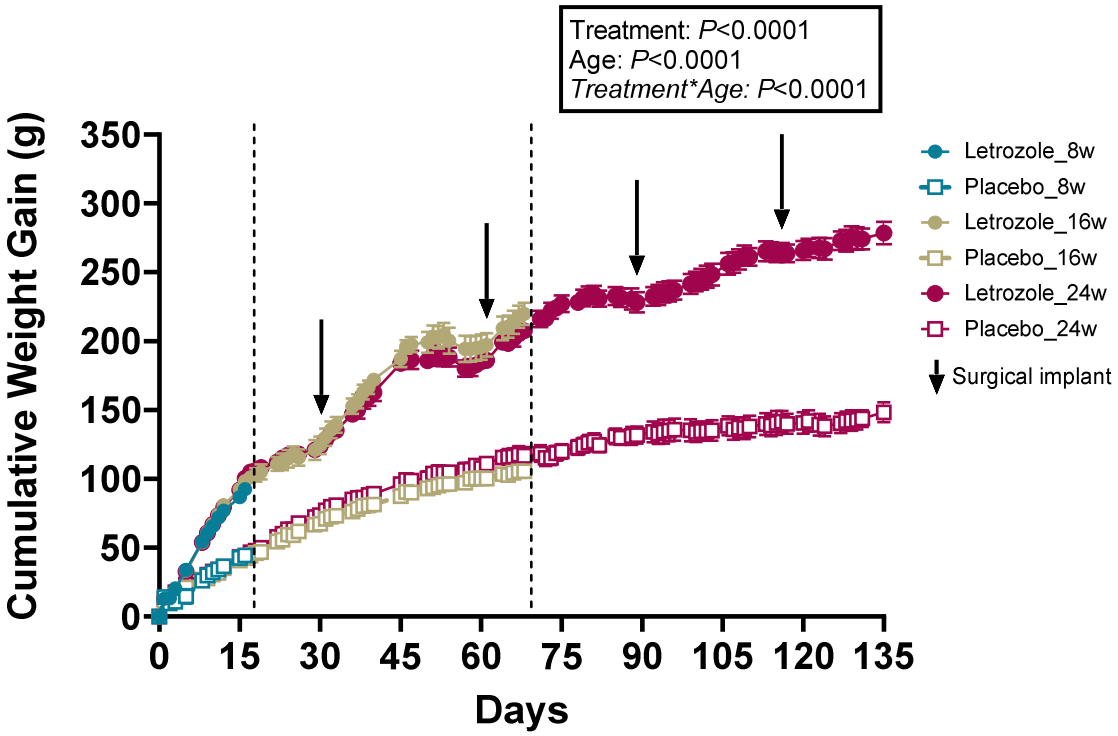

Figure 3-2. Cumulative body weight gain of rats on letrozole and placebo across 8, 16, and 24 wk of age. Data are means ± SEMs; n = 6. Main effects of letrozole and age were tested in a linear mixed-model of repeated measures at significance $P < 0.05$.

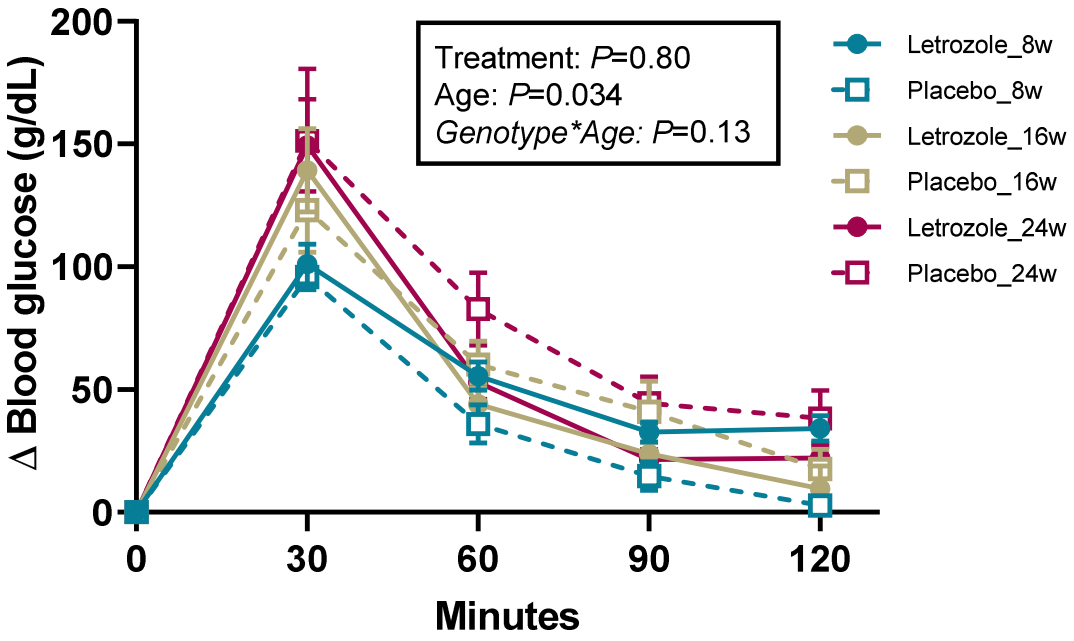

Figure 3-3. Change in blood glucose concentrations in rats on letrozole vs. placebo following an intraperitoneal glucose tolerance test. Data are means ± SEMs; n = 6. Main effects of letrozole and age were tested in a linear mixed-model of repeated measures at significance $P < 0.05$.

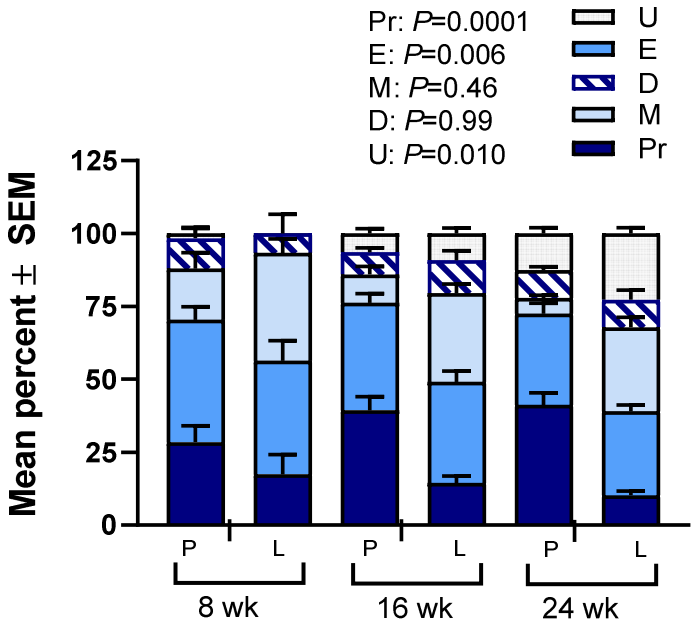

Figure 3-4. Percent frequency of days spent in each stage of the estrous cycle for a total of 30 d. Data are means ± SEMs of the percent frequency; n = 6. Main effects of letrozole and age were tested in a linear mixed-model at significance $P < 0.05$. Abbreviations used: Pr, proestrus; E, estrus; M, metestrus; D, diestrus; and U, pseudodiestrus; P, placebo; and L, letrozole.

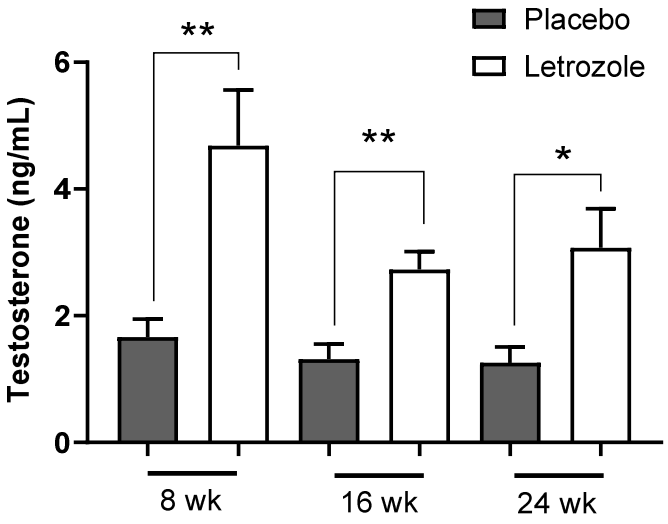

Figure 3-5. Serum testosterone concentrations for letrozole-induced and placebo control SD rats. Data are means ± SEMs; n = 6. Significant differences were assessed by unpaired t-test; $^{*}P < 0.05$, $^{**}P < 0.01$.

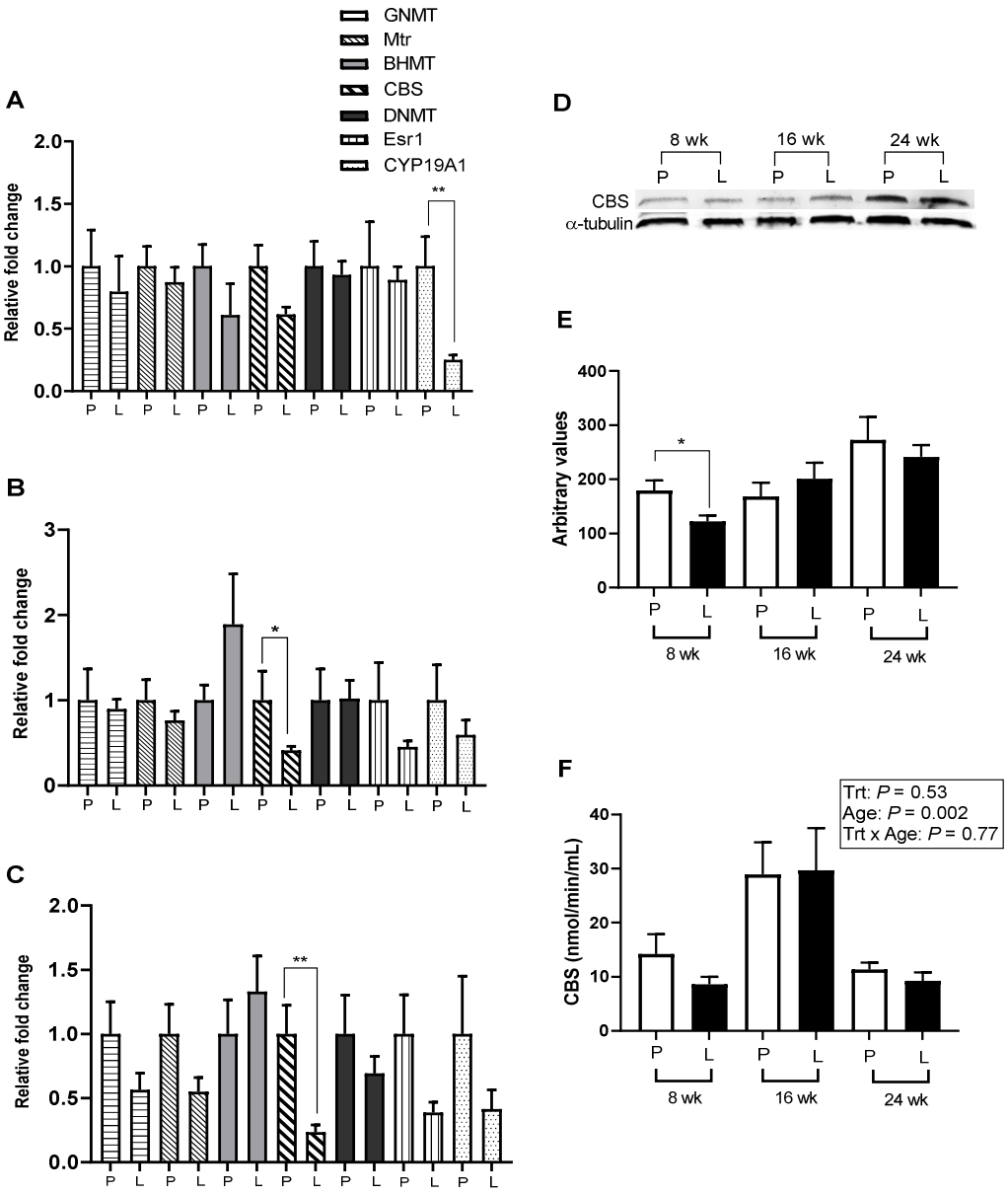

Figure 3-6. Ovarian mRNA abundance of select proteins in letrozole-induced and placebo control SD rats at 8 (A), 16 (B), and 24 (C) wk of age, representative western blot (D), CBS protein abundance (E), and CBS enzyme activity (F). The abundance of mRNA were normalized to 18S ribosomal mRNA and expressed as relative to placebo rats. Data are means ± SEMs of the relative fold change of mRNA transcript abundance, protein abundance, and enzymatic activity, respectively; n = 6/group. Relative fold change, protein abundance, and enzyme activity were compared via an unpaired t-test within in age group and deemed significant at $P < 0.05$. Abbreviations used: *L*, letrozole; *P*, proestrus; *Gnmt,* glycine n-methyltransferase*; Mtr,* methionine synthase*; Bhmt,* betaine-homocysteine S-methyltransferase*; Cbs,* cystathionine beta-synthase*; Dnmt,* DNA methyltransferase*; Esr1,* estrogen receptor 1*; Cyp19A1, cytochrome P450 isoform 19a1*

Table 3-1. Primer sequences for Rattus Norvegicus mRNA qRT-PCR quantification[1].

	Gnmt	TM	GC%
5' to 3'	CAGCAGGAGATGGCTTTGA	57.44	52.63
5' to 3' antisense	CCATGCTTGCGATGTTCTTTAG	58.31	45.45
	Mtr		
5' to 3'	CAGACAGATGAGTGGAGGAATG	58.21	50
5' to 3' antisense	CTGGCTTCTTCAGTGTCTTCA	57.88	47.62
	Bhmt		
5' to 3'	CACCTGTGATTGGTGCTAGTTA	58.06	45.45
5' to 3' antisense	CTGTGGACTTCTCCTTTCTTCC	58.33	50
	Cbs		
5' to 3'	CTTAGCAGTTCCTCCTCACATC	58.21	50
5' to 3' antisense	AGGTAGACATGACCACAGGTA	57.53	47.62
	Dnmt		
5' to 3'	CAGAGGAGAGAGACCAGGATAA	57.82	50
5' to 3' antisense	GGCCTTACTCGTTCAGGTTT	57.82	50
	Esr1		
5' to 3'	AGGCTGCAAGGCTTTCTT	57.06	50
5' to 3' antisense	CAACTCTTCCTCCGGTTCTTATC	58.57	47.83
	Cyp19a1		
5' to 3'	ATTTGTGTGTGTGTGTGTGTG	62	42.9
5' to 3' antisense	GCTCCTACTCCAGGTCTAGTAA	62	50
	18S		
5' to 3'	AAGACGAACCAGAGCGAAAG	62	50
5' to 3' antisense	TCGGAACTACGACGGTATCT	62	50

[1]Abbreviations used: *Gnmt,* glycine n-methyltransferase*; Mtr,* methionine synthase*; Bhmt,* betaine-homocysteine S-methyltransferase*; Cbs,* cystathionine β-synthase*; Dnmt,* DNA methyltransferase*; Esr1,* estrogen receptor 1*; Cyp19A1,* aromatase.

Table 3-2. Relative organ weights of letrozole-induced or placebo Sprague Dawley rats at 8, 16, or 24 wk of age[1].

	8 wk		16 wk		24 wk		P-value		
Tissue	**LET**	**Placebo**	**LET**	**Placebo**	**LET**	**Placebo**	**Trt**	**Age**	**Trt ×Age**
BW (g)	222 ± 4.2	186 ± 3.7	363 ± 5.8	239 ± 4.1	410 ± 9.2	275 ± 8.5	<0.0001	<0.0001	<0.0001
UH (g)	1.14 ± .014**	2.15 ± 21.1	.047 ± .002***	2.42 ± .035	.052 ± .002**	2.73 ± .058	<0.0001	0.76	0.12
Ovary	26.5 ± 1.8*	20.6 ± 0.9	16.4 ± 1.1	14.8 ± 1.3	16.8 ± 0.7	18.7 ± 1.5	0.08	<0.0001	0.02
Kidney (g)	3.4 ± 1.0	3.1 ± 1.0	2.6 ± 1.0	2.9 ± 0.9	2.5 ± 1.1	2.8 ± 0.7	0.20	0.0002	0.06
Adipose	1.0 ± 0.2	0.9 ± 0.0	2.9 ± 0.4	2.2 ± 0.2	3.7 ± 0.3	3.2 ± 0.3	0.14	<0.0001	0.73
Liver	3.8 ± 0.1	3.7 ± 0.1	2.9 ± 0.1	3.0 ± 0.1	2.7 ± 0.1	2.8 ± 0.1	0.61	<0.0001	0.87
BG (g/dL)	86.3 ± 4.5	95.0 ± 3.2	119.8 ± 8.9	108.0 ± 7.3	114.7 ± 3.6	116.0 ± 7.4	0.90	0.0005	0.26

[1] Data are means ± SEMs; n = 6/group. Different from placebo group (*P < 0.05, **P < 0.01, ***P < 0.001). Data within age group determined by unpaired t-test. Overall main (Trt and Age) effects and their interaction (Trt x Age) were determined via a linear mixed model. Abbreviations used: BG, blood glucose; BW, body weight; LET, letrozole; and UH, uterine horn.

CHAPTER 4. POLYCYSTIC OVARY SYNDROME MODULATES BETAINE HOMOCYSTEINE S-METHYLTRANSFERASE IN 8 WEEK OLD FEMALE LETHAL YELLOW AGOUTI MICE

A manuscript prepared for submission to the *Journal of Nutrition*

Amanda E. Bries, Joseph L. Webb, Brooke Vogel, Claudia Carrillo, Samantha K. Pritchard, Aileen F. Keating, and Kevin L. Schalinske

Abstract

Background Polycystic ovary syndrome (PCOS) is a condition that has linked poor oocyte quality with inadequate methyl group supply, yet the literature regarding the pathophysiology of methyl group/one-carbon metabolism (OCM) mediated in PCOS is not well understood.

Objectives The objective of this study was to examine the effects of metabolically perturbed PCOS on OCM in the ovary and liver of mice during the progression of PCOS.

Methods Five wk old female lethal yellow agouti mice (KK.CG-A^y/J; agouti; n = 18), and their wild type (WT) controls (a/a; n = 18), were obtained and acclimated for one wk. Mice were placed on a modified standard AIN93G diet. All mice were randomly assigned to be euthanized in proestrus, at 8, 16, and 24 wk of age, whereas acyclic agouti mice (24 wk of age) were euthanized in diestrus (n = 6/group/genotype). mRNA abundance of the OCM enzymes was evaluated via RT-qPCR. Betaine homocysteine *S*-methyltransferase (BHMT) protein abundance was determined via western blotting. Serum testosterone concentrations were determined via ELISA, and all analyses were performed using an unpaired t-test on each experimental age group ($P < 0.05$).

Results Circulating testosterone concentrations were markedly higher in agouti vs. WT at 16 and 24 wk of age. When compared to WT mice, 8 wk agouti exhibited a 4.6-fold increase and a 27% decrease in *Bhmt* transcript abundance in the ovary and liver, respectively. There was a trend for

decreased hepatic BHMT protein abundance in 8 wk old agouti mice. By 16 wk of age, an observed 44% reduction in ovarian glycine *N*-methyltransferase (*Gnmt*) transcript abundance, along with a 33% reduction in hepatic *Gnmt* at 24 wk old agouti mice was detected. **Conclusion** These data suggest that *Bhmt* is modulated in the ovary and liver during the early onset of PCOS prior to phenotypic changes.

Introduction

Upwards of 20% of premenopausal women are diagnosed with polycystic ovary syndrome (PCOS), an endocrine disorder that is characterized by hyperandrogenism, impaired oogenesis, and ultimately infertility (1). Moreover, the etiology of PCOS is unknown and has been attributed to a combination of both genetic and environmental factors (2), making it challenging to elucidate the mechanisms of this disorder. There is also a high prevalence of comorbidities, such as cardiovascular disease, type 2 diabetes, and obesity in women diagnosed with PCOS (3). Management of PCOS varies on a per-patient basis, as the diagnostic criteria is a complex set of symptoms (4). Therefore, the first line of treatment for PCOS includes lifestyle modifications to induce weight loss as a means to improve ovarian function and lessen the burden of hyperinsulinemia and metabolic anomalies that disrupt the hypothalamic-pituitary-ovarian axis.

Emerging research has identified that women with PCOS present elevated serum homocysteine concentrations, whether obese or not (5). Several studies have also reported an observed vitamin B_{12} deficiency as a secondary indicator of hyperhomocysteinemia in subpopulations with PCOS (6). Homocysteine is regulated by methyl group/one-carbon metabolism (OCM), and homeostasis involves several key substrates and cofactors, specifically, methionine, betaine, choline, and B-vitamins, folate, B_{12}, B_6, and B_2. The interplay and sufficiency of all of these nutrients are critical for maintaining proper methylation status,

antioxidants like glutathione, and homocysteine balance. One carbon metabolism not only influences the pathogenesis of the disease, but the literature indicates that DNA methylation is critical in the maintenance of oocytes quality and maturation – key components of fertility (7,8). Subsequently, inadequate production of methyl groups affects downstream gene expression, which may influence genes involved in androgen production, insulin resistance, among other metabolic anomalies.

The literature surrounding the mechanistic reasoning for the observed perturbations in methyl group-mediated OCM in PCOS is very limited. Research has primarily focused on the physiological role of methylation status on oogenesis and oocyte quality in livestock (9–11), but given the metabolic complexities of PCOS, it is essential to observe these outcomes under conditions representative of human PCOS. Therefore, this study's objective was to investigate and characterize OCM in the ovary and liver during the progression of PCOS with concomitant obesity and impaired metabolic outcomes. This research aims to determine whether PCOS represents a condition further characterized by abnormal OCM, to provide a strategic means of addressing these PCOS-related complications through dietary intervention strategies that support OCM.

Materials and Methods

Animals and Diets. All animal studies were approved by the Institutional Animal Care and Use Committee at Iowa State University (IACUC # 18-294) and were performed according to the Iowa State University Laboratory Animal Resources Guidelines. Female agouti lethal yellow mice (KK.Cg-A^y/J; n = 18) and their wild-type non-agouti mice (a/a; n = 18) were purchased at 4 wk of age from the Jackson Laboratory (Bar Harbor, ME; stock no: 002468). According to their genotype, mice were dual caged with a 12-h light-dark cycle in a temperature-controlled room. All rats were acclimated on a semi-purified diet (AIN-93G) for one wk. Both agouti and

wild-type (WT) mice were randomly assigned to cage and age of sacrifice (8, 16, or 24 wk of age). Mice were given *ab libitum* access to water and a modified standard AIN93G diet containing 50.4% carbohydrate; 17.3% protein, and 32.3% fat from energy. Body weights were recorded daily, and during the last 30 d of the experimental period, vaginal cytology was monitored to determine the patterns of their estrous cycle, as previously described (12). Intraperitoneal glucose tolerance tests (IPGTT) were performed 3 days prior to euthanasia at 8, 16, and 24 weeks of age (n = 6/age/genotype). All WT mice were euthanized in proestrus, and agouti mice were euthanized in proestrus until they reached acyclicity, in which they were euthanized in diestrus (24 wk of age). Mice were anesthetized via a single intraperitoneal injection of ketamine:xylazine (90:10 mg/kg BW) prior to euthanasia via bilateral thoracotomy. Whole blood was collected via cardiac puncture for serum separation, and the epididymal fat pad, liver, kidneys, and ovaries were removed and weighed. One ovary and liver, kidney, and adipose tissue samples were stored in *RNA*later. Sections of the liver, kidney, and adipose were snap-frozen in liquid nitrogen, and all tissues were stored at -80°C until subsequent analysis.

Intraperitoneal glucose tolerance test. Three days prior to euthanasia, mice underwent an IPGTT test over 120 min as described in the Methods section of Chapter 3 in this dissertation.

Assessment of estrous cyclicity. To determine the cyclicity of the mice, vaginal smears were performed in the last 30 d of life. Briefly, vaginal smears were performed from 8-9 am via a lavage using 15 µL of sterile PBS solution. Smears were allowed to dry, followed by staining with methylene blue, as previously described (13,14). Classification of the estrous stage was determined based on the proportion of leukocytes, nucleated epithelial cells, and desquamated

(cornified) epithelial cells (15). Proestrus consisted primarily of nucleated epithelial cells, with a few cornified cells; estrus was characterized by the predominant presence of cornified epithelial cells, with a few nucleated cells; metestrus was classified by the presence of a few cornified cells with an abundance of leukocytes; diestrus was determined by the presence of polymorphonuclear leukocytes and nucleated epithelial cells.

Testosterone. Serum testosterone concentrations were determined using a mouse-specific commercially available enzyme linked-immunosorbent assay (Crystal Chem; Elk Grove Village, IL).

RNA extractions

Total RNA was isolated from one-half of an ovary. Briefly, the ovarian tissue was lysed in RNA lysis buffer, and total RNA was extracted and purified using 15 uL of elution buffer from Zymo Research Quick RNA-miniprep extraction kit (R1054; Zymo Research, Irvine, CA). Before reverse transcription cDNA conversion using the Agilent High Capacity cDNA kit (Thermo-Fisher Scientific), total RNA concentrations were measured via spectrophotometry (λ= 260/280 nm of ~2.0) using a Nanodrop 2000 (Thermo Fisher Scientific).

Quantitative real-time PCR (qRT-PCR)

Primers (**Table 4-1**) were designed and obtained from Integrated DNA Technologies (Coralville, IA) using the NCBI accession number for the corresponding gene. Quantitative reverse transcription PCR reactions were performed on each sample in triplicate using 30ng of cDNA, a forward and reverse final primer concentration of 0.3 µM, and LightCycler FastStart Master

SYBR Green 1 (no. 03003230001; Roche) on a LightCyler 96-well Real-time PCR System (Roche) according to manufacturer's instructions. CT values were normalized to 18S ribosomal mRNA and presented as a relative-fold change to the WT mice. Amplification efficiencies of target and reference gene assays were verified, and data were analyzed using the Livak, delta-delta CT method for relative mRNA expression (16).

Western blot. Liver (20 mg) was homogenized in 500 µL in lysis buffer [Tris-HCl (50 mmol/L, pH 7.4), 1 mmol/L of EDTA, EGTA, DTT, glycerol (10%, w/v), and Triton-X (1%, w/v)] with halt protease inhibitor cocktail (Thermo Fisher Scientific, no. 78439). Liver lysates were diluted to 2.0 µg/µL in Laemmli loading buffer with protein quantities determined via Pierce Coomassie Bradford assay (ThermoFisher Scientific, no. 23236). A total of 40 µg protein was loaded onto a 15% sodium dodecyl sulfate-polyacrylamide gel and separated via electrophoresis (80 min; 200V) in cold 1X Tris-Glycine SDS buffer. After separation, proteins were transferred to a nitrocellulose membrane via a fully-wet transfer in cold towbin buffer (25 mM Tris, 192 mM glycine, 20% v/v methanol, pH 8.3) for 120 min at 100V. All membranes were stained with Ponceau S to verify equal loading and transfer efficiency. Membranes were washed with PBS and incubated with BHMT (1:200 dilution) and α-tubulin (1:400 dilution) primary antibodies (BHMT, santa cruz, H-7 sc-69708; α-tubulin, cat. no sc-5286; ThermoFisher Scientific) in 5% non-fat dry milk/PBS-tween buffer, overnight at 4˚C. After 3 washes with PBS-tween, membranes were incubated with a secondary antibody (IRDye 800CW Goat anti-Mouse cat no. 926-32210 and 600CW Goat anti-rabbit cat. no 926-68021) at a dilution of 1:5,000 for 1 h at room temperature. Membranes were washed 4 times, 10 min each, in PBS-tween before imaging via digital fluorescence detection using an Odyssey CLx imaging system (Li-Cor). The net

intensity of each band was determined using Empiria Studio Software (Li-Cor) and normalized to α-tubulin.

Statistical Analysis. All data were analyzed with SAS 9.4 Statistic Software (Cary, NC), and residuals were assessed for normal distribution of the data. Normally distributed data are presented as means ± SEMs and analyzed using unpaired t-tests between genotypes (i.e. WT and agouti) within each age, as detailed previously (17). A linear mixed model with an analysis of main effects of genotype and age in addition to simple effects were reported when the function of age was considered (e.g. IPGTT and BW). Satterthwaite approximations were used to estimate degrees of freedom for post-hoc tests. Statistical significance for both methods of testing was determined at a level of $P < 0.05$.

Results

Cumulative body weight gain differed between genotypes and as a function of age. Significant main effects on change in cumulative body weight gain were detected ($P < 0.001$) as both a result in the genotype and age of the mice **(Figure 4-1)**. Furthermore, there was a significant interaction between age and genotype on cumulative body weight gain, but analysis of simple effects did not detect differences between genotypes within age groups (Figure 4-1). Interestingly, when t-tests were performed on absolute body weight at each experimental age (i.e., 8, 16, and 24 wk), only agouti mice at 16 wk of age had significantly higher final body weight when compared to their WT counterparts ($P = 0.03$; **Table 4-2**).

Agouti mice exhibited higher fasting blood glucose than wild-type mice. When examining the main effects of the IPGTT, there was a significant finding of the genotype on glucose intolerance ($P < 0.001$; **Figure 4-2**). Additionally, there was a significant main effect of glucose intolerance

on age ($P = 0.013$). There was no significant interaction between genotype and age ($P = 0.49$); therefore no simple effects were performed. When examining differences in fasting blood glucose (BG), fasting BG concentrations were 38% higher at 8 and 16 wk of age in the agouti mice when compared to the WT mice ($P = 0.02$ and $P = 0.001$, respectively; **Table 4-2**). Interestingly, fasting BG concentrations were not found to differ between genotypes in mice at 24 wk of age ($P = 0.26$).

Agouti mice had perturbed estrous cyclicity by 24 wk of age. Percent frequency of occurrence in each stage of the estrous cycle are presented in **Figure 4-3.** When examining the main effects of frequency in proestrus, overall, WT mice cycled exhibited increased frequency ofproestrus compared to agouti mice ($P = 0.03$). Similarly, WT mice were in estrus at a higher percentage of time compared to their agouti counterparts ($P < 0.006$). Conversely, overall main effects demonstrated that agouti mice were in diestrus more frequent than WT mice ($P < 0.0001$). When examining simple effects, agouti mice exhibited acyclicity at 24 wk of age with a decrease in the frequency of proestrus ($P = 0.002$) and estrus ($P = 0.007$) when compared to WT mice. Moreover, by 24 wk of age, agouti mice arrested in diestrus (80% of the last 30 d of life), compared to WT mice ($P <0.0001$) that were in diestrus 31% of the time. Significant differences in perturbed estrous cyclicity between the genotypes at a given age were not reported at 8 wk or 16 wk of age, however, trends for decreased frequency of estrus ($P = 0.06$) and increased frequency of diestrus ($P = 0.07$) in the agouti mice compared to WT were observed.

Organ weights. As expected, there was a significant main effect of genotype on uterine horn weight ($P < 0.0001$; **Table 4-2**). This was primarily driven by the agouti mice that exhibited a

68% reduction in uterine horn weight compared to their WT counterparts ($P < 0.0001$). It is not surprising that these findings were not observed at 8 or 16 wk of age mice, as the 24 wk old mice were euthanized in diestrus as a result of acyclicity, introducing discrepancies in uterine horn weight.

Agouti mice had elevated circulating testosterone concentrations. Testosterone concentrations are presented in **Figure 4-4.** There were significant differences in serum testosterone concentrations in the agouti mice compared to the WT at 16 and 24 wk of age. Specifically, circulating testosterone concentrations were 38% higher in the agouti mice compared to the WT mice ($P = 0.04$; Figure 4-4) at 16 wk of age. By 24 wk of age, agouti exhibited 68% elevated serum testosterone concentrations when compared to WT control mice ($P = 0.008$; Figure 4-4). No differences were observed in circulating testosterone concentrations between the agouti and WT mice at 8 wk of age ($P = 0.26$; Figure 4-4).

Agouti mice presented a transient response to ovarian and hepatic BHMT mRNA abundance. We characterized the transcript abundance of the central enzymes in the OCM pathway in both the ovary and liver of agouti and WT mice at 8, 16, and 24 wk of age. These results are presented in **Figure 4-5.** Interestingly, agouti mice displayed a transient response in *Bhmt* and *Dnmt1* mRNA abundance, resulting in 4.56-fold ($P = 0.04$) and 2.2-fold $P = 0.05$) higher transcript abundance, respectively, at 8 wk of age when compared to WT mice; whereas this was not observed at 16 or 24 wk of age (Figure 4-5). Conversely, in agouti mice hepatic *Bhmt* mRNA abundance was attenuated 27% in the agouti mice compared to WT mice at 8 wk of age ($P =$ 0.03). Likewise, there was no significant difference in hepatic *Bhmt* transcript abundance at 16 or

24 wk of age. In agouti mice, a 44% reduction in *Gnmt* transcript abundance was observed in the ovary at 16 wk of age ($P = 0.03$), and a 33% reduction in *Gnmt* occurred in the liver of agouti mice at 24 wk of age ($P = 0.009$). No differences were observed in ovarian or hepatic *Gnmt* at any other age. All other mRNA transcript abundances for the genes encoding the remaining OCM enzymes were unchanged.

Western blots. When examining the relative protein abundance of hepatic BHMT, there was a tendency for diminished BHMT protein abundance in the agouti mice at 8wk of age ($P = 0.09$; **Figure 4-6**). There were no observed differences in BHMT protein abundance at 16 or 24 wk of age.

Discussion

Polycystic ovary syndrome is a condition with an array of metabolic insults, often manifesting in comorbidities such as diabetes, obesity, and cardiovascular disease (4,18). Hyperhomocysteinemia has been long appreciated as an independent risk factor for cardiovascular disease, but it has also been implicated in PCOS. For instance, several prospective studies have reported elevated homocysteine levels in patients with PCOS, irrespective of obesity (5,19). The role of hyperhomocysteinemia and its determinants in the pathogenesis of disease remains inconclusive. Intervention trials employing micronutrients that support OCM have demonstrated promising results in correcting circulating homocysteine concentrations, thereby reducing disease risk (20–22). Moreover, the provision of methyl groups is critical for folliculogenesis, ovulation, and reproduction as a whole (8); therefore, we hypothesized that the progression of PCOS would be characterized by altered one-carbon metabolism. To address this question, we chose the lethal yellow agouti mouse, as it is an excellent model for progressive obesity, and it is accompanied by acyclicity and disrupted folliculogenesis, providing a strong

model for PCOS (23). The time points selected were based on the model providing temporally compromised fertility, concomitant with hyperinsulinemia, insulin resistance, hyperphagia, and obesity beginning at 12 wk of age (24–26).

Homocysteine is a non-proteinogenic amino acid that contains a sulfur group and is endogenously biosynthesized from the essential amino acid, methionine (27). Homocysteine concentrations are regulated via three pathways: 1) folate-dependent remethylation; 2) folate-independent remethylation; and 3) transsulfuration. The conversion of methionine to homocysteine is critical for the catabolic generation of cysteine and subsequent glutathione production. Furthermore, homocysteine is a central product of S-adenosylmethionine (SAM)-dependent transmethylation reactions, whereby the donated methyl groups are used in the epigenetic regulation of DNA silencing and posttranslational modifications. Several nutrients, such as folate, vitamin B_{12}, B_2, B_6 and choline, play an essential role in one-carbon metabolism, and insufficient supply in any one of these nutrients over time leads to hyperhomocysteinemia (28). It is important to explore the OCM characteristics in a PCOS model given the association-based studies that have been reported (19,20,29) to mechanistically examine the effects of PCOS and identify an intervention strategy.

PCOS progression was verified in our agouti lethal yellow model as indicated by acyclicity by 24 wk of age, accompanied by a decrease in the frequency of time spent in proestrus and estrus, leading to prolonged diestrus. Our findings are corroborated by previous studies employing this model (23,26). Circulating testosterone concentrations were also used as a confirmatory measure, as the heterogeneity of the agouti genotype can introduce variable ectopic agouti protein expression levels, resulting in a spectrum of metabolic severity (30). We did identify significantly elevated serum testosterone concentrations but only at 16 and 24 wk of age.

This is consistent with previous reports of metabolic characteristics such as hyperinsulinemia, impaired fasting blood glucose, and increased body weight observed as early as 12 wk of age (23). It is important to note that our findings were not associated with cumulative body weight gain, but we hypothesize this phenotypic outcome may have been influenced by exposure to a moderately high-fat diet (37% kcal from fat). The a/a wild-type mice's growth rate was comparable to the agouti mice at 24 wk of age, but the inverse was reported at 8 and 16 wk of age. These observations have been demonstrated in the KK.CG-a/a mice continuously fed a high-fat diet between 20-26 wk of age (31), whereby there was a significant effect of high-fat diet on the growth rate in the wild type mice when compared to its control on the standard chow diet. Despite these observations, we did verify the presence of altered estrous cyclicity and metabolic anomalies characteristic of PCOS in our agouti model.

To our knowledge, only two studies to date have examined the OCM pathway in an animal model of PCOS. In gilts with polycystic ovaries, an observed increase in follicular homocysteine concentrations was reported in association with an upregulation of several key OCM enzymes (10,11). Poor oocyte quality as an outcome of PCOS has also been associated with high serum homocysteine concentrations in cohorts undergoing assisted reproductive treatment (32). There is no mechanistic research describing these associations, but elevated homocysteine has been observed as a product of aging, endometriosis, and ovarian cancer (33–35). The corollary is that elevated homocysteine indirectly inhibits nitric oxide production, which may explain the poor oocyte quality as diminished nitric oxide concentrations can lead to arrest in ovulation, follicular atresia, and impaired early embryonic development (34,36). Furthermore, the irreversible catabolism of homocysteine is essential for the downstream production of glutathione via the transsulfuration pathway. Elevated follicular homocysteine concentrations

have been subject to lower intracellular glutathione concentrations due to decreased cystathionine β-synthase enzymatic activity (37). Taken together, the lack of nitric oxide and glutathione production may account for increased reactive oxygen species, leading to a propensity for low quality follicles and impaired reproduction. These molecular mechanisms have yet to be explored under conditions reflective of PCOS, but experiments assessing these indicators are warranted.

Numerous studies have demonstrated epigenetic modifications, namely, altered methylation patterns in oocytes under various environmental conditions (37,38). The establishment of DNA methylation via DNMTs is crucial for the proper regulation of gene expression and genomic imprinting during oogenesis (39–41). Failure to regulate repetitive sequences during folliculogenesis alters the genetic expression of subsequent genes (39). DNA methyltransferase-1 (DNMT1) catalyzes the methylation of CpG-rich regions, requiring the biosynthesis of the ubiquitous methyl donor, s-adenosylmethionine (SAM). Interestingly, *Dnmt1* expression is decreased in oocytes of aging mice (42,43) and hyperandrogenized mice treated with dehydroepiandrosterone (44), suggesting imbalanced methylation patterns as a result of senescence and hyperandrogenism. On the contrary, Jia et al. (10) reported elevated *Dnmt1,* accompanied by hypermethylated mitochondrial DNA in ovaries of gilts with PCOS. The consequences of hypermethylated mitochondrial DNA was associated with impaired oocyte quality (10). Similarly, our results demonstrated a 2.2-fold elevation in *Dnmt1* transcript abundance, but only in our 8 wk old agouti model. These results, combined with findings in the literature, suggest perturbed methylation patterns during the early onset of PCOS.

In addition to *Dnmt1,* our 8 wk old agouti mice exhibited increased ovarian *Bhmt* mRNA abundance, but attenuated hepatic *Bhmt* abundance. Bhmt is a metalloenyzme that requires zinc

as a cofactor for its catalytic function in recycling homocysteine back to methionine via the folate-independent remethylation pathway (27). BHMT is also important for the biosynthesis of SAM; therefore, inhibition of BHMT leads to hyperhomocysteinemia and hypomethylation, owing to depletion in SAM concentrations (45). Studies determining the role of BHMT in PCOS remain scant, but few studies have reported perturbed BHMT activity during oocyte maturation (10,37,46). Tian et al. determined that oocyte BHMT inhibition resulting from acute zinc deficiency, led to drastic shifts in global DNA methylation and compromised oocyte integrity (47). They attributed the alterations in oocyte quality to hypomethylation, as zinc deficient oocytes supplemented with s-adenosylmethionine (SAM) restored oocyte maturation. It is important to note that this in vitro model does not entirely reflect the conditions of PCOS. Furthermore, the determinants exhibited by SAM supplementation on oocytes are similar to ovarian response to circulating levels of SAM. Therefore, it is possible that our observed decrease in hepatic *Bhmt* more closely aligns with the results of the zinc-deficient model. Considering the liver is a significant supplier of methyl groups for subsequent organs, the observed alterations in ovarian *Bhmt, Dnmt1,* and *Gnmt* may reflect its response to disrupted hepatic OCM. Moreover, it is important to distinguish that these findings were only detected in our 8wk old mice, but elevated ovarian *Bhmt* has been reported in a gilt (10), androgen-receptor knockout mouse model (48), and reported in a letrozole-induced rat model of PCOS (Chapter 3).

Several limitations should be considered when determining the impact of PCOS on ovarian and hepatic OCM. First, in order to adequately characterize the effects of PCOS on OCM to set the foundation for future nutrition intervention studies, we employed a modified AIN93G diet containing 37% kcal from fat, whereas standard AIN93G diet for rodent contains 17% kcal from fat. We recognize that our diet was a moderately high fat diet, as 45% kcal from

fat is considered to be a high fat diet, potentially introducing variable phenotypic outcomes between the agouti and wild-type mice, such as cumulative body weight gain and fasting blood glucose indicators. Future studies will examine the effects of diets supplemented with dietary methyl groups in order to understand how nutrition may play a role in the OCM burden of progressive PCOS. This study's control diet is the same control diet that will be used for future dietary methyl group intervention studies. Another limitation was that we did not verify the follicular or homocysteine concentrations in our model, as this has been explored and reported on numerous occasions (10,11,17,49), and we plan to make these observations in a dietary intervention study in a model of PCOS.

Conclusion

Our data and findings, in combination with our chemically-induced model of PCOS (Chapter 3 of this dissertation) suggest that BHMT and CBS-mediated hyperhomocysteinemia may be a result of the onset and progression of PCOS in response to perturbed hepatic OCM regulation. Although the data presented in this paper are primarily descriptive, our findings make substantial strides towards better understanding the implications of PCOS on OCM beyond biomarker association studies. Determining the transient response of OCM in both the liver and ovaries of progressive PCOS allows us to further explore the pathogenesis and identify a suitable nutrition-based strategy in attenuating the long-term metabolic consequences from PCOS.

References

1. Wolf WM, Wattick RA, Kinkade ON, Olfert MD. Geographical Prevalence of Polycystic Ovary Syndrome as Determined by Region and Race/Ethnicity. *Int J Environ Res Public Health*. 2018; 15.

2. Rosenfield RL, Ehrmann DA. The Pathogenesis of Polycystic Ovary Syndrome (PCOS): The Hypothesis of PCOS as Functional Ovarian Hyperandrogenism Revisited. *Endocr Rev*. 2016; 37:467–520.

3. Caldwell ASL, Middleton LJ, Jimenez M, Desai R, McMahon AC, Allan CM, Handelsman DJ, Walters KA. Characterization of reproductive, metabolic, and endocrine features of polycystic ovary syndrome in female hyperandrogenic mouse models. *Endocrinology*. 2014; .

4. Ibáñez L, Oberfield SE, Witchel S, Auchus RJ, Chang RJ, Codner E, Dabadghao P, Darendeliler F, Elbarbary NS, Gambineri A, et al. An International Consortium Update: Pathophysiology, Diagnosis, and Treatment of Polycystic Ovarian Syndrome in Adolescence. *Horm Res Paediatr*. 2017; 88:371–95.

5. Maleedhu P, Vijayabhaskar M, Sharma SSB, Kodumuri PK, Vasundhara Devi D. Status of homocysteine in polycystic ovary syndrome. *J Clin Diagnostic Res*. 2014; 8:31–3.

6. Kaya C, Cengiz SD, Satıroğlu H. Obesity and insulin resistance associated with lower plasma vitamin B12 in PCOS. *Reprod Biomed Online*. 2009; 19:721–6.

7. Wei Y, Lang J, Zhang Q, Yang CR, Zhao ZA, Zhang Y, Du Y, Sun Y. DNA methylation analysis and editing in single mammalian oocytes. *Proc Natl Acad Sci U S A*. 2019; 116:9883–92.

8. Sagvekar P, Kumar P, Mangoli V, Desai S, Mukherjee S. DNA methylome profiling of granulosa cells reveals altered methylation in genes regulating vital ovarian functions in polycystic ovary syndrome. *Clin Epigenetics*. 2019; 11:61.

9. Boddicker RL, Koltes JE, Fritz-Waters ER, Koesterke L, Weeks N, Yin T, Mani V, Nettleton D, Reecy JM, Baumgard LH, et al. Genome-wide methylation profile following prenatal and postnatal dietary omega-3 fatty acid supplementation in pigs. *Anim Genet*. 2016; 47:658–71.

10. Jia L, Li J, He B, Jia Y, Niu Y, Wang C, Zhao R. Abnormally activated one-carbon metabolic pathway is associated with mtDNA hypermethylation and mitochondrial malfunction in the oocytes of polycystic gilt ovaries. *Sci Rep*. 2016; 6.

11. Jia L, Zeng Y, Hu Y, Liu J, Yin C, Niu Y, Wang C, Li J, Jia Y, Hong J, et al. Homocysteine impairs porcine oocyte quality via deregulation of one-carbon metabolism and hypermethylation of mitochondrial DNA†. *Biol Reprod*. 2019; 100:907–16.

12. Ganesan S, Nteeba J, Keating AF. Impact of obesity on 7,12-dimethylbenz[a]anthracene-induced altered ovarian connexin gap junction proteins in female mice. *Toxicol Appl Pharmacol*. 2015; 282:1–8.

13. Nteeba J, Ortinau LC, Perfield JW, Keating AF. Diet-induced obesity alters immune cell infiltration and expression of inflammatory cytokine genes in mouse ovarian and peri-ovarian adipose depot tissues. *Mol Reprod Dev*. 2013; 80:948–58.

14. Yener T, Turkkani Tunc A, Aslan H, Aytan H, Caliskan AC. Determination of oestrous cycle of the rats by direct examination: How reliable? *J Vet Med Ser C Anat Histol Embryol*. 2007; 36:75–7.

15. Byers SL, Wiles M V., Dunn SL, Taft RA. Mouse estrous cycle identification tool and images. *PLoS One*. 2012; 7:e35538.

16. Livak KJ, Schmittgen TD. Analysis of Relative Gene Expression Data Using Real-Time Quantitative PCR and the 2−ΔΔCT Method. *Methods*. 2001; 25:402–8.

17. Nteeba J, Ganesan S, Keating AF. Progressive Obesity Alters Ovarian Folliculogenesis with Impacts on Pro-Inflammatory and Steroidogenic Signaling in Female Mice1. *Biol Reprod*. 2014; 91:86.

18. Guzick DS. Cardiovascular Risk in PCOS. *J Clin Endocrinol Metab*. 2004; 89:3694–5.

19. Salehpour S, Manzor-Al-Ajdad O, Samani EN, Abadi A. Evaluation of homocysteine levels in patients with polycystic ovarian syndrome. *Int J Fertil Steril*. 2011; 4:168–71.

20. Eskandari Z, Sadrkhanlou RA, Nejati V, Tizro G. PCOS women show significantly higher homocysteine level, independent to glucose and E2 level. *Int J Reprod Biomed*. 2016; 14:495–500.

21. Regidor P-A, Schindler AE, Lesoine B, Druckman R. Management of women with PCOS using myo-inositol and folic acid. New clinical data and review of the literature. *Horm Mol Biol Clin Investig*. 2018; 0.

22. Asemi Z, Karamali M, Esmaillzadeh A. Metabolic response to folate supplementation in overweight women with polycystic ovary syndrome: A randomized double□blind placebo□controlled clinical trial. *Mol Nutr Food Res*. 2014; 58:1465–73.

23. Nteeba J, Ganesan S, Keating AF. Progressive Obesity Alters Ovarian Folliculogenesis with Impacts on Pro-Inflammatory and Steroidogenic Signaling in Female Mice1. *Biol Reprod*. 2014; 91:86.

24. Granholm NH, Jeppesen KW, Japs RA. Progressive infertility in female lethal yellow mice (A(y)/a; strain C57BL/6J). *J Reprod Fertil*. 1986; 76:279–87.

25. Brannian JD, Furman GM, Diggins M. Declining fertility in the lethal yellow mouse is related to progressive hyperleptinemia and leptin resistance. *Reprod Nutr Dev*. 2005; 45:143–50.

26. Nteeba J, Ganesan S, Keating AF. Impact of Obesity on Ovotoxicity Induced by 7,12-dimethylbenz[a]anthracene in Mice1. *Biol Reprod*. 2014; 90:68.

27. Schalinske KL, Smazal AL. Homocysteine Imbalance: a Pathological Metabolic Marker. *Adv Nutr*. 2012; 3:755–62.

28. Selhub J. Homocysteine Metabolism. *Annu Rev Nutr*. 1999; 19:217–46.

29. Berker B, Kaya C, Aytac R, Satiroglu H. Homocysteine concentrations in follicular fluid are associated with poor oocyte and embryo qualities in polycystic ovary syndrome patients undergoing assisted reproduction. *Hum Reprod*. *Narnia*. 2009; 24:2293–302.

30. Dolinoy DC. The agouti mouse model: an epigenetic biosensor for nutritional and environmental alterations on the fetal epigenome. *Nutr Rev*. 2008; 66 Suppl 1:S7-11.

31. O'Brien SP, Smith M, Ling H, Phillips L, Weber W, Lydon J, Maloney C, Ledbetter S, Arbeeny C, Wawersik S. Glomerulopathy in the KK.Cg- Ay/J mouse reflects the pathology of diabetic nephropathy. *J Diabetes Res*. 2013; 2013:13.

32. Berker B, Kaya C, Aytac R, Satiroglu H. Homocysteine concentrations in follicular fluid are associated with poor oocyte and embryo qualities in polycystic ovary syndrome patients undergoing assisted reproduction. *Hum Reprod*. 2009; 24:2293–302.

33. Razi Y, Eftekhar M, Fesahat F, Dehghani Firouzabadi R, Razi N, Sabour M, Razi MH. Concentrations of homocysteine in follicular fluid and embryo quality and oocyte maturity in infertile women: a prospective cohort. *J Obstet Gynaecol* 2020; 1-6.

34. Ocal P, Ersoylu B, Cepni I, Guralp O, Atakul N, Irez T, Idil M. The association between homocysteine in the follicular fluid with embryo quality and pregnancy rate in assisted reproductive techniques. *J Assist Reprod Genet*. 2012; 29:299–304.

35. Zhu H, Blake S, Chan KT, Pearson RB, Kang J. Cystathionine β-Synthase in Physiology and Cancer. *Biomed Res Int*. 2018; 3205125.

36. Maul H, Longo M, Saade G, Garfield R. Nitric Oxide and its Role During Pregnancy: From Ovulation to Delivery. *Curr Pharm Des*. 2005; 9:359–80.

37. Kwong WY, Adamiak SJ, Gwynn A, Singh R, Sinclair KD. Endogenous folates and single-carbon metabolism in the ovarian follicle, oocyte and pre-implantation embryo. *Reprod*. 2010; 139:705–15.

38. Ge ZJ, Schatten H, Zhang CL, Sun QY. Oocyte ageing and epigenetics. *Reprod.* 2015; 149:R103–14.

39. Kierszenbaum AL. Genomic imprinting and epigenetic reprogramming: Unearthing the garden of forking paths. *Mol Reprod Dev*. 2002; 63:269–72.

40. Branco MR, Oda M, Reik W. Safeguarding parental identity: Dnmt1 maintains imprints during epigenetic reprogramming in early embryogenesis. *Genes and Dev*. 2008. p. 1567–71.

41. Lodde V, Modina SC, Franciosi F, Zuccari E, Tessaro I, Luciano AM. Localization of DNA methyltransferase-1 during oocyte differentiation, in vitro maturation and early embryonic development in cow. *Eur J Histochem*. 2009; 53:24.

42. Hamatani T, Falco G, Carter MG, Akutsu H, Stagg CA, Sharov AA, Dudekula DB, VanBuren V, Ko MSH. Age-associated alteration of gene expression patterns in mouse oocytes. *Hum Mol Genet*. 2004; 13:2263–78.

43. Pan H, Ma P, Zhu W, Schultz RM. Age-associated increase in aneuploidy and changes in gene expression in mouse eggs. *Dev Biol*. 2008; 316:397–407.

44. Eini F, Novin MG, Joharchi K, Hosseini A, Nazarian H, Piryaei A, Bidadkosh A. Intracytoplasmic oxidative stress reverses epigenetic modifications in polycystic ovary syndrome. *Reprod Fertil Dev*. 2017; 29:2313–23.

45. Collinsova M, Strakova J, Jiracek J, Garrow TA. Inhibition of Betaine-Homocysteine S-Methyltransferase Causes Hyperhomocysteinemia in Mice. *J Nutr*. 2006; 136:1493–7.

46. Li D, Liu HX, Fang YY, Huo JN, Wu QJ, Wang TR, Zhou YM, Wang XX, Ma XX. Hyperhomocysteinemia in polycystic ovary syndrome: decreased betaine-homocysteine methyltransferase and cystathionine β-synthase-mediated homocysteine metabolism. *Reprod Biomed Online*. 2018; 37:234–41.

47. Tian X, Diaz FJ. Acute dietary zinc deficiency before conception compromises oocyte epigenetic programming and disrupts embryonic development. *Dev Biol*. 2013; 376:51–61.

48. Shiina H, Matsumoto T, Sato T, Igarashi K, Miyamoto J, Takemasa S, Sakari M, Takada I, Nakamura T, Metzger D, et al. Premature ovarian failure in androgen receptor-deficient mice. *Proc Natl Acad Sci*. 2006; 103:224–9.

49. Ganesan S, Nteeba J, Keating AF. Impact of obesity on 7,12-dimethylbenz[a]anthracene-induced altered ovarian connexin gap junction proteins in female mice. *Toxicol Appl Pharmacol*. 2015; 282:1–8.

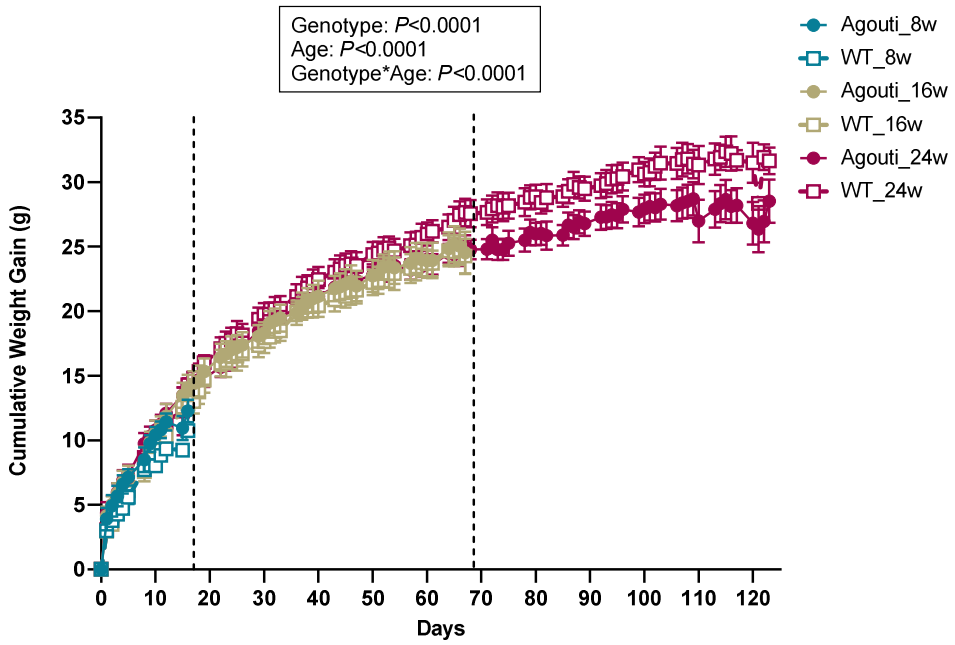

Figure 4-1: Cumulative body weight gain of agouti and wild-type mice across 8, 16, and 24 wk of age. Vertical dotted lines represent the end of an experimental period at 8 and 16 wk of age. Data are means ± SEMs; $n = 6$. Main effects of genotype and age were tested in a linear mixed-model of repeated measures at significance $P < 0.05$.

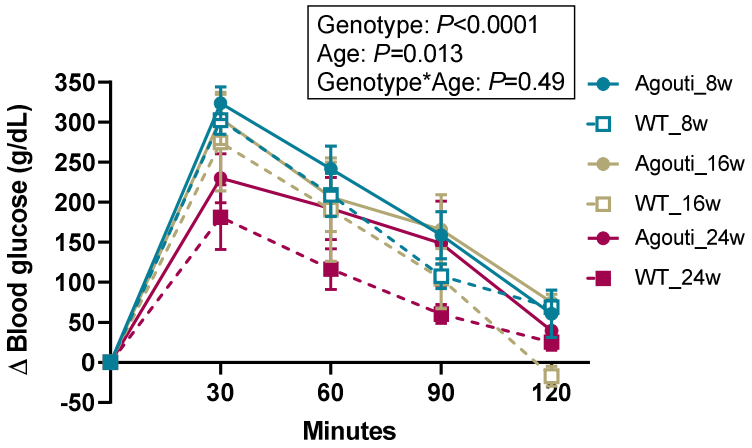

Figure 4-2: Change in blood glucose concentrations in agouti and their wild-type mice following an intraperitoneal glucose tolerance test. Data are means ± SEMs; $n = 6$. Main effects of genotype and age were tested in a linear mixed-model of repeated measures at significance $P < 0.05$.

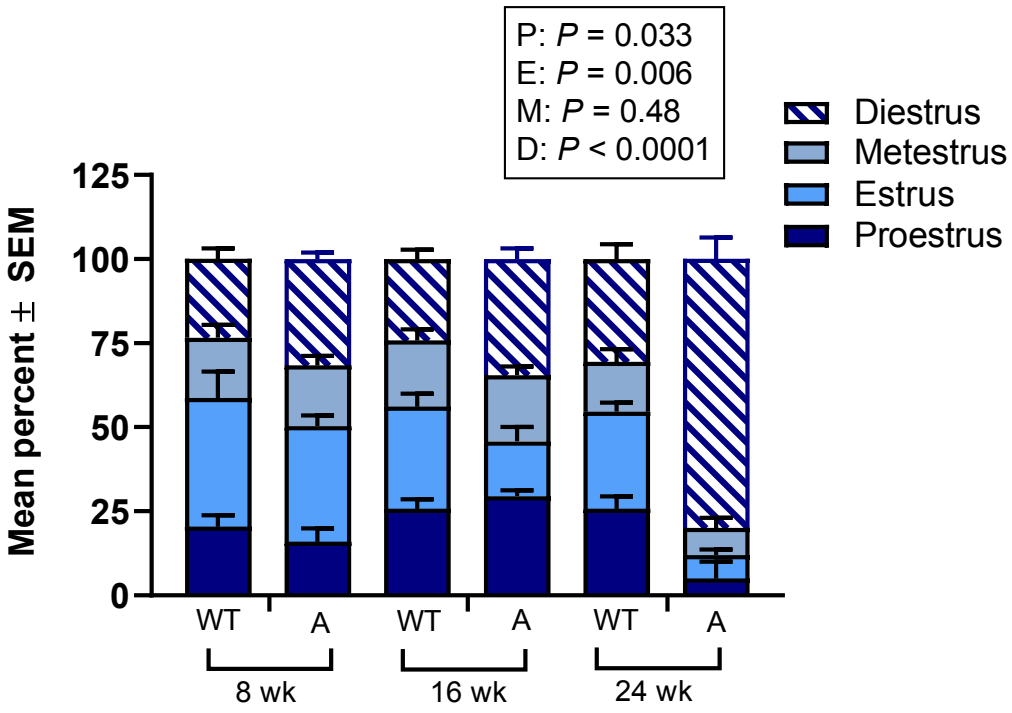

Figure 4-3: Distribution of the days spent in the four stages of the estrous cycle over a total of 30d. Data are means ± SEMs of the percent frequency; $n = 6$. Main effects of genotype and age were tested in a linear mixed-model at significance $P < 0.05$. Abbreviations used: P, proestrus; E, estrus; M, metestrus; and D, diestrus; WT, wild type; and A, agouti.

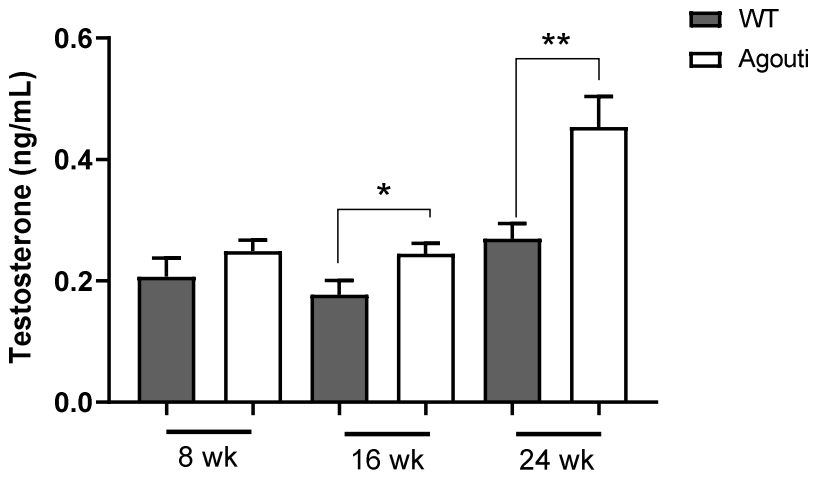

Figure 4-4: Serum testosterone concentrations (ng/mL) in agouti and WT mice. Data are means ± SEMs; $n = 6$/group, *P < 0.05, **P < 0.01. Data were analyzed via unpaired t-test at a significance of $P < 0.05$. Abbreviations used: WT, wild type.

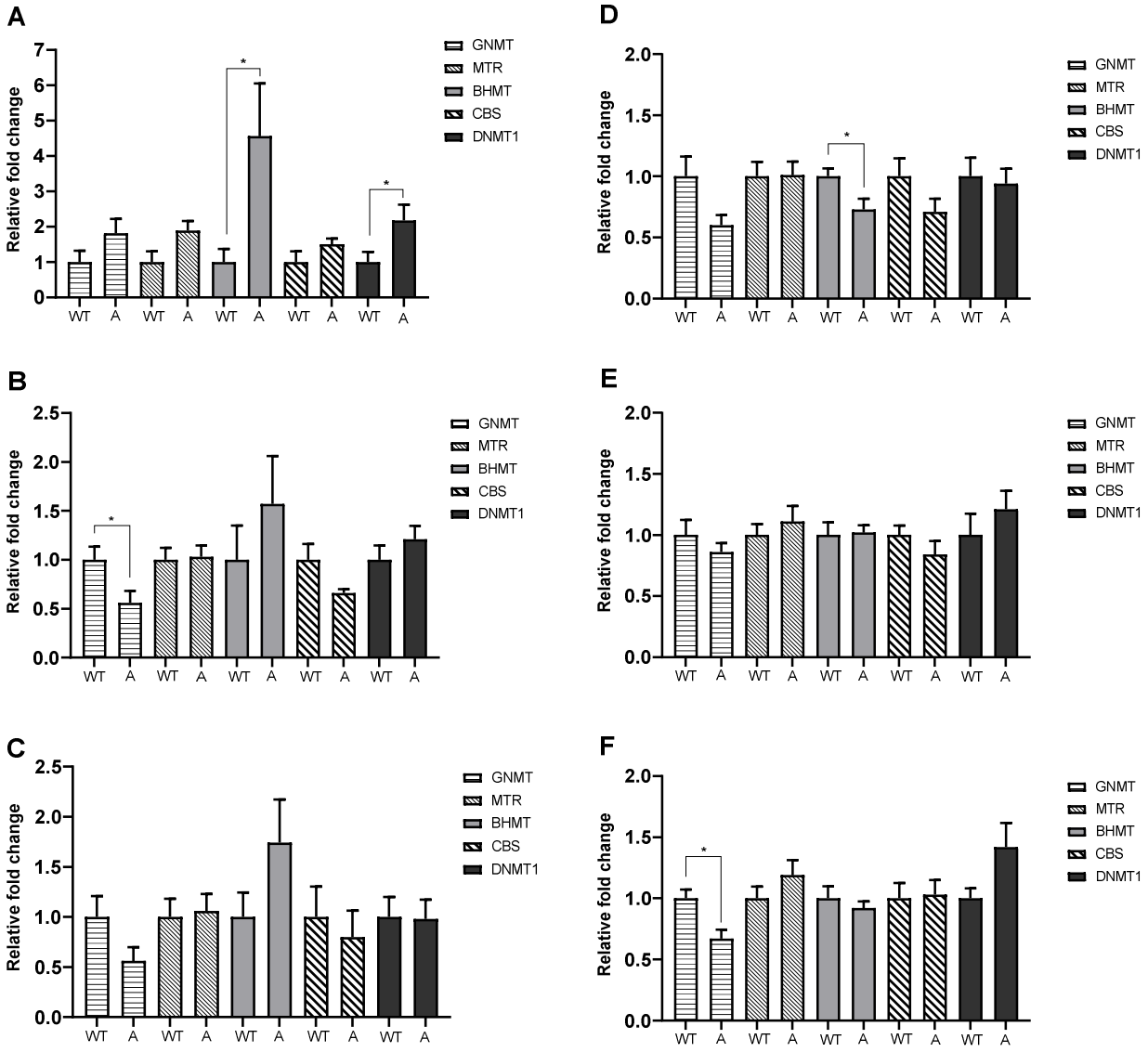

Figure 4-5: Ovarian one carbon metabolism enzyme mRNA abundance at 8 (A), 16 (B), and 24 (C) wk of age and hepatic mRNA abundance at 8 (D), 16 (E), and 24 (F) wk of age as determined by real-time polymerase chain reaction. Transcript abundance of the target genes was normalized against 18S ribosomal mRNA and reported as relative fold-change. Relative fold-change was compared using t-tests for relative abundance compared to WT mice. Data are means ± SEMs; $n = 6$/group, $^*P < 0.05$. Abbreviations used: A, agouti; WT, wild type; GNMT, glycine N-methyltransferase; BHMT, betaine homocysteine S-methyltransferase; CBS, cystathionine β-synthase; MTR, 5-methyltetrahydrofolate-homocysteine methyltransferase; and DNMT1, DNA (cytosine-5)-methyltransferase-1.

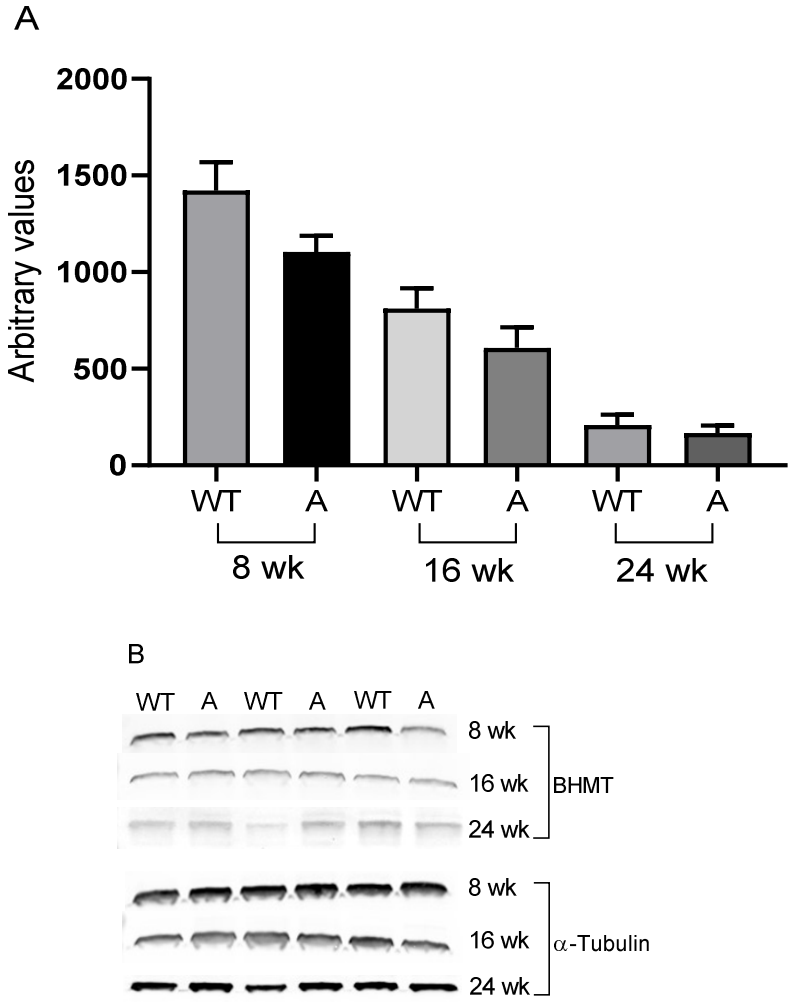

Figure 4-6: Hepatic BHMT protein abundance (A) and representative western blots of BHMT and α-tubulin (B) at 8, 16, and 24 wk of age for agouti and WT mice fed a modified standard AIN93G diet. Data are means ± SEMs; $n = 6$/group, $^*P < 0.05$. Abbreviations used: WT, wild type; and A, agouti.

Table 4-1: Primer sequences for Mus Musculus mRNA qRT-PCR quantification.

	Gnmt	TM	GC%
5' to 3'	GTGACCTGACCAAGGACATTAC	62	50
5' to 3' antisense	GAACTTACTGAAGCCAGGAGAG	62	50
	Mtr		
5' to 3'	CTGTGGATGGCTTGGTGAATA	62	47.6
5' to 3' antisense	GGGACTCTTGGCTTACACTTT	62	47.6
	Bhmt		
5' to 3'	TGATGAAGGAGACGCTTTGG	62	50
5' to 3' antisense	CCTCTAGCTGTTGGCGAAATA	62	47.6
	Cbs		
5' to 3'	GGATGGGCACAGACTACAATAG	62	50
5' to 3' antisense	CCACACAATCAGTCCAAGGT	62	50
	Dnmt		
5' to 3'	CCATCTTCTTGTCTCCCTGTATG	62	47.8
5' to 3' antisense	GGTGCTTTGTCCTTCTCCTT	62	50
	18S		
5' to 3'	CTGAGAAACGGCTACCACATC	62	52.4
5' to 3' antisense	GCCTCGAAAGAGTCCTGTATTG	62	50

[1]Abbreviations used: *Gnmt,* glycine n-methyltransferase*; Mtr,* methionine synthase*; Bhmt,* betaine-homocysteine S-methyltransferase*; Cbs,* cystathionine β-synthase*;* and *Dnmt,* DNA methyltransferase.

Table 4-2: Relative organ weights of agouti lethal yellow and wild-type mice at 8, 16, or 24 wk of age[1].

Tissue	**8 week**		**16 week**		**24 week**			**P-value**	
	Agouti	WT	Agouti	WT	Agouti	WT	Genotype	Age	Genotype*Age
Body weight (g)	37.2 ± 1.47	34.1 ± 1.08	49.5 ± 0.91	46.6 ± 0.74*	51.7 ± 1.46	54.7 ± 0.95	0.38	<0.001	0.065
Uterine horn (mg)[1]	-	-	24.7 ± 3.90	36.9 ± 5.84	15.1 ± 1.26	47.8 ± 4.60***	<0.0001	0.88	0.03
IPGTT (AUC)[2,3]	22647 ± 2618	19613 ± 1882	21450 ± 3644	16925 ± 4937	17720 ± 3870	11122 ± 2566	0.04	0.06	0.83
Fasting BG (g/dL)[3]	216.5 ± 27.2*	132.2 ± 18.9	254.0 ± 20.7**	156.0 ± 7.46	165.2 ± 11.4	139.8 ± 18.1	0.001	0.06	0.20

[1] Data are means ± SEMs; *n* = 6/group. Different from wild-type control group (*P < 0.05, **P < 0.01, ***P < 0.001). Data within age group determined by unpaired t-test. Overall main (Genotype and Age) effects and their interaction (Genotype x Age) were determined via a linear mixed model. Abbreviations used: BG, blood glucose; AUC, area under the curve; and WT, wild type.

CHAPTER 5. GENERAL CONCLUSIONS

Overall summary and conclusions

Polycystic ovary syndrome is a multifactorial disorder that has several metabolic and reproductive ramifications in women of childbearing age (1). The etiology of PCOS remains elusive. Consequently, identifying a treatment strategy that addresses the underpinning of PCOS is challenging. Several research studies have reported aberrations in the global methylation of oocytes at different stages of oogenesis (2,3), as well as environmental insults that may impose an increased risk of developing PCOS (4–6). Moreover, association-based studies have detected key biochemical markers that correlate with PCOS - including elevated homocysteine levels (7,8) and micronutrient deficiencies (9–12). Notably, the overall theme of these studies is their implication in methyl group metabolism. Several research studies have noted the beneficial role of nutrients that support methyl group metabolism (i.e., B_{12} and folate) on key outcomes such as homocysteine and methylation status in women with PCOS seeking reproductive assistance (13–15). Despite these reports, research has not characterized the fundamental mechanisms of methyl group metabolism in the progression nor management of PCOS. The studies presented in this dissertation examine the perturbations of methyl group metabolism as a result of various stages of PCOS. By employing both a chemically-induced and genetic model of PCOS, the research demonstrates that there are critical enzymes in the methyl group metabolism pathways that are fluctuating as a result of dysfunctional metabolism due to PCOS.

In the first study, we sought to examine the impact of letrozole-induced PCOS, on ovarian methyl group metabolism. To date, this is the first study that has examined the methyl group or one carbon metabolism enzymes in a rodent model of PCOS; therefore, the data presented herein - is exploratory in nature. The descriptive results of the metabolic and

phenotypic outcomes of the PCOS model include normal glucose tolerance, unaltered organ weights, and significantly higher body weight gain accompanied by normal epididymal adipose tissue. In order to determine the potential effects of PCOS on methyl group metabolism, we selected three age groups of 8, 16, and 24 wk of age. Observations from the vaginal lavage indicated that implantation of the letrozole slow-release bead did work within days, as determined by disrupted estrous cyclicity, and PCOS was confirmed by significantly elevated serum testosterone concentrations. Notably, in the letrozole-induced model of PCOS, *Cbs* transcript abundance decreased as a function of age, but this effect of reduced mRNA abundance on subsequent protein abundance was only explained in the rats at 8 wk of age. When examining the gene transcript abundance in the liver across 8, 16 and 24 wk of age, no differences were detected between the letrozole-induced and placebo control rats. One of the most interesting findings was the observed increase in *Bhmt* transcript abundance as a function of age, but only among the letrozole-induced rats. Conclusions from this study do point to potential methyl group metabolism imbalances, particularly in the folate-independent (BHMT) and transsulfuration (CBS)-mediated pathways.

Based on the findings from the first study in the chemically-induced model, we aimed to assess the same primary outcomes of interest in a metabolically perturbed model of PCOS. In the second study, we examined the ovarian and hepatic outcomes of methyl group metabolism in a progressively obese model of PCOS. As previous research has reported, agouti mice become obese and are acyclic by 24 wk of age. Therefore, in order to assess this gradual impact, we also examined agouti and their wild type control mice at 8, 16, and 24 wk of age. The phenotypic outcomes of the animal model recapitulate the classic metabolic disturbances that are present in women with PCOS, such as increased body weight gain, adiposity, fasting blood glucose, and

impaired glucose tolerance. An interesting finding from this second study was that in 8wk old agouti mice there was a 4.6-fold increase in ovarian *Bhmt* transcript abundance – an outcome similar to that of the chemically-induced model. Notably, an inverse effect of *Bhmt* transcript abundance was observed in the liver, whereby a 27% reduction in abundance was detected, exclusively at 8 wk of age. Moreover, when examining the results as a function of age, there was a significant increase in *Bhmt* transcript abundance in the agouti mice with age. It is important to note that these results were not supported by an alteration in protein abundance. Results from this second study also concluded a decrease in *Gnmt* in the ovaries at 16 wk of age and in the liver at 24 wk of age, but these findings were not further explored on the protein and activity levels.

Overall, the collective observations from these two studies suggest that BHMT may play a critical role in the progression of PCOS. It is important to highlight that *Bhmt* transcript abundance was elevated in both the letrozole-induced and agouti rodent models of PCOS as a function of age and between experimental groups, respectively. Given the inverse observation between the ovaries and the liver in the agouti mouse model of PCOS, we suspect that the ovaries are either responding to elevated circulating Hcy concentrations due to diminished hepatic *Bhmt* transcript abundance, or that the ovary has increased demand for methyl groups, as evidenced by the increased abundance of the *Bhmt* transcript.

In conclusion, the findings from these characterization research studies suggest that there are underlying alterations in methyl group metabolism at various stages of PCOS progression, and more so, differences in methyl group outcomes are depicted by the phenotypic dissimilarities between the two PCOS models used. Future studies are warranted to determine some of the metabolic parameters that are affected by PCOS due to changes in methyl group metabolism, such as serum insulin, Hcy, FSH, LH, and follicular Hcy concentrations. Moreover, it is

necessary to examine the mechanistic outcomes of providing a micronutrient rich diet to support methyl group metabolism to determine if such dietary intervention strategies attenuate PCOS-related anomalies.

References

1. Goodarzi MO, Dumesic DA, Chazenbalk G, Azziz R. Polycystic ovary syndrome: Etiology, pathogenesis and diagnosis. *Nature Rev Endocrinol.* 2011. p. 219–31.

2. Lodde V, Modina SC, Franciosi F, Zuccari E, Tessaro I, Luciano AM. Localization of DNA methyltransferase-1 during oocyte differentiation, in vitro maturation and early embryonic development in cow. *Eur J Histochem*. 2009; 53:24.

3. Wei Y, Lang J, Zhang Q, Yang CR, Zhao ZA, Zhang Y, Du Y, Sun Y. DNA methylation analysis and editing in single mammalian oocytes. *Proc Natl Acad Sci U S A*. 2019; 116:9883–92.

4. Xu N, Azziz R, Goodarzi MO. Epigenetics in polycystic ovary syndrome: a pilot study of global DNA methylation. *Fertil Steril*. 2010; 94:781.

5. Zhou Y, Zhang A, Gong M, Lu Y, Zhao C, Shen X, Zhang X, Wang L, Chen J, Ju R. Maternal Testosterone Excess Contributes to Reproductive System Dysfunction of Female Offspring Mice. *Endocrinology*. 2020; 161.

6. Echiburú B, Milagro F, Crisosto N, Pérez-Bravo F, Flores C, Arpón A, Salas-Pérez F, Recabarren SE, Sir-Petermann T, Maliqueo M. DNA methylation in promoter regions of genes involved in the reproductive and metabolic function of children born to women with PCOS. *Epigenetics*. 2020; 11:1178-1194.

7. Razi Y, Eftekhar M, Fesahat F, Dehghani Firouzabadi R, Razi N, Sabour M, Razi MH. Concentrations of homocysteine in follicular fluid and embryo quality and oocyte maturity in infertile women: a prospective cohort. *J Obstet Gynaecol.* 2020; 1-6.

8. Berker B, Kaya C, Aytac R, Satiroglu H. Homocysteine concentrations in follicular fluid are associated with poor oocyte and embryo qualities in polycystic ovary syndrome patients undergoing assisted reproduction. *Hum Reprod*. 2009; 24:2293–302.

9. Schiuma N, Costantino A, Bartolotti T, Dattilo M, Bini V, Aglietti MC, Renga M, Favilli A, Falorni A, Gerli S. Micronutrients in support to the one carbon cycle for the modulation of blood fasting homocysteine in PCOS women. *J Endocrinol Invest*. 2020; 43:779–86.

10. Kaya C, Cengiz SD, Satıroğlu H. Obesity and insulin resistance associated with lower plasma vitamin B12 in PCOS. *Reprod Biomed Online*. 2009; 19:721–6.

11. Kazerooni T, Asadi N, Dehbashi S, Zolghadri J. Effect of folic acid in women with and without insulin resistance who have hyperhomocysteinemic polycystic ovary syndrome. *Int J Gynecol Obstet*. 2008; 101:156–60.

12. Guler I, Himmetoglu O, Turp A, Erdem A, Erdem M, Onan MA, Taskiran C, Taslipinar MY, Guner H. Zinc and homocysteine levels in polycystic ovarian syndrome patients with insulin resistance. *Biol Trace Elem Res*. 2014; 158:297–304.

13. Asemi Z, Karamali M, Esmaillzadeh A. Metabolic response to folate supplementation in overweight women with polycystic ovary syndrome: A randomized double□blind placebo□controlled clinical trial. *Mol Nutr Food Res*. 2014; 58:1465–73.

14. Palomba S, Falbo A, Giallauria F, Russo T, Tolino A, Zullo F, Colao A, Orio F. Effects of metformin with or without supplementation with folate on homocysteine levels and vascular endothelium of women with polycystic ovary syndrome. *Diabetes Care*. 2010; 33:246–51.

15. Bahmani F, Karamali M, Shakeri H, Asemi Z. The effects of folate supplementation on inflammatory factors and biomarkers of oxidative stress in overweight and obese women with polycystic ovary syndrome: a randomized, double-blind, placebo-controlled clinical trial. *Clin Endocrinol.* 2014; 81:582–7.

APPENDIX A. WHOLE EGG CONSUMPTION INCREASES GENE EXPRESSION WITHIN THE GLUTATHIONE PATHWAY IN THE LIVER OF ZUCKER DIABETIC FATTY RATS

Joe L. Webb*, Amanda E. Bries*, Brooke Vogel, Claudia Carrillo, Lily Harvison, Timothy A. Day, Michael J. Kimber, Rudy J. Valentine, Matthew J. Rowling, Stephanie Clark, Elizabeth McNeill, and Kevin L. Schalinske., Whole egg consumption increases gene expression within the glutathione pathway in the liver of Zucker Diabetic fatty rats. *PloS One*. 2020. 15:11, e0240885, reprinted by permission.

*JLW and AEB contributed equally to this work.

Abstract

Background: Nutrigenomic evidence supports the idea that Type 2 Diabetes Mellitus (T2DM) arises due to the interactions between the transcriptome, individual genetic profiles, lifestyle, and diet.

Objective: Since eggs are a nutrient dense food containing bioactive ingredients that modify gene expression, our goal was to examine the role of whole egg consumption on the transcriptome during T2DM. We analyzed whether whole egg consumption in Zucker Diabetic Fatty (ZDF) rats alters microRNA and mRNA expression across the adipose, liver, kidney, and prefrontal cortex tissue.

Methods: Male ZDF (fa/fa) rats (n = 12) and their lean controls (fa/+) (n = 12) were obtained at 6 wk of age. Rats had *ad libitum* access to water and were randomly assigned to a modified semi-purified AIN93G casein-based diet or a whole egg-based diet, both providing 20% protein (w/w). TotalRNA libraries were prepared using QuantSeq 3' mRNA-Seq and Lexogen smallRNA library prep kits and were further sequenced on an Illumina HighSeq3000.

Differential gene expression was conducted using DESeq2 in R and Benjamini-Hochberg adjusted *P*-values controlling for false discovery rate at 5%.

Results: We identified 9 microRNAs and 583 genes that were differentially expressed in response to 8 wk of consuming whole egg-based diets. Kyto Encyclopedia of Genes and Genomes/Gene ontology pathway analyses demonstrated that 12 genes in the glutathione metabolism pathway were upregulated in the liver and kidney of ZDF rats fed whole egg. Whole egg consumption primarily altered glutathione pathways such as conjugation, methylation, glucuronidation, and detoxification of reactive oxygen species.

Conclusion: These pathways are often negatively affected during T2DM, therefore this data provides unique insight into the nutrigenomic response of dietary whole egg consumption during the progression of T2DM.

Introduction

Type 2 Diabetes Mellitus (T2DM) is an insulin independent metabolic disease characterized by chronic hyperglycemia and concomitant insulin resistance and it is estimated that greater than 415 million adults worldwide have T2DM [1]. Oxidative stress is a potential key mediator in the pathogenesis of T2DM and may underlie the progressive development of hyperglycemia and insulin resistance [2]. More specifically, reports demonstrate that glutathione (a major intracellular antioxidant) enzymes are diminished in the liver and brain of T2DM animal models [3]. Sekhar and colleagues examined the ability of patients with uncontrolled and controlled T2DM to synthesize glutathione via measuring isotopically labelled glycine [4,5]. They reported that patients with uncontrolled T2DM were severely deficient in the ability to maintain glutathione metabolism in cardiac tissue [4], which may be, in part, due to hyperglycemia decreasing L-cysteine concentrations [5] and the reduced flux of methionine to

cysteine [6]. Because of the deleterious effects of hyperglycemia on organ function, it is important to consider the global transcriptomic effects of T2DM. Similar to humans, the Zucker Diabetic Fatty (ZDF) rat model of T2DM also displays increased oxidative stress [7], whereby endogenous protective antioxidants like glutathione are similarly downregulated in ZDF rats [8]. The gene expression profiles in animal models of T2DM, such as the ZDF rat, is consistent with gene expression profiles of humans with T2DM [9], making this a suitable model to explore the global gene expression effects of diet in the ZDF rat.

Dietary treatments with bioactive foods such as cocoa or Shenyuan granules [10,11] in ZDF rats have been shown to reduce oxidative stress or attenuate renal injury in the presence of T2DM-related nephropathy [12]. Consumption of eggs as a bioactive food during T2DM in humans remains controversial [13–15], but eggs have been shown to display antioxidative properties, which may be beneficial during the progression of T2DM [16]. Additionally, our laboratory has consistently reported that long-term whole egg (WE) consumption improves metabolic parameters during T2DM such as the maintenance of circulating vitamin D concentrations, decreased weight gain, and nephroprotection via reduced proteinuria in male ZDF rats [17–20]. These are important findings, as vitamin D deficiency, increased adiposity, and kidney failure have collectively been suggested to exacerbate oxidative stress during T2DM [21].

While the literature surrounding the effects of dietary WE on insulin resistance during T2DM is inconclusive in both rodent [17] and human population studies [22], there are no studies to date examining the molecular mechanisms underlying how WE consumption affects the transcriptome across multiple tissues. Longitudinal, prospective, and comprehensive meta-analyses have been performed to assess the independent risk factors of increased dietary egg

consumption on chronic diseases [23,24]. Because of the highly controversial science of whole egg consumption on increased cardiovascular disease in patients with T2DM, it is important to examine the possible underlying molecular targets and drivers of whole egg consumption on disease. Ultimately, analyzing the transcriptomic impact of egg consumption would provide us with a better understanding of the nutrigenomic actions that dietary egg consumption contributes to T2DM, and bridge the gap in our understanding of how whole eggs may effect the physiological progression of T2DM. Therefore, the objective of this study was to determine the influence of WE consumption on gene and microRNA expression profiles in a ZDF rat model of progressive T2DM. We examined the transcriptomes from the adipose, liver, kidney, and prefrontal cortex (PFC) tissues to determine how WE consumption alters gene expression and examined whether these changes correspond to altered microRNA expression profiles in T2DM.

Results and Discussion

Whole eggs have predominantly been criticized for their associated risk of developing chronic diseases [25], yet the benefits of WE consumption have also been reported [26]. For instance, several groups have suggested that WE provide antioxidant properties [12,27] , either through antioxidant peptides in the egg yolk [12] or other reactive oxygen species-reducing nutrients [28]. Other studies examining the role of quail egg consumption in rat models of T2DM have demonstrated upregulation of glutathione metabolism in alloxan-induced T2DM in Wistar rats [29] and improved oxidative stress profiles in streptozotocin-injected rats [30]. Raza and colleagues [30] identified that in diabetic rat liver glutathione content and glutathione S-transferase (GST) activity were decreased 65% while also observing that brain glutathione and GST activity were increased two-fold as a result of a T2DM phenotype.

Total RNASeq differential expression. When comparing the WE versus casein (CAS) in ZDF rats and their lean controls, differential expression analyses of the mRNAseq data resulted in 583 differentially expressed genes (DEGs) across four tissues in both genotypes **(Table 1)**. **S1 Table** contains the results from DESeq2 with the results for each gene across all four tissues with data on individual genes. **S2 Table** contains raw mRNA read counts for each tissue and rat across both genotypes. Among the lean controls, 13 genes were differentially expressed in the adipose tissue, 32 in the liver, and 6 in the kidney. Notably, none of the genes were differentially expressed in the PFC between dietary treatments in the lean rats. In the ZDF rats, dietary WE consumption resulted in 532 total DEGs across all tissues where 50 genes were differentially expressed in adipose tissue, 474 in the liver, 6 in the kidney and 2 genes in the PFC following multiple testing correction using the false discovery rate (FDR) threshold of 5%. We demonstrated that consuming WE-based diets for 8 wk resulted in significant alterations in oxidative stress pathways, as well as glutathione metabolism pathways. While there were tissue-specific changes in gene expression, glutathione metabolism was altered in the kidney and liver among ZDF rats, and in the kidney of lean controls were significantly upregulated. Overall, these data highlight how consumption of WE-based diets can provide beneficial effects through modifying gene expression of oxidative reduction targets.

We previously demonstrated that WE consumption for 8 wk is effective at improving serum vitamin D status and providing nephroprotective benefits [31,32]; however, despite our gene expression findings in this study we still have yet to elucidate the mechanism underlying how WE consumption leads to decreased weight gain. We also identified that ZDF rats fed WE upregulated 11 genes involved in glutathione metabolism in the liver and kidney. In the PFC, WE consumption had differing effects whereby in the lean PFC, WE consumption did not

change the transcriptome, whereas in the ZDF rats WE consumption strongly downregulated the expression of 2, AY172581 exon transcripts. These exon transcripts have yet to be characterized and future proteomic studies may reveal their biological importance. Across both genotypes, the most significantly altered genes were involved in the Kyoto Encyclopedia of Genes and Genomes (KEGG) pathways of: glutathione metabolism, metabolic pathways, steroid biosynthesis, and cholesterol metabolism. After controlling for the genetic background differences of our ZDF rats, a combined analysis indicated that 428 unique genes were differentially expressed across these tissues as a product of WE consumption. Moreover, 13 different glutathione metabolism genes were significantly upregulated across the liver and kidney in both genotypes suggesting that increased whole egg consumption, may increase glutathione metabolism independent of T2DM, and attenuate the decreased glutathione metabolism during diabetes.

To visualize the global differences in the transcriptomes based on dietary treatment, we performed principal component analysis (PCA) and generated volcano plots for genes that exhibited ≥1.5-fold change, respectively. **Fig 1** displays the samples in a three-dimensional principal component space, whereby samples are colored in red or black to distinguish either WE or CAS, respectively. In the mRNA samples, rats on the same dietary treatment (i.e. black or red) clustered together, while animals belonging to different dietary treatments separated, indicating distinctly different patterns across global mRNA expression. These results were further visualized using volcano plots for each tissue as presented in **Fig 2.** These volcano plots demonstrate the degree to which genes were upregulated or downregulated across each tissue. For instance, volcano plots indicate a relatively equal number of upregulated and downregulated

genes in the lean PFC following WE consumption, whereas WE consumption primarily resulted in downregulated gene expression in the ZDF PFC.

During T2DM, reports indicate that genes within the oxidative stress-related pathways upregulated [28]. Evans et al. suggested that oxidative stress was driven by the hyperglycemic environment concomitant with increased concentrations of free fatty acids in the plasma [28]. Corbett et al. [31] reported that protective antioxidant genes such as glutathione peroxidase are downregulated during T2DM, and both glutathione s-transferases (GSTs) and glutathione-dependent enzymes are important in the regulation of pathophysiological alterations in numerous chronic diseases, especially T2DM [33]. Previous work has shown that dietary intervention with direct glutathione supplementation was protective against diabetic nephropathy in an insulin dependent streptozotocin-induced T1DM model [30]. This current study provides new transcriptomic evidence supporting our previous report demonstrating that WE consumption protects against diabetic nephropathy, where WE consumption leads to altered gene expression in the kidney. In this study, we noted that the strongest alterations in glutathione metabolism were in the liver, potentially because hepatic glutathione is produced at much higher concentrations (10 mM), whereas intracellular glutathione concentrations are approximately 1-2 mM [30]. This body of previous work is important in relation to our findings that several GSTs and glutathione-dependent enzymes are significantly altered during WE consumption in lean controls and during diabetes in the kidneys and livers across both genotypes. Future mechanistic studies identifying the beneficial impact of these two enzymes in chronic diseases like T2DM are warranted.

Outside of the glutathione pathways, we also observed that there were significant differences in early growth response-1 (*Egr-1*) gene expression following WE consumption. Egr-

1 has been implicated in the onset of insulin-resistance, as previous studies in insulin-resistant T2DM mice identified that loss of function in Egr-1 restores insulin sensitivity via increased phosphorylation of the insulin receptor substrate-1 tyrosine kinase [34]. Notably, we observed a 30% decrease in hepatic *Egr-1* expression in the ZDF rats fed WE. This is an interesting finding as research by Garnett et al. [35] determined that exposing beta cells to hyperglycemic conditions resulted in a temporal and dose-dependent increase in *Egr-1* transcription and translation. Furthermore, Egr-1 null mice are known for their inability of displaying diabetic and obese phenotypes [36] owing to their increased energy expenditure. These data suggest that consumption of WE may lead to altered Egr-1 expression which may play a key role in regulating energy expenditure.

We also demonstrated that WE consumption resulted in tissue-specific alterations in gene expression and that there were distinct transcriptomic differences between genotypes. WE consumption did not influence gene expression in the PFC of lean animals, while 2 genes were significantly altered in the ZDF PFC. There were more stark differences when comparing the liver tissues between the two genotypes, where more than 400 genes were altered in ZDF livers that were not altered in the liver of lean controls. It has been shown that T2DM impacts a variety of tissues [1] but previous studies have provided very little evidence of how T2DM alters the nutrigenomic responses to foods in specific tissues. It is still unknown which specific egg components lead to phenotypic differences in gene expression and future studies should focus on identifying the specific egg constituents that mediate these gene expression differences. These collective findings are likely mediated through the alteration of several genes; therefore, we aimed to further examine microRNA changes involved in the underlying progression of T2DM during WE consumption.

MicroRNA sequencing differential expression. We examined if endogenously expressed microRNA profiles in the adipose, liver, kidney, and prefrontal cortex tissues would be altered following 8 wk consumption of dietary WE. Differential expression analyses of the ZDF microRNA data resulted in 1 differentially expressed microRNA in the adipose tissue, none in the liver, none in the kidney and 2 in the PFC that surpassed multiple testing correction. Among the lean rats, there were 2 marginally differentially expressed microRNAs in the adipose tissue, 4 in the liver, none in the kidney and none in the PFC that survived multiple testing correction. Table 2 presents the differentially expressed microRNAs in the adipose, liver, kidney, and PFC tissues across both genotypes. S3 Table contains results from DESeq2 with the results for each microRNA across all four tissues and raw microRNA read counts are contained in S4 Table.

Based on the microRNA sequencing analysis, 9 microRNAs were differentially expressed following multiple testing correction. Several of these microRNAs have been previously correlated with gestational diabetes or show to be altered in the plasma of individuals with diabetes. Very few studies to date have examined the tissue-specific changes of endogenous microRNA expression in response to dietary patterns and this is the first study to demonstrate that endogenous microRNA expression in the liver, adipose, and PFC can be altered following 8 wks of WE consumption. Future studies should focus on identifying if similar foods such as quail eggs alter microRNA expression in these tissues and determine the smallest effective dosage of egg required to recapitulate these changes in microRNAs.

Mapping between microRNAs and target genes. Next, we sought to determine if these significantly altered microRNAs were responsible for the tissue-specific differential expression of their predicted target genes. MicroRNA mapping analyses of the differentially expressed microRNAs and their target genes demonstrates that in each of the tissues with differentially

expressed microRNAs, key target genes of these microRNAs were altered. For instance, in the lean liver microRNA-181a-3p was upregulated and two of its mRNA target genes were differentially expressed, Cytochrome P450 Family 7 Subfamily A Member 1 (Cyp7a1) and stearoyl-CoA desaturase (Scd). Similarly, in the lean adipose, microRNA-125b-5p was downregulated while its target gene phosphoglycolate phosphatase (Pgp) was upregulated. The microRNAs in the PFC and kidney tissue did not map to any differentially expressed genes. Table 4 summarizes the mapping between microRNAs and their gene targets.

While examining the relationship between significantly altered microRNAs and their target genes, we identified that in the livers of lean rats fed WE, the upregulated microRNA-181a-5p affected target genes involved in steroid hormone biosynthesis such as Cyp7a1 and Scd. Notably, only Cyp7a1 was upregulated in the liver of ZDF rats fed the WE-based diet while both Scd and Cyp7a1 were upregulated in the livers of lean control rats. In rodent models of diabetes, liver expression of Cyp7a1 has been shown to be decreased and thought to play a key role in regulating whole body energy homeostasis [37]. Similarly, transgenic mice overexpressing Cyp7a1 were shown to become resistant to weight gain and fatty liver disease [37]. Experiments examining the role of Scd in rat hepatocytes has demonstrated that Scd expression regulates hepatic insulin resistance during diabetes [38], but very few studies have determined the expression of Scd genes in the context of dietary consumption. Based on the data, WE consumption more strongly upregulated hepatic expression of Cyp7a1 in ZDF animals than in the lean controls and this might suggest that WE consumption can prevent or reverse the loss of hepatic Cyp7a1 expression due to diabetes.

In our lean rats, we also identified that microRNA-125b-5p was downregulated in adipose tissue where its gene target Pgp was strongly upregulated. Pgp is known to hydrolyze

glycerol-3-phosphate into glycerol, and overexpression experiments in rodents showed that upregulation of Pgp leads to a reduction in body weight gain and improves hepatic glucose regulation [39]. Additionally, we observed the upregulation of liver microRNA-9a-5p, which has been correlated with gestational diabetes in humans [40]. While the gene targets of microRNA-9a-5p were not differentially expressed in the liver, future studies should look into whether endogenous microRNA expression fluctuates in response to consuming other eggs, such as quail eggs, or egg yolk alone.

KEGG and GO functional enrichment analysis. To further examine the molecular function of the identified DEGs, KEGG pathway analysis indicated that the most prevalent pathways influenced by dietary WE across multiple tissues in the ZDF rats were: glutathione metabolism; oxidation-reduction; metabolism of xenobiotics; steroid hormone biosynthesis; and fatty acid synthesis pathways. In the livers of lean control rats, the most significantly expressed pathways included metabolic pathways and retinol metabolism. All the differentially expressed genes that map to KEGG and gene ontology (GO) pathways analyses are presented in S5 Table.

To further investigate the specific genes involved in the glutathione metabolism pathways, genes were categorized into the corresponding reactions identified by Reactome.org in **Fig 3.** Glutathione metabolism functions in antioxidant defense, signal transduction, cytokine production, and other cellular processes such as detoxification. The role of GST, GSTK, GSTO dimers, and GPX1 which function in glutathione conjugation, glucuronidation, methylation, and detoxification of reactive oxygen species, respectively, are detailed within **Fig 3**. These reactions within glutathione metabolism are essential for recycling of glutathione disulfide or the conjugation of GSH that can be utilized in redox reactions.

KEGG pathway analysis highlighted that in addition to an upregulation of glutathione metabolism pathways, several of the same gene products mediate metabolism of xenobiotics, a pathway upregulated in our rats fed WE-based diets. Xenobiotic metabolism has previously been shown to be downregulated during insulin dependent T1DM [30], where in this study these pathways were upregulated in response to feeding WE-based diets. These observed effects appear to be tissue specific, as these alterations were the most prominent in ZDF liver, whereas one gene, glutathione s-transferase p (*Gstp1*), was differentially upregulated in the kidney of ZDF rats while glutathione s-transferase mu 1 (*Gstm1*) was upregulated in the lean kidney. These findings support the previous observation that WE consumption affects obese phenotypes differently than a lean phenotype [13], in part, due to the different transcriptomic responses to dietary WE. We previously hypothesized that these differences in response to WE consumption were not due to satiety, because there was increased food intake in the WE group [13]; the present study identifies a potential molecular response to egg partially explaining these previous findings. Other suggested mechanisms that might explain differences between obese and lean genotypes include thermogenesis [42], altered methylation patterns [43], intestinal microbiome alterations [44], and changes in energy expenditure [33]. While there have been numerous studies highlighting differences in the microbiota between obese and lean phenotypes in rats [33] and humans [42], one recent study examining WE consumption concluded that it did not influence the intestinal microbiome in postmenopausal women [45]. Taken together, these observations support the idea that phenotypic alterations during T2DM may depend strongly on obesity status and energy expenditures on a molecular level, potentially in response to changes in the transcriptome.

qPCR analyses. Finally, we examined the relationship between our qPCR data for several genes to validate the results from the Quantseq analysis. Confirmatory analysis with qPCR demonstrated that across the genes selected, the qPCR data highly correlates with the mRNA Quantseq results (R2 = 0.72; S1 Fig) indicating strong similarities between these two methods.

Strengths and Limitations

The strengths and limitations of this study should be addressed to better understand how these results fit into the larger context of the current literature. It is estimated that in 2019, people in the United States consumed on average, 5.6 eggs per week [46]. The dose of egg used in this study would equate to roughly 14 eggs per day for a human. While our study demonstrated that consuming a large dose of WE may alter gene expression of various metabolic pathways, particularly during T2DM, this quantity of egg would not be a standard dietary practice in humans. We do recognize that our whole egg dosage was high, but the goal was to examine whether there was a transcriptomic response from consuming dietary whole egg in a T2DM model. It is worth noting that our laboratory has previously reported in ZDF rats that even smaller dosages, such as the human equivalent of <2 eggs/day, significantly reduced weight gain in the ZDF rat and therefore may be effective in identifying oxidative stress outcomes from long-term dietary whole egg consumption [13]. After the examination of the transcriptome following our high WE-based diet, it is warranted to examine these specific genes in a follow-up intervention study. Future studies will focus on titrating down the egg dosages to discern the smallest dosage to elicit similar transcriptomic responses to egg consumption that will be more translatable to human consumption patterns. Overall, our findings are significant as we are the first to report that whole hen egg consumption promotes glutathione metabolism expression during T2DM and alters the transcriptome of multiple tissues using next-generation sequencing.

Additionally, we provide evidence supporting the idea that egg consumption modifies endogenous microRNA expression in a tissue-specific manner.

In summary, we examined whether feeding WE modifies expression of microRNAs or gene expression profiles across multiple tissues in a diabetic versus a lean rat model. Across all tissues examined with next generation sequencing, we identified that 9 microRNAs were differentially expressed in response to consuming WE. Additionally, we have shown that these microRNAs were related to tissue-specific changes in gene expression, and that 8 wk of consuming diets high in whole egg modified 583 genes across the PFC, kidney, liver, and adipose tissue. KEGG/GO analyses identified that glutathione metabolism was highly upregulated in response to feeding WE and qPCR results validated the sequencing results. These data suggest that high WE consumption may provide beneficial effects during T2DM by improving glutathione metabolism gene expression across multiple tissues and decreasing gene expression in oxidative stress pathways.

Materials and Methods

The data discussed in this publication have been deposited in NCBI's Gene Expression Omnibus [47] and are accessible through GEO Series accession number GSE157491 (https://www.ncbi.nlm.nih.gov/geo/query/acc.cgi?acc=GSE157491). All protocols used within this study have been made publicly available at protocols.io. Protocols have been zipped into one file and can be accessed at dx.doi.org/10.17504/protocols.io.bjgakjse.

Animal housing and experimental design This animal study was approved by the Institutional Animal Care and Use Committee (IACUC) at Iowa State University. All animal care was performed according to Laboratory Animal Resources Guidelines at Iowa State University. Male ZDF (*fa/fa*) rats (n = 12) and their lean controls (*fa*/+; n = 12) were obtained at 6-wk of age

(Charles River, Wilmington, MA). Rats were dual-caged and acclimated for 72 h in conventional cages in a temperature-controlled room (25°C) with a 12-h light-dark cycle. Rats were randomly assigned to an experimental diet (Table 4) consisting of either a casein (CAS)-based diet, or a WE-based diet containing dried WE powder (Rose Acre Farms).

Both diets provided 20% protein (w/w) from either vitamin-free CAS or WE powder. To match the diets for total lipid content (18.3%), corn oil was added to the control diet. Both diets were prepared in-house weekly by mixing all ingredients into a powdered form and administered daily in a standard amount for both lean and ZDF rats. For the remainder of the study, rats were fed *ad libitum* for 8 wk and at the end of the experimental period, rats were anesthetized with a dissociative agent combination of ketamine:xylaxine (90:10 mg/kg body weight) via an intraperitoneal injection of 1µL/g body weight. Two methods of animal euthanasia were performed according to the American Veterinary Medical Association guidelines for the Euthanasia of Animals: 2020 edition [47]. Cardiac exsanguination of whole blood on the anesthetized rat was performed and serum was subsequently stored at −80°C for downstream analysis. The second method of exsanguination was the procurement of organs. Following cardiac puncture, tissues were immediately excised, weighed, and snap frozen in liquid nitrogen for storage at −80°C in RNA*Later*.

RNA extraction and analysis. Tissue samples (20 mg) were rapidly thawed on ice and largeRNA and smallRNA fractions were extracted from the same isolate using the RNA SPLIT Kit (Lexogen) according to the manufacturer's instructions. Briefly, samples were homogenized in an isolation buffer and phase separated using a phenol/chloroform extraction followed by a spin column-based purification procedure. All samples were aliquoted and stored at −80°C for downstream analysis. Following extraction, sample concentrations for the largeRNA fraction

were analyzed using a Qubit 2.0 fluorometer (Thermo Fisher) using the Qubit™ Broad Range RNA Assay Kit. RNA integrity was assessed using the Bioanalyzer 2100 (Agilent Technologies) and samples with low RNA integrity number (RIN) values <5 were discarded and re-extracted. SmallRNA concentrations were measured using a Qubit 2.0 fluorometer (Thermo Fisher) using the Qubit™ microRNA Assay Kit.

TotalRNA and smallRNA sequencing. Libraries for totalRNA were prepared using an automated protocol according to the manufacturer's instructions for half reactions on the QuantSeq 3' mRNA-Seq Library Prep Kit (Lexogen) using a MANTIS® Liquid Handler pipetting robot (Formulatrix). All totalRNA samples were multiplexed together across two lanes on an Illumina High-Seq 3000. SmallRNA Libraries were prepared manually using the SmallRNA-Seq Library Prep Kit (Lexogen). Briefly, 100 ng of enriched smallRNA was used as input and 3' and 5' adapters were ligated followed by column purifications. Subsequently, the ligation products were reverse transcribed and double stranded cDNA libraries were generated. Finally, individual sample barcodes for multiplexing were introduced via 17 cycles of PCR. All libraries were assessed on the Bioanalyzer 2100 (Agilent) to examine if adapter dimers formed during PCR. All libraries were further prepared using a bead purification module (Lexogen) and pooled into a single sample at 2 nM (20 µL reaction) for sequencing.

Sequencing quality control and adapter trimming. For both totalRNA and smallRNA samples, the resulting FASTQ files were analyzed using Fast-QC [21] and sequencing adapters were trimmed using on BBDUK [48] with an example of the trimming procedure: bbduk.sh in=reads.fq out=clean.fq maq=10 ref= /bbmap/resources/adapters.fa. For smallRNA samples, reads were additionally trimmed using the literal flag to remove the Lexogen specific sequence "5'-TGGAATTCTCGGGTGC CAAGGAACTCCAGTCAC – 3'" following similar trimming

procedures. Briefly, any read segments that matched Illumina Truseq or Nextera adapters, along with reads containing integrity scores <10 were trimmed out.

Alignment and read quantification. For totalRNA, reads were mapped to the Ensembl release 94 of the Rattus Norvegicus RNO_6.0 genome using RNA STAR [49]. TotalRNA read counts were generated during the read alignment using the --genecounts function in STAR. For smallRNA samples, reference fasta files from www.RNACentral.org were downloaded for microRNA, piwiRNA, snRNA, nRNA, rRNA, and tRNA. Indexes were generated using Bowtie [50] and alignment was conducted using the smallrnaseq python tool [51]. Read counts for all reference indices and IsomiRs were generated using the smallrnaseq python tool.

Data filtering and normalization. Following read count generation, Quantseq gene expression data was merged into a single data frame for analysis in R (version 3.6.0). Genes were discarded from the analysis if there were <3 samples without a single read for that given gene. TotalRNA data initially generated read counts for 32,883 genes and over 50% of the trimmed reads from each sample mapped to the RNO_6 version 94 genome. Prior to normalization, remaining gene counts across all four tissues contained between 8,700-12,000 genes for analysis. The microRNA data originally generated read counts for over 350 microRNAs and the formal analysis was conducted on 60-150 targets across each tissue. For totalRNA and smallRNA fractions, all samples were normalized using the Trimmed Mean of M values (TMM) method [52]. Briefly, TMM accounts for variable depth between samples by normalizing them according to the weighted trimmed mean of the log expression ratios across all samples prior to analysis.

Differential expression analysis. All differential expression analyses were conducted using R (version 3.6.0). Differential expression was conducted using DESeq2 from Bioconductor.

DESeq-DataSetFromMatrix generated p-values and Benjamini-Hochberg [53] adjusted P-values controlling false discovery rate (FDR) at 5%. Significance was determined at adj $P<0.05$.

Heatmaps, principal component analysis, and volcano plots. Principal Component Analysis (PCA) was used to visualize sample relatedness across treatments and tissues. Subsequent hierarchical clustering grouped samples according to transcriptomic relatedness, while volcano plots were constructed to visualize samples with absolute log-fold changes >1.5. All figures were generated with MatplotLib in Python version 3.2.0rc1.

KEGG/GO pathway analysis. Biological pathways for each DEG were generated using the KEGG pathway analysis and GO analysis conducted via the Database for Annotation, Visualization, and Integrated Discovery (DAVID) v6.7 software tool.

qPCR validation analyses. TotalRNA from each tissue was aliquoted and frozen at -80°C, and 2 µg of total RNA was reverse-transcribed into cDNA using the High-Capacity cDNA Reverse Transcription Kit (Applied Biosystems, Catalog # 4368813). cDNA was diluted to 250 ng/µL and qPCR reactions were performed using 250 ng of total cDNA with primers at 300 nM concentration in 10 µL FastStart Sybr Green Master (Roche) according to the manufacturer's instructions. Briefly, the thermocycling protocol followed a pre-incubation at 95°C for 10 minutes, followed by 45 cycles of 3-Step amplification: 1) denature at 95°C for 20 seconds; 2) anneal and extend at 60°C for 20 seconds; and 3) elongate at 72°C for 20 seconds. All qPCR reactions were conducted in a Roche LightCycler 96 Real-Time PCR System. Primers sequences for qPCR are as follows: Fatty Acid Synthase FWD: GGCGAGTCTATGCCACTATTC, REV: GCTGATACAGAGAACGGATGAG; Indolethylamine N-methyltransferase FWD: CTGGAGAAGGAGACGGTAGAA, REV: CGGGCAACCACGAAGTATAA; Cytochrome

P450, family 2, subfamily c, polypeptide 22 FWD: AGAGAGAGAGAGAGAGAGAGAGA, REV: GAGACCCTCTGCATCTCAATAC; 18S Ribosomal Subunit FWD: AAGACGAACCAGAGCGAAAG, REV:TCGGAACTACGACGGTATCT; Cytochrome P450, family 51 FWD: CCTTCCAGTGGTGCTCTTATT, REV: CTAAGCCACTACCCAAAGACTATAC. In all qPCR experiments, 18s RNA expression was used to normalize gene expression within each tissue sample that was processed in triplicate. All data were analyzed using the Livak Delta-Delta CT method [54].

MicroRNA bioinformatic analysis. All microRNA fastq files were processed using the smallrnaseq [51] package in python. Smallrnaseq automates standard bioinformatic processes for quantification and analysis of small non-coding RNA species such as microRNA quantification and novel microRNA prediction. Briefly, smallrnaseq uses bowtie to align fastq files to user defined reference fasta sequences and all reference sequences were downloaded from www.RNAcentral.org (version 14). Following alignment to the Rattus Norvegicus genome and reference tRNA, rRNA, microRNA, lncRNA, and snRNA files, novel microRNA predictions are conducted using microRNADeep2. Additionally, differential expression was automated using the DEseq2 package in R.

Acknowledgements

We would like to thank Dr. Peng Liu, Department of Statistics, for aiding in planning this project, and the ISU DNA facility staff members Kevin Calvalin, Tanya Murtha and Dr. Mike Baker for their assistance sequencing our samples. Additionally, the authors would like to thank the undergraduate research assistants that helped conduct the experiments and work with the rats.

References

1. Zheng Y, Ley SH, Hu FB. Global aetiology and epidemiology of type 2 diabetes mellitus and its complications. Nature Reviews Endocrinology. Nature Publishing Group; 2018. pp. 88–98. doi:10.1038/nrendo.2017.151

2. Folli F, Corradi D, Fanti P, Davalli A, Paez A, Giaccari A, et al. The Role of Oxidative Stress in the Pathogenesis of Type 2 Diabetes Mellitus Micro- and Macrovascular Complications: Avenues for a Mechanistic-Based Therapeutic Approach. Current Diabetes Reviews. 2012;7: 313–324. doi:10.2174/157339911797415585

3. Raza H, John A, Howarth FC. Increased Oxidative Stress and Mitochondrial Dysfunction in Zucker Diabetic Rat Liver and Brain. Cellular Physiology and Biochemistry. 2015;35: 1241–1251. doi:10.1159/000373947

4. Raza H, John A, Howarth FC. Alterations in glutathione redox metabolism, oxidative stress, and mitochondrial function in the left ventricle of elderly zucker diabetic fatty rat heart. International Journal of Molecular Sciences. 2012;13: 16241–16254. doi:10.3390/ijms131216241

5. Kanikarla-Marie P, Micinski D, Jain SK. Hyperglycemia (high-glucose) decreases l-cysteine and glutathione levels in cultured monocytes and blood of Zucker diabetic rats. Molecular and Cellular Biochemistry. 2019;459: 151–156. doi:10.1007/s11010-019-03558-z

6. Tessari P, Coracina A, Kiwanuka E, Vedovato M, Vettore M, Valerio A, et al. Effects of insulin on methionine and homocysteine kinetics in type 2 diabetes with nephropathy. Diabetes. 2005;54: 2968–2976. doi:10.2337/diabetes.54.10.2968

7. Patel D, Rooney R, Groom S. Gene Expression Profiles for the Zucker Fatty Rat Versus Zucker Diabetic Fatty Rat are Highly Consistent with Those Observed in Human Patients. Available: www.criver.com

8. Cordero-Herrera I, Martín MÁ, Goya L, Ramos S. Cocoa intake ameliorates hepatic oxidative stress in young Zucker diabetic fatty rats. Food Research International. 2015;69: 194–201. doi:10.1016/j.foodres.2014.12.039

9. Zou XR, Zhan LR, Chen L, Long QH, Yuan J, Wang L, et al. Influence of the klotho/FGF23/egr1 signaling pathway on calciumphosphorus metabolism in diabetic nephropathy and the intervention of shenyuan granules. Journal of Biological Regulators and Homeostatic Agents. 2019;33: 1695–1702. doi:10.23812/19-207-A

10. Fuller NR, Caterson ID, Sainsbury A, Denyer G, Fong M, Gerofi J, et al. The effect of a high-egg diet on cardiovascular risk factors in people with type 2 diabetes: The Diabetes and Egg (DIABEGG) study- A 3-mo randomized controlled trial. American Journal of Clinical Nutrition. 2015;101: 705–713. doi:10.3945/ajcn.114.096925

11. Djoussé L, Khawaja OA, Gaziano JM. Egg consumption and risk of type 2 diabetes: A meta-analysis of prospective studies. American Journal of Clinical Nutrition. 2016;103: 474–480. doi:10.3945/ajcn.115.119933

12. Yousr M, Howell N. Antioxidant and ACE inhibitory bioactive peptides purified from egg yolk proteins. International Journal of Molecular Sciences. 2015;16: 29161–29178. doi:10.3390/ijms161226155

13. Saande CJ, Webb JL, Curry PE, Rowling MJ, Schalinske KL. Dietary Whole Egg Reduces Body Weight Gain in a Dose-Dependent Manner in Zucker Diabetic Fatty Rats. The Journal of Nutrition. 2019;149: 1766–1775. doi:10.1093/jn/nxz143

14. Virtanen JK, Mursu J, Tuomainen TP, Virtanen HEK, Voutilainen S. Egg consumption and risk of incident type 2 diabetes in men: The kuopio ischaemic heart disease risk factor study. American Journal of Clinical Nutrition. 2015;101: 1088–1096. doi:10.3945/ajcn.114.104109

15. Rong Y, Chen L, Zhu T, Song Y, Yu M, Shan Z, et al. Egg consumption and risk of coronary heart disease and stroke: Dose-response meta-analysis of prospective cohort studies. BMJ (Online). 2013;346. doi:10.1136/bmj.e8539

16. Garcés-Rimón M, González C, Uranga JA, López-Miranda V, López-Fandiño R, Miguel M. Pepsin Egg White Hydrolysate Ameliorates Obesity-Related Oxidative Stress, Inflammation and Steatosis in Zucker Fatty Rats. Peterson J, editor. PLOS ONE. 2016;11: e0151193. doi:10.1371/journal.pone.0151193

17. Saande CJ, Steffes MA, Webb JL, Valentine RJ, Rowling MJ, Schalinske KL. Whole Egg Consumption Impairs Insulin Sensitivity in a Rat Model of Obesity and Type 2 Diabetes. Current Developments in Nutrition. 2019;3. doi:10.1093/CDN/NZZ015

18. Saande CJ, Jones SK, Rowling MJ, Schalinske KL. Whole Egg Consumption Exerts a Nephroprotective Effect in an Acute Rodent Model of Type 1 Diabetes. Journal of Agricultural and Food Chemistry. 2018;66: 866–870. doi:10.1021/acs.jafc.7b04774

19. Dhas Y, Mishra N, Banerjee J. Vitamin D Deficiency and Oxidative Stress in Type 2 Diabetic Population of India. Cardiovascular & Hematological Agents in Medicinal Chemistry. 2017;14: 82–89. doi:10.2174/1871525714666160426150233

20. Wimalawansa SJ. Vitamin D deficiency: Effects on oxidative stress, epigenetics, gene regulation, and aging. Biology. MDPI AG; 2019. doi:10.3390/biology8020030

21. Andrews S. FASTQC. A quality control tool for high throughput sequence data. 2010 [cited 5 Apr 2020]. Available: https://www.bibsonomy.org/person/1f230a919c34360709aa298734d63dca3/author/0

22. Pourafshar S, Akhavan NS, George KS, Foley EM, Johnson SA, Keshavarz B, et al. Egg consumption may improve factors associated with glycemic control and insulin sensitivity in adults with pre- and type II diabetes. Food and Function. 2018;9: 4469–4479. doi:10.1039/c8fo00194d

23. Dehghan M, Mente A, Rangarajan S, Mohan V, Lear S, Swaminathan S, et al. Association of egg intake with blood lipids, cardiovascular disease, and mortality in 177,000 people in 50 countries. 14: 34. doi:10.1093/ajcn/nqz348

24. Geiker NRW, Lytken Larsen M, Dyerberg J, Stender S, Astrup A. Egg consumption, cardiovascular diseases and type 2 diabetes. European Journal of Clinical Nutrition. Nature Publishing Group; 2018. pp. 44–56. doi:10.1038/ejcn.2017.153

25. Tran NL, Barraj LM, Heilman JM, Scrafford CG. Egg consumption and cardiovascular disease among diabetic individuals: A systematic review of the literature. Diabetes, Metabolic Syndrome and Obesity: Targets and Therapy. Dove Medical Press Ltd.; 2014. pp. 121–137. doi:10.2147/DMSO.S58668

26. Fuller NR, Sainsbury A, Caterson ID, Markovi TP. Egg consumption and human cardio-metabolic health in people with and without diabetes. Nutrients. MDPI AG; 2015. pp. 7399–7420. doi:10.3390/nu7095344

27. Patrick Emeka Aba, Domnic Chibuike Igwebuike, Jonas Anayo Onah. Effects of Various Concentrations of Quail Egg Solution on Glycemia and Antioxidant Parameters of Alloxan-induced Diabetic Rats. Journal of Advances in Medical and Pharmaceutical Sciences. 2015.

28. Evans JL, Goldfine ID, Maddux BA, Grodsky GM. Are oxidative stress - Activated signaling pathways mediators of insulin resistance and β-cell dysfunction? Diabetes. American Diabetes Association; 2003. pp. 1–8. doi:10.2337/diabetes.52.1.1

29. Suchocka Z, Kobylińska K, Pachecka J. Activity of glutathione-dependent enzymes in long term diabetes. II. Glutathione contents and activity of glutathione-dependent enzymes: S-transferase and peroxidase in the kidney cytosol of alloxan induced diabetic rats. Acta Pol Pharm. 1995;52.

30. Raza H, Ahmed I, John A, Sharma AK. Modulation of xenobiotic metabolism and oxidative stress in chronic streptozotocin-induced diabetic rats fed with Momordica charantia fruit extract. In: J Biochem Mol Toxicol [Internet]. 2000 [cited 26 Apr 2020]. Available: https://www.ncbi.nlm.nih.gov/pubmed/10711628

31. Quigley JD. Effects of spray-dried whole egg and biotin in calf milk replacer. Journal of Dairy Science. 2002;85: 198–203. doi:10.3168/jds.S0022-0302(02)74068-X

32. Chen X, Du Y, Boni GF, Liu X, Kuang J, Geng Z. Consuming egg yolk decreases body weight and increases serum HDL and brain expression of TrkB in male SD rats. Journal of the Science of Food and Agriculture. 2019;99: 3879–3885. doi:10.1002/jsfa.9610

33. Corbett SW, Stern JS, Keesey RE. Energy expenditure in rats with diet-induced obesity. The American journal of clinical nutrition. 1986;44: 173–80. doi:10.1093/ajcn/44.2.173

34. Shen N, Yu X, Pan FY, Gao X, Xue B, Li CJ. An early response transcription factor, Egr-1, enhances insulin resistance in type 2 diabetes with chronic hyperinsulinism. Journal of Biological Chemistry. 2011;286: 14508–14515. doi:10.1074/jbc.M110.190165

35. Garnett KE, Chapman P, Chambers JA, Waddell ID, Boam DSW. Differential gene expression between Zucker Fatty rats and Zucker Diabetic Fatty rats: a potential role for the immediate-early gene Egr-1 in regulation of beta cell proliferation. Journal of molecular endocrinology. 2005;35: 13–25. doi:10.1677/jme.1.01792

36. Zhang J, Zhang Y, Sun T, Guo F, Huang S, Chandalia M, et al. Dietary obesity-induced Egr-1 in adipocytes facilitates energy storage via suppression of FOXC2. Scientific Reports. 2013;3: 1–10. doi:10.1038/srep01476

37. Tiangang Li, Erika Owsley, Michelle Matozel, Peter Hsu, John Y.L. Chiang. Transgenic expression of CYP7A1 in the liver prevents high fat diet-induced obesity and insulin resistance in mice | The FASEB Journal. Pharmacology/Experimental Therapeutics. 2010.

38. Gutiérrez-Juárez R, Pocai A, Mulas C, Ono H, Bhanot S, Monia BP, et al. Critical role of stearoyl-CoA desaturase - 1 (SCD1) in the onset of diet-induced hepatic insulin resistance. Journal of Clinical Investigation. 2006;116: 1686–1695. doi:10.1172/JCI26991

39. Mugabo Y, Zhao S, Seifried A, Gezzar S, Al-Mass A, Zhang D, et al. Identification of a mammalian glycerol-3-phosphate phosphatase: Role in metabolism and signaling in pancreatic β-cells and hepatocytes. Proceedings of the National Academy of Sciences of the United States of America. 2016;113: E430–E439. doi:10.1073/pnas.1514375113

40. Zhang M, Zhu X. miR-9-5p plays an important role in gestational diabetes mellitus (GDM) progression by targeting HK-2. Int J Clin Exp Med. 2018. Available: www.ijcem.com/

41. Jassal B, Matthews L, Viteri G, Gong C, Lorente P, Fabregat A, et al. The reactome pathway knowledgebase. Nucleic Acids Research. 2020;48. doi:10.1093/nar/gkz1031

42. Karst H, Steiniger J, Noack R, Steglich HD. Diet-induced thermogenesis in man: Thermic effects of single proteins, carbohydrates and fats depending on their energy amount. Annals of Nutrition and Metabolism. 1984;28: 245–252. doi:10.1159/000176811

43. Kvaløy K, Page CM, Holmen TL. Epigenome-wide methylation differences in a group of lean and obese women – A HUNT Study. Scientific Reports. 2018;8: 1–9. doi:10.1038/s41598-018-34003-8

44. Chen J, He X, Huang J. Diet Effects in Gut Microbiome and Obesity. Journal of Food Science. 2014;79: R442-51. doi:10.1111/1750-3841.12397

45. Zhu C, Sawrey-Kubicek L, Bardagjy AS, Houts H, Tang X, Sacchi R, et al. Whole egg consumption increases plasma choline and betaine without affecting TMAO levels or gut microbiome in overweight postmenopausal women. Nutrition Research. 2020 [cited 26 Apr 2020]. doi:10.1016/j.nutres.2020.04.002

46. M. Shahbandeh, Statistica 2020. Per capita consumption of eggs in the U.S. 2020 | Statista. In: Statistica.com [Internet]. 28 Jan 2020 [cited 6 Aug 2020]. Available: https://www.statista.com/statistics/183678/per-capita-consumption-of-eggs-in-the-us-since-2000/

47. Leary S, Johnson CL. AVMA GUIDELINES FOR THE EUTHANASIA OF ANIMALS: 2020 EDITION AVMA Guidelines for the Euthanasia of Animals: 2020 Edition* Members of the Panel on Euthanasia AVMA Staff Consultants. 2020.

48. Bushnell B, Rood J, Singer E. BBMerge – Accurate paired shotgun read merging via overlap. PLoS ONE. 2017;12. doi:10.1371/journal.pone.0185056

49. Dobin A, Davis CA, Schlesinger F, Drenkow J, Zaleski C, Jha S, et al. STAR: Ultrafast universal RNA-seq aligner. Bioinformatics. 2013;29: 15–21. doi:10.1093/bioinformatics/bts635

50. Langmead B, Salzberg SL. Fast gapped-read alignment with Bowtie 2. Nature Methods. 2012;9: 357–359. doi:10.1038/nmeth.1923

51. Farrell D. smallrnaseq : short non coding RNA-seq analysis with Python. Bioarxiv. 2017; 110585. doi:10.1101/110585

52. Robinson MD, Oshlack A. A scaling normalization method for differential expression analysis of RNA-seq data. Genome Biology. 2010;11: R25. doi:10.1186/gb-2010-11-3-r25

53. Benjamini, Yoav ; Hochberg Y. Controlling the False Discovery Rate - a Practical and Powerful Approach to Multiple Testing. Journal of the Royal Statistical Society Series B-Methodological 1995.pdf. Journal of the Royal Statistical Society Series B (Methological). 1995. doi:10.2307/2346101

54. Livak KJ, Schmittgen TD. Analysis of Relative Gene Expression Data Using Real-Time Quantitative PCR and the 2 C T Method. METHODS. 2001;25: 402–408. doi:10.1006/meth.2001.1262

Tables and Figures

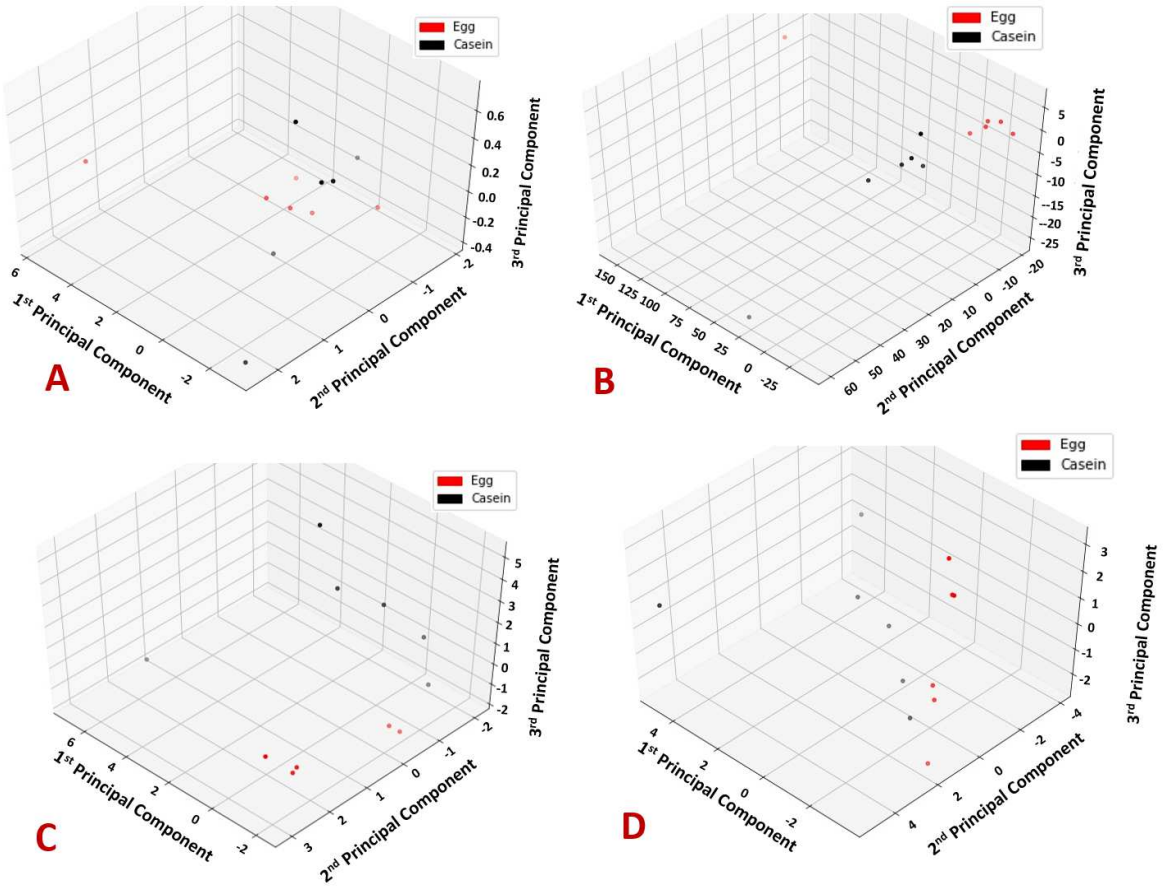

Figure A-1. Principle component analysis for both mRNA and microRNA data according to each genotype**.** Samples in the first three principle component space are colored in red or black for either WE or CAS, respectively. Each panel displays PCA results using microRNA data or mRNA data are colored by dietary treatment groups with A) ZDF microRNA, B) ZDF mRNA, C) lean microRNA, D) lean mRNA.

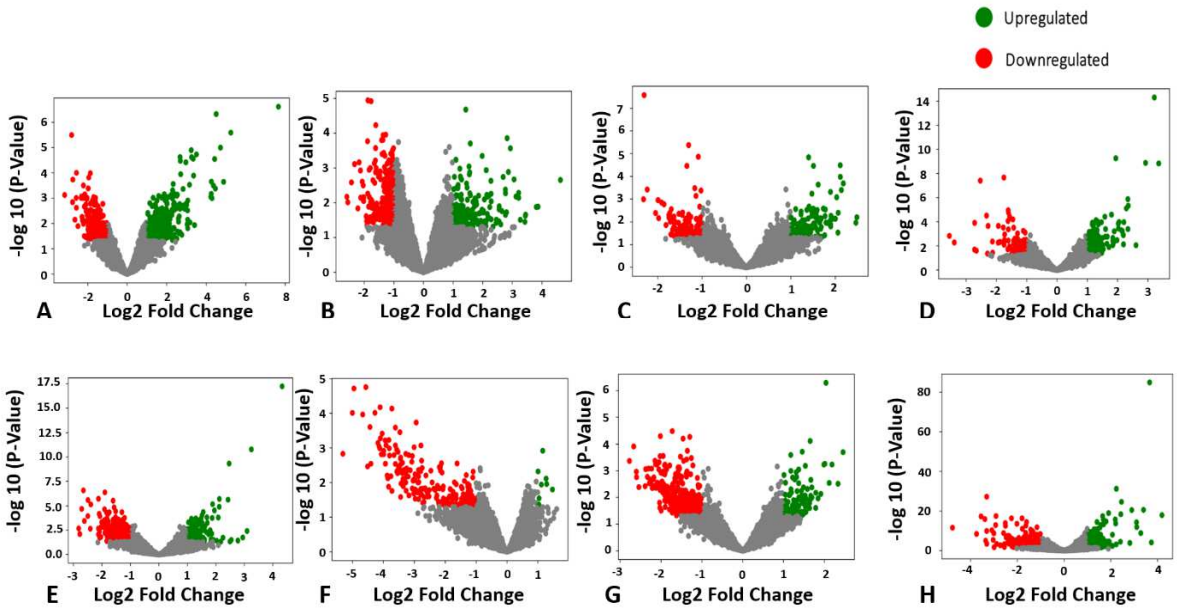

Figure A-2. Volcano plots indicating the directionality of the differentially expressed genes. Genes upregulated (green) or downregulated (red) by WE consumption, correspond to a 1.5 decrease or increase in log fold changes. Each panel corresponds to a tissue in a given genotype: A) lean adipose; B) lean PFC; C) lean kidney; D) lean liver; E) ZDF adipose; F) ZDF PFC; G) ZDF kidney; and H) ZDF liver.

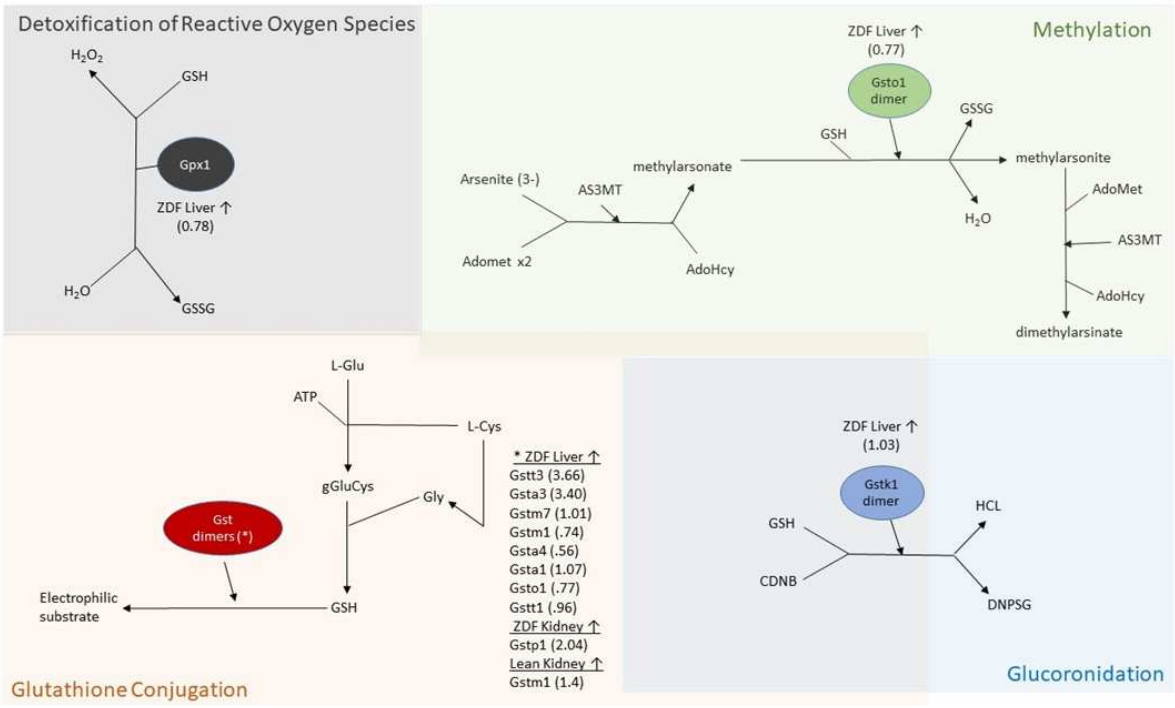

Figure A-3. Differentially Expressed Genes Involved in Glutathione Metabolism. This figure was adapted from D'Eustachio, P., and Jassal, B. from the Reactome [41]. Glutathione metabolism reactions can be categorized into glutathione conjugation, glucuronidation, methylation, or detoxification of reactive oxygen species. All genes are listed within each reaction category followed by their corresponding log2fold change in parentheses for each given tissue. Abbreviations used: ZDF, Zucker Diabetic fatty rat; GSSG, glutathione disulfide; GSH, glutathione; AS3MT, arsenite 3-methyltransferase; AdoMet, S-adenosyl methionine; AdoHcy, S-adenosyl homocysteine; CDNB, 1-chloro-2, 4-dinitrobenzene; DNPSG, S-(2,4-dinitrophenyl)glutathione; glu, glutamate; cys, cysteine; gly, glycine; gGluCys, gamma-glutamyl-L-cysteine; GST, glutathione s-transferase; and GPX, glutathione peroxidase.

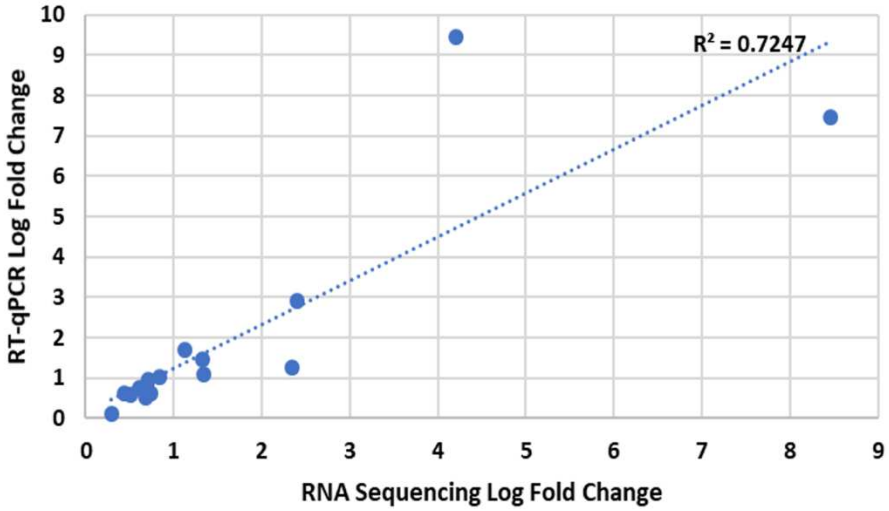

Supplemental Figure A-1. qPCR Correlation with mRNA Sequencing**.** Log fold change comparisons between qPCR and mRNA sequencing of several genes suggesting strong relationship between these two methods.

Table A-1: Differentially expressed genes in the liver, kidney, adipose and PFC tissues stratified according to each genotype[1-3].

Genotype	Tissue	Ensembl_ID (ENSRNO)	Symbol	Gene Name	L2FC	P-value[3]
ZDF	**Adipose Down-regulated**	G00000011039	Gch1	GTP cyclohydrolase 1	-2.71	2.1E-05
		G00000040108	RGD1565355	similar to fatty acid translocase/CD36	-2.65	2.7E-07
		G00000011024	Zdhhc20	zinc finger DHHC-type palmitoyltransferase 20	-2.49	1.2E-04
		G00000006946	Arhgap9	Rho GTPase activating protein 9	-2.49	2.6E-06
		G00000006715	Ccr1	C-C motif chemokine receptor 1	-2.39	7.4E-06
		G00000032546	Dot1l	DOT1 like histone lysine methyltransferase	-2.12	1.9E-06
		G00000034230	Fcrl1	Fc receptor-like 1	-2.09	6.9E-05
		G00000019283	P2ry2	purinergic receptor P2Y2	-2.07	1.2E-04
		G00000022975	Nfam1	NFAT activating protein with ITAM motif 1	-1.92	3.1E-04
		G00000013917	Igsf10	immunoglobulin superfamily, member 10	-1.91	2.4E-05
		G00000049115	Ccr5	C-C motif chemokine receptor 5	-1.89	4.3E-07
		G00000015895	B4galt6	beta-1,4-galactosyltransferase 6	-1.84	5.1E-05

Table A-1 Continued.

Genotype	Tissue	Ensembl_ID (ENSRNO)	Symbol	Gene Name	L2FC	P-value[3]
		G00000020479	Pik3c2a	phosphatidylinositol-4-phosphate 3-kinase, catalytic subunit type 2 alpha	-1.83	2.2E-04
		G00000061379	C7	complement C7	-1.82	1.8E-04
		G00000011927	Sdc3	syndecan 3	-1.82	2.3E-04
		G00000026644	Glipr1	GLI pathogenesis-related 1	-1.77	6.4E-05
		G00000011946	Ptn	pleiotrophin	-1.74	4.8E-05
		G00000013922	Dok2	docking protein 2	-1.61	2.7E-04
		G00000013526	Rassf4	Ras association domain family member 4	-1.60	3.1E-06
		G00000001989	Alcam	activated leukocyte cell adhesion molecule	-1.57	1.5E-05
		G00000016643	Lpcat2	lysophosphatidylcholine acyltransferase 2	-1.52	2.9E-04
		G00000003835	Slc43a2	solute carrier family 43 member 2	-1.52	1.6E-04
		G00000019077	Lipa	lipase A, lysosomal acid type	-1.51	3.8E-05
		G00000009347	Arhgap25	Rho GTPase activating protein 25	-1.49	2.1E-04
		G00000000257	Smpd3	sphingomyelin phosphodiesterase 3	-1.47	2.8E-04
		G00000012616	Ppt1	palmitoyl-protein thioesterase 1	-1.41	2.7E-04
		G00000009331	Hck	HCK proto-oncogene, Src family tyrosine kinase	-1.30	4.6E-05
		G00000010183	Gask1b	golgi associated kinase 1B	-1.26	2.7E-04
		G00000017022	Cerk	ceramide kinase	-1.25	3.2E-04
		G00000008465	Tmem176b	transmembrane protein 176B	-1.23	2.4E-04
		G00000010208	Timp1	TIMP metallopeptidase inhibitor 1	-1.20	1.8E-04
ZDF	**Adipose Up-regulated**	**Ensembl_ID (ENSRNO)**	**Gene Symbol**	**Gene Name**	**L2FC**	**P-value**
		G00000015072	Ptgr1	prostaglandin reductase 1	1.15	2.2E-04
		G00000010389	Ndrg2	NDRG family member 2	1.30	2.0E-04
		G00000037446	Pxmp2	peroxisomal membrane protein 2	1.30	2.3E-04
		G00000002896	Prdx6	peroxiredoxin 6	1.37	3.1E-04
		G00000019328	Phgdh	phosphoglycerate dehydrogenase	1.45	3.4E-04
		G00000021316	Tmem98	transmembrane protein 98	1.48	2.1E-04
		G00000046858	MGC109340	similar to Microsomal signal peptidase 23 kDa subunit (SPase 22 kDa subunit)	1.52	9.7E-05

Table A-1 Continued.

Genotype	Tissue	Ensembl_ID (ENSRNO)	Symbol	Gene Name	L2FC	P-value[3]
				(SPC22/23)		
		G00000017012	Coq7	coenzyme Q7, hydroxylase	1.56	4.5E-05
		G00000021524	Mrap	melanocortin 2 receptor accessory protein	1.69	1.6E-04
		G00000017226	Slc2a4	solute carrier family 2 member 4	1.87	1.8E-04
		G00000002579	Parm1	prostate androgen-regulated mucin-like protein 1	1.89	7.0E-06
		G00000001001	Retn	resistin	1.95	3.0E-05
		G00000008615	Mal2	mal, T-cell differentiation protein 2	2.09	1.6E-04
		G00000019412	Rhbg	Rh family B glycoprotein	2.12	1.3E-05
		G00000009715	Me1	malic enzyme 1	2.13	2.0E-06
		G00000012404	Thrsp	thyroid hormone responsive	2.43	2.4E-06
		G00000019914	Tlcd3b	TLC domain containing 3B	2.47	4.8E-10
		G00000045636	Fasn	fatty acid synthase	3.25	1.7E-11
		G00000049911	LOC102556347	carbonyl reductase [NADPH] 1-like	4.33	6.0E-18
Lean	**Adipose Down-regulated**	**Ensembl_ID (ENSRNO)**	**Gene Symbol**	**Gene Name**	**L2FC**	**P-value**
		G00000016700	Tcf21	transcription factor 21	-2.82	3.2E-06
Lean	**Adipose Up-regulated**	**Ensembl_ID (ENSRNO)**	**Gene Symbol**	**Gene Name**	**L2FC**	**P-value**
		G00000013733	Ppp4r1	protein phosphatase 4, regulatory subunit 1	2.68	2.4E-05
		G00000009536	Pgp	phosphoglycolate phosphatase	2.69	3.4E-05
		G00000031789	Rangap1	RAN GTPase activating protein 1	2.97	3.9E-05
		G00000005082	Irf6	interferon regulatory factor 6	3.25	1.3E-05

Table A-1 Continued.

Genotype	Tissue	Ensembl_ID (ENSRNO)	Symbol	Gene Name	L2FC	P-value[3]
		G00000031934	Enah	ENAH, actin regulator	3.26	2.4E-05
		G00000011296	Cenpn	centromere protein N	3.34	2.8E-05
		G00000056550	Epb41l4b	erythrocyte membrane protein band 4.1 like 4B	3.51	1.9E-05
		G00000021589	Nexmif	neurite extension and migration factor	4.43	2.9E-05
		G00000008713	Slc41a2	solute carrier family 41 member 2	4.51	4.8E-07
		G00000033262	Reep6	receptor accessory protein 6	4.72	1.0E-05
		G00000003098	Prom1	prominin 1	5.25	2.6E-06
		G00000015403	Cd52	CD52 molecule	7.66	2.5E-07
ZDF	**PFC Down-regulated**	**Ensembl_ID (ENSRNO)**	**Gene Symbol**	**Gene Name**	**L2FC**	**P-value**
		G00000033932	AY172581.22-201	AY172581.22-201	-5.21	1.1E-05
		G00000032112	AY172581.14	AY172581.14	-4.73	1.5E-05
ZDF	**PFC Up-regulated**	**Ensembl_ID (ENSRNO)**	**Gene Symbol**	**Gene Name**	**L2FC**	**P-value**
		None				
Lean	**PFC Down-regulated**	**Ensembl_ID (ENSRNO)**	**Gene Symbol**	**Gene Name**	**L2FC**	**P-value**
		None				
Lean	**PFC Up-regulated**	**Ensembl_ID (ENSRNO)**	**Gene Symbol**	**Gene Name**	**L2FC**	**P-value**
		None				
ZDF	**Kidney Down-regulated**	**Ensembl_ID (ENSRNO)**	**Gene Symbol**	**Gene Name**	**L2FC**	**P-value**
		G00000020204	Srp19	signal recognition particle 19	-1.72	3.3E-05
		G00000004794	Rtn1	reticulon 1	-2.01	5.1E-05
		G00000055471	Ywhah	tyrosine 3-monooxygenase/tryptophan 5-monooxygenase activation protein, eta	-1.29	5.5E-05

Table A-1 Continued.

Genotype	Tissue	Ensembl_ID (ENSRNO)	Symbol	Gene Name	L2FC	P-value[3]
		G00000003357	Col3a1	collagen type III alpha 1 chain	-1.46	6.4E-05
ZDF	**Kidney Up-regulated**	**Ensembl_ID (ENSRNO)**	**Gene Symbol**	**Gene Name**	**L2FC**	**P-value**
		G00000018237	Gstp1	glutathione S-transferase pi 1	2.04	5.2E-07
		G00000018940	CNT1	solute carrier family 28 member 1	1.65	7.8E-05
Lean	**Kidney Down-regulated**	**Ensembl_ID (ENSRNO)**	**Gene Symbol**	**Gene Name**	**L2FC**	**P-value**
		G00000020151	Cdh1	cadherin 1	-1.08	1.4E-05
		G00000013062	Cyp24a1	cytochrome P450, family 24, subfamily a, polypeptide 1	-1.30	4.3E-06
		G00000012956	Tgm2	transglutaminase 2	-1.34	3.5E-05
		G00000004019	Phlda1	pleckstrin homology-like domain, family A, member 1	-2.30	2.7E-08
Lean	**Kidney Up-regulated**	**Ensembl_ID (ENSRNO)**	**Gene Symbol**	**Gene Name**	**L2FC**	**P-value**
		G00000029726	Gstm1	glutathione S-transferase mu 1	1.40	1.5E-05
		G00000053811	Arg2	arginase 2	1.51	3.5E-05
		G00000000576	Anapc16	anaphase promoting complex subunit 16	2.11	3.3E-05
ZDF	**Liver Down-regulated**	**Ensembl_ID (ENSRNO)**	**Gene Symbol**	**Gene Name**	**L2FC**	**P-value**
		G00000014320	Inhba	inhibin subunit beta A	-4.77	3.2E-12
		G00000007923	Cgref1	cell growth regulator with EF hand domain 1	-3.74	4.4E-09
		G00000004307	Tor3a	torsin family 3	-3.55	6.1E-18
		G00000034190	Ighm	immunoglobulin heavy constant mu	-3.38	1.4E-16
		G00000003802	Pttg1	PTTG1 regulator of sister chromatid separation	-3.35	1.2E-05
		G00000007060	Plin2	perilipin 2	-3.31	6.8E-28

Table A-1 Continued.

Genotype	Tissue	Ensembl_ID (ENSRNO)	Symbol	Gene Name	L2FC	P-value[3]
		G00000045636	Fasn	fatty acid synthase	-3.31	1.5E-10
		G00000022256	Cxcl10	C-X-C motif chemokine ligand 10	-3.30	4.4E-04
		G00000009019	Slc6a6	solute carrier family 6 member 6	-3.09	6.0E-11
		G00000025691	Pla2g7	phospholipase A2 group VII	-3.03	4.5E-06
		G00000020035	Cyp17a1	cytochrome P450	-3.00	2.1E-09
		G00000020480	Fads1	fatty acid desaturase 1	-2.93	1.5E-13
		G00000000658	Acacb	acetyl-CoA carboxylase beta	-2.91	4.0E-18
		G00000030154	Cyp4a2	cytochrome P450	-2.88	5.0E-04
		G00000021802	Isg15	ISG15 ubiquitin-like modifier	-2.72	2.4E-03
		G00000001052	Slc25a30	solute carrier family 25	-2.58	1.8E-09
		G00000001963	Mx2	MX dynamin like GTPase 2	-2.56	2.1E-03
		G00000040151	Sdr16c6	short chain dehydrogenase/reductase family 16C	-2.55	6.3E-04
		G00000017914	Cavin3	caveolae associated protein 3	-2.51	1.4E-14
		G00000006859	Insig1	insulin induced gene 1	-2.50	3.4E-13
		G00000006204	Slc30a3	solute carrier family 30 member 3	-2.47	3.0E-07
		G00000016353	Nim1k	NIM1 serine/threonine protein kinase	-2.40	3.6E-08
		G00000016011	Plekhg1	pleckstrin homology and RhoGEF domain containing G1	-2.40	7.8E-05
		G00000028137	Mki67	marker of proliferation Ki-67	-2.38	1.5E-04
		G00000014476	Evl	Enah/Vasp-like	-2.37	3.4E-04
		G00000008022	Apaf1	apoptotic peptidase activating factor 1	-2.36	7.1E-05

Table A-1 Continued.

Genotype	Tissue	Ensembl_ID (ENSRNO)	Symbol	Gene Name	L2FC	P-value[3]
		G00000053891	Phf11	PHD finger protein 11	-2.34	6.4E-08
		G00000010819	Hspa4l	heat shock protein family A (Hsp70) member 4 like	-2.32	6.9E-06
		G00000021150	Plcb3	phospholipase C beta 3	-2.31	3.1E-05
		G00000001414	Serpine1	serpin family E member 1	-2.27	1.2E-04
		G00000016924	Acly	ATP citrate lyase	-2.25	5.5E-17
		G00000045560	Gvin1	GTPase	-2.25	2.1E-06
		G00000020503	Cbln3	cerebellin 3 precursor	-2.22	1.4E-06
		G00000052444	Samd9	sterile alpha motif domain containing 9	-2.22	3.3E-04
		G00000005209	Spred1	sprouty-related	-2.21	1.7E-05
		G00000010888	Ankrd33b	ankyrin repeat domain 33B	-2.20	2.1E-06
		G00000047218	Clic5	chloride intracellular channel 5	-2.20	1.7E-03
		G00000009481	Ddhd1	DDHD domain containing 1	-2.19	2.0E-04
		G00000022242	Cxcl9	C-X-C motif chemokine ligand 9	-2.16	1.3E-05
		G00000008807	Rp1	RP1	-2.08	4.7E-05
		G00000014426	Lox	lysyl oxidase	-2.07	1.9E-03
		G00000015498	Il17rb	interleukin 17 receptor B	-2.07	2.3E-04
		G00000051965	Smad4	SMAD family member 4	-2.07	8.7E-04
		G00000017512	Aldh3b1	aldehyde dehydrogenase 3 family	-2.05	1.0E-04
		G00000057092	Slfn4	schlafen family member 4	-2.05	6.2E-06
		G00000012685	Adck1	aarF domain containing kinase 1	-2.04	1.8E-03
		G00000011268	Chd5	chromodomain helicase DNA binding protein 5	-2.02	2.3E-03

Table A-1 Continued.

Genotype	Tissue	Ensembl_ID (ENSRNO)	Symbol	Gene Name	L2FC	P-value[3]
		G00000032374	Paqr9	progestin and adipoQ receptor family member 9	-2.01	3.3E-14
		G00000020272	Elapor1	endosome-lysosome associated apoptosis and autophagy regulator 1	-1.97	1.0E-04
		G00000061118	LOC102551095	uncharacterized LOC102551095	-1.96	9.6E-05
		G00000061527	Gck	glucokinase	-1.93	4.4E-07
		G00000053460	Acot3	acyl-CoA thioesterase 3	-1.91	1.4E-04
		G00000005043	Cpeb2	cytoplasmic polyadenylation element binding protein 2	-1.91	2.0E-03
		G00000017332	Dapk2	death-associated protein kinase 2	-1.87	3.8E-04
		G00000034013	Acaca	acetyl-CoA carboxylase alpha	-1.86	4.5E-05
		G00000017611	Tnp1	transition protein 1	-1.86	2.0E-03
		G00000012603	Sestd1	SEC14 and spectrin domain containing 1	-1.85	1.2E-03
		G00000025558	Palm2	paralemmin 2	-1.84	5.7E-06
		G00000018461	Pdgfrb	platelet derived growth factor receptor beta	-1.82	1.0E-03
		G00000016123	Rnf144b	ring finger protein 144B	-1.80	5.5E-17
		G00000013111	Mettl3	methyltransferase-like 3	-1.78	6.7E-04
		G00000045679	Apoa1	apolipoprotein A1	-1.78	1.1E-11
		G00000001926	Cldn1	claudin 1	-1.78	1.8E-06
		G00000005600	Nr4a2	nuclear receptor subfamily 4	-1.77	4.2E-04
		G00000012148	Trio	trio Rho guanine nucleotide exchange factor	-1.76	7.0E-04
		G00000004626	Slc34a2	solute carrier family 34 member 2	-1.76	8.7E-05
		G00000009360	Sh3bp1	SH3-domain binding protein 1	-1.74	2.2E-03
		G00000010890	Bmp1	bone morphogenetic protein 1	-1.71	1.8E-07

Table A-1 Continued.

Genotype	Tissue	Ensembl_ID (ENSRNO)	Symbol	Gene Name	L2FC	P-value[3]
		G00000011820	Acp3	acid phosphatase 3	-1.69	1.1E-04
		G00000007591	Slc45a3	solute carrier family 45	-1.68	8.9E-05
		G00000006170	Bach2	BTB domain and CNC homolog 2	-1.68	1.2E-03
		G00000028895	Rtp4	receptor (chemosensory) transporter protein 4	-1.66	5.3E-05
		G00000002773	Rgs4	regulator of G-protein signaling 4	-1.65	5.0E-04
		G00000007234	Cyp51	cytochrome P450	-1.64	1.2E-09
		G00000020918	Ccnd1	cyclin D1	-1.64	7.0E-09
		G00000028941	Zbed3	zinc finger	-1.63	8.4E-06
		G00000012681	Lgals9	galectin 9	-1.63	2.8E-13
		G00000001640	Tomm70	translocase of outer mitochondrial membrane 70	-1.63	2.6E-03
		G00000009117	Otub2	OTU deubiquitinase	-1.62	1.9E-04
		G00000005726	Pclo	piccolo (presynaptic cytomatrix protein)	-1.62	6.2E-04
		G00000051171	G6pc	glucose-6-phosphatase	-1.61	1.6E-04
		G00000016552	Hmgcs1	3-hydroxy-3-methylglutaryl-CoA synthase 1	-1.60	4.4E-15
		G00000004577	Fez2	fasciculation and elongation protein zeta 2	-1.60	1.9E-04
		G00000000547	Tspyl4	TSPY-like 4	-1.59	5.0E-04
		G00000017120	Abhd2	abhydrolase domain containing 2	-1.59	1.9E-07
		G00000015906	Tgif1	TGFB-induced factor homeobox 1	-1.56	1.1E-03
		G00000008144	Irf1	interferon regulatory factor 1	-1.54	2.4E-06
		G00000007319	Trib3	tribbles pseudokinase 3	-1.54	8.5E-06
		G00000018467	Mitd1	microtubule interacting and trafficking domain containing 1	-1.52	1.9E-03

Table A-1 Continued.

Genotype	Tissue	Ensembl_ID (ENSRNO)	Symbol	Gene Name	L2FC	P-value[3]
		G00000023238	Dgkd	diacylglycerol kinase	-1.52	1.2E-05
		G00000020776	Dhcr7	7-dehydrocholesterol reductase	-1.51	1.1E-05
		G00000033824	Gpd2	glycerol-3-phosphate dehydrogenase 2	-1.51	5.5E-04
		G00000003442	Adora1	adenosine A1 receptor	-1.50	2.3E-06
		G00000025689	Abhd1	abhydrolase domain containing 1	-1.50	2.1E-07
		G00000018198	Dapk1	death associated protein kinase 1	-1.48	5.3E-04
		G00000029668	Wfdc21	WAP four-disulfide core domain 21	-1.45	1.6E-04
		G00000006280	Pcsk9	proprotein convertase subtilisin/kexin type 9	-1.44	4.7E-07
		G00000008215	Trim47	tripartite motif-containing 47	-1.44	1.3E-04
		G00000014013	Map4k4	mitogen-activated protein kinase kinase kinase kinase 4	-1.43	1.1E-05
		G00000018627	Plekhb1	pleckstrin homology domain containing B1	-1.43	8.9E-05
		G00000007713	Tmcc3	transmembrane and coiled-coil domain family 3	-1.43	2.6E-05
		G00000000987	Ptcd1	pentatricopeptide repeat domain 1	-1.43	1.0E-03
		G00000014702	Elovl2	ELOVL fatty acid elongase 2	-1.43	2.8E-11
		G00000037595	Gpbp1l1	GC-rich promoter binding protein 1-like 1	-1.41	2.3E-04
		G00000001205	Agpat3	1-acylglycerol-3-phosphate O-acyltransferase 3	-1.41	3.8E-09
		G00000019776	Sh3gl3	SH3 domain containing GRB2 like 3	-1.40	4.1E-05
		G00000012622	Mmp15	matrix metallopeptidase 15	-1.40	1.9E-03
		G00000023856	Agxt	alanine--glyoxylate and serine--pyruvate aminotransferase	-1.39	7.5E-11
		G00000042560	Bag4	BCL2-associated athanogene 4	-1.38	1.2E-03
		G00000013841	Dcaf1	DDB1 and CUL4 associated factor 1	-1.38	2.1E-03

Table A-1 Continued.

Genotype	Tissue	Ensembl_ID (ENSRNO)	Symbol	Gene Name	L2FC	P-value[3]
		G00000019995	Dnajc18	DnaJ heat shock protein family (Hsp40) member C18	-1.37	2.4E-04
		G00000019996	Slc16a1	solute carrier family 16 member 1	-1.36	1.6E-04
		G00000023226	S100a10	S100 calcium binding protein A10	-1.35	2.2E-04
		G00000006227	Ifih1	interferon induced with helicase C domain 1	-1.35	7.5E-04
		G00000019005	Pde8a	phosphodiesterase 8A	-1.34	1.5E-03
		G00000021259	Prnp	prion protein	-1.33	1.7E-03
		G00000055909	Apoa4	apolipoprotein A4	-1.33	2.6E-10
		G00000008012	Abcb4	ATP binding cassette subfamily B member 4	-1.33	4.1E-10
		G00000021405	Cyp2c7	cytochrome P450	-1.32	1.0E-08
		G00000012181	Lpl	lipoprotein lipase	-1.31	5.3E-05
		G00000056041		AABR07062570	-1.30	2.5E-03
		G00000016815	Tmem135	transmembrane protein 135	-1.29	4.1E-05
		G00000019422	Egr1	early growth response 1	-1.29	1.1E-05
		G00000054077		Aabr07024870	-1.29	1.4E-03
		G00000008194	Znfx1	zinc finger	-1.28	5.5E-04
		G00000009076	Ttpal	alpha tocopherol transfer protein like	-1.27	1.7E-03
		G00000005825	Lyz2	lysozyme 2	-1.26	2.7E-05
		G00000032293	Polg	DNA polymerase gamma	-1.26	2.9E-04
		G00000008586	Aldh1l2	aldehyde dehydrogenase 1 family	-1.26	3.5E-04
		G00000010805	Fabp4	fatty acid binding protein 4	-1.25	2.5E-03
		G00000016044	Mab21l3	mab-21 like 3	-1.25	1.0E-04

Table A-1 Continued.

Genotype	Tissue	Ensembl_ID (ENSRNO)	Symbol	Gene Name	L2FC	P-value[3]
		G00000000459	Psmb9	proteasome 20S subunit beta 9	-1.25	7.4E-04
		G00000015124	Gpam	glycerol-3-phosphate acyltransferase	-1.25	1.4E-03
		G00000020871	Ltbp4	latent transforming growth factor beta binding protein 4	-1.22	2.1E-03
		G00000016516	Mbp	myelin basic protein	-1.22	1.2E-04
		G00000007324	Plxna2	plexin A2	-1.22	2.4E-07
		G00000001821	Adipoq	adiponectin	-1.21	2.7E-03
		G00000020573	Efna1	ephrin A1	-1.19	1.7E-04
		G00000004606	Meis1	Meis homeobox 1	-1.19	8.3E-04
		G00000001647	Ets2	ETS proto-oncogene 2	-1.17	9.1E-09
		G00000059043	Itch	itchy E3 ubiquitin protein ligase	-1.17	1.4E-03
		G00000006787	Dhcr24	24-dehydrocholesterol reductase	-1.16	1.9E-12
		G00000015121	N4bp1	Nedd4 binding protein 1	-1.15	3.0E-04
		G00000042771	Apol3	apolipoprotein L	-1.14	7.6E-08
		G00000023664	Lepr	leptin receptor	-1.12	2.5E-03
		G00000000451	RT1-Ba	RT1 class II	-1.12	1.1E-03
		G00000012782	Cemip2	cell migration inducing hyaluronidase 2	-1.11	1.0E-05
		G00000014766	Galt	galactose-1-phosphate uridylyltransferase	-1.11	1.7E-05
		G00000014718	Acsl3	acyl-CoA synthetase long-chain family member 3	-1.11	1.4E-03
		G00000017428	Map1b	microtubule-associated protein 1B	-1.10	1.7E-03
		G00000018517	Trim21	tripartite motif-containing 21	-1.09	2.0E-03
		G00000001426	Prkrip1	PRKR interacting protein 1	-1.09	2.2E-03

Table A-1 Continued.

Genotype	Tissue	Ensembl_ID (ENSRNO)	Symbol	Gene Name	L2FC	P-value[3]
		G00000028448	Elovl1	ELOVL fatty acid elongase 1	-1.08	2.2E-03
		G00000005695	Mgp	matrix Gla protein	-1.07	1.2E-03
		G00000017558	Tubb2a	tubulin	-1.07	7.2E-04
		G00000012876	Slc6a13	solute carrier family 6 member 13	-1.07	7.1E-05
		G00000018960	Syne1	spectrin repeat containing nuclear envelope protein 1	-1.07	7.3E-05
		G00000017993	Abcb10	ATP binding cassette subfamily B member 10	-1.05	8.6E-05
		G00000007545	Angptl4	angiopoietin-like 4	-1.04	4.1E-07
		G00000007990	Adipor2	adiponectin receptor 2	-1.04	1.1E-04
		G00000020134	Upf1	UPF1	-1.03	5.1E-04
		G00000027434	Fitm2	fat storage-inducing transmembrane protein 2	-1.02	1.7E-05
		G00000048315	Eif2ak2	eukaryotic translation initiation factor 2-alpha kinase 2	-1.02	6.7E-05
		G00000005642	Frs2	fibroblast growth factor receptor substrate 2	-1.02	7.7E-04
		G00000014604	Sigmar1	sigma non-opioid intracellular receptor 1	-1.01	4.9E-09
		G00000002175	Clock	clock circadian regulator	-1.01	2.4E-04
		G00000042785	Sesn2	sestrin 2	-1.00	1.7E-05
		G00000023463	Parp9	poly (ADP-ribose) polymerase family	-0.99	3.5E-04
		G00000043377	Fdps	farnesyl diphosphate synthase	-0.99	1.6E-03
		G00000000593	Rev3l	REV3 like	-0.98	2.0E-03
		G00000019283	P2ry2	purinergic receptor P2Y2	-0.98	1.0E-03
		G00000024061	Rarb	retinoic acid receptor	-0.98	2.7E-03
		G00000017220	Tcirg1	T-cell immune regulator 1	-0.98	3.3E-04

Table A-1 Continued.

Genotype	Tissue	Ensembl_ID (ENSRNO)	Symbol	Gene Name	L2FC	P-value[3]
		G00000021032	Sphk2	sphingosine kinase 2	-0.97	2.3E-05
		G00000001585	Nrip1	nuclear receptor interacting protein 1	-0.97	1.1E-03
		G00000003882	Cep350	centrosomal protein 350	-0.96	5.2E-04
		G00000005292	Trip11	thyroid hormone receptor interactor 11	-0.96	2.4E-06
		G00000046889	Dbi	diazepam binding inhibitor	-0.96	2.3E-05
		G00000000664	Tpst2	tyrosylprotein sulfotransferase 2	-0.95	2.1E-03
		G00000014900	Crem	cAMP responsive element modulator	-0.95	2.0E-03
		G00000024115	C6	complement C6	-0.93	2.9E-04
		G00000030225	Clpx	caseinolytic mitochondrial matrix peptidase chaperone subunit X	-0.92	3.8E-05
		G00000038012	Commd6	COMM domain containing 6	-0.91	1.8E-04
		G00000007302	Fbn1	fibrillin 1	-0.91	1.4E-03
		G00000018420	Slc22a7	solute carrier family 22 member 7	-0.90	4.1E-04
		G00000002635	Dexi	Dexi homolog	-0.89	1.6E-06
		G00000007728	Gsdmd	gasdermin D	-0.89	2.3E-03
		G00000026942	RGD1311595	similar to KIAA2026 protein	-0.88	2.9E-05
		G00000034066	Hspa8	heat shock protein family A (Hsp70) member 8	-0.87	3.0E-04
		G00000019372	Pc	pyruvate carboxylase	-0.87	8.5E-06
		G00000000177	Plpp2	phospholipid phosphatase 2	-0.87	9.6E-04
		G00000056703	Atrx	ATRX	-0.86	2.0E-04
		G00000016219	Vnn1	vanin 1	-0.86	1.5E-04
		G00000014338	Slc25a25	solute carrier family 25 member 25	-0.86	6.6E-04

Table A-1 Continued.

Genotype	Tissue	Ensembl_ID (ENSRNO)	Symbol	Gene Name	L2FC	P-value[3]
		G00000013391	Sorbs2	sorbin and SH3 domain containing 2	-0.84	9.9E-06
		G00000016692	Hsdl2	hydroxysteroid dehydrogenase like 2	-0.83	1.3E-04
		G00000024145	Trim65	tripartite motif-containing 65	-0.83	5.9E-05
		G00000010947	Mmp14	matrix metallopeptidase 14	-0.83	1.7E-03
		G00000018584	Ptma	prothymosin alpha	-0.83	1.5E-05
		G00000008274	Xpc	XPC complex subunit	-0.83	3.6E-04
		G00000011261	Ttc14	tetratricopeptide repeat domain 14	-0.83	2.7E-03
		G00000047386	Smg1	SMG1	-0.82	2.7E-03
		G00000007400	Srebf2	sterol regulatory element binding transcription factor 2	-0.82	4.0E-04
		G00000028801	Gsap	gamma-secretase activating protein	-0.82	2.1E-03
		G00000007700	Inhbc	inhibin subunit beta C	-0.81	5.3E-04
		G00000013178	Cmip	c-Maf-inducing protein	-0.81	6.6E-04
		G00000032394	Tymp	thymidine phosphorylase	-0.80	5.0E-04
		G00000031709	Ppfibp1	PPFIA binding protein 1	-0.79	6.6E-04
		G00000003020	Slc25a47	solute carrier family 25	-0.79	1.5E-03
		G00000019450	Etf1	eukaryotic translation termination factor 1	-0.78	1.6E-03
		G00000010497	RGD1305807	hypothetical LOC298077	-0.77	1.7E-05
		G00000000184	Tmprss6	transmembrane serine protease 6	-0.75	3.7E-04
		G00000004709	Foxn3	forkhead box N3	-0.73	2.2E-04
		G00000007681	Brd3	bromodomain containing 3	-0.72	2.1E-03
		G00000033593	Osbpl9	oxysterol binding protein-like 9	-0.72	7.9E-04

Table A-1 Continued.

Genotype	Tissue	Ensembl_ID (ENSRNO)	Symbol	Gene Name	L2FC	P-value[3]
		G00000002212	Hsd17b13	hydroxysteroid (17-beta) dehydrogenase 13	-0.70	5.2E-06
		G00000053550	Itga1	integrin subunit alpha 1	-0.68	1.6E-03
		G00000030700	COX3	cytochrome c oxidase subunit 3	-0.67	2.8E-04
		G00000020425	Stim1	stromal interaction molecule 1	-0.66	1.0E-03
		G00000057814	Nsdhl	NAD(P) dependent steroid dehydrogenase-like	-0.66	2.0E-05
		G00000056371	Pik3ca	phosphatidylinositol-4	-0.66	1.5E-03
		G00000016266	Mphosph10	M-phase phosphoprotein 10	-0.65	2.2E-03
		G00000015441	Il4r	interleukin 4 receptor	-0.65	1.8E-03
		G00000009102	Fermt2	fermitin family member 2	-0.62	2.2E-03
		G00000005015	Rabep1	rabaptin	-0.62	1.8E-03
		G00000020151	Cdh1	cadherin 1	-0.60	2.4E-03
		G00000013135	Ptpn12	protein tyrosine phosphatase	-0.58	2.7E-04
		G00000057623	Copb1	COPI coat complex subunit beta 1	-0.53	4.7E-04
		G00000011140	Prxl2a	peroxiredoxin like 2A	-0.51	2.0E-03
		G00000018849	Tcerg1	transcription elongation regulator 1	-0.51	2.0E-03
		G00000008305	Sc5d	sterol-C5-desaturase	-0.47	2.0E-03
		G00000009263	Ifi27	interferon	-0.47	2.2E-03
		G00000004345	Daam1	dishevelled associated activator of morphogenesis 1	-0.46	2.7E-03
		G00000016963	Trip12	thyroid hormone receptor interactor 12	-0.43	1.7E-03
ZDF	**Liver Up-regulated**	**Ensembl_ID (ENSRNO)**	**Gene Symbol**	**Gene Name**	**L2FC**	**P-value**
		G00000003119	Gc	GC	0.45	1.1E-03

Table A-1 Continued.

Genotype	Tissue	Ensembl_ID (ENSRNO)	Symbol	Gene Name	L2FC	P-value[3]
		G00000000610	Cisd1	CDGSH iron sulfur domain 1	0.46	7.7E-04
		G00000019629	Lamp1	lysosomal-associated membrane protein 1	0.50	8.8E-05
		G00000000701	Iscu	iron-sulfur cluster assembly enzyme	0.51	4.0E-05
		G00000037850	Mtarc2	mitochondrial amidoxime reducing component 2	0.51	6.0E-04
		G00000019048	Sod2	superoxide dismutase 2	0.54	2.8E-04
		G00000007967	Sdhb	succinate dehydrogenase complex iron sulfur subunit B	0.54	1.8E-03
		G00000013928	Dsp	desmoplakin	0.54	1.5E-03
		G00000016794	Phyhd1	phytanoyl-CoA dioxygenase domain containing 1	0.55	2.0E-03
		G00000019626	Slc27a5	solute carrier family 27 member 5	0.55	8.8E-05
		G00000028368	Etnk2	ethanolamine kinase 2	0.55	1.4E-03
		G00000011535	Gcsh	glycine cleavage system protein H	0.56	9.9E-04
		G00000008921	Dynll2	dynein light chain LC8-type 2	0.56	1.5E-03
		G00000030449	Gsta4	glutathione S-transferase alpha 4	0.56	1.1E-03
		G00000018604	Tufm	Tu translation elongation factor	0.59	2.2E-03
		G00000017672	Akr1c14	aldo-keto reductase family 1	0.59	3.1E-04
		G00000020994	Slc25a39	solute carrier family 25	0.59	7.3E-04
		G00000047708	Gstz1	glutathione S-transferase zeta 1	0.59	1.1E-04
		G00000013704	Cps1	carbamoyl-phosphate synthase 1	0.60	5.4E-04
		G00000043404	Uroc1	urocanate hydratase 1	0.60	1.6E-05
		G00000007395	Baat	bile acid CoA:amino acid N-acyltransferase	0.60	5.3E-04
		G00000017577	Bphl	biphenyl hydrolase like	0.60	6.8E-04

Table A-1 Continued.

Genotype	Tissue	Ensembl_ID (ENSRNO)	Symbol	Gene Name	L2FC	P-value[3]
		G00000007069	Adhfe1	alcohol dehydrogenase	0.62	4.9E-04
		G00000023538	Aldh5a1	aldehyde dehydrogenase 5 family	0.62	4.9E-04
		G00000006653	Slc38a4	solute carrier family 38	0.62	1.2E-04
		G00000001333	Azgp1	alpha-2-glycoprotein 1	0.62	8.6E-06
		G00000016339	Uox	urate oxidase	0.63	2.8E-05
		G00000061876	Tas1r2	taste 1 receptor member 2	0.63	2.4E-04
		G00000006916	Sardh	sarcosine dehydrogenase	0.63	8.6E-05
		G00000029549	Eci3	enoyl-Coenzyme A delta isomerase 3	0.63	8.9E-04
		G00000048723	Pros1	protein S	0.64	4.9E-04
		G00000009005	Slco2a1	solute carrier organic anion transporter family	0.64	2.7E-05
		G00000007839	Slc16a7	solute carrier family 16 member 7	0.64	8.2E-04
		G00000010389	Ndrg2	NDRG family member 2	0.65	5.7E-04
		G00000014165	Ssr1	signal sequence receptor subunit 1	0.65	1.0E-04
		G00000029735	Pid1	phosphotyrosine interaction domain containing 1	0.65	1.9E-03
		G00000033466	Apon	apolipoprotein N	0.65	1.1E-03
		G00000000158	Cdo1	cysteine dioxygenase type 1	0.65	6.6E-06
		G00000008364	Cat	catalase	0.67	1.1E-03
		G00000061883	Aqp9	aquaporin 9	0.68	1.3E-03
		G00000021916	Slc16a12	solute carrier family 16	0.68	2.5E-03
		G00000007743	Mgst1	microsomal glutathione S-transferase 1	0.68	1.8E-05
		G00000003653	Fh	fumarate hydratase	0.68	1.6E-03

Table A-1 Continued.

Genotype	Tissue	Ensembl_ID (ENSRNO)	Symbol	Gene Name	L2FC	P-value[3]
		G00000013223	Fah	fumarylacetoacetate hydrolase	0.69	2.4E-04
		G00000014700	Ttc36	tetratricopeptide repeat domain 36	0.69	8.4E-05
		G00000030862	Atp6v1h	ATPase H+ transporting V1 subunit H	0.69	4.9E-04
		G00000030667	Ppm1b	protein phosphatase	0.71	4.7E-06
		G00000004139	Ndel1	nudE neurodevelopment protein 1-like 1	0.72	3.8E-05
		G00000007927	Mettl7b	methyltransferase like 7B	0.72	5.0E-05
		G00000004147	Abca8a	ATP-binding cassette	0.73	1.4E-03
		G00000029726	Gstm1	glutathione S-transferase mu 1	0.74	1.3E-03
		G00000003370	Otc	ornithine carbamoyltransferase	0.74	6.8E-06
		G00000013039	Add1	adducin 1	0.74	4.2E-04
		G00000014727	Fahd1	fumarylacetoacetate hydrolase domain containing 1	0.75	4.2E-04
		G00000059463	Slc39a1	solute carrier family 39 member 1	0.76	1.6E-03
		G00000004302	Pah	phenylalanine hydroxylase	0.76	3.4E-07
		G00000029651	Rdh16	retinol dehydrogenase 16	0.76	8.2E-04
		G00000028746	Gsto1	glutathione S-transferase omega 1	0.77	3.2E-04
		G00000018426	NEWGENE_2134	apolipoprotein C1	0.77	1.3E-06
		G00000001053	Tmed2	transmembrane p24 trafficking protein 2	0.77	6.7E-04
		G00000016173	Cyp1a2	cytochrome P450	0.77	6.7E-04
		G00000004089	Enpp2	ectonucleotide pyrophosphatase/phosphodiesterase 2	0.78	3.5E-04
		G00000042274	Fbxo31	F-box protein 31	0.78	2.3E-03

Table A-1 Continued.

Genotype	Tissue	Ensembl_ID (ENSRNO)	Symbol	Gene Name	L2FC	P-value[3]
		G00000000186	Tst	thiosulfate sulfurtransferase	0.78	8.6E-05
		G00000048812	Gpx1	glutathione peroxidase 1	0.79	5.0E-04
		G00000047986	Sult2a1	sulfotransferase family 2A member 1	0.79	2.5E-03
		G00000006345	Sec61b	SEC61 translocon subunit beta	0.79	6.2E-04
		G00000009779	Krt8	keratin 8	0.79	2.2E-03
		G00000006623	Cd302	CD302 molecule	0.80	1.5E-04
		G00000005987	Suox	sulfite oxidase	0.81	1.1E-03
		G00000061890	Ust5r	integral membrane transport protein UST5r	0.81	2.3E-04
		G00000020879	Nags	N-acetylglutamate synthase	0.81	3.3E-04
		G00000008902	Pon1	paraoxonase 1	0.82	9.7E-07
		G00000018904	Dtymk	deoxythymidylate kinase	0.82	2.1E-03
		G00000023116	Agmo	alkylglycerol monooxygenase	0.82	4.0E-05
		G00000047816	Ccs	copper chaperone for superoxide dismutase	0.84	1.3E-04
		G00000012142	Glyat	glycine-N-acyltransferase	0.84	5.6E-07
		G00000021206	Plaat3	phospholipase A and acyltransferase 3	0.84	7.5E-04
		G00000012962	Nudt16	nudix hydrolase 16	0.85	1.9E-04
		G00000050315	Dcxr	dicarbonyl and L-xylulose reductase	0.86	2.9E-06
		G00000000024	Hebp1	heme binding protein 1	0.86	2.7E-04
		G00000000386	Pbld1	phenazine biosynthesis-like protein domain containing 1	0.87	1.3E-05
		G00000007378	Acox2	acyl-CoA oxidase 2	0.87	7.0E-05
		G00000003307	Gcdh	glutaryl-CoA dehydrogenase	0.87	2.2E-08

Table A-1 Continued.

Genotype	Tissue	Ensembl_ID (ENSRNO)	Symbol	Gene Name	L2FC	P-value[3]
		G00000002205	Ociad1	OCIA domain containing 1	0.87	1.4E-03
		G00000014645	Aldh7a1	aldehyde dehydrogenase 7 family	0.88	8.2E-08
		G00000008638	Angptl3	angiopoietin-like 3	0.88	2.9E-09
		G00000011351	Mat1a	methionine adenosyltransferase 1A	0.89	3.6E-05
		G00000009421	Ivd	isovaleryl-CoA dehydrogenase	0.89	1.9E-09
		G00000036894	Cisd3	CDGSH iron sulfur domain 3	0.89	4.0E-04
		G00000014128	Ecsit	ECSIT signaling integrator	0.90	1.6E-03
		G00000017619	Aldh1a1	aldehyde dehydrogenase 1 family	0.90	3.1E-05
		G00000018662	Amacr	alpha-methylacyl-CoA racemase	0.90	3.9E-07
		G00000020000	Tmem219	transmembrane protein 219	0.90	5.2E-04
		G00000001957	Sult1e1	sulfotransferase family 1E member 1	0.90	2.8E-06
		G00000051860	Rnase4	ribonuclease A family member 4	0.91	1.3E-09
		G00000014160	Tcp1	t-complex 1	0.91	2.2E-04
		G00000048114	Echdc3	enoyl CoA hydratase domain containing 3	0.91	2.7E-07
		G00000003291	Creg1	cellular repressor of E1A-stimulated genes 1	0.92	1.3E-07
		G00000008837	Ass1	argininosuccinate synthase 1	0.92	7.7E-04
		G00000018159	Anxa4	annexin A4	0.92	2.3E-04
		G00000010993	Dpm1	dolichyl-phosphate mannosyltransferase subunit 1	0.92	9.1E-04
		G00000019982	Ethe1	ETHE1	0.92	2.4E-05
		G00000023177	Esrp2	epithelial splicing regulatory protein 2	0.93	9.8E-07
		G00000013409	Gclm	glutamate cysteine ligase	0.93	3.0E-04

Table A-1 Continued.

Genotype	Tissue	Ensembl_ID (ENSRNO)	Symbol	Gene Name	L2FC	P-value[3]
		G00000001806	Fetub	fetuin B	0.93	2.9E-04
		G00000017291	Sord	sorbitol dehydrogenase	0.94	7.2E-09
		G00000053362	Gabarapl1	GABA type A receptor associated protein like 1	0.94	1.4E-07
		G00000021174	Macrod1	mono-ADP ribosylhydrolase 1	0.95	7.1E-05
		G00000014268	Abca2	ATP binding cassette subfamily A member 2	0.95	9.8E-04
		G00000049771	Gstt1	glutathione S-transferase theta 1	0.96	8.4E-05
		G00000011226	Timm8a1	translocase of inner mitochondrial membrane 8A1	0.96	4.5E-06
		G00000005175	Sgpp1	sphingosine-1-phosphate phosphatase 1	0.97	2.0E-03
		G00000049464	Cyp2c13	cytochrome P450	0.97	6.0E-10
		G00000002210	Hsd17b11	hydroxysteroid (17-beta) dehydrogenase 11	0.97	4.4E-10
		G00000012786	Pgrmc1	progesterone receptor membrane component 1	0.99	1.2E-07
		G00000004327	Ddc	dopa decarboxylase	0.99	4.8E-05
		G00000046357	Adh5	alcohol dehydrogenase 5 (class III)	0.99	1.2E-11
		G00000054049	Prelid2	PRELI domain containing 2	0.99	7.6E-04
		G00000004442	Dglucy	D-glutamate cyclase	0.99	1.6E-03
		G00000014876	Lpin2	lipin 2	1.00	3.9E-04
		G00000012911	Erlin1	ER lipid raft associated 1	1.00	6.8E-04
		G00000055314	Msrb1	methionine sulfoxide reductase B1	1.00	1.1E-07
		G00000006619	Dnajc9	DnaJ heat shock protein family (Hsp40) member C9	1.01	6.5E-04
		G00000018937	Gstm7	glutathione S-transferase	1.01	1.6E-04
		G00000027016	Cobll1	cordon-bleu WH2 repeat protein-like 1	1.01	1.4E-04

Table A-1 Continued.

Genotype	Tissue	Ensembl_ID (ENSRNO)	Symbol	Gene Name	L2FC	P-value[3]
		G00000046007	Cldn3	claudin 3	1.02	2.8E-04
		G00000033609	Irx1	iroquois homeobox 1	1.02	2.0E-03
		G00000017777	Ahcy	adenosylhomocysteinase	1.02	1.5E-05
		G00000019180	Acsl4	acyl-CoA synthetase long-chain family member 4	1.02	1.0E-08
		G00000022932	Serhl2	serine hydrolase-like 2	1.03	1.5E-04
		G00000016484	Gstk1	glutathione S-transferase kappa 1	1.03	1.5E-07
		G00000003620	Fmo3	flavin containing dimethylaniline monoxygenase 3	1.04	1.7E-05
		G00000032895	Cyp4f4	cytochrome P450	1.04	5.0E-08
		G00000032737	F7	coagulation factor VII	1.05	2.1E-04
		G00000023816	Aph1a	aph-1 homolog A	1.05	1.6E-03
		G00000015205	Cyb5a	cytochrome b5 type A	1.06	9.6E-07
		G00000008079	Ugp2	UDP-glucose pyrophosphorylase 2	1.06	4.1E-08
		G00000011559	Cnn3	calponin 3	1.07	5.6E-05
		G00000013484	Gsta1	glutathione S-transferase alpha-1	1.07	4.2E-10
		G00000050595	Mup5	major urinary protein 5	1.07	1.5E-04
		G00000026775	Pmpca	peptidase	1.08	3.9E-04
		G00000001338	Hpd	4-hydroxyphenylpyruvate dioxygenase	1.08	7.7E-06
		G00000001618	Ripk4	receptor-interacting serine-threonine kinase 4	1.09	2.3E-03
		G00000000768	Ubd	ubiquitin D	1.10	2.4E-05
		G00000007508	Lrtm2	leucine-rich repeats and transmembrane domains 2	1.10	1.8E-08
		G00000031769	Chchd7	coiled-coil-helix-coiled-coil-helix domain containing 7	1.10	4.4E-04

Table A-1 Continued.

Genotype	Tissue	Ensembl_ID (ENSRNO)	Symbol	Gene Name	L2FC	P-value[3]
		G00000013291	Cyp2c23	cytochrome P450	1.10	4.4E-07
		G00000017188	Cyp27a1	cytochrome P450	1.11	1.7E-08
		G00000058327			1.13	7.4E-04
		G00000025079	Fam126b	family with sequence similarity 126	1.13	4.7E-04
		G00000061215	Crym	crystallin	1.14	2.1E-04
		G00000017752	Mccc2	methylcrotonoyl-CoA carboxylase 2	1.16	1.8E-05
		G00000016166	Pdlim1	PDZ and LIM domain 1	1.16	7.7E-07
		G00000010079	Ca3	carbonic anhydrase 3	1.17	4.7E-10
		G00000013728	Polg2	DNA polymerase gamma 2	1.17	6.2E-04
		G00000062298	Rpl13a	ribosomal protein L13A	1.19	2.6E-03
		G00000013751	Plpbp	pyridoxal phosphate binding protein	1.19	2.3E-06
		G00000001442	Por	cytochrome p450 oxidoreductase	1.19	1.2E-09
		G00000042253	Ecd	ecdysoneless cell cycle regulator	1.20	6.0E-04
		G00000020254	Per2	period circadian regulator 2	1.20	3.1E-04
		G00000007949	Rgn	regucalcin	1.21	8.8E-08
		G00000003253	Qdpr	quinoid dihydropteridine reductase	1.21	3.4E-09
		G00000003515	Ephx1	epoxide hydrolase 1	1.22	7.9E-07
		G00000011039	Gch1	GTP cyclohydrolase 1	1.23	2.8E-07
		G00000038746	Bco2	beta-carotene oxygenase 2	1.24	6.3E-07
		G00000005861	Hsd11b1	hydroxysteroid 11-beta dehydrogenase 1	1.24	4.3E-09
		G00000000588	Slc16a10	solute carrier family 16 member 10	1.24	1.6E-05

Table A-1 Continued.

Genotype	Tissue	Ensembl_ID (ENSRNO)	Symbol	Gene Name	L2FC	P-value[3]
		G00000020202	Asrgl1	asparaginase and isoaspartyl peptidase 1	1.25	2.7E-03
		G00000017826	Mtrr	5-methyltetrahydrofolate-homocysteine methyltransferase reductase	1.26	1.6E-03
		G00000033700	Bud23	BUD23	1.27	1.7E-03
		G00000000281	Prodh1	proline dehydrogenase 1	1.28	2.1E-11
		G00000042084	Acsm2	acyl-CoA synthetase medium-chain family member 2	1.30	3.4E-09
		G00000006972	Zfp189	zinc finger protein 189	1.30	1.5E-03
		G00000027784	Tsku	tsukushi	1.32	7.2E-04
		G00000012387	Glyatl2	glycine-N-acyltransferase-like 2	1.33	7.3E-07
		G00000011714	Sat2	spermidine/spermine N1-acetyltransferase family member 2	1.33	6.9E-05
		G00000045799	Rup2	urinary protein 2	1.34	7.8E-04
		G00000021924	Cyp2c22	cytochrome P450	1.35	9.3E-08
		G00000018494	Ppp1r3c	protein phosphatase 1	1.36	4.1E-11
		G00000004693	Pbx1	PBX homeobox 1	1.36	1.4E-03
		G00000001258	Snx8	sorting nexin 8	1.37	2.0E-04
		G00000020698	Rnd2	Rho family GTPase 2	1.37	6.0E-05
		G00000051227			1.38	6.2E-04
		G00000052810	Cyp2c11	cytochrome P450	1.39	2.0E-11
		G00000012436	Adh6	alcohol dehydrogenase 6 (class V)	1.41	4.4E-15
		G00000015936	Gng5	G protein subunit gamma 5	1.41	2.6E-03
		G00000018413	Per3	period circadian regulator 3	1.42	1.6E-04

Table A-1 Continued.

Genotype	Tissue	Ensembl_ID (ENSRNO)	Symbol	Gene Name	L2FC	P-value[3]
		G00000016967	Hfe	homeostatic iron regulator	1.42	2.9E-07
		G00000001376	Mettl7a	methyltransferase like 7A	1.43	3.1E-04
		G00000056940	Cited2	Cbp/p300-interacting transactivator	1.44	1.5E-11
		G00000015002	Abhd15	abhydrolase domain containing 15	1.44	1.5E-04
		G00000032959	Adh7	alcohol dehydrogenase 7 (class IV)	1.45	7.6E-09
		G00000050232	LOC680406	similar to Urinary protein 2 precursor (RUP-2)	1.46	1.5E-09
		G00000020700	Rnaseh2c	ribonuclease H2	1.48	7.7E-04
		G00000011635	Ces2e	carboxylesterase 2E	1.49	2.9E-08
		G00000015354	Aox1	aldehyde oxidase 1	1.54	2.6E-12
		G00000061450	Homer2	homer scaffold protein 2	1.54	2.5E-05
		G00000009629	Car2	carbonic anhydrase 2	1.55	2.9E-05
		G00000042111	Sult1c2a	sulfotransferase family	1.55	2.3E-03
		G00000057072	Slc12a3	solute carrier family 12 member 3	1.55	3.1E-04
		G00000004009	Xpnpep2	X-prolyl aminopeptidase 2	1.57	1.1E-08
		G00000013313	Nceh1	neutral cholesterol ester hydrolase 1	1.57	8.8E-07
		G00000015438	LOC501233	LRRGT00080	1.58	1.2E-13
		G00000015076	Cyp26b1	cytochrome P450	1.62	6.3E-04
		G00000016456	Il33	interleukin 33	1.65	4.2E-18
		G00000001766	Tfrc	transferrin receptor	1.67	1.1E-04
		G00000011718	C1rl	complement C1r subcomponent like	1.68	1.2E-06
		G00000013949	Idh2	isocitrate dehydrogenase (NADP(+)) 2	1.68	2.3E-16

Table A-1 Continued.

Genotype	Tissue	Ensembl_ID (ENSRNO)	Symbol	Gene Name	L2FC	P-value[3]
		G00000018740	Ugt1a6	UDP glucuronosyltransferase family 1 member A6	1.69	6.1E-14
		G00000016807	Oat	ornithine aminotransferase	1.72	1.2E-05
		G00000025418	Armc9	armadillo repeat containing 9	1.74	4.5E-04
		G00000023778	Gcnt2	glucosaminyl (N-acetyl) transferase 2 (I blood group)	1.77	6.8E-05
		G00000056596	Alas1	5'-aminolevulinate synthase 1	1.80	2.3E-15
		G00000046643	Cyp3a9	cytochrome P450	1.82	5.3E-04
		G00000003260	Nr1i3	nuclear receptor subfamily 1	1.84	6.4E-05
		G00000001158	Abcg1	ATP binding cassette subfamily G member 1	1.86	3.0E-05
		G00000020250	Pcgf6	polycomb group ring finger 6	1.88	9.2E-04
		G00000006420	Rbm38	RNA binding motif protein 38	1.89	2.0E-04
		G00000012458	Cyp2e1	cytochrome P450	1.91	1.3E-19
		G00000002258	Tmem150c	transmembrane protein 150C	1.94	9.3E-05
		G00000013982	Hsd17b2	hydroxysteroid (17-beta) dehydrogenase 2	1.94	5.1E-04
		G00000021027	Dbp	D-box binding PAR bZIP transcription factor	1.94	3.2E-05
		G00000004437	Map2k6	mitogen-activated protein kinase kinase 6	2.07	1.1E-08
		G00000032246	Acsm3	acyl-CoA synthetase medium-chain family member 3	2.19	2.3E-16
		G00000014490	Bdh2	3-hydroxybutyrate dehydrogenase 2	2.21	2.5E-14
		G00000036687	Alyref	Aly/REF export factor	2.23	8.9E-04
		G00000015519	Ces1d	carboxylesterase 1D	2.24	6.9E-32
		G00000009598	Ncaph2	non-SMC condensin II complex	2.41	3.8E-05
		G00000043131	LOC100360095	urinary protein 1-like	2.43	4.9E-19

Table A-1 Continued.

Genotype	Tissue	Ensembl_ID (ENSRNO)	Symbol	Gene Name	L2FC	P-value[3]
		G00000034191	Fmo1	flavin containing dimethylaniline monoxygenase 1	2.46	2.8E-25
		G00000005985	Kcnma1	potassium calcium-activated channel subfamily M alpha 1	2.82	1.6E-04
		G00000011250	Inmt	indolethylamine N-methyltransferase	2.90	3.9E-21
		G00000058904	Tex13b	testis expressed 13B	3.10	5.9E-15
		G00000012772	Nqo1	NAD(P)H quinone dehydrogenase 1	3.11	1.5E-12
		G00000001388	Sds	serine dehydratase	3.29	1.7E-09
		G00000056847	Gsta3	glutathione S-transferase alpha 3	3.40	3.1E-21
		G00000001242	Gstt3	glutathione S-transferase	3.66	1.2E-85
		G00000051912	Acnat2	acyl-coenzyme A amino acid N-acyltransferase 2	3.74	8.9E-05
		G00000009488	Cyp7a1	cytochrome P450 family 7 subfamily A member 1	4.19	1.4E-18
Lean	**Liver Down-regulated**	**Ensembl_ID (ENSRNO)**	**Gene Symbol**	**Gene Name**	**L2FC**	**P-value**
		G00000029668	Wfdc21	WAP four-disulfide core domain 21	-2.72	1.3E-04
		G00000020480	Fads1	fatty acid desaturase 1	-2.53	4.0E-08
		G00000006859	Insig1	insulin induced gene 1	-2.32	3.2E-05
		G00000057557	Prlr	prolactin receptor	-2.27	2.3E-04
		G00000055909	Apoa4	apolipoprotein A4	-1.93	2.3E-04
		G00000030154	Cyp4a2	cytochrome P450	-1.75	2.2E-08
		G00000019776	Sh3gl3	SH3 domain containing GRB2 like 3	-1.62	8.9E-05
		G00000046889	Dbi	diazepam binding inhibitor	-1.61	1.1E-05
		G00000014702	Elovl2	ELOVL fatty acid elongase 2	-1.60	1.8E-05

Table A-1 Continued.

Genotype	Tissue	Ensembl_ID (ENSRNO)	Symbol	Gene Name	L2FC	P-value[3]
		G00000032297	Msmo1	methylsterol monooxygenase 1	-1.56	3.6E-05
		G00000007234	Cyp51	cytochrome P450	-1.56	4.9E-05
		G00000020989	Tm7sf2	transmembrane 7 superfamily member 2	-1.45	6.6E-05
Lean	**Liver Up-regulated**	**Ensembl_ID (ENSRNO)**	**Gene Symbol**	**Gene Name**	**L2FC**	**P-value**
		G00000001376	Mettl7a	methyltransferase like 7A	1.16	1.7E-04
		G00000048114	Echdc3	enoyl CoA hydratase domain containing 3	1.17	1.2E-04
		G00000023116	Agmo	alkylglycerol monooxygenase	1.21	1.7E-04
		G00000002643	Ugdh	UDP-glucose 6-dehydrogenase	1.29	7.6E-05
		G00000015354	Aox1	aldehyde oxidase 1	1.33	1.2E-04
		G00000004089	Enpp2	ectonucleotide pyrophosphatase/phosphodiesterase 2	1.34	9.6E-05
		G00000034191	Fmo1	flavin containing dimethylaniline monoxygenase 1	1.37	1.7E-04
		G00000013291	Cyp2c23	cytochrome P450	1.47	1.1E-04
		G00000003809	Sat1	spermidine/spermine N1-acetyl transferase 1	1.58	3.9E-05
		G00000018740	Ugt1a6	UDP glucuronosyltransferase family 1 member A6	1.80	2.6E-05
		G00000015519	Ces1d	carboxylesterase 1D	1.94	5.6E-10
		G00000033570	Arhgap8	Rho GTPase activating protein 8	2.03	1.5E-04
		G00000051912	Acnat2	acyl-coenzyme A amino acid N-acyltransferase 2	2.05	1.1E-04
		G00000001158	Abcg1	ATP binding cassette subfamily G member 1	2.21	1.1E-04
		G00000001388	Sds	serine dehydratase	2.29	8.0E-06
		G00000047613	AABR07048463.1	AABR07048463.1	2.34	1.4E-06

Table A-1 Continued.

Genotype	Tissue	Ensembl_ID (ENSRNO)	Symbol	Gene Name	L2FC	P-value[3]
		G00000013552	Scd	stearoyl-CoA desaturase	2.36	4.8E-06
		G00000001242	Gstt3	glutathione S-transferase	2.93	1.4E-09
		G00000021924	Cyp2c22	cytochrome P450	3.22	5.2E-15
		G00000009488	Cyp7a1	cytochrome P450 family 7 subfamily A member 1	3.36	1.5E-09

[1]All genes were analyzed using DESeq2 for differential analysis
[2]Abbreviations used: ZDF, Zucker Diabetic Fatty; L2FC, log2 fold change; PFC, prefrontal cortex
[3] Benjamini-Hochberg adjusted P-values controlling for false discovery rate at 5%, where P< 0.05 was considered significant.

Table A-2: Differentially expressed microRNAs in WE vs CAS-based diets in ZDF rats and their lean controls[1-3]**.**

Genotype	Tissue	MicroRNA	L2FC	Non adjusted p-value	*P*-value[3]
ZDF	Adipose Downregulated	rno-miR-221-3p	-1.60	9.53E-05	0.007
ZDF	PFC Upregulated	rno-miR-29a-3p	0.59	0.0001	0.022
ZDF	PFC Upregulated	rno-miR-151-5p	0.89	0.0005	0.036
Lean	Adipose Downregulated	rno-miR-125a-5p	-1.48	0.0022	0.069
Lean	Adipose Downregulated	rno-miR-125b-5p	-1.78	0.0029	0.069
Lean	Liver Upregulated	rno-miR-9a-5p	1.89	9.08E-05	0.0063
Lean	Liver Upregulated	rno-miR-181a-5p	1.10	0.0007	0.024
Lean	Liver Upregulated	rno-miR-10b-5p	1.37	0.0011	0.024
Lean	Liver Downregulated	rno-miR-192-5p	-0.57	0.0013	0.024

[1]All miRNAs were analyzed using DESeq2 for differential analysis
[2]Abbreviations used: ZDF, Zucker Diabetic Fatty; WE, whole egg; CAS, casein; L2FC, log2 fold change; and PFC, prefrontal cortex
[3]Benjamini-Hochberg adjusted P-values controlling for false discovery rate at 5%, where P< 0.05 was considered significant.

Table A-3: Differentially expressed microRNAs and their corresponding target genes that were differentially regulated by dietary WE consumption[1-3].

MicroRNA	Tissue	Gene Name	L2FC	Non-adj p-value	Human Symbol	Ensembl Rat ID (RNOG)	Rat Symbol	Gene Name
miR-125b-5p (down-regulated)	lean adipose	Pgp	2.69	0.00003	PGP	00000009536	Pgp	phosphoglycolate phosphatase
rno-miR-181a-5p (up-regulated)	lean liver	CYP7A1	3.36	0.000000001	Cyp7a1	00000009488	Cyp7a1	Cytochrome P450-Family-7 SubfamilyA-Member 1
rno-miR-181a-5p (up-regulated)	lean liver	Scd	2.35	0.0000048	Scd	00000013552	SCD	stearoyl-CoA desaturase

[1]All miRNAs were analyzed using DESeq2 for differential analysis

[2]Abbreviations used: miR, microRNAS; rno, rattus norvegicus; WE, whole egg; and L2FC, log2 fold change.

[3]Gene targets for *Rattus Norvegicus* and humans were determined by DRSC Integrative Ortholog Prediction Tool.

Table A-4: Composition of the CAS and WE based diets fed to lean and ZDF rats for 8 wk[1].

Ingredient (g/kg)	CAS	WE
Casein	200	-
Whole Egg[2]	-	435
Cornstarch	417	365
Corn Oil	183	-
Glucose Monohydrate	150	150
Mineral Mix	35	35
Vitamin Mix	10	10
Choline Bitartrate	2	2
L-methionine	3	3
Biotin (1%)	-	0.4
Macronutrients (% total kcal)[3]		
Protein	17	17
Carbohydrate	48	48
Fat	35	35
Caloric Content	4,715	4,715

[1]All ingredients were purchased from Envigo except for dried whole egg (Rose Acre Farms, Guthrie Center, IA), as well as L-methionine and choline bitartrate (Sigma-Aldrich). Abbreviations used: CAS, casein-based diet, WE, whole egg-based diet

[2] Total protein and lipid content provided by 435 g of dried WE was 46% (200 g) and 42% (183 g), respectively.

[3] To formulate all diets such that protein was provided at 20% (w/w).

APPENDIX B. LARGE AND SMALL RNA SEQUENCING REVEALS OXIDATIVE-REDUCTION PATHWAYS ARE MODIFID BY SHORT-TERM WHOLE EGG CONSUMPTION.

A manuscript prepared for submission to *Molecular Nutrition and Food Research*

Amanda E. Bries*, Joe L. Webb*, Brooke Vogel, Claudia Carrillo, Lily Harvison, Timothy A. Day, Michael J. Kimber, Rudy J. Valentine, Matthew J. Rowling, Stephanie Clark, Elizabeth McNeill, and Kevin L. Schalinske. *AEB and JLW contributed equally to this work.

Abstract

Scope: Eggs are protein-rich, nutrient-dense, and contain bioactive ingredients that have been shown to modify gene expression.

Methods: In order to understand the effects that egg consumption has on tissue-specific mRNA and microRNA gene expression, we examined the role of whole egg consumption (20% protein, w/w) on differentially expressed genes (DEGs) between rat (n =12) transcriptomes in the prefrontal cortex (PFC), liver, kidney and adipose tissue. Principal component analysis with hierarchical clustering were used to examine transcriptomic profiles between treatment groups. Finally, we performed Gene Ontology and Kyoto Encyclopedia of Genes and Genomes (KEGG) pathway analysis to examine which metabolic pathways were the most predominantly altered each tissue.

Results: Overall, these data demonstrate that whole egg consumption for 2 wk modified the expression of 52 genes in the PFC, 20 genes in the adipose, and two genes in the liver (adj $P <$ 0.05). Additionally, miR125b-5p was downregulated in the adipose, and miR-192-5p and miR-10b-5p were downregulated in the PFC. The main pathways influenced by WE consumption were glutathione metabolism in the adipose and cholesterol biosynthesis in the PFC.

Conclusion: These data highlight potential microRNA targets and the genes that may be modified by acute consumption of whole egg based diets.

Introduction

Eggs are a low-cost, nutrient-dense food comprised of numerous vitamins, bioactive compounds and have been proposed to play a role in disease prevention[1,2]. Dietary whole eggs and their derived compounds[3] have been linked to several mechanisms of modulating gene expression, such as vitamin D-mediated transcriptional regulation and methyl group metabolism by supplying choline, methionine, folate, B_{12}, B_6, and B_2[4]. Despite the beneficial components of eggs, they remain one of the most controversial foods[5], due to their level of cholesterol [6,7]. Observational studies examining the role of long-term egg intake on the risk of developing cardiovascular disease (CVD) have reported inconsistent results[8], but most recently, Dehghan and others reported no significant association between whole egg intake and major CVD events in a conglomerate of 50 studies[9]. Although the role of whole egg (WE) consumption has been extensively examined in population-based studies[10,11], only a few studies have thoroughly identified the biological role of the individual egg components.

For instance, egg yolk peptides have been shown to display anti-oxidative properties[12] and lutein, a carotenoid that is high in egg yolk, has been demonstrated to protect dopaminergic neurons from oxidative damage in a model of Parkinson's Disease (PD)[13]. Similar effects of lutein administration have also been shown in other animal models of aging and cognitive impairment[14,15]; however, the role of these egg components and their influence on their global gene expression remains elusive. In addition to WE decreasing oxidative stress, our laboratory has previously reported that consuming a WE-based diet reduced body weight gain in rats with type 2 diabetes[16,17]. To date, very few studies have focused on identifying the molecular

mechanisms that are altered by WE consumption in additional to the global gene expression changes in the rats fed WE vs. casein (CAS)-based protein diets. By gaining an in-depth understanding of gene-diet interactions, we can shed light on the molecular mechanisms underlying WE consumption, and identify targets for future therapeutics in metabolic or aging diseases.

In this study, male Sprague Dawley rats were fed WE-based diets to examine the influence of short-term WE consumption on gene and microRNA expression in comparison with CAS-based diets. We examined the transcriptomic profiles of the prefrontal cortex (PFC), adipose, liver, and kidney tissues to identify metabolic pathways that may be altered by WE consumption and mapped these changes to microRNAs. The primary aim of this study was to first identify if WE consumption had a significant impact on global gene expression, and if there were potential molecular drivers, such as microRNAs that were upstream effects of these observed transcriptomic differences.

Materials and methods

Animals and Diets. This animal study was approved by the Institutional Animal Care and Use Committee at Iowa State University and was performed according to the Iowa State University Laboratory Animal Resources Guidelines. Male Sprague Dawley rats (n =12) were obtained at 6 wk of age (151-175 g) from Charles River Laboratories (Wilmington, MA). Rats were individually housed in conventional cages in a temperature-controlled environment (22°C ± 2°C) following a 12-h light-dark cycle. All rats were acclimated for one week on a standard rat chow diet, whereby they were randomly assigned to one of two dietary intervention groups. There were no significant differences in baseline weights between groups (P=0.62). Rats were either placed on the control casein (CAS)-based diet, or a whole egg (WE)-based diet **(Table B-1**)

matched for 20% protein (w/w). For 72 h, animals underwent a controlled fasted-refeeding protocol to train them to consume food *ad libitum* within a 4h window **(Figure B-1).** After training, animals were fasted overnight for 10 h with water provided *ad libitum,* followed by controlled feeding (4 g) of either the CAS- or WE-based diet. At 7 wk of age, serum was collected via tail vein at 0, 2, 4, 6, and 8 h immediately following refeeding. Following the serum time curve collection, rats were maintained on their respective diets for 2-wk with food intake and body weight gain monitored daily. Following the dietary intervention, 9-wk old rats underwent a 12 h overnight fast with water provided *ad libitum*; rats were anesthetized with a ketamine:xylazine cocktail (90:10 mg/kg bw) via a single intraperitoneal injection. Whole blood was collected via cardiac puncture and stored at -80°C. The epididymal adipose, kidney, liver, and PFC tissues were procured, weighed, and stored in *RNA*later.

Large and small RNA Extraction & Sequencing. Total RNA and microRNA were extracted using a SPLIT Total RNA Extraction Kit (Lexogen, Greenland, NH). RNA quantities were measured using the Qubit Fluorometer (ThermoFisher Scientific), and integrity was assessed using a Bioanalyzer 2100 (Agilent Technologies). Large RNA libraries were prepared using an automated protocol for the QuantSeq 3' mRNA-Seq Library Prep Kit (Lexogen, Greenland, NH) and small RNA libraries were prepared using Small RNA Library Prep Kits (Lexogen, Greenland, NH). Total RNA samples were multiplexed across two lanes using an Illumina High-Seq 3000 resulting in an average of 7.5 million reads per sample prior to quality control. Small RNA libraries were also multiplexed and run on a separate lane on an Illumina High-Seq 3000.

Quality Control & Adapter Trimming. All large and small RNA reads were inspected using Fastqc and were trimmed to remove adapter sequences using BBDUK[18]. Read segments matching common Illumina Truseq or Nextera adapter sequences were removed for the reverse-

complement or forward sequence of the adapters during processing. Subsequently, low-quality reads with average quality < 10 were discarded.

Read Alignment & Quantification. Reference genome (fasta) and genome annotation files (gtf) were obtained from the Ensembl genome browser. Reads were aligned to the RNO version 6 release 94 of the Ensembl genome using the STAR v2.5.2 aligner[19]. Transcripts aligning to specific genes were counted using the STAR - quantMode geneCounts function to map transcripts to each genome. Files containing microRNA counts and gene counts for all samples are supplemental and not included in this dissertation**.** Small RNA samples were processed using the smallrnaseq python tool[20], which aligns samples using Bowtie and quantifies small RNA read counts using reference fasta and gtf files from RNAcentral.org.

Data Filtering & Quality Control. All data analysis was conducted in Python within an IPython notebook unless otherwise specified. Genes were filtered out if they were not expressed in any samples or had fewer than 10 counts in half of the samples for each gene. Data filtering and alignment settings were adapted from Lexogen‘s QuantSeq 3‘ mRNA-Seq Kit and integrated Data Analysis Pipeline on Bluebee® platform according to the manufacturer’s instructions.

Differential Expression Analysis using DESeq2. Read normalization was conducted using a weighted trimmed mean of the log expression ratios (trimmed mean of M values (TMM)) method to account for variable sequencing depth between samples. Differential expression analysis was conducted using the DESeq2[21] package in the R programming language. When applying DESeq2, DESeqDataSetFromMatrix was used to generate P values and adjusted p-values were calculated using the Benjamini-Hochberg method[22] of false discovery rate (FDR)

correction. For all analyses, FDR was controlled at 1% and all adjusted p-values < 0.01 were considered significant.

Heatmaps, Principal Component Analysis, & Volcano Plots. Principal Component Analysis (PCA) was conducted for the initial clustering and characterization of RNAseq data. Hierarchical clustering was used to create a dendrogram classifying samples according to similar transcriptomic profiles, while volcano plots were constructed to visualize genes which surpass a log-fold change of >1.5 increase or decrease to assess biological significance. PCA, clustering, and volcano plots were all constructed using MatplotLib in python version 3.2.0rc1.

Functional Enrichment Annotations. Pathway-based analysis was performed using the Kyoto Encyclopedia of Genes and Genomes (KEGG) database that contains annotated biological functions for genes[23]. All KEGG pathway analysis was performed in python using the KEGG package version bio2bel-kegg 0.2.5. All differentially expressed genes (DEGs) were additionally categorized based on cellular localization, function, and processes using Gene Ontology (GO) Analysis using the Database for Annotation, Visualization and Integrated Discovery (DAVID) v6.8 database through the online web application[24]. MicroRNA target genes were identified through TargetScan analysis tools and target genes were then downloaded and deidentified through the Ensembl software[25]. Gene identifiers were then cross-validated through our differentially expressed genes on the basis of significance at FDR correction of <0.05.

qRT-PCR Validation Analyses. Total RNA from each tissue was aliquoted and reverse transcribed into cDNA using the High-Capacity cDNA Reverse Transcription Kit (Applied Biosystems, Catalog # 4368813). The cDNA was diluted to 100ng/uL and qPCR reactions were performed using 200ng of total cDNA with primers at 300nM concentration in 10 uL FastStart Sybr Green Master (Roche) according to the manufacturer's instructions. All qPCR reactions

were conducted in a Roche LightCycler 96 Real-Time PCR System. Primers sequences for qPCR are were obtained from Integrated DNA Technology (IDT) and 18s RNA was used as an internal control for normalization in each tissue. Each sample was assessed in triplicate. All data were analyzed using the Livak Delta-Delta CT method[26].

Protein-Protein Interaction Network Mapping. The STRING database was used for analyzing protein-protein interaction networks between DEGs using their online web portal https://string-db.org/ . These interactions include direct (physical) and indirect (functional) associations from other published studies and databases.

Results

RNA Seq Differential Expression. Differential gene expression analyses of the resulted in 52 DEGs in the PFC, 20 in the adipose tissue, 2 in the liver, and 0 in the kidney. Of the 74 DEGs that surpassed multiple testing corrections (adjusted $P < 0.05$), 1 gene was differentially upregulated across both the PFC (5.6-fold increase) and adipose (3.2-fold increase) tissue - indolethylamine N-methyltransferase (INMT). **Table B-2** describes the DEGs in each tissue, whereas supplemental data not contained in this dissertation contains adjusted *P*-value results for all genes.

KEGG & GO Functional Enrichment Analysis. To examine the function pathway for each DEG, mRNA were mapped to KEGG/GO pathway terms, which are described in **Table B-3.** The primary KEGG enrichment analyses of the DEGs indicated that in adipose tissue, the top KEGG pathway that was upregulated by consuming a WE-based diet was glutathione metabolism. In the PFC, glutathione metabolism was ranked third, while steroid biosynthesis and terpenoid backbone biosynthesis were the other top biological pathways. In the liver, there were no pathway processes that were determined from the differentially expressed gene pool.

To further investigate the molecular function and localization of these DEGs, GO analyses revealed that all 74 genes could be classified according to their biological processes, cellular components, and molecular functions. GO Functional Analysis of DEGs indicated that in the PFC, the top altered pathways were oxidation-reduction processes, cholesterol biosynthetic processes, metal ion binding pathways, and fatty acid biosynthetic processes. In the adipose, the main pathways were organic acid transmembrane transport, phosphate ion transmembrane transport, and glutathione metabolic processes. A table of the GO analysis results are described in **Table B-3.**

microRNA Seq Differential Expression. Differential expression analyses of the microRNAs, resulted in 6 upregulated microRNAs and 10 downregulated microRNAs across all four tissues based on non-adjusted $P < 0.05$. No microRNAs survived multiple testing correction with FDR correction at 5%. **Table B-4** describes the differentially expressed microRNAs in each tissue, and likewise, adjusted *P* values results for all microRNAs are in supplemental files. Interestingly, across the PFC, adipose, and liver, miR-10b-5p was downregulated in both the adipose and PFC (non-adjusted; $P=0.03$ and $P=0.02$, respectively) and miR-192-5p was downregulated in both the liver and PFC (non-adjusted; $P=0.02$ and $P=0.05$, respectively).

MicroRNA Gene Target Analysis. Differentially expressed microRNAs from Table B-2 were mapped against their human genetic targets, and cross-referenced against the DEGs from Table 3. For instance, **Table B-5** indicates the targets of the downregulated miR-10b-5p in the PFC. The DEG that was upregulated in the PFC as it relates to miR-10b-5p was the Arrestin Domain Containing 3 protein (*Arrdc3).* Nine DEGs were identified in the PFC and were correlated with the suppression of miR-192-5p in the PFC (Table B-4).

Serum MicroRNA Refeeding Analysis. There was no significant effects of dietary treatment on serum microRNA at 0, 2, 4, 6, or 8 h immediately following refeeding based on multiple testing corrective measures using FDR adjusted $P < 0.05$.

Principal Component Analysis (PCA) & Hierarchical Clustering. To examine the similarity between transcriptomic profiles, lowly expressed genes across all tissues were filtered and illustrated in a PCA, as shown in **Figure B-2A**. The PCA plots indicate that these rat samples cluster by diet (WE vs. CAS). Subsequently, the top DEGs were visualized using a hierarchical clustering heatmap for each tissue that displays distinct differential expression patterns according to each diet, as shown in **Figure B-2 (B-D).** To visualize which of these DEGs may have biological significance, each tissue was plotted using volcano plots, as displayed in **Figure B-3.**

qRT-PCR validation. To validate the RNA-seq data, 5 DEGs were selected for qRT-PCR analysis in each tissue. The PCR gene expression data were correlated with the RNA-seq data in **Figure B-4,** suggesting that RNA-seq and PCR results were in alignment with one another.

Food Intake & Body Weight Gain. There was no significant effect of dietary treatment on food intake or total energy intake throughout the study (*data not shown*). Additionally, there was no statistically significant effect of dietary treatment on final body weight or cumulative body weight gain at 8 wk of age. There were also no differences in organ weights at tissue collection except for the liver, where rats on the WE-based diets had 16% increased relative liver weight ($P<0.01$).

Discussion

Previous studies have examined specific egg components, such as hen egg lysozymes in altering gene expression in pig intestinal tissues[27], but very little information is known about how

dietary WE affects endogenous gene expression across multiple tissues. Our laboratory has consistently demonstrated the beneficial role of a WE-based diet in maintaining vitamin D status and modulating phenotypic outcomes in both a type 1 diabetes (T1D) and type 2 diabetes (T2D) animal model[17,28]; however, we have yet to investigate how WE consumption modulates gene expression in a standard rodent model. RNA-sequencing is a powerful tool that can examine the influence of dietary patterns on whole genome gene expression. Since nutrition was one of the first major environmental factors that was identified as an epigenetic influencer, it's important to look at more global effects of WE consumption in a standard rodent model to better understand how consuming WE alone, influences genetic expression. Measuring these effects is especially important when it comes to better understanding the molecular drivers of disease. By assessing the genes that are influenced by WE, we can contribute to scientifically sound intervention strategies using dietary WE as a means of disease mitigation or supplementation.

In this study, next generation sequencing revealed that consuming WE for 2-wk significantly modified the expression of 74 different genes across the PFC, liver, and adipose tissue. In the PFC, the top three represented GO pathways were oxidation-reduction process, cholesterol biosynthetic process, and metal ion binding. Notably, profiling the DEGs within the given pathways indicated that 9 out of the 12 DEGs in the oxidation-reduction process pathway were downregulated. Two cytochrome P450 genes, *Cyp2c22,* and *Cyp4A1* were upregulated in the PFC of the animals fed WE- vs. CAS-based diets. Moreover, squalene epoxidase *(Sqle),* a rate-limiting gene in the sterol biosynthesis pathway[29], was significantly downregulated (-31-fold) within the PFC of rats fed WE-based vs. CAS-based diets. *Sqle* is important for steroidal synthesis, and previous studies have demonstrated that ablation of *Sqle* may disrupt tumorigenesis, owing to blunted cholesterol biosynthesis[30]. Moreover, the dysregulation of *Sqle*

has been observed during the onset of diabetes[31,32]. Q Ge et al.[33] indicated a significant upregulation in the expression of *Sqle*, as well as an abundance in the protein in a chemically-induced diabetic animal model[34]. Another contrast between the diabetic animal model and our WE dietary fed animals is the observed increased expression of the *Cyp* genes, whereas, there was a global reduction in *Cyp51* and other cytochrome P450 genes in the liver of diabetic animals. Similar findings have been reported in other diabetic animal models, where it's been detected that *Cyp2c22* was markedly reduced in a T2D mouse[35]. Interestingly, Ding et al[31] conducted a cross-sectional study in an obese population of men, examining the relationship between body mass index and DEGs. They reported the close association between body mass index and increased expression of *Fads1, Sqle, Scd, Cyp51a1* whereas, in a weight-loss intervention study, *Sqle* expression was significantly reduced. Similar to these findings, we observed downregulation of *Fads1 and Sqle* in animals fed the WE- vs. CAS-based diets. The results from our findings may indicate a potential benefit of WE-based diet on the increased expression of these cytochrome P450 enzymes, which may have a beneficial role in correcting the progression of T2D.

Functional annotation of the DEGs to GO terms indicated that the two targeted genes of the glutathione S-transferase (GST) pathway were glutathione S-transferase zeta 1 (*Gstz1*) and glutathione S-transferase pi 1 (*Gstp1*), which were upregulated 1.9- and 3.7-fold, respectively in the adipose tissue of the SD animals fed WE-based diets. Previously, it has been reported that deficiency of glutathione-related pathways alters antioxidant responses[36], suggesting that our data may indicate an upregulation of glutathione with WE consumption, providing protection against oxidative stress. In a recent study, a *Gstp1* polymorphism was associated with increased glucose intolerance and greater androgen production in non-obese women with polycystic ovary

syndrome[37]. Moreover, the literature indicates that dysregulated GST production has been implicated in conditions of obesity and T2D[38]. It was previously reported that glutathione metabolism is regulated by egg yolk peptide consumption in a porcine model of oxidative stress[39], while in Zucker Diabetic Fatty rats, egg white hydrolysate consumption increased glutathione concentrations in the liver[40]. In a meta-analysis of clinical studies with long-term egg consumption, there were no observed effects of WE consumption on blood inflammatory markers[41], whereas other researchers have reported elevation in endothelial and arterial inflammation from WE consumption[42] and some report vascular inflammation to be exclusive to egg white consumption and not WE[43,44]. It is important that we examined these differences in gene expression, as we identified upregulation not only in the adipose tissue, but also observed an increase of glutathione S-transferase mu 2 *(Gstm2)* expression in the brain of rats fed WE-based diet. These are important considerations as the data from clinical trials regarding WE consumption on inflammation-mediated cardiovascular disease is indeterminate.

To better understand how the DEGs interact with one another, we used the STRING-DB to interrogate potential protein-protein interactions using models based on gene pathways and functional categories. K-nearest-neighbor (KNN) clustering was used to more granularly define relationships between DEGs and identify sub-networks in our data. In adipose tissue, very few genes interacted and KNN clustering revealed 3 main pathways that corroborated the KEGG analysis: 1) glutathione processing, 2) carbamoyl-phosphate processing and 3) peroxisome proliferator activated genes. One of the most intriguing findings resulted from examining the PFC, where distinct protein-protein interaction networks occurred among the DEG genes. Nearly all of the fatty acid biosynthesis genes and cholesterol synthesis genes physically interacted, while very few of the genes in any other pathways were interrelated. KNN clustering also

revealed 3 common clusters in the PFC according to the protein interaction maps, with two main subgroups: 1) steroid biosynthesis processing; and 2) fatty acid synthesis, with the remaining genes not interacting.

Although in this study we demonstrated multiple genes were differentially expressed across these tissues, each of these genes highlighted here should be investigated further to confirm if they are regulated through WE consumption. After examining whether these DEGs were changing across all of the sequenced tissues, we did not identify any DEGs that were globally affected by WE consumption, which was a rigorous assessment. Additionally, we wanted to interrogate the mechanism by which these 74 genes were being altered by WE consumption, by performing smallRNA sequencing. Surprisingly, there was no observed effect of acute WE consumption on postprandial serum microRNAs within 8h of testing. Previous research by Zemplini et al. reported robust effects of egg consumption on transient plasma microRNA expression[45,46]. While it is controversial whether diet consumption directly influences circulating microRNA status[47], we didn't observe any serum changes in microRNAs between the two dietary treatments. MicroRNAs are a great tool for biomarker detection[48], as well as granular mediators in the pathogenesis of various diseases[49,50]. By using next generation sequencing to observe serum microRNA changes, we concluded that diet alone, is not promising to elicit acute changes in microRNA status. The tissue microRNA profiles however, may change due to diet, thus we examined the microRNA expression changes in rats following 2-wk consumption.

Since we observed prominent pathways that were altered by WE consumption, we wanted to explore whether these gene changes could be associated by their microRNA targets. Interestingly, of the target microRNAs detected as influencers of the glutathione-mediated

pathways, 5 microRNAs were detected from the small RNA-Seq in the adipose tissue that are targets of glutathione-related genes, but only was deemed significant. MicroRNA-125b-5p was downregulated (-1.4-fold) by the WE-based diet, with a non-adjusted *P*-value of (*P*=0.007). miR-125b-5p does logically link with the upregulation in *Gstz1* and *Gstp1* in the adipocytes.

The biological significance of miR-125b-5p in the adipocytes has been examined in both human and animal models. Brovkina et al. reported an upregulation of miR-125b-5p in the subcutaneous adipose tissue in individuals T2D and obesity[51]. Additionally, in a population with T1D, Satake and others[52] reported a strong positive correlation between hemoglobinA1c and the expression of miR-125b-5p, and this has also been reported in a diabetic *db/db* mouse model[53]. Future mechanistic studies exploring the relationship between miR-125b-5p and glutathione metabolism in a diabetic animal model are warranted.

In this study, we examined the effects of rats consuming a WE-based diet for 2 wk on gene expression in multiple tissues, revealing 74 novel DEGs across the PFC, liver, adipose and kidney transcriptomes in Sprague Dawley rats using Illumina HiSeq 3000 platform. In the adipose, KEGG analyses highlighted that glutathione metabolism was upregulated by WE consumption accompanied by downregulated miR-125b-5p in the adipose tissue of rats fed a WE-based diet. GO analysis showed that multiple reduction-oxidation reactions in the PFC were also altered by consuming WE. These results indicate that WE-based diets attenuate the expression of glutathione and oxidative-reduction processes as a result of WE-based diets. Together, these results may provide utility in diseased models where these given pathways are involved in the pathogenesis.

References

1. Park, S. J., Jung, J. H., Choi, S. W. & Lee, H. J. Association between egg consumption and metabolic disease. *Korean Journal for Food Science of Animal Resources* **38**, 209–223 (2018).

2. Andersen, C. J. Bioactive egg components and inflammation. *Nutrients* **7**, 7889–7913 (2015).

3. Nimalaratne, C. & Wu, J. Hen egg as an antioxidant food commodity: A review. *Nutrients* **7**, 8274–8293 (2015).

4. Wallace, T. C. & Fulgoni, V. L. Usual choline intakes are associated with egg and protein food consumption in the United States. *Nutrients* **9**, (2017).

5. Miranda, J. M. *et al.* Egg and egg-derived foods: Effects on human health and use as functional foods. *Nutrients* **7**, 706–729 (2015).

6. Alexander, D. D., Miller, P. E., Vargas, A. J., Weed, D. L. & Cohen, S. S. Meta-analysis of Egg Consumption and Risk of Coronary Heart Disease and Stroke. *Journal of the American College of Nutrition* **35**, 704–716 (2016).

7. Zhong, V. W. *et al.* Associations of Dietary Cholesterol or Egg Consumption with Incident Cardiovascular Disease and Mortality. *JAMA - J. Am. Med. Assoc.* **321**, 1081–1095 (2019).

8. Drouin-Chartier, J. P. *et al.* Egg consumption and risk of cardiovascular disease: Three large prospective US cohort studies, systematic review, and updated meta-analysis. *The BMJ* **368**, (2020).

9. Dehghan, M. *et al.* Association of egg intake with blood lipids, cardiovascular disease, and mortality in 177,000 people in 50 countries. *Am. J. Clin. Nutr.* (2020). doi:10.1093/ajcn/nqz348

10. Fuller, N. R. *et al.* Effect of a high-egg diet on cardiometabolic risk factors in people with type 2 diabetes: The Diabetes and Egg (DIABEGG) Study - Randomized weight-loss and follow-up phase. *Am. J. Clin. Nutr.* **107**, 921–931 (2018).

11. DiMarco, D. M. *et al.* Intake of up to 3 Eggs/Day Increases HDL Cholesterol and Plasma Choline While Plasma Trimethylamine-N-oxide is Unchanged in a Healthy Population. *Lipids* **52**, 255–263 (2017).

12. Yousr, M. & Howell, N. Antioxidant and ACE inhibitory bioactive peptides purified from egg yolk proteins. *Int. J. Mol. Sci.* **16**, 29161–29178 (2015).

13. Nataraj, J., Manivasagam, T., Justin Thenmozhi, A. & Essa, M. M. Lutein protects dopaminergic neurons against MPTP-induced apoptotic death and motor dysfunction by ameliorating mitochondrial disruption and oxidative stress. *Nutr. Neurosci.* **19**, 237–246 (2016).

14. Akbaraly, N. T., Faure, H., Gourlet, V., Favier, A. & Berr, C. Plasma carotenoid levels and cognitive performance in an elderly population: results of the EVA Study. *J. Gerontol. A. Biol. Sci. Med. Sci.* **62**, 308–16 (2007).

15. Binawade, Y. & Jagtap, A. Neuroprotective effect of lutein against 3-nitropropionic acid-induced huntington's disease-like symptoms: Possible behavioral, biochemical, and cellular alterations. *J. Med. Food* **16**, 934–943 (2013).

16. Saande, C. J., Webb, J. L., Curry, P. E., Rowling, M. J. & Schalinske, K. L. Dietary Whole Egg Reduces Body Weight Gain in a Dose-Dependent Manner in Zucker Diabetic Fatty Rats. *J. Nutr.* **149**, 1766–1775 (2019).

17. Saande, C. J. *et al.* Dietary Whole Egg Consumption Attenuates Body Weight Gain and Is More Effective than Supplemental Cholecalciferol in Maintaining Vitamin D Balance in Type 2 Diabetic Rats. *J. Nutr.* jn254193 (2017). doi:10.3945/jn.117.254193

18. BBMap: A Fast, Accurate, Splice-Aware Aligner. Available at: https://escholarship.org/uc/item/1h3515gn. (Accessed: 28th January 2020)

19. Dobin, A. *et al.* STAR: Ultrafast universal RNA-seq aligner. *Bioinformatics* **29**, 15–21 (2013).

20. Farrell, D. smallrnaseq : short non coding RNA-seq analysis with Python. *Bioarxiv* 110585 (2017). doi:10.1101/110585

21. Love, M. I., Huber, W. & Anders, S. Moderated estimation of fold change and dispersion for RNA-seq data with DESeq2. *Genome Biol.* **15**, (2014).

22. Benjamini, Y. & Hochberg, Y. Benjamini-1995.pdf. *Journal of the Royal Statistical Society B* **57**, 289–300 (1995).

23. Kanehisa, M. & Goto, S. *KEGG: Kyoto Encyclopedia of Genes and Genomes*. *Nucleic Acids Research* **28**, (2000).

24. DAVID Functional Annotation Bioinformatics Microarray Analysis. Available at: https://david.ncifcrf.gov/home.jsp. (Accessed: 23rd March 2020)

25. Ensembl genome browser 99. Available at: https://useast.ensembl.org/index.html. (Accessed: 25th March 2020)

26. Livak, K. J. & Schmittgen, T. D. Analysis of relative gene expression data using real-time quantitative PCR and the 2-ΔΔCT method. *Methods* **25**, 402–408 (2001).

27. Lee, M. *et al.* Hen egg lysozyme attenuates inflammation and modulates local gene expression in a porcine model of dextran sodium sulfate (DSS)-Induced Colitis. *J. Agric. Food Chem.* **57**, 2233–2240 (2009).

28. Jones, S. K., Koh, G. Y., Rowling, M. J. & Schalinske, K. L. Whole Egg Consumption Prevents Diminished Serum 25-Hydroxycholecalciferol Concentrations in Type 2 Diabetic Rats. *J. Agric. Food Chem.* **64**, 120–124 (2016).

29. Boone, L. R., Brooks, P. A., Niesen, M. I. & Ness, G. C. Mechanism of Resistance to Dietary Cholesterol. *J. Lipids* **2011**, 1–9 (2011).

30. Garcia-Bermudez, J. *et al.* Squalene accumulation in cholesterol auxotrophic lymphomas prevents oxidative cell death. *Nature* **567**, 118–122 (2019).

31. Ding, J. *et al.* Alterations of a cellular cholesterol metabolism network are a molecular feature of obesity-related type 2 diabetes and cardiovascular disease. *Diabetes* **64**, 3464–3474 (2015).

32. Seiki, S. & Frishman, W. H. Pharmacologic inhibition of squalene synthase and other downstream enzymes of the cholesterol synthesis pathway: A new therapeutic approach to treatment of hypercholesterolemia. *Cardiology in Review* **17**, 70–76 (2009).

33. Ge, Q. *et al.* Mulberry leaf regulates differentially expressed genes in diabetic mice liver based on RNA-seq analysis. *Front. Physiol.* **9**, (2018).

34. Ge, Q. *et al.* RNA-Seq analysis of the pathogenesis of STZ-induced male diabetic mouse liver. *J. Diabetes Complications* **34**, 107444 (2020).

35. Pass, G. J. *et al.* Effect of hyperinsulinemia and type 2 diabetes-like hyperglycemia on expression of hepatic cytochrome p450 and glutathione s-transferase isoforms in a New Zealand obese-derived mouse backcross population. *J. Pharmacol. Exp. Ther.* **302**, 442–50 (2002).

36. Blackburn, A. C. *et al.* Deficiency of glutathione transferase zeta causes oxidative stress and activation of antioxidant response pathways. *Mol. Pharmacol.* **69**, 650–657 (2006).

37. Savic-Radojevic, A. *et al.* Glutathione S-transferase (GST) polymorphism could be an early marker in the development of PCOS: An insight from non-obese and non-insulin resistant adolescents. *Endokrynol. Pol.* **69**, 366–374 (2018).

38. Dastidar, S. G. *et al.* Glutathione s-transferase p deficiency induces glucose intolerance via jnk-dependent enhancement of hepatic gluconeogenesis. *Am. J. Physiol. - Endocrinol. Metab.* **315**, E1005–E1018 (2018).

39. Young, D., Fan, M. Z. & Mine, Y. Egg Yolk Peptides Up-regulate Glutathione Synthesis and Antioxidant Enzyme Activities in a Porcine Model of Intestinal Oxidative Stress. *J. Agric. Food Chem.* **58**, 7624–7633 (2010).

40. Garcés-Rimón, M. *et al.* Pepsin Egg White Hydrolysate Ameliorates Obesity-Related Oxidative Stress, Inflammation and Steatosis in Zucker Fatty Rats. *PLoS One* **11**, e0151193 (2016).

41. Sajadi Hezaveh, Z., Sikaroudi, M. K., Vafa, M., Clayton, Z. S. & Soltani, S. Effect of egg consumption on inflammatory markers: a systematic review and meta-analysis of randomized controlled clinical trials. *Journal of the Science of Food and Agriculture* **99**, 6663–6670 (2019).

42. David Spence, J. Dietary cholesterol and egg yolk should be avoided by patients at risk of vascular disease. *J. Transl. Intern. Med.* **4**, 20–24 (2016).

43. Jiayu, Y. *et al.* Egg white consumption increases GSH and lowers oxidative damage in 110-week-old geriatric mice hearts. *J. Nutr. Biochem.* **76**, 108252 (2020).

44. Njike, V., Faridi, Z., Dutta, S., Gonzalez-Simon, A. L. & Katz, D. L. Daily egg consumption in hyperlipidemic adults - Effects on endothelial function and cardiovascular risk. *Nutr. J.* **9**, 28 (2010).

45. Zempleni, J., Baier, S. R., Howard, K. M. & Cui, J. Gene regulation by dietary microRNAs. *Canadian Journal of Physiology and Pharmacology* **93**, 1097–1102 (2015).

46. Baier, S. R., Nguyen, C., Xie, F., Wood, J. R. & Zempleni, J. MicroRNAs Are Absorbed in Biologically Meaningful Amounts from Nutritionally Relevant Doses of Cow Milk and Affect Gene Expression in Peripheral Blood Mononuclear Cells, HEK-293 Kidney Cell Cultures, and Mouse Livers. *J. Nutr.* **144**, 1495–1500 (2014).

47. Witwer, K. W. & Zhang, C. Y. Diet-derived microRNAs: Unicorn or silver bullet? *Genes and Nutrition* **12**, 15 (2017).

48. Mosallaei, M. *et al.* PBMCs: a new source of diagnostic and prognostic biomarkers. *Arch. Physiol. Biochem.* 1–7 (2020). doi:10.1080/13813455.2020.1752257

49. Akbar, N. *et al.* Endothelium-derived extracellular vesicles promote splenic monocyte mobilization in myocardial infarction. *JCI insight* **2**, (2017).

50. Fulga, T. A. *et al.* A transgenic resource for conditional competitive inhibition of conserved Drosophila microRNAs. *Nat. Commun.* **6**, 7279 (2015).

51. Brovkina, O. *et al.* Role of MicroRNAs in the Regulation of Subcutaneous White Adipose Tissue in Individuals With Obesity and Without Type 2 Diabetes. *Front. Endocrinol. (Lausanne).* **10**, (2019).

52. Satake, E. *et al.* Circulating miRNA profiles associated with hyperglycemia in patients with type 1 diabetes. *Diabetes* **67**, 1013–1023 (2018).

53. Villeneuve, L. M. *et al.* Enhanced levels of microRNA-125b in vascular smooth muscle cells of diabetic db/db mice lead to increased inflammatory gene expression by targeting the histone methyltransferase Suv39h1. *Diabetes* **59**, 2904–2915 (2010).

Tables and Figures

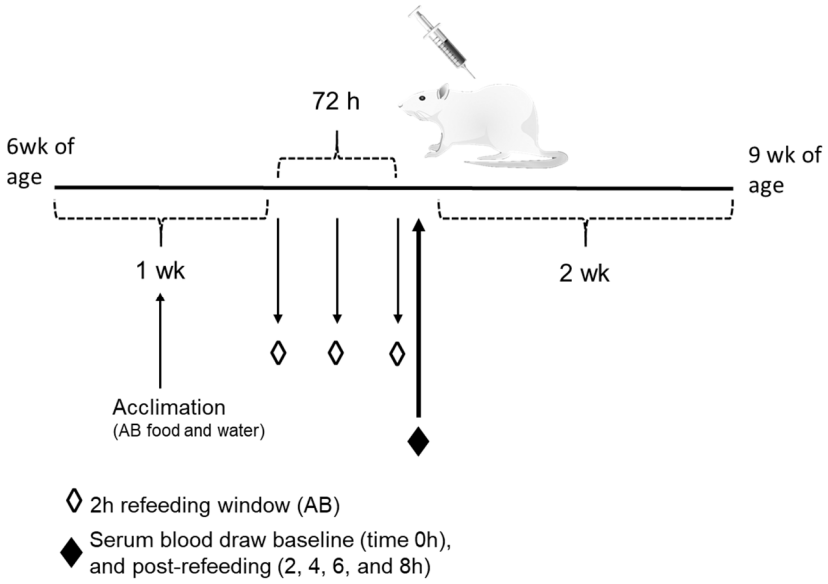

Figure B-1. Schematic of the study design.

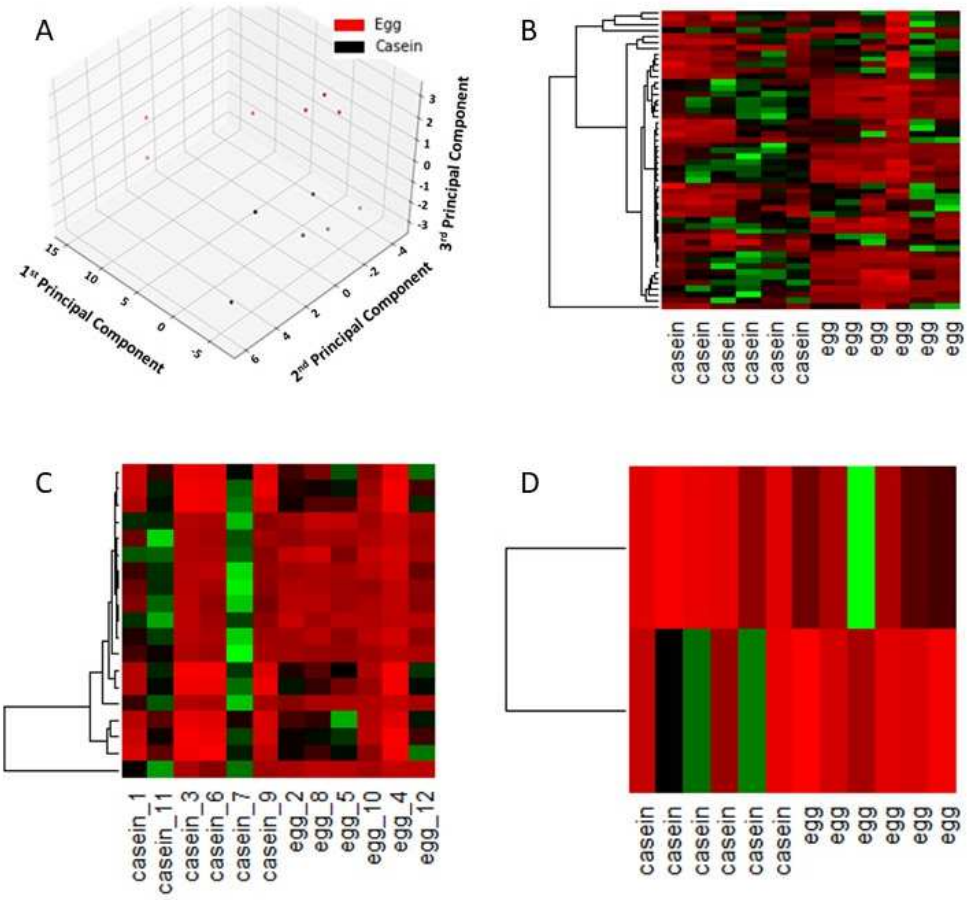

Figure B-2. Principle component analysis (A) and hierarchical clustering of genes between casein and whole egg based diets in the Prefrontal cortex (B), adipose (C) and liver (D) of Sprague Dawley rats. Samples in the first three principle component space are colored in red or black for either WE or CAS, respectively.

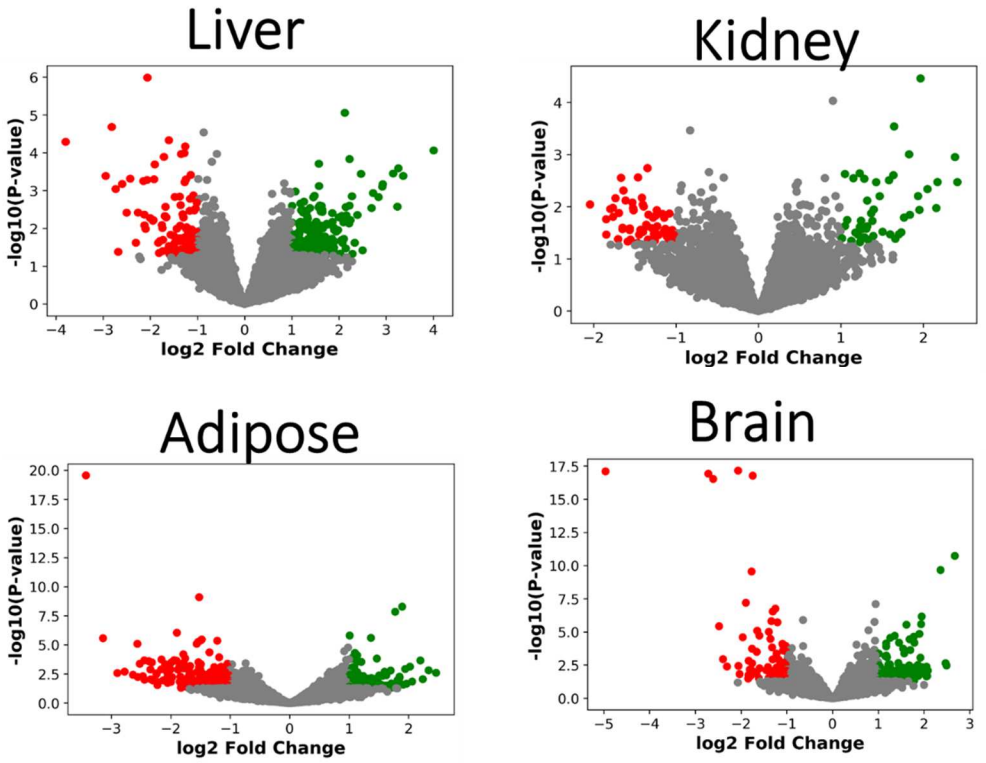

Figure B-3. Volcano plots indicating the directionality of the differentially expressed genes. Genes upregulated (green) or downregulated (red) by WE consumption, correspond to a 1.5 decrease or increase in log fold changes. Each panel corresponds to a tissue in a given genotype: A) lean adipose; B) lean PFC; C) lean kidney; D) lean liver; E) ZDF adipose; F) ZDF PFC; G) ZDF kidney; and H) ZDF liver.

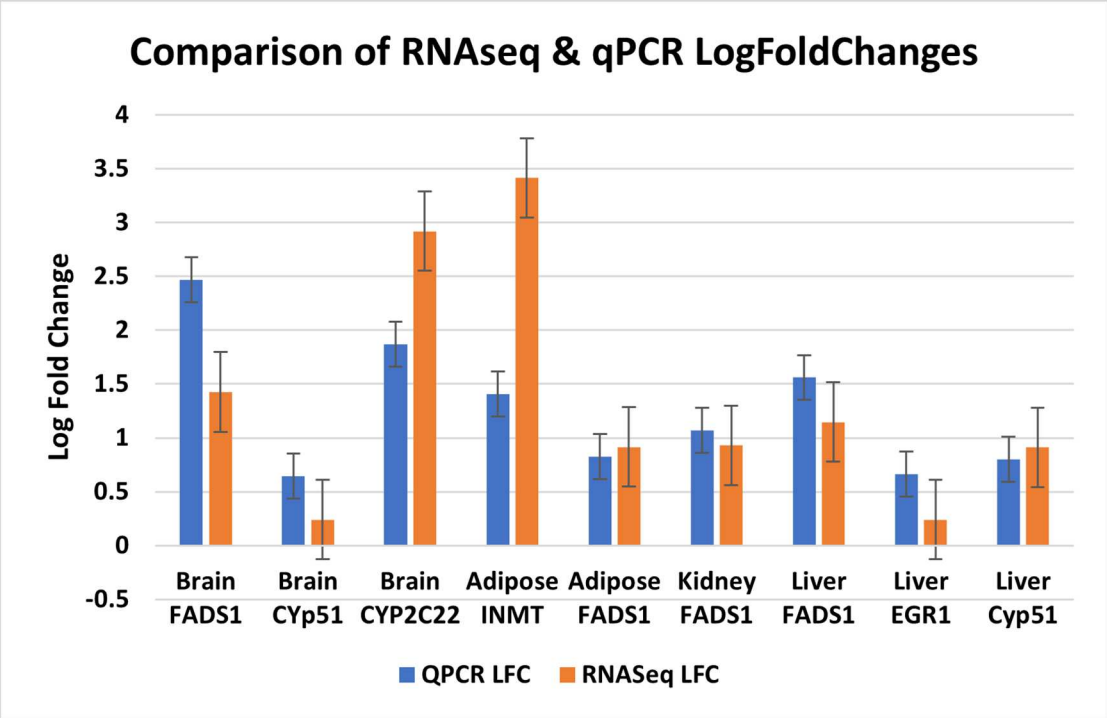

Figure B-4. qPCR results for select differentially expressed genes from mRNA Sequencing. Log fold change comparisons between qPCR and mRNA sequencing of several genes validating the sequencing results.

Table B-1. Composition of the WE- and CAS-based diets fed to male Sprague Dawley rats for 2 wk.

Ingredient (g/kg)	CAS	WE
Casein	200	0
Whole Egg	-	435
Cornstarch	417	365
Glucose monohydrate	150	150
Lard	-	200
Corn Oil	183	0
Mineral Mix	35	35
Vitamin Mix	10	10
Choline Bitartrate	2	2
L-methionine	3	3
Biotin (1%)	-	0.4

[1]All ingredients were purchased from Envigo except for dried whole egg (Rose Acre Farms, Guthrie Center, IA), as well as L-methionine and choline bitartrate (Sigma-Aldrich). Abbreviations used: CAS, casein-based diet, WE, whole egg-based diet
[2] Total protein and lipid content provided by 435 g of dried whole egg was 46 (200 g) and 42% (183 g), respectively.
[3] To formulate all diets such that protein was provided at 20% (w/w).

Table B-2. List of Differentially Expressed Genes in the PFC, Liver, Adipose, and Kidney.

Tissue	Ensembl_ID (ENSRNO)	Symbol	Gene Name	L2FC	P-value[3]
Adipose Up-regulated					
	G00000018237	Gstp1	glutathione S-transferase pi 1	1.89	1.65E-05
	G00000011250	Inmt	indolethylamine N-methyltransferase	1.78	3.42E-05
	G00000013484	Gsta3	glutathione S-transferase alpha-3	1.37	3.20E-03
	G00000058571	N/A	unclassified	1.14	3.76E-02
	G00000033206	Entpd5	ectonucleoside triphosphate diphosphohydrolase 5	1.10	2.57E-02
	G00000032745	Slc17a3	solute carrier family 17 member 3	1.06	5.08E-02

Table B-2. Continued

Tissue	Ensembl_ID (ENSRNO)	Symbol	Gene Name	L2FC	P-value[3]
	G00000011573	Csad	cysteine sulfinic acid decarboxylase	1.01	2.49E-03
	G00000008755	Acox1	acyl-CoA oxidase 1	0.98	1.07E-02
	G00000047708	Gstz1	glutathione S-transferase zeta 1	0.92	2.08E-02
Adipose Down-regulated	G00000017672	Akr1c14	aldo-keto reductase family 1, member C14	-3.43	2.66E-16
	G00000043451	Spp1	secreted phosphoprotein 1	-3.14	3.20E-03
	G00000010047	Ddit4l	DNA-damage-inducible transcript 4-like	-2.56	5.51E-03
	G00000013704	Cps1	carbamoyl-phosphate synthase 1	-1.90	1.72E-03
	G00000010833	Mthfd2	methylenetetrahydrofolate dehydrogenase (NADP+ dependent) 2, methenyltetrahydrofolate cyclohydrolase	-1.79	3.24E-02
	G00000058739	Snn	stannin	-1.56	5.51E-03
	G00000004626	Slc34a2	solute carrier family 34 member 2	-1.54	4.45E-03
	G00000014453	Anxa5	annexin A5	-1.52	3.81E-06
	G00000002579	Parm1	prostate androgen-regulated mucin-like protein 1	-1.50	3.81E-03
	G00000003120	Prelp	proline and arginine rich end leucine rich repeat protein	-1.48	3.63E-03
	G00000015550	Ptgds	prostaglandin D2 synthase	-1.35	2.45E-02
	G00000018351	Thap4	THAP domain containing 4	-1.22	3.81E-03
	G00000009019	Slc6a6	solute carrier family 6 member 6	-1.19	5.08E-02
Liver Up-regulated	G00000003144	Gprc5c	G protein-coupled receptor, class C, group 5, member C	2.13	4.43E-02
Liver Down-regulated	G00000019422	Egr1	early growth response 1	-2.06	1.04E-02
PFC Up-regulated	G00000010262	Hdc	histidine decarboxylase	2.67	2.77E-08
	G00000011250	Inmt	indolethylamine N-methyltransferase	2.36	2.76E-07
	G00000000961	Glt1d1	glycosyltransferase 1 domain containing 1	1.95	4.70E-04
	G00000061527	Gck	glucokinase	1.94	1.29E-03
	G00000013851	Spry4	sprouty RTK signaling antagonist 4	1.90	5.19E-03
	G00000010337	Slc13a2	solute carrier family 13 member 2	1.79	1.70E-02
	G00000013552	Scd	stearoyl-CoA desaturase	1.78	7.50E-03
	G00000020869	mrpl9	mitochondrial ribosomal protein L9	1.70	4.23E-02
	G00000032246	Acsm3	acyl-CoA synthetase medium-chain family member 3	1.69	1.03E-02
	G00000009597	Cyp4a1	cytochrome P450, family 4, subfamily a, polypeptide 1	1.62	1.34E-03
	G00000021924	Cyp2c22	cytochrome P450, family 2, subfamily c, polypeptide 22	1.55	3.56E-02
	G00000057072	Slc12a3	solute carrier family 12 member 3	1.46	1.70E-02
	G00000045649	Arrdc3	arrestin domain containing 3	1.36	6.69E-03
	G00000000978	N/A	unclassified	1.26	8.58E-03
	G00000019587	Ptprn	protein tyrosine phosphatase, receptor type, N	1.17	1.86E-02
	G00000011648	Aqp1	aquaporin 1	1.17	2.70E-02
	G00000018937	Gstm2	glutathione S-transferase mu 2	0.94	7.05E-05

Table B-2. Continued

Tissue	Ensembl_ID (ENSRNO)	Symbol	Gene Name	L2FC	P-value[3]
	G00000003515	Ephx1	epoxide hydrolase 1	0.93	1.27E-02
	G00000009421	Ivd	isovaleryl-CoA dehydrogenase	0.93	4.42E-02
	G00000004009	Xpnpep2	X-prolyl aminopeptidase 2	0.92	9.78E-04
	G00000013949	NADP	isocitrate dehydrogenase	0.92	4.04E-02
	G00000010017	Wee1	WEE1 G2 checkpoint kinase	0.79	3.19E-03
	G00000000645	Reep3	receptor accessory protein 3	0.76	4.59E-02
	G00000011747	Tmem205	transmembrane protein 205	0.71	2.70E-02
	G00000003038	Sft2d2	SFT2 domain containing 2	0.53	2.21E-02
PFC Down-regulated	G00000009550	Sqle	squalene epoxidase	-4.96	3.53E-14
	G00000016690	Idi1	isopentenyl-diphosphate delta isomerase 1	-2.71	3.53E-14
	G00000020480	fasn	fatty acid desaturase 1	-2.61	5.31E-14
	G00000012819	Gdnf	glial cell derived neurotrophic factor	-2.48	1.65E-03
	G00000007234	Cyp51	cytochrome P450, family 51	-2.06	3.53E-14
	G00000006859	Insig1	insulin induced gene 1	-1.96	8.06E-03
	G00000006280	Pcsk9	proprotein convertase subtilisin/kexin type 9	-1.89	6.29E-05
	G00000016552	Hmgcs1	3-hydroxy-3-methylglutaryl-CoA synthase 1	-1.77	3.11E-07
	G00000036615	RGD1560242	similar to RIKEN cDNA 1700028P14	-1.76	3.56E-02
	G00000032297	Msmo1	methylsterol monooxygenase 1	-1.74	3.76E-14
	G00000011622	Echdc1	ethylmalonyl-CoA decarboxylase 1	-1.65	3.32E-03
	G00000005871	Il1rn	interleukin 1 receptor antagonist	-1.60	6.69E-03
	G00000043377	Fdps	farnesyl diphosphate synthase	-1.39	3.81E-03
	G00000006787	Dhcr24	24-dehydrocholesterol reductase	-1.36	9.88E-03
	G00000045636	Fasn	fatty acid synthase	-1.34	9.14E-04
	G00000020704	Tkfc	triokinase and FMN cyclase	-1.32	3.07E-02
	G00000016924	Acly	ATP citrate lyase	-1.30	2.15E-04
	G00000016122	Hmgcr	3-hydroxy-3-methylglutaryl-CoA reductase	-1.25	1.43E-04
	G00000018755	Acss2	acyl-CoA synthetase short-chain family member 2	-1.20	9.88E-04
	G00000032508	Acot5	acyl-CoA thioesterase 5	-1.09	1.95E-02
	G00000002212	17-beta	hydroxysteroid	-1.08	2.36E-02
	G00000023348	Tbc1d2	TBC1 domain family, member 2	-1.08	4.42E-02
	G00000000658	Acacb	acetyl-CoA carboxylase beta	-1.02	2.59E-02
	G00000013387	Tpcn2	two pore segment channel 2	-0.92	4.04E-02
	G00000046889	Dbi	diazepam binding inhibitor, acyl-CoA binding protein	-0.89	3.39E-02
	G00000057814	Nsdhl	NADP-dependent steroid dehydrogenase-like	-0.64	8.06E-04
	G00000004903	Ebo	emopamil binding protein (sterol isomerase)	-0.64	2.60E-02

[1]All genes were analyzed using DESeq2 for differential analysis

[2]Abbreviations used: L2FC, log2 fold change; and PFC, prefrontal cortex

[3]Benjamini-Hochberg adjusted P-values controlling for false discovery rate at 5%, where $P < 0.05$ was considered significant.

Table B-3. Kegg Pathway and Gene Ontology (GO) Analysis.

Category	GO_ID	Term	Count	P-Value	Gene Symbols
Adipose					
	GO:1903825	organic acid transmembrane transport	2	4.80E-03	*Slc17a3, Slc6a6*
	GO:0044341	sodium-dependent phosphate transport	2	7.70E-03	*Slc17a3, Slc34a2*
	GO:0006817	phosphate ion transport	2	9.70E-03	*Slc17a3, Slc34a2*
	GO:0035435	phosphate ion transmembrane transport	2	1.70E-02	*Slc17a3, Slc34a2*
	GO:0006749	glutathione metabolic process	2	4.90E-02	*Gstz1, Gstp1*
	GO:0043200	response to amino acid	2	5.50E-02	*Cps1, Gstp1*
	GO:0048545	response to steroid hormone	2	5.80E-02	*Cps1, Spp1*
	GO:0098869	cellular oxidant detoxification	2	6.50E-02	*Gstz1, Gstp1*
	GO:0035725	sodium ion transmembrane transport	2	6.60E-02	*Slc17a3, Slc34a2*
	GO:0005436	sodium:phosphate symporter activity	2	6.70E-03	*Slc17a3, Slc34a2*
	GO:0015321	sodium-dependent phosphate transmembrane transporter activity	2	7.70E-03	*Slc17a3, Slc34a2*
	GO:0042301	phosphate ion binding	2	1.10E-02	*Mthfd2, Slc34a2*
	GO:0004602	glutathione peroxidase activity	2	2.00E-02	*Gstz1, Gstp1*
	GO:0005504	fatty acid binding	2	2.60E-02	*Ptgds, Acox1*
	GO:0004364	glutathione transferase activity	2	4.10E-02	*Gstz1, Gstp1*
	KEGG	Metabolic pathways	6	8.70E-03	*Cps1, Mthfd2, Csad, Ptgds, Gstz1, Acox1*
Brain	GO:0006695	cholesterol biosynthetic process	8	3.90E-13	*Hmgcr, Hmgcs1, sterol isomerase, Nsdhl, Dhcr24, Idi1, Fdps*
	GO:0006633	fatty acid biosynthetic process	6	1.10E-07	*Scd, Acsm3, Acacb, Fasn, Acly, Msmo1*
	GO:0055114	oxidation-reduction process	12	8.70E-07	*17-beta, Scd, Hmgcr, Fads1, Fasn, Sqle, Cyp2c22, Cyp51, Nsdhl, Dhcr24, Cyp4a1, Msmo1*
	GO:0016126	sterol biosynthetic process	4	5.10E-06	*Insig1, Sqle, sterol isomerase, Msmo1*
	GO:0008610	lipid biosynthetic process	4	8.00E-06	*Scd, Fasn, Acly, Acss2*
	GO:0008203	cholesterol metabolic process	5	2.30E-05	*Pcsk9, Insig1, Sqle, Nsdhl, Dhcr24*
	GO:0008299	isoprenoid biosynthetic process	4	2.30E-05	*Hmgcr, Hmgcs1, Idi1, Fdps*
	GO:0006084	acetyl-CoA metabolic process	3	1.50E-04	*Acacb, Fasn, Acly*
	GO:0006641	triglyceride metabolic process	4	1.70E-04	*Pcsk9, Scd, Insig1, Dbi*

Table B-3. Continued

Category	GO_ID	Term	Count	P-Value	Gene Symbols
	GO:0014070	response to organic cyclic compound	6	7.80E-04	*Hmgcs1, Fads1, Acacb, Ephx1, Il1rn, Gstm2*
	GO:0006637	acyl-CoA metabolic process	3	2.50E-03	*Acsm3, Acot5, Dbi*
	GO:0019932	second-messenger-mediated signaling	2	8.00E-03	*Gck, Ptprn*
	GO:0043588	skin development	3	9.90E-03	*Arrdc3, Dhcr24, Dbi*
	GO:0006085	acetyl-CoA biosynthetic process	2	1.10E-02	*Acly, Acss2*
	GO:0031999	negative regulation of fatty acid beta-oxidation	2	1.30E-02	*Acacb, Dbi*
	GO:0006725	cellular aromatic compound metabolic process	2	1.90E-02	*Ephx1, Sqle*
	GO:0030157	pancreatic juice secretion	2	2.10E-02	*Aqp1, Dbi*
	GO:0006629	lipid metabolic process	3	2.40E-02	*Fads1, Il1rn, Acly*
	GO:0009725	response to hormone	3	2.90E-02	*Hmgcs1, Aqp1, Dhcr24*
	GO:0021670	lateral ventricle development	2	3.20E-02	*Aqp1, Dbi*
	GO:0070723	response to cholesterol	2	3.40E-02	*Hmgcs1, Fdps*
	GO:0046889	positive regulation of lipid biosynthetic process	2	3.70E-02	*17-beta, Dbi*
	GO:0006636	unsaturated fatty acid biosynthetic process	2	3.70E-02	*Scd, Fads1*
	GO:0032869	cellular response to insulin stimulus	3	4.30E-02	*Gck, Pcsk9, Insig1*
	GO:0042493	response to drug	5	5.20E-02	*Hmgcs1, Aqp1, Acacb, Il1rn, Fdps*
	GO:0001889	liver development	3	5.80E-02	*Pcsk9, Hmgcs1, Ephx1*
	GO:0008584	male gonad development	3	5.90E-02	*Hmgcs1, Gdnf, Fdps*
	GO:0046835	carbohydrate phosphorylation	2	6.20E-02	*Gck, Tkfc*
	GO:0010033	response to organic substance	3	6.30E-02	*Hmgcs1, Fads1, Sqle*
	GO:0006694	steroid biosynthetic process	2	8.20E-02	*Cyp51, Dbi*
	GO:0019369	arachidonic acid metabolic process	2	8.20E-02	*Fads1, Cyp4a1*
	GO:0030073	insulin secretion	2	9.00E-02	*Ptprn, Il1rn*
	GO:0070542	response to fatty acid	2	9.90E-02	*Scd, Insig1*
	GO:0005506	iron ion binding	5	1.80E-03	*Scd, Cyp2c22, Cyp51, Cyp4a1, Msmo1*

Table B-3. Continued

Category	GO_ID	Term	Count	P-Value	Gene Symbols
	GO:0016491	oxidoreductase activity	4	4.30E-03	*17-beta, Scd, Fads1, Dhcr24*
	GO:0050660	flavin adenine dinucleotide binding	3	1.40E-02	*Sqle, Dhcr24, Ivd*
	GO:0000287	magnesium ion binding	4	1.70E-02	*Gck, NADP, Wee1, Idi1*
	GO:0016831	carboxy-lyase activity	2	2.80E-02	*Echdc1, Hdc*
	GO:0070402	NADPH binding	2	4.10E-02	*Hmgcr, Fasn*
	GO:0005215	transporter activity	3	4.40E-02	*Slc13a2, Aqp1, Slc12a3*
	GO:0042803	protein homodimerization activity	6	5.50E-02	*Hmgcr, Hmgcs1, Fasn, Hdc, Gdnf, Gstm2*
	GO:0046872	metal ion binding	8	6.10E-02	*Scd, Acsm3, Acacb, Xpnpep2, Acly, Idi1, Tkfc, Fdps*
	GO:0020037	heme binding	3	6.80E-02	*Cyp2c22, Cyp51, Cyp4a1*
	GO:0019899	enzyme binding	4	7.90E-02	*Ephx1, Dhcr24, Gstm2, Slc12a3*
	GO:0000062	fatty-acyl-CoA binding	2	9.40E-02	*Ivd, Dbi*
	KEGG	Metabolic pathways	23	9.50E-10	*Gck, Hmgcs1, Acsm3, Acacb, Fasn, NADP, sterol isomerase, Sqle, Hdc, Acly, Acot5, Nsdhl, Cyp51, Acss2, Dhcr24, Idi1, Cyp4a1, Tkfc, Fdps, Hmgcr, Cyp2c22, Ivd, Msmo1*
	KEGG	Biosynthesis of antibiotics	12	1.60E-09	*Gck, Hmgcr, Hmgcs1, NADP, Sqle, Acly, Acss2, Cyp51, Nsdhl, Idi1, Msmo1, Fdps*
	KEGG	Steroid biosynthesis	6	2.10E-08	*Sqle, sterol isomerase, Cyp51, Nsdhl, Dhcr24, Msmo1*
	KEGG	Terpenoid backbone biosynthesis	4	1.40E-04	*Hmgcr, Hmgcs1, Idi1, Fdps*
	KEGG	Propanoate metabolism	3	7.00E-03	*Echdc1, Acacb, Acss2*
	KEGG	Biosynthesis of unsaturated fatty acids	3	7.50E-03	*Scd, Fads1, Acot5*
	KEGG	Carbon metabolism	4	1.70E-02	*Gck, NADP, Acss2, Tkfc*
	KEGG	AMPK signaling pathway	4	2.00E-02	*Scd, Hmgcr, Acacb, Fasn*
	KEGG	Fatty acid metabolism	3	2.40E-02	*Scd, Fads1, Fasn*
	KEGG	Bile secretion	3	4.10E-02	*Hmgcr, Aqp1, Ephx1*
	KEGG	PPAR signaling pathway	3	4.70E-02	*Scd, Cyp4a1, Dbi*
	KEGG	Fatty acid biosynthesis	2	6.10E-02	*Acacb, Fasn*
	KEGG	Chemical carcinogenesis	3	6.30E-02	*Ephx1, Cyp2c22, Gstm2*

[1]All pathway analyses were determined via g:Profiler
[2]Abbreviations used: GO, gene ontology; KEGG, Kyto Encyclopedia of Genes and Genomes

Table B-4. Differentially Expressed MicroRNAs between Sprague Dawley Rats Fed Dietary Whole Egg Compared to Casein Control.

Tissue	MicroRNA	Log2Fold	FDR non-adjusted P-value
Adipose Upregulated	rno-miR-221-3p	0.8928	0.023787818
Adipose Downregulated	rno-miR-140-3p	-1.01197	0.001986062
	rno-miR-125b-5p	-1.17509	0.007240392
	rno-miR-191a-5p	-0.7673	0.011564826
	rno-miR-10b-5p	-0.49055	0.033921745
Brain Upregulated	rno-let-7e-5p	1.339427	0.005181862
	rno-miR-30a-3p	0.388272	0.029746435
	rno-miR-98-5p	0.960443	0.035167986
Brain Downregulated	rno-miR-10a-5p	-1.42826	0.025129776
	rno-miR-10b-5p	-1.35052	0.027749043
	rno-miR-29a-3p	-0.89674	0.03613351
	rno-miR-192-5p	-0.82033	0.057313629
Liver Upregulated	rno-miR-30c-5p	0.352427	0.027632486
	rno-miR-30d-5p	0.32298	0.056044331
Liver Downregulated	rno-miR-21-5p	-0.44345	0.003247421
	rno-miR-192-5p	-0.19144	0.021920638

[1]All miRNAs were analyzed using DESeq2 for differential analysis
[2]Abbreviations used: L2FC, log2 fold change; and PFC, prefrontal cortex
[3]Benjamini-Hochberg adjusted P-values controlling for false discovery rate at 5%, where $P < 0.05$ was considered significant.

Table B-5. MicroRNA Targets of Differentially Expressed Genes in the PFC and Adipose Tissue of Sprague Dawley Rats Fed Dietary Whole Egg vs. Casein.

MicroRNA	Tissue	Human GeneID	Log2fold change	Log fold change	Rat Symbol	Non-adj p value
miR-10b-5p (down regulated)	Brain	ARRDC3	1.36E+00	1.85E+00	Arrdc3	1.96E-05
miR-192-5p (down regulated)	Brain	AMER1	1.26E+00	1.58E+00	Amer1	2.81E-03
		BLCAP	-4.96E-01	-2.46E-01	Blcap	1.10E-02
		MYLK	-4.61E-01	-2.12E-01	Mylk	1.16E-02
		FABP3	1.33E+00	1.78E+00	Fabp3	1.64E-02
		TAOK1	-5.43E-01	-2.95E-01	Taok1	1.74E-02
		PCDH17	1.21E+00	1.46E+00	Pcdh17	2.01E-02
		FRMD4B	8.81E-01	7.76E-01	Frmd4b	2.62E-02
		KIF1B	4.56E-01	2.08E-01	Kif1b	3.37E-02
		C4orf46	-5.31E-01	-2.82E-01	RGD1560010	3.72E-02
		COL5A1	1.41E+00	2.00E+00	Col5a1	4.17E-02
		ZFP36L1	4.13E-01	1.71E-01	Zfp36l1	4.86E-02
		NIPAL1	6.36E-01	4.05E-01	Nipal1	5.19E-02
		PDHB	-4.43E-01	-1.96E-01	Pdhb	5.49E-02
		SNX33	4.25E-01	1.81E-01	Snx33	5.88E-02
miR-125b-5p (down regulated)	Adipose	PARM1	-1.50E+00	-2.24E+00	Parm1	4.19E-06
		DNAJC14	-9.69E-01	-9.39E-01	Dnajc14	4.79E-04

APPENDIX C. ACUTE SERUM AND NON-TRANSFERRIN BOUND IRON AND GASTROINTESTINAL SYMPTOMS WITH 3 WEEK CONSUMPTION ARE LOWER WITH IRON-ENRICHED ASPERGILLUS ORYZAE COMPARED TO FERROUS SULFATE

Amanda E. Bries, Chong Wang, Isaac Agbemafle, Brian Wels, and Manju B. Reddy., Acute serum and non-transferrin bound iron and gastrointestinal symptoms with 3 week consumption are lower with iron-enriched Aspergillus oryzae compared to ferrous sulfate. *Curr Dev Nutr* 2019, 3:12, nzz127, reprinted by permission of Oxford University Press.

Abstract

Background: Iron deficiency anemia (IDA) is a widespread nutritional deficiency and iron supplementation, especially with ferrous sulfate ($FeSO_4$) is the most common strategy to treat IDA; however, compliance is often poor with daily $FeSO_4$ due to negative side effects. In a previous study, iron from iron-enriched *A. oryzae* [Ultimine® Koji Iron, (ULT)] was similarly absorbed as $FeSO_4$.

Objective: The main objective of this study was to assess the safety of consuming ULT in terms of increasing non-transferrin bound iron (NTBI) and gastrointestinal distress.

Methods: Young female participants (n=16) with serum ferritin < 40μg/L were randomized to a double-blind, 9-wk cross-over study with a 3-wk placebo/washout period between treatments. Oral $FeSO_4$ and ULT supplements containing 65 mg Fe mg/dose were administered daily, for 21 consecutive days. On day 1, serum iron (SI), percentage transferrin saturation (%TS), and NTBI were measured for 8h on the first day of iron consumption. Changes in biochemical indicators were evaluated after 3 wk consumption. Side effects questionnaires were completed weekly on 2 randomly selected weekdays and 1 weekend day for the entire of the study.

Results: SI, %TS, and NTBI were all markedly higher during hours 2-8 ($P < 0.001$) with $FeSO_4$ than with ULT. Oxidative stress, inflammatory, and kidney and liver function markers remained unchanged with both supplementations compared with placebo. Changes in iron status markers were not significantly different among the 3 treatments. Individual or global side effects were not significantly different among all treatments. Even when common side effects of nausea, constipation, and diarrhea were combined, $FeSO_4$ treatment had a significantly higher effect than ULT ($P = 0.04$) and placebo ($P = 0.004$) only at week 3, but the difference was not significant between ULT and placebo.

Conclusions: Low NTBI production and fewer common gastrointestinal side effects with ULT suggest that it is a safe oral iron supplement to treat IDA. This trial was registered at clinicaltrials.gov as NCT04018300.

Introduction

An estimated 12.5% of the global population has iron deficiency anemia (IDA) (1) and it is the most common nutritional deficiency in the world, especially among women and children in developing countries. Negative consequences of IDA include reduced cognitive and physical development and increased mortality of children (2, 3). The WHO guidelines are aimed toward using food fortification, home fortification, or supplementation strategies in treatment of IDA (4). Food iron fortification is one of the most economical strategies to address anemia; however, iron supplementation is more effective in short-term treatment. Ferrous sulfate ($FeSO_4$), the most commonly used oral iron supplement, is highly absorbed and improves iron status, but causes adverse effects such as constipation, diarrhea, and nausea (5). Owing to the quick absorption of $FeSO_4$, iron influx into blood is rapid, saturating transferrin transiently and producing non-transferrin-bound iron (NTBI) (6). Under normal iron status, transferrin is capable of binding

iron present in circulation. It is well known that in chronic iron overload conditions, the capacity of transferrin to bind iron decreases, causing high transferrin saturation and production of NTBI, a highly reactive iron, which induces oxidative stress owing to its involvement in free radical production, as well as potentially damaging DNA, protein, and lipids (7). Research has also demonstrated that circulating NTBI is likely to appear despite the presence of available binding sites on transferrin if the rate of iron influx into plasma exceeds the rate of iron acquisition by transferrin (8). Further consequences of circulating NTBI constitute increased bacterial-pathogenic infections, due to the free iron being utilized by the parasite, causing increased infections and even death in malaria–endemic areas (9). Therefore, it is important to maintain low iron saturation levels to minimize the production of NTBI and thereby reduce systemic inflammation and bacterial infections (10). Furthermore, research indicates that maintaining percentage transferrin saturation (%TS) <35% delays biological aging and lessens the risk of age-associated diseases induced by oxidative stress (11).

$FeSO_4$ is the gold-standard treatment of anemia, especially in pregnant women, but concerns about high soluble iron supplements during pregnancy continue to emerge owing to high amounts of unabsorbed reactive iron in the gut, causing diarrhea, inflammation, and constipation, resulting in low patient compliance (5). There is also a need for a low-risk and safe iron supplement targeted to vulnerable populations with increased physiological need, who may be susceptible to infection.

Ultimine® Koji Iron (ULT) is a source of natural iron produced by fermentation with *Aspergillus oryzae*, also known as *koji* culture. Most of the iron is stored within the mycelia of the *koji* culture. Our recent publication showed that the iron from ULT is as bioavailable as $FeSO_4$ in humans (12). The main objective of this study was to compare the acute effect of

consuming 65 mg Fe from $FeSO_4$ and ULT with food, in young female subjects, on serum iron (SI) and NTBI production as a function of time. In addition, we evaluated the effectiveness in improving iron status and safety of 65 mg Fe/d from these supplements by assessing changes in gastrointestinal-related side effects, oxidative stress, and biochemical indicators after 3 wk oral intake.

Materials and Methods

Subjects and Study Design. Women 18–40 y of age were recruited via an Iowa State University (ISU)-wide email. Consented subjects (n = 126) completed a prescreening online health questionnaire including demographics (age, gender, education, and ethnicity) and questions pertaining to the initial inclusion criteria: a BMI (in kg/m^2) of 18.5–30; no medication use (except noniron combination oral contraceptives); no blood donation within 2 mo; nonsmoking; nonpregnant or lactating; no history of chronic diseases; no gastrointestinal-associated conditions or dietary intolerances; and no intake of vitamin, mineral, or herbal supplements 1 wk before and during the study period. Subjects were excluded based on the following criteria: hemoglobin (Hb) < 12 g/dL, serum ferritin (SF) ≥ 40 μg/L, or abnormal kidney, liver, and basic metabolic panel indicators. A total of 91 consented subjects were screened, of whom only 17 were eligible based on the set inclusion criteria and were randomly assigned to their respective treatment groups. One subject dropped out during placebo treatment because of reported side effects of gastrointestinal discomfort. A total of 16 subjects completed the 3 arms of the study. We estimated a sample size of 15 subjects for each group was needed to provide a power of 80% (β=0.20) to detect an intrasubject difference of 30% in NTBI with α = 0.05. Written informed consent was obtained from each participant and the study was approved by the Institutional Review Board (IRB) at ISU: IRB# 17-365.

This 9-wk intervention was conducted at the Nutrition and Wellness Research Center at ISU and was aimed at assessing the acute influx of iron into serum and NTBI as a function of time over 8 h after oral Fe supplementation and change in iron status, safety, and gastrointestinal distress with 3-wk consumption of iron. Seventeen female subjects were enrolled in a double-blind crossover study. They were randomly assigned to receive daily capsules containing 65 mg Fe as either $FeSO_4$ or ULT for 3-wk periods with a 3-wk placebo/washout before treatment crossover (Figure C-1). A gastrointestinal side effects questionnaire (GISQ) was distributed electronically to participants over 2 randomly chosen weekdays and 1 weekend day during each intervention period. The SI response and NTBI determination procedures are described below. Subjects acted as their own controls and side effects from iron supplementation were monitored throughout the study. General compliance was recorded by documenting the remaining capsules from the returned containers. Safety of supplementation was evaluated via kidney function [blood urea nitrogen (BUN), creatinine, and estimated glomerular filtration rate (eGFR)]; liver function [aspartate aminotransferase (AST) and alanine aminotransferase (ALT)]; oxidative stress [protein carbonyls (PCOs) and thiobarbituric acid reactive substances (TBARS)]; and inflammatory indicators [C-reactive protein (CRP) and hepcidin].

Iron Supplements. Each iron supplement contained 65 mg Fe as $FeSO_4$ (Nature Made®) or as ULT (iron-enriched *A. oryzae* containing 8.7% Fe) and placebo capsules were prepared with dextrose monohydrate. Similarly to our previous study (12), a commercial sample of ULT (13) was supplied by Cura Global Health, Inc. All pills were prepared in opaque-colored, pharmaceutical-grade gelatin capsules (Capsuline). New pill containers with 21 capsules (a 3-wk supply) were given to subjects on day 1 of each treatment period to prevent cross-contamination.

Subjects were explicitly instructed to only take 1 capsule daily with food, even if they forgot to take it on prior days.

Biochemical Assessment. Biochemical indicators were assessed at baseline (day 1) and end (day 21) of treatment period 1 and baseline (day 42) and end (day 63) of treatment period 2. The effect of the washout period (placebo) was evaluated using the week 3 and week 6 time points. Whole blood and serum were collected and sent to a certified diagnostic laboratory (Quest Diagnostics) for Hb, SI, total iron-binding capacity, %TS, ALT, AST, BUN, eGFR, and creatinine analyses. The SF concentration was determined using an S-22 Spectro Ferritin Kit (Ramco Laboratories, Inc.). Serum aliquots were collected at all 4 visits and stored at −80°C until oxidative indicators were measured within 3 mo of time of collection. Circulating hepcidin, CRP, and soluble transferrin receptor concentrations were measured using commercial ELISA kits (DRG International, Inc.; American Laboratory Products Company; and Ramco Laboratories, Inc., respectively). Lipid peroxidation (TBARS) was measured as a malondialdehyde colorimetric assay (Cayman Chemical). Serum PCOs were measured based on a modified assay (14).

Acute SI response and NTBI production. To determine NTBI and SI concentrations after iron supplements ($FeSO_4$ and ULT) consumed with a semipurified meal (egg albumin, maltodextrose, and corn oil) after a 10-h fast on days 1 and 42, serum was collected at time points 0 (time of supplementation), 1, 2, 3, 4, 6, and 8 h after supplementation. The ingredients and procedure used in preparing the meals were as previously described (12). During the 8-h period, the subjects consumed unfortified white bread with cheese and butter at 3 h and an apple at 6 h. The NTBI was determined as previously described (15, 16) with modifications. In brief, serum aliquots were rapidly thawed at 37°C for 10 min and incubated with resin-treated 400 mM

nitriloacetic acid (NTA) at pH 7.0 for 30 min at room temperature. The serum–NTA complex was then centrifuged in a 30 kD microcon ultracel-30 column (Millipore Sigma) at 7437 × *g* for 90 min. Sample ultrafiltrates were diluted to a final concentration of 10 mM NTA. To ensure negligible concentrations of NTBI, pooled serum ultrafiltrate obtained from the screening serum of the subjects with SF < 15 μg/L was used to prepare blanks and standards. A pooled ultrafiltrate (10 mM NTA) was used as blank and spiked with 2 and 5 μg/L of iron as quality controls.

Serum NTBI from the Fe–NTA filtered complex was measured using graphite furnace atomic absorption spectrometry (Perkin Elmer AAnalyst600). The lower limit and upper limit of detection were 0.1 and 60 μg/L, respectively. Linearity was established from 0.1 to 60 μg/L ($r = 0.99$) with the iron containing the pooled filtrate. The percentage recovery was 96% with a known 60 μg/L standard, ensuring the accuracy of the measurement.

Side Effects Questionnaire. We used a modified GISQ assessment tool that was based on a previously reported oral iron supplement questionnaire (17). The GISQ covers gastrointestinal-related side effects commonly reported with oral $FeSO_4$ supplementation. We asked subjects to report the following common side effects due to the iron supplement intake: nausea, heartburn, abdominal discomfort, fatigue, diarrhea, and constipation. The severity of the side effects was recorded on a 7-point Likert scale (0 = absent, 1 = somewhat mild, 2 = mild, 3 = somewhat moderate, 4 = moderate, 5 = somewhat severe, 6 = severe). Frequency of weekly side effects was the number of reported side effects for 2 randomly selected weekdays and 1 weekend day over the 9-wk study period. From the 6 side effects reported, the most common ones related to iron were nausea, diarrhea, and constipation, which are likely to cause abdominal discomfort (5); these were combined to test the effect of the supplements.

Statistical Analysis. Analysis was performed by intention to treat, consistent with CONSORT guidelines (18). All analyses were performed using SAS version 9.4 (2018; SAS Institute Inc.). Changes in SI, TS, and NTBI from baseline to 8 h after administration of 65 mg $FeSO_4$ or ULT were analyzed using repeated-measures regression models over the 8 h time. The biochemical variable values (mean ± SEM) refer to the change from baseline to end for their respective time points within the crossover design. Normality for the biochemical data was tested using the Shapiro–Wilk test and geometric means (95% CIs) were reported for non-normally distributed data. Effects of the treatments on the change were compared using SAS PROC GLIMMIX for repeated-measures ANOVAs with Tukey multiple comparisons to test the difference between least-square means. A total of 16 subjects were included in all biochemical and questionnaire analyses, whereas 15 subjects were included in SI, NTBI, and TS analyses, because 1 subject had difficulty with multiple blood draws.

Data for the side effects were obtained from the online survey of the GISQ exported from Qualtrics™ into Microsoft Excel. The severity of the side effects was recoded from the 7-point Likert scale into 4 levels: 0 = absent, 1 = mild (somewhat mild and mild), 2 = moderate (somewhat moderate and moderate), 3 = severe (somewhat severe and severe). To record the frequency of side effects, we created a dichotomous variable from the 7-point Likert scale as follows: 0 = absent and 1 = present (somewhat mild, mild, somewhat moderate, moderate, somewhat severe, and severe). After the 3-wk supplementation, the frequency of weekly side effects was aggregated to total reported side effects over the 3-wk supplemental period. The models included fixed effects for treatment, period, and sequence; they also included random effects for subjects nested within sequence. Descriptive statistics were presented as frequencies for the side effects. Differences between treatments in the frequency of reported side effects were

specified using SAS PROC GLIMMIX. For all statistical analysis, $P < 0.05$ was considered statistically significant.

Results

Subject Characteristics. Age, BMI, and biochemical characteristics of the 16 subjects at baseline are shown in Table C-1. The mean age and BMI of subjects in the study were 21 y and 22.9, respectively. At screening, all participants had normal Hb concentrations (≥12 g/dL) and suboptimal SF concentrations (19.3 ± 8.4 μg/L). One subject was borderline for the SF cutoff concentration at baseline (40.4 μg/L); however, it was 37.4 μg/L at screening.

Acute Response of Serum Iron, Transferrin saturation, and NTBI. Mean changes in both %TS and SI concentrations peaked at 4 h with $FeSO_4$ (39.6% ± 5.2% and 27.8 ± 3.6 μM, respectively) and with ULT (11.7% ± 2.0% and 8.3 ± 1.6 μM, respectively) supplements, but the change was less distinct with ULT. The SI progressively decreased after 4 h for $FeSO_4$, but values did not return to baseline within 8 h with either $FeSO_4$ or ULT supplements (Figure C-2). TS percent rapidly spiked with a 65-mg dose of $FeSO_4$, but the same effect did not occur with ULT (Figure 2). NTBI concentrations peaked at 4 h (0.35 ± 0.17 μM) with $FeSO_4$ and remained above baseline even at 8 h post-dosing, although they were not statistically different from baseline concentrations (Figure C-3). On the contrary, at all time points, ULT NTBI concentrations were nearly unchanged from baseline. As expected, both SI ($r = 0.52$, $P = 0.0001$) and %TS ($r = 0.54$, $P = 0.0001$) were significantly correlated with NTBI when both treatments were combined (**Supplemental Figure C-1**).

Biochemical Indicators. There were no significant differences in the change of biochemical indicators among the iron supplements and placebo (Table C-2). Although, nonsignificantly, SI with ULT was higher than with $FeSO_4$ (mean ± SD: 12.7 ± 11.6 μg/dL and −5.69 ± 10.5 μg/dL,

respectively) at the end of the 3-wk supplementation period. Unlike a decline with placebo, improvements in SF were found both with ULT and with $FeSO_4$ supplementation (ULT: 2.03 ± 3.44 μg/L; $FeSO_4$: 9.38 ± 4.91 μg/L; Table C-2) but the differences were not statistically significant between the 2 treatments ($P = 0.23$). No other iron indicators were significantly different among the 3 treatments. Nonsignificant changes in inflammatory and oxidative stress markers were observed between treatment groups ($P > 0.05$). Based on kidney and liver function markers, the changes with ULT were not significantly different from those with $FeSO_4$. Compared with $FeSO_4$ and placebo, there were slight improvements in eGFR with ULT (ULT: 6.0 ± 2.46; $FeSO_4$: −0.81 ± 3.42; placebo: −1.63 ± 2.29; Table 2) but the differences were nonsignificant ($P = 0.09$). ALT concentrations for placebo were significantly higher from baseline to end than for ULT (Table 2; $P = 0.01$).

Gastrointestinal side effects. Compliance was 97%, 93%, and 95.2% for ULT, $FeSO_4$, and placebo, respectively. Although nonsignificantly, $FeSO_4$ tended to contribute higher incidence of constipation, diarrhea, nausea, and abdominal discomfort than did ULT and placebo (Table C-3). The differences for global side effects (combined effects) were not significant among the treatments ($P = 0.37$). Even when we combined the most common symptoms (nausea, diarrhea, and constipation) associated with $FeSO_4$, the differences were only significant at week 3 of $FeSO_4$ supplementation compared with both ULT and placebo ($P = 0.04$ and $P = 0.004$, respectively; data not shown), but no differences were found at the preceding weeks.

Discussion

Despite $FeSO_4$ being the most commonly used supplement for its effectiveness in treating anemia, its rapid absorption is of concern. When a bolus of iron enters the blood quickly, this exceeds the capacity for transferrin to bind the circulating iron, resulting in a transient increase in

NTBI concentrations. The catalytically reactive NTBI can promote oxidative stress and inflammatory response in the body (19). Therefore, there is a need for safer alternatives to $FeSO_4$ (20), without compromising iron absorption.

Based on the similar absorption of ULT to $FeSO_4$ in our previous stable isotope study in humans (12), the low SI response with ULT suggested its slow release mechanism, not low absorption. Several studies have demonstrated that the rate in which iron is taken up by the body is dependent on the dose, form of iron, and whether it was taken with or without food (21–23). Both %TS levels and SI concentrations did not return to baseline, even at 8 h post-supplementation, with either iron source. The %TS data are in agreement with a previous study demonstrating that %TS could reach baseline levels only after 24 h of supplementation (24).

Although nonsignificantly, change in SI was higher (after a 10-h overnight fast) with ULT compared with $FeSO_4$ after 3 wk consumption, suggesting that ULT iron may be released beyond 8 h (Table C-2). On the contrary, improvement in ferritin was less with ULT, but the change was nonsignificantly different from that with $FeSO_4$. Although we do not know the form of iron in ULT, Perls stain, and DAB/H_2O_2 iron intensification confirmed that >90% of the iron is inside the *A. oryzae* mycelia (data not shown). We can postulate that the iron from the complex fungal matrix is digested over a longer period of time than $FeSO_4$ and the digested iron may be taken up into enterocytes, processed, and released slowly. Also, it doesn't rule out absorption in the large intestine. Nearly 5 decades ago, a study showed a delayed peak of circulating iron with Hb iron compared with $FeSO_4$, because of its slow absorption and its alternative heme-absorption pathway (25). Evidence indicates that heme-iron absorption may be saturable because of the lack of dose-response observed after a 15-mg Fe dose (26). Therefore,

the slow mechanism of release observed in this trial may support a heme-like alternative absorption pathway.

The use of the SI curve as a surrogate for iron absorption is well established (27), and we may interpret that ULT absorption is 3 times lower than that of $FeSO_4$ based on our results. However, caution should be taken when examining different iron sources owing to the differences in digestion rate and mucosal processing time. Our study showed a much lower SI change with ULT than with $FeSO_4$ but based on that we cannot necessarily predict the iron absorption. For example, despite having high bioavailability shown in many studies, plasma iron release in 270 min with NaFeEDTA was much lower than with $FeSO_4$ (23). The limitation in applying SI curves for predicting iron absorption was clearly discussed by Schümann et al., especially in reference to Hb iron because of its complex digestibility (23). Therefore, ULT absorption is similar to $FeSO_4$ (12), despite low SI supporting the aforementioned hypothesis.

Under normal physiological conditions, the iron is bound to transferrin in circulation, resulting in negligible amounts of NTBI (20). When a bolus of iron enters blood with a high dose of iron supplementation, the transferrin becomes quickly saturated, causing a transient increase in NTBI concentrations and a propensity for associated adverse side effects. One study (28) reported that 6.5 mg Fe as $FeSO_4$ resulted in no NTBI production (similar to placebo), but a 65-mg Fe dose induced a 300-fold increase in the AUC of NTBI. Because higher iron doses are given to anemic subjects (200 mg/d) and a 65-mg dose was used in a previous study to assess NTBI (6), this was a reasonable amount for us to use in this study for subjects with an SF < 40 µg/L. The significant association found between SI and both %TS and NTBI suggests the importance iron influx has for %TS and NTBI production. Hence, it is critical for the controlled

absorption of iron to thereby reduce the elevation in SI concentrations, minimize the saturation of transferrin, and the subsequent production of NTBI.

NTBI has become a concern because of the involvement of free iron in promoting infection (20). In a large iron supplementation intervention trial in Pemba, adverse effects, including death, were observed when iron-replete children with malaria were given iron daily (9). This was primarily attributed to the role of NTBI in promoting the parasitic growth of malaria (29). More recent evidence from Parkkinen et al. (10) aligns with this observation in a study where they gave hemodialysis patients 100 mg intravenous iron. In their study, they identified significantly higher bacterial growth when cultured in the serum of hemodialysis patients with 80% TS, and the authors directly related it to NTBI availability (10). Although we cannot directly compare intravenous results and our oral supplementation results, a single 65-mg dose of $FeSO_4$ in healthy subjects in this study reached an absolute mean of 64% TS and ≤97% TS in some of the subjects. The mean %TS from ULT was half of that from $FeSO_4$ (34%) and remained at normal concentrations throughout the 8 h. Interestingly, the AUC for NTBI was 19-fold higher for $FeSO_4$ (97.5 ± 61.9) than for ULT (5.5 ± 6.6) (Figure C-3, data not shown).

Our findings suggest that %TS > 60% (as seen with $FeSO_4$) may produce NTBI concentrations at levels that promote systemic inflammation and other adverse effects. On the contrary, iron supplements, like ULT, with no NTBI production may result in less inflammation with long-term administration. Despite our observations of significantly reduced PCOs in rats fed ULT compared with $FeSO_4$ (30), in our short-term human study we found no differences in inflammatory and oxidative stress markers (CRP, PCOs, and TBARS) between ULT and $FeSO_4$. This could be attributed to several confounding variables such as the young age of our subjects, and resilience to acute oxidative stress induction.

One of the goals of this research was also to assess the safety and advantage of ULT supplementation as an alternative supplement to $FeSO_4$, to mitigate the commonly reported negative gastrointestinal side effects and low patient compliance. The higher individual side effects with $FeSO_4$ were not significantly different from those found with ULT. With a larger sample size, we may have detected significant differences; however, the sample size was based on NTBI as the primary outcome. Based on the most common side effects (nausea, diarrhea, and constipation) that were reported in a meta-analysis (5), the combined effects of those 3 gradually increased from week 1 to week 3 for $FeSO_4$ and were significantly different at week 3 compared with ULT and placebo. The increase with time in the reported number of side effects with $FeSO_4$ suggests the body's inability to tolerate its long-term use. On the contrary, side effects with ULT decreased with time. The natural encapsulation of the iron within the fungal matrix may have resulted in slower digestion, potentially reducing the liberation of free reactive iron in the gut. We expect less reactive unbound iron in the distal colon for bacterial growth, creating less oxidative stress, inflammation, and gastrointestinal-related side effects with ULT iron. The inability of the body to tolerate $FeSO_4$ compared with ULT may have accounted for the severe abdominal discomfort and lower compliance with $FeSO_4$ supplementation. Although there was no carryover effect from one iron supplementation to the other, the high frequency of side effects reported in week 1 for the placebo group is in agreement with previous studies (17) and may indicate inflammatory insult to the gut for continued short periods of time after switching to placebo. In a meta-analysis examining the incidence of gastrointestinal symptoms with $FeSO_4$ in 20 trials, the authors reported significant side effects when compared with placebo; however, most of these placebo-controlled trials were not truly double-blind (5). In Pereira et al.'s (17) double-blind 1-wk intervention study (not crossover), higher side effects were reported in the

group supplemented with $FeSO_4$ than in the group on placebo. In their study, symptoms still existed during the washout period after $FeSO_4$ supplementation, suggesting a 7-d washout period is not long enough. The strength in our study was that our treatments were double-blind, with a crossover study of 21 d supplementation and a 21-d washout period between treatments. The limitation of our study was that we were not able to identify significant differences in gastrointestinal side effects between treatment groups. This limitation may have been due to an inadequate sample size, the duration of supplementation, or the duration of the washout period resulting in potential residual side effects. Because our primary objective was to determine the implications of these 2 supplements for NTBI production, we did not account for the power needed for gastrointestinal side effect outcomes. Lastly, although we did see the acute effects of iron supplementation on NTBI production, this was not supported by our inflammatory and oxidative stress measurements. Longer supplementation periods are warranted to potentially see a response in healthy subjects. Kidney and liver function markers were similarly affected by ULT and $FeSO_4$, suggesting the safety of ULT consumption.

In conclusion, significantly lower production of NTBI and slightly fewer gastrointestinal side effects (although nonsignificant) were found with ULT consumption than with $FeSO_4$. ULT iron is safe to consume because oxidative stress, inflammatory, and kidney and liver function markers were not elevated. Therefore, ULT may be a safer alternative to oral $FeSO_4$ in maintaining healthy kidney and liver function, as well as iron status in young women. The results we have to date indicate that ULT has a slow release mechanism, but further studies are needed to identify the form of iron and the mechanism of ULT absorption in humans.

Acknowledgements

We thank Jeanne Stewart for scheduling and organizing the nurses and phlebotomists at the Nutrition and Wellness Research Center and blinding the supplemental treatments. In addition, we thank Olivia Meier, Casey Johnson, and Nicole Hanson for helping during the study. The authors' responsibilities were as follows—AEB and MBR: designed the study; AEB: conducted the study, analyzed the data, and prepared the manuscript; MBR: supervised the study and the final content of the manuscript overall; CW: provided the statistical expertise in data analysis; IA: assisted in performing statistical analyses on the qualitative data and was responsible for editing the manuscript; BW: optimized the method and performed the NTBI analysis; and all authors: read and approved the final manuscript.

References

1. WHO. Micronutrient deficiencies. *Geneva: WHO*; 2015.

2. Murray-Kolb LE, Beard JL. Iron treatment normalizes cognitive functioning in young women. *Am J Clin Nutr*. 2007;85:778–87.

3. Scott S, Chen-Edinboro L, Caulfield L, Murray-Kolb L. The impact of anemia on child mortality: an updated review. *Nutrients.* 2014;6:5915–32.

4. WHO. Fortification of condiments and seasonings with vitamins and minerals in public health: from proof of concept to scaling up. *Geneva: WHO*; 2014.

5. Tolkien Z, Stecher L, Mander AP, Pereira DIA, Powell JJ. Ferrous sulfate supplementation causes significant gastrointestinal side-effects in adults: a systematic review and meta-analysis. *PLoS One*. 2015;10:e0117383.

6. Hutchinson C, Al-Ashgar W, Liu DY, Hider RC, Powell JJ, Geissler CA. Oral ferrous sulphate leads to a marked increase in pro-oxidant nontransferrin-bound iron. *Eur J Clin Invest*. 2004;34:782–4.

7. Brissot P, Ropert M, Le Lan C, Loréal O. Non-transferrin bound iron: a key role in iron overload and iron toxicity. *Biochim Biophys Acta*. 2012;1820:403–10.

8. Cazzola M, Huebers HA, Sayers MH, MacPhail AP, Eng M, Finch CA. Transferrin saturation, plasma iron turnover, and transferrin uptake in normal humans. *Blood.* 1985;66:935–9.

9. Sazawal S, Black RE, Ramsan M, Chwaya HM, Stoltzfus RJ, Dutta A, Dhingra U, Kabole I, Deb S, Othman MK et al. .. Effects of routine prophylactic supplementation with iron and folic acid on admission to hospital and mortality in preschool children in a high malaria transmission setting: community-based, randomised, placebo-controlled trial. *Lancet.* 2006;367:133–43.

10. Parkkinen J, von Bonsdorff L, Peltonen S, Grönhagen Riska C, Rosenlöf K. Catalytically active iron and bacterial growth in serum of haemodialysis patients after i.v. iron–saccharate administration. *Nephrol Dial Transplant*. 2000;15:1827–34.

11. Shin C, Baik I. Transferrin saturation concentrations associated with telomeric ageing: a population-based study. *Br J Nutr*. 2017;117:1693–701.

12. Reddy MB, Armah SM, Stewart JW, O'Brien KO. Iron absorption from iron-enriched *Aspergillusoryzae* is similar to ferrous sulfate in healthy female subjects. *Curr Dev Nutr.* 2018;2(3):nzy004.

13. Bian Y, Wicking JB, inventors; Cura Global Health (bvi) Ltd, assignee. Nutritional supplement containing iron. *Australia Patent*; AU2013315341B2 2013.

14. Colombo G, Clerici M, Garavaglia ME, Giustarini D, Rossi R, Milzani A, Dalle-Donne I. A step-by-step protocol for assaying protein carbonylation in biological samples. *J Chromatogr B*. 2016;1019:178–90.

15. Jakeman A, Thompson T, McHattie J, Lehotay DC. Sensitive method for nontransferrin-bound iron quantification by graphite furnace atomic absorption spectrometry. *Clin Biochem.* 2001;34:43–7.

16. Singh S, Hider RC, Porter JB. A direct method for quantification of non-transferrin-bound iron. *Anal Biochem.* 1990;186:320–3.

17. Pereira DI, Couto Irving SS, Lomer MC, Powell JJ. A rapid, simple questionnaire to assess gastrointestinal symptoms after oral ferrous sulphate supplementation. *BMC Gastroenterol*. 2014;4:103.

18. Schulz KF, Altman DG, Moher D, CONSORT Group. CONSORT 2010 statement: updated guidelines for reporting parallel group randomised trials. *BMJ.* 2010;340:c332.

19. Killilea DW, Jiang Q, Hudes M, Madden J, Porter J, Evans P, Vichinsky E, Harmatz P. Oxidative stress and inflammation in iron-overloaded patients with β-thalassaemia or sickle cell disease. *Br J Haematol.* 2006;135:254–63.

20. Prentice AM, Mendoza YA, Pereira D, Cerami C, Wegmuller R, Constable A, Spieldenner J. Dietary strategies for improving iron status: balancing safety and efficacy. *Nutr Rev.* 2017;75:49–60.

21. Cook JD, Reddy MB. Efficacy of weekly compared with daily iron supplementation. *Am J Clin Nutr.* 1995;62:117–20.

22. Brittenham GM, Andersson M, Egli I, Foman JT, Zeder C, Westerman ME, Hurrell RF. Circulating non-transferrin-bound iron after oral administration of supplemental and fortification doses of iron to healthy women: a randomized study. *Am J Clin Nutr*. 2014;100:813–20.

23. Schümann K, Solomons NW, Romero-Abal M-E, Orozco M, Weiss G, Marx J. Oral administration of ferrous sulfate, but not of iron polymaltose or sodium iron ethylenediaminetetraacetic acid (NaFeEDTA), results in a substantial increase of non-transferrin-bound iron in healthy iron-adequate men. *Food Nutr Bull*. 2012;33:128–36.

24. Moretti D, Goede JS, Zeder C, Jiskra M, Chatzinakou V, Tjalsma H, Melse-Boonstra A, Brittenham G, Swinkels DW, Zimmermann MB. Oral iron supplements increase hepcidin and decrease iron absorption from daily or twice-daily doses in iron-depleted young women. *Blood.* 2015;126:1981–9.

25. Callender ST, Mallett BJ, Smith MD. Absorption of haemoglobin iron. *Br J Haematol.* 1957;3:186–92.

26. Pizarro F, Olivares M, Hertrampf E, Mazariegos DI, Arredondo M. Research communication: heme-iron absorption is saturable by heme-iron dose in women. *J Nutr.* 2003;133:2214–17.

27. Conway RE, Geissler CA, Hider RC, Thompson RPH, Powell JJ. Serum iron curves can be used to estimate dietary iron bioavailability in humans. *J Nutr.* 2006;136:1910–14.

28. Ginanjar E, Indrawati L, Setianingsih I, Atmakusumah D, Harahap A, Timan I, Marx J. Iron absorption in iron-deficient women, who received 65 mg Fe with an Indonesian breakfast, is much better from NaFe(III)EDTA than from Fe(II)SO_4, with an acceptable increase of plasma NTBI. A randomized clinical trial. *Pharmaceuticals.* 2018;11:85.

29. WHO. Daily iron supplementation in children 24–59 months of age in malaria-endemic areas. *Geneva: WHO*; 2017.

30. Reddy MB, Armah SM. Impact of iron-enriched Aspergillus oryzae on iron bioavailability, safety, and gut microbiota in rats. *J Agric Food Chem*. 2018;66:6213–8.

Table and Figures

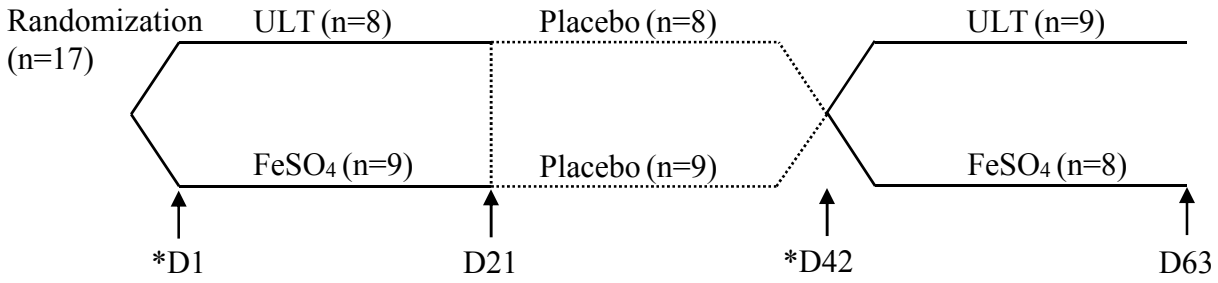

Figure C-1. Study design for the double blind cross-over study with young female subjects (n=16). *8h NTBI and serum iron curve analyses; arrows indicate biochemical parameters testing.

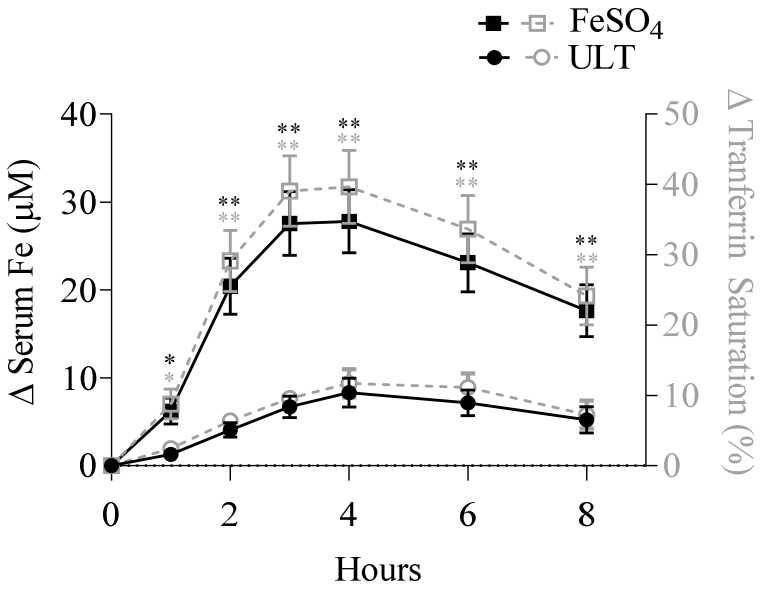

Figure C-2. Mean ± SEM (n=15) change in serum iron (solid lines) and % transferrin saturation (dotted lines) from baseline over 8 h after administration of 65 mg $FeSO_4$ or ULT with a semi-purified meal. One subject was removed due to blood draw complications. Differences between treatments at each time point was analyzed with two-way repeated-measures of ANOVA. *P < 0.01, **P < 0.0001.

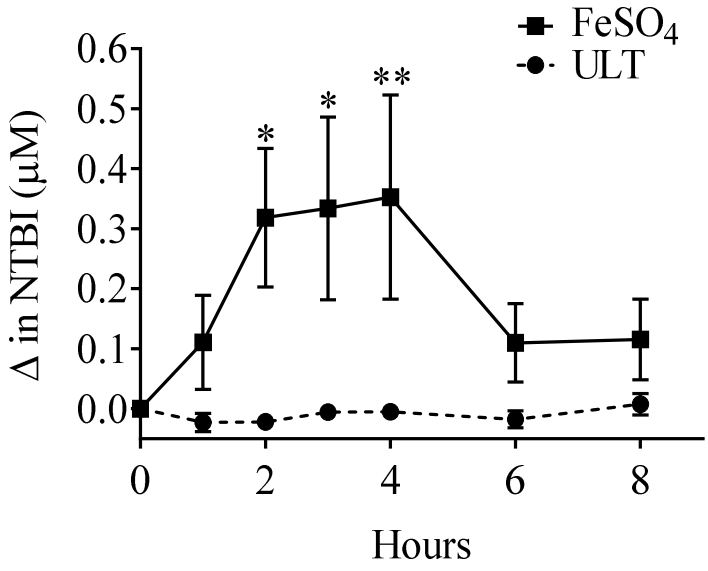

Figure C-3. Mean ± SEM (n=15) change in non-transferrin bound iron (NTBI) from baseline over 8 h after administration of 65 mg $FeSO_4$ or ULT with a semi-purified meal. One subject was removed due to blood draw complications. Differences between treatments at each time point was analyzed with two-way repeated-measures of ANOVA. *$P < 0.01$, **$P < 0.0001$.

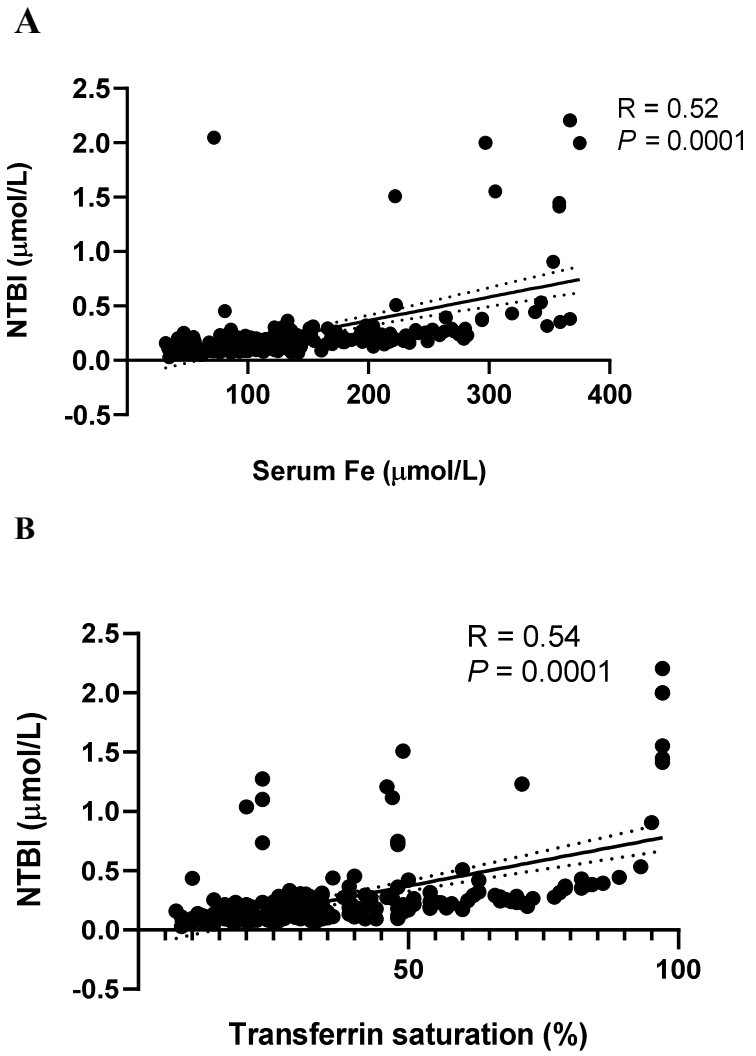

Supplemental Figure C-S1. Correlation between SI and NTBI (Fig A) and TS and NTBI (Fig B). Values represent 194 pairs combining ULT and $FeSO_4$.

Table C-1. Age, body mass index and biochemical indicators of subjects at baseline (n=16)*

Age, y	20.6 ± 1.4
Anthropometric measures	
BMI, kg/m^2	22.9 ± 2.8
Laboratory measures	
Hemoglobin, g/dL	13.3 ± 0.8
Hematocrit, %	39.2 ± 2.3
Serum ferritin[1], µg/L	19.3 [15.1, 24.7]
Serum iron, µg/dL	90.5 ± 35.7
Transferrin saturation, %	23.8 ± 8.9
Soluble transferrin receptor[1], ng/mL	4.6 [3.9, 5.4]
Hepcidin[1], ng/mL	4.4 [3.3, 5.8]
C-reactive protein[1], mg/L	1.0 [0.4, 2.3]
Glomerular filtration rate, mL/min/1.73m^2	100.9 ± 13.0
Creatinine, mg/dL	0.8 ± 0.1
Blood urea nitrogen, mg/dL	11.1 ± 3.1
Aspartate aminotransferase, U/L	16.4 ± 3.5
Alanine aminotransferase, U/L	13.2 ± 5.4

* mean ± SD or [1] geometric mean [95% Cls]

Table C-2. Change from baseline to 3 weeks with supplementation of ULT, $FeSO_4$ and placebo (n=16)*

Biochemical Indicators	ULT	$FeSO_4$	Placebo
Iron Status			
Hemoglobin, *g/dL*	0.07 ± 0.12	-0.04 ± 0.13	0.06 ± 0.16
Hematocrit, *%*	-0.07 ± 0.31	-0.59 ± 0.44	0.12 ± 0.40
Serum ferritin, *µg/L*	2.03 ± 3.44	9.38 ± 4.91	-2.61 ± 4.0
Soluble transferrin receptor, *ng/mL*	-0.02 ± 0.22	-0.13 ± 0.21	0.04 ± 0.18
Serum iron, *µg/dL*	12.7 ± 11.6	-5.69 ± 10.5	-5.63 ± 12.5
Transferrin saturation, *%*	4.63 ± 3.39	0.63 ± 2.72	-3.44 ± 3.61
Total iron binding capacity, *µg/dL*	-6.06 ± 4.71^{A}	-36.19 ± 9.08^{B}	20.19 ± 8.49^{C}
Inflammatory Markers			
C-reactive protein, *mg/L*	-0.41 ± 0.37	-0.27 ± 0.85	-0.27 ± 0.52
Hepcidin, *ng/mL*	0.53 ± 1.0	-1.47 ± 1.25	-0.09 ± 0.65
Oxidative stress			
TBARS, µM	0.73 ± 0.97	1.94 ± 0.95	0.90 ± 0.90
Protein carbonyls, *nmol/mL*	-0.24 ± 2.0	2.23 ± 3.06	-6.13 ± 3.91
Kidney and Liver Function			
Glomerular filtration rate, *mL/min/1.73m²*	6.0 ± 2.46^{A}	-0.81 ± 3.42^{AB}	-1.63 ± 2.29^{B}
Creatinine, *mg/dL*	-0.04 ± 0.02	0.01 ± 0.02	-0.69 ± 0.69
Blood urea nitrogen, *mg/dL*	0.63 ± 0.94	-0.43 ± 0.76	0.57 ± 1.47
Aspartate aminotransferase, *U/L*	-0.94 ± 0.85	0.06 ± 1.15	-2.19 ± 1.07
Alanine aminotransferase, *U/L*	0.31 ± 0.63^{A}	0.06 ± 0.93^{AB}	3.44 ± 1.02^{B}

*Mean ± SEM of change from baseline to final for each treatment period. Different letters indicate statistical significance at alpha=0.05 using a One-way ANOVA with Tukey multiple comparison test. TBARS, thiobarbituric acid reactive substances.

Table C-3. Frequency of reported gastrointestinal side effects during the 3 week supplementation of ULT, $FeSO_4$ and placebo* (n=16)

Symptom	ULT	$FeSO_4$	Placebo
Constipation	1.13 ± 0.42^a	1.56 ± 0.50^a	1.06 ± 0.37^a
Diarrhea	0.63 ± 0.22^a	1.00 ± 0.33^a	0.5 ± 0.24^a
Nausea	0.38 ± 0.18^a	0.75 ± 0.30^a	0.44 ± 0.16^a
Abdominal Discomfort	2.5 ± 0.5^a	2.81 ± 0.56^a	2.75 ± 0.78^a
Heartburn	0.13 ± 0.09^a	0.13 ± 0.09^a	0 ± 0^a
Fatigue	1.9 ± 0.55^a	1.81 ± 0.54^a	2.00 ± 0.47^a

*Mean ± SEM of frequency of reported gastrointestinal side effects over the 3-week supplementation period for each treatment period. Sharing same letters indicate no statistical significance at P=0.05 using a generalized linear mixed model of effects.

IRB Approval Memo

IOWA STATE UNIVERSITY
OF SCIENCE AND TECHNOLOGY

Institutional Review Board
Office for Responsible Research
Vice President for Research
2420 Lincoln Way, Suite 202
Ames, Iowa 50014
515 294-4566

Date: 1/16/2018

To: Dr. Manju Reddy
220 MacKay Hall

From: Office for Responsible Research

Title: Assessment of patient-reported gastrointestinal symptoms and compliancy after oral ferrous sulfate and iron-enriched Aspergillus oryzae supplementation; a randomized, double-blinded, cross-over study

IRB ID: 17-365

Approval Date:	1/16/2018	**Date for Continuing Review:**	7/31/2018
Submission Type:	Modification	**Review Type:**	Full Committee

The project referenced above has received approval from the Institutional Review Board (IRB) at Iowa State University according to the dates shown above. Please refer to the IRB ID number shown above in all correspondence regarding this study.

To ensure compliance with federal regulations (45 CFR 46 & 21 CFR 56), please be sure to:

- **Use only the approved study materials** in your research, **including the recruitment materials and informed consent documents that have the IRB approval stamp.**
- **Retain signed informed consent documents for 3 years after the close of the study,** when documented consent is required.
- **Obtain IRB approval prior to implementing any changes** to the study by submitting a Modification Form for Non-Exempt Research or Amendment for Personnel Changes form, as necessary.
- **Immediately inform the IRB of** (1) **all serious and/or unexpected adverse experiences** involving risks to subjects or others; and (2) **any other unanticipated problems involving risks** to subjects or others.
- **Stop all research activity if IRB approval lapses,** unless continuation is necessary to prevent harm to research participants. Research activity can resume once IRB approval is reestablished.
- **Complete a new continuing review form** at least three to four weeks prior to the **date for continuing review** as noted above to provide sufficient time for the IRB to review and approve continuation of the study. We will send a courtesy reminder as this date approaches.

Please be aware that IRB approval means that you have met the requirements of federal regulations and ISU policies governing human subjects research. **Approval from other entities may also be needed.** For example, access to data from private records (e.g. student, medical, or employment records, etc.) that are protected by FERPA, HIPAA, or other confidentiality policies requires permission from the holders of those records. Similarly, for research conducted in institutions other than ISU (e.g., schools, other colleges or universities, medical facilities, companies, etc.), investigators must obtain permission from the institution(s) as required by their policies. **IRB approval in no way implies or guarantees that permission from these other entities will be granted.**

Upon completion of the project, please submit a Project Closure Form to the Office for Responsible Research, 202 Kingland, to officially close the project.

Please don't hesitate to contact us if you have questions or concerns at 515-294-4566 or IRB@iastate.edu.

APPENDIX D. IRON SUPPLEMENTATION CONFERS PROTECTION AGAINST DISEASE SEVERITY IN DEXTRAN SODIUM SULFATE (DSS)-INDUCED COLITIS IN RATS

A manuscript prepared for submission to *Current Developments in Nutrition*

Amanda E. Bries, Rachel J. Derscheid, Paige Curry, Joseph L. Webb, Olivia N. Meier, Casey Johnson, Taylor Ferrere, Matthew J. Rowling, and Manju B. Reddy

Abstract

Background: Koji iron, enriched with ferrous sulfate ($FeSO_4$), otherwise known as Ultimine® (ULT), is a novel source of supplemental iron. Previously, we reported ULT had similar absorption as $FeSO_4$, while resulting in less circulating non-transferrin bound iron in young women. Iron deficiency anemia is a common manifestation of inflammatory bowel disease (IBD) due to malabsorption of iron and gastrointestinal (GI) bleeding.

Objective: The objective of our study was to assess the efficacy of two forms of iron supplementation on improving impaired GI integrity and anemia caused by dextran sulfate sodium (DSS)-induced colitis.

Methods: Six wk old Sprague Dawley rats (n = 40) were randomly assigned to one of four treatment groups (n =10/group): 1) control with no DSS; 2) control + DSS only (NFe); 3) DSS + ULT; and 4) DSS + $FeSO_4$. Animals were maintained on the AIN-93G diets for 7 days. Colitis was induced by administering fresh 3.5% (w/v) DSS in water *ad libitum* throughout the study. Daily iron supplementation (6 mg Fe/kg body weight) was provided in a pulverized treat, and disease activity indices were measured (gross bleeding, stool consistency and weight loss). Histological scoring of colonic ulcerations, inflammation and grade were assessed. Basic iron status indicators and circulating inflammatory markers were determined via ELISA and multiplex bead assays, respectively.

Results: The severity score of IBD was significantly higher in the animals without iron supplementation than those treated with iron ($P < 0.0001$). Moreover, iron supplementation protected against diminished hemoglobin and hematocrit levels as a result of DSS treatment (P=0.001 and P=0.03, respectively); whereas, these parameters were not significantly (NS) different between ULT and $FeSO_4$. A trend for improvement of post-mortem disease scores for DSS-induced rats on ULT compared to $FeSO_4$ and NFe by 14% and 39%, respectively (NS). Among all groups, $FeSO_4$ had significantly elevated circulating interleukin-17A (P<0.05).

Conclusions: The results of this study highlight the beneficial effects iron supplementation has on the disease activity promoted by severe GI inflammation. Furthermore, this data suggests that $FeSO_4$, but not ULT, may lead to increased chronic inflammation.

Introduction

Inflammatory Bowel Disease (IBD) is an idiopathic condition that affects upwards of 1.3 million people in the United States (1). IBD is sub-classified into either Crohn's disease or ulcerative colitis, whereby the hallmark of both conditions is gastrointestinal inflammation – leading to nutrient malabsorption, gastrointestinal bleeding, and hematochezia (2). Because of these chronic occurrences, iron deficiency anemia (IDA) often manifests in patients with IBD (3). In healthy adults, approximately 1-2 mg of iron is lost daily from desquamation of mucosal epithelial tissue; however, in IBD patients a myriad of precursors, such as rapid epithelial turnover, blood loss, and inflammatory-mediated iron sequestration can lead to IDA (4).

therefore often need iron therapy in order to maintain adequate iron stores. Currently, the recommended first line of treatment for IDA is elemental iron at a dose of 200 mg/day in highly bioavailable forms like ferrous sulfate ($FeSO_4$) (5). It has been of concern with production of non-transferrin bound iron (NTBI) due to the rapid absorption of $FeSO_4$ (6). The deleterious

consequences of circulating NTBI leads to the generation of reactive oxygen species, potentiating systemic inflammation.

NTBI also has been implicated increasing bacterial-pathogenic infections in vulnerable populations (7). The perturbed microbiome in patients with IBD is not only a result from the clinical aberrations, but oral iron supplementation can induce microbial dysbiosis (8). Approximately 90% of unabsorbed oral iron salts end up in the colon, creating an environment that favors the growth of iron-dependent pathogenic bacteria (9–11). For instance, studies have reported growth of pathogenic *Enterobacteriacae* and increased virulence following oral iron supplementation in patients with IBD (11). Not only does iron shift the microbial population, but compounds like $FeSO_4$ have been shown to exacerbate intestinal ulcerations and gastrointestinal inflammation, raising concerns of $FeSO_4$ use (8,10).

Koji iron, Ultimine® (ULT), is a natural compound that is enriched with approximately 8% iron. Koji is capable of providing a relatively high amount of iron because of its ability to harbor it in the mycelium. The bioavailability and efficacy was tested in human subjects, whereby results indicated that ULT was as bioavailable as $FeSO_4$, in addition to a slower rate of absorption with ULT, and reduced protein carbonyl concentrations (12–14). Previously, we reported in young females that ULT produced almost untraceable amounts of NTBI in circulation compared to $FeSO_4$, despite an observed serum iron peak at 4 h post ingestion (13). In the same study, we reported no adverse effects or systemic inflammatory changes in patients that were administered ULT for 3 wk (13). With the collective results from cell culture, animal, and human studies testing the safety, efficacy, and bioavailability of the koji iron, the objective of our current study was to examine the effects of oral koji iron compared to $FeSO_4$ when treating the progression of disease in an acute model of IBD. Our goal was to determine whether the koji iron

could be a safe iron compound for long-term therapy in IBD patients without exacerbating common clinical symptoms.

Material and Methods

Chemicals and Reagents. Colitis grade dextran sulfate sodium (DSS) with a molecular weight of 36-50 kDa was purchased from MP Biologics (Santa Ana, CA), hemoglobin was assessed by the HemoCue HB 201 device (Brea, CA), hemoccult assay kit was from Beckman Coulter, Inc. (San Diego, CA), qRT-PCR SYBR green was purchased from Zymo Research (Irvine, CA), and custom designed hepcidin mRNA and 18S ribosomal primers were obtained from Integrated DNA technologies (Davenport, IA). ULT was kindly donated from Cura Global Health, Inc. and $FeSO_4$ by Paul Lohman Company, Germany.

Animals and Diets. This animal study was approved by the Institutional Animal Care and Use Committee at Iowa State University and performed according to the Iowa State University Laboratory Animal Resources Guidelines. Forty, 6 wk old male Sprague Dawley rats (140-160 g) from Charles River Laboratories (Wilmington, MA) were obtained. Rats were individually housed in *innovive* cages (San Diego, CA) at 22°C ± 2°C temperature-controlled environment and a 12 h light-dark cycle. Following acclimation for 72 h on a standard rat chow diet. Rats were placed on a semi-purified AIN-93G diet containing 65 ppm iron, 39.75% corn sugar; 20% vitamin-free casein lactic; 10% granulated sugar; 13.20% dextran; 3.5% mineral mix (AIN-93); 1% vitamin mix (AIN-93); 0.30% L-Cysteine; and 0.25% choline bitartrate from Envigo Laboratories (Madison, WI TD.97184) throughout the experimental period.

Induction of colitis and iron supplementation. Rats (*n* =10) were randomly assigned to one of four treatment groups: 1) no DSS, no Fe (control); 2) DSS, no Fe (NFe); 3) DSS + ULT; and 4) DSS + $FeSO_4$. Colitis was induced by giving rats fresh 3.5% (w/v) of DSS consumed food *ad libitum*, daily, throughout the study for the respective treatment groups. Iron supplementation was provided in a vehicle of pulverized rat treats containing alfalfa sprouts, apple, corn oil, peas, parsley and wheat (Sunseed Animal Lovens Bowling Green, OH) with no vitamin C contribution. Treats were weighed in 3 g portions and pelleted with 30 mg agar-agar. Each iron treat was supplemented with 6 mg Fe/kg BW/d based on the average baseline weight of all DSS treatment groups (140 grams), equating to 0.84 mg Fe/day. ULT dry weight contained 8.7% iron, whereas $FeSO_4$ contained 32% iron enrichment. The human equivalent dose of the iron administered to the rats was 58 mg Fe (for a 60 kg adult human) based on a 6.2 conversion rate using the estimate of a 0.15 kg rat (15). Individual iron treatments were incorporated and administered daily via the same vehicle treat, with groups 1 and 2 devoid of iron. Consumption of the iron supplemental treats were monitored and adjusted for final hemoglobin regeneration efficiency (HRE) ratios, as previously described (16–19).

Rats were maintained on the same AIN-93G diet for 7 days, along with daily DSS administration and iron supplementation for respective groups. On the morning of day 8 following a 10 h overnight fast with water provided *ad libitum*, rats were anesthetized with a ketamine:xylazine cocktail (90:10 mg/kg BW) via a single intraperitoneal injection. Liver and kidney tissues were procured and weighed; whole blood was collected via cardiac puncture. The intestine was removed, measured for length and photographed for total disease assessment. All tissues were sectioned and either fixed in 4% paraformaldehyde or snap frozen in liquid nitrogen and stored at -80°C.

Disease activity index. Disease activity index (DAI) is a proxy to assess the severity of inflammation and colitis conditions for in vivo models. Disease activity index was calculated by taking the cumulative score based on the magnitude of percent daily weight loss, stool consistency, and gross bleeding of the rats as previously described (20,21). Daily water intake was measured and assessed between groups administered DSS to determine if disease severity was attributed to DSS consumption. Total post-mortem disease scores were summed after binary-assessment of the presence of: cecal atrophy, enlarged cecal tonsil, cecal emptying, absence of formed fecal pellets in colon, as well as watery/mucoid, luminal blood, and tissue thickening in both the colon and cecum. Assessment of these parameters were performed in a blinded fashion by a Veterinary Pathologist.

Histological scoring of the distal colon. Following fixation of the tissues in 4% paraformaldehyde for 24 h, liver, kidney and colon were paraffin embedded. Blocks were sectioned to 5 μm thick and stained with hematoxylin and eosin (H&E) for histological scoring and evaluation. The lesion and inflammation index were evaluated based on a modified method by Toblli et al (22). Briefly, the areas were scored based on the levels of damage, as well as, each of these was given an additional grade of the percentage of the area (in 25% increments) affected by the damage or inflammation as follows: 0=intact crypt, 1=1/3 loss, 2=2/3 loss, 3=loss of crypt, intact surface, 4=crypt loss+ulceration; 0=normal, 1=lamina propria, 2=inflammation+gland dropout, and 3=complete abscesses. A cumulative score was assessed by the percent affected of crypt damage **(Table D-1)**. Degree of lesion and inflammatory severity is described as: 1) crypt hypertrophy; 2) crypt abscesses; and 3) ulceration (**Figure D-1**). Lesion and inflammatory scores and their respective grades were summed, and compared as individual

indicators and total disease scores among groups. Distal colon thickness was also measured to determine level of proliferative epithelial tissue.

Iron status indicators. Nonheme-iron was assessed as previously described (23). Briefly, livers were homogenized in water and subjected to trichloroacetic acid (TCA) protein precipitation at 65°C for 20 h. Nonheme iron assay was determined colorimetrically using ferrozine in thioglycolic acid measuring the absorbance of soluble iron (ug/g) as percent solubility. Hematocrit was determined as a ratio of red blood cells to total blood volume following hematocrit centrifugation (24), and hemoglobin (Hb) was assessed at baseline and final endpoints of the study. To determine the efficiency of converting dietary Fe into Hb among all groups, the hemoglobin regeneration efficiency (HRE) ratio was calculated as described previously (16–18). Fecal hemoccult tests were performed to determine positive or negative presence of blood in the fecal content.

Cytokine and inflammatory markers. Serum inflammatory analytes, interleukin (IL)-1 alpha, IL-beta, IL-2, IL-6, IL-10, IL-17A, IL-18, and interferon-gamma were analyzed using a multiplex magnetic bead array from Millipore Sigma (Burlington, MA). Liver mRNA was isolated using the Autogen QuickGene RNA tissue kits II (Holliston, MA) and verified for a 260/280 ratio of 2.0 using the nanodrop followed by cDNA conversion using the high capacity cDNA reverse transcription kit from Applied Biosystems (Beverly, MA). Fecal S100A8/S100A9 calprotectin, a biomarker for inflammatory gastrointestinal disease, was analyzed using a commercially available kit.

Statistical methods. All statistical analyses were performed using SAS (version 9.4, 2018, SAS Institute Inc., Cary, NC). Evaluation of statistically significance ($P < 0.05$) between group means was performed using a one-way ANOVA. When LS means between each group were compared Tukey post hoc analyses were utilized; whereas, when treatments were compared to the no DSS control animals, a Dunnett post hoc analyses were used for LS mean comparisons. Temporal data were analyzed using repeated measures test.

Results

Iron supplementation delayed the progression of disease activity in DSS-induced rats. All DSS-induced animals expressed higher total post-mortem disease scores compared to healthy controls ($P < 0.001$; **Figure D-1A**). There were no observed significant differences among the DSS-induced rats with and without iron, verifying presence of IBD. Moreover, when comparing all DSS groups to the control rats, $FeSO_4$ protected against a significant reduction in body weight gain ($P < 0.05$); whereas the DSS + ULT and DSS, NFe groups gained significantly less weight ($P < 0.01$ and $P < 0.001$, respectively). As expected, all animals treated with DSS, resulted in significantly higher DAI scores compared to the animals without DSS ($P < 0.001$; **Figure D-2A**). When comparing DSS-induced animals, those on iron supplementation (ULT and $FeSO_4$) had reduced disease severity when compared to the rats on DSS alone ($P < 0.001$; Figure D-1A). Animals on the DSS consumed significantly less water compared to the no DSS group ($P < 0.001$, data not shown); however, there were no differences in water consumption among three DSS-induced groups (data not shown), indicating no effect of consumption on disease severity. Notably, when compared to the no DSS group, the iron supplemented animals displayed a significant reduction in intestinal length ($P < 0.05$); whereas the difference between control and alone was highly significant ($P < 0.001$; **Figure D-2B**).

Histological lesion scoring of distal colon. All DSS-induced animals had significantly higher crypt lesions, inflammation, and hypertrophy of their distal colons compared to the healthy controls ($P < 0.001$; **Table D-2**). There was a tendency for higher scores in all three parameters (crypt, inflammation, and total disease score) for the DSS, no Fe group, although not significant.

Iron status indicators. As expected, the DSS groups supplemented with both ULT and $FeSO_4$ protected against reduction in Hb from baseline when compared to no DSS healthy control, although it was borderline significant ($P = 0.07$ and $P = 0.06$, respectively). In contrast, NFe group resulted in significantly depleted Hb from baseline compared to no DSS control group ($P < 0.05$; **Figure D-3A).** Likewise, the same was observed for hematocrit among the three groups when compared to the healthy control ($P = 0.12$, ULT; $P = 0.15$, $FeSO_4$; $P < 0.05$, NFe; **Figure D-3B).** No significant differences were detected in total non-heme iron stores in the liver among all groups **(Figure D-3C)**.

Fecal disease indicators were significantly higher in the rats void of iron supplementation. Hemoccult is a test to determine the presence of hematochezia by a simple test strip. All rats treated with DSS exhibited higher incidence of hematochezia compared to the control rats ($P<0.05$). Although not significantly different from one another, the percentage of rats testing positive in the DSS, $FeSO_4$ group was 100%, 90% in the DSS, NFe group, and 80% in the DSS, ULT group. Calprotectin, a clinical test used to distinguish the difference between inflammatory-related bowel disease, and non-inflammatory related, was 46% higher in DSS alone compared to DSS, ULT ($P<0.0001$) and 32% higher than DSS, $FeSO_4$ ($P<0.001$; **Figure D-4**). Traceable

calprotectin concentrations were detected in the control rats, but were lower compared to DSS-treated rats (P<0.0001).

Interleukin-17A and interleukin-1 alpha were elevated DSS-induced rats supplemented with $FeSO_4$. After multiplexing 8 different cytokines/chemokines, the only two that were statistically significant among groups were IL-1α and IL-17A. Interestingly, IL-1α was only detectable in the DSS treated rats on iron supplementation **(Table D-3).** DSS, ULT rats did not have significantly higher IL-1α compared to the DSS and no DSS control rats; however, DSS, $FeSO_4$ rats exhibited higher circulating IL-1α concentrations compared to the no DSS and DSS, NFe control rats (P<0.001), but was not statistically different from DSS, ULT rats (Table D-3). Lastly, there were no significant differences among the control, DSS, NFe; and DSS, ULT groups for concentrations of IL-17A. The DSS-induced rats supplemented with $FeSO_4$ did exhibited elevated circulating IL-17A concentrations when compared among all groups (P<0.05; Table 3).

Discussion

Anemia of chronic disease or inflammation, is one of the most common anemia's that exits among the elderly and chronically ill in the United States (25). Chronic diseases that are compounded by inflammation, such as obesity, kidney disease, and cancer often result in iron deficiency due to the elevation in circulating hepcidin (26,27). The increase in hepcidin production is directly proportional to inflammation and since its hormonal mode of action is to block the efflux of iron into circulation, chronic elevation in hepcidin concentrations can manifest in anemia. Therefore, one of the most prevalent complications of IBD is anemia, which can vastly affect the rate of remission and long-term progress of patients with this disorder. The impact of IBD can be much more severe due to the multifactorial insults of iron malabsorption,

increased intestinal desquamation, and elevated hepcidin, which in turn, blocks iron mobilization. All of these warrant to identify a safe and effective iron supplement that is effective in treating anemia, but does not exacerbate these conditions and allows for increased patient compliance during long-term iron regimens.

Previously, we have reported in a stable iron isotope clinical study that ULT is as bioavailable as $FeSO_4$ (28), as well as resulted in no significant gastrointestinal related side effects and nearly untraceable amounts of serum NTBI (13). Furthermore, we reported no effect on serum C-reactive protein and hepcidin levels following 3 wk of ULT consumption. These studies demonstrated the safety and efficacy of this oral koji iron supplement for potential use in chronic diseases, such as IBD. In this study, we administered the koji iron supplement to an acute chemical-induced rodent model of IBD. Dextran sulfate sodium is one of the most commonly used chemicals for recapitulating the clinical aberrations observed in human IBD (29). Because of the localized impact of DSS on the colon, it more closely mimics conditions of ulcerative colitis. This is an important distinction, as iron is predominantly absorbed in the duodenum and proximal jejunum (30). Although the intestinal lining is compromised in the colon as a result of DSS, upstream inflammation may advance due to colonic atrophy and an increase in inflammatory signaling cascades.

Numerous studies have examined the effects of oral iron compounds, dosage, and duration in a chemical-induced rodent model of IBD (8,10,31,32). The effectiveness of improving iron stores in an IBD animal model with ferrous-fumarate, that has high bioavailability was promising, however the animals exhibited exacerbated gastrointestinal inflammation and diminished colonic integrity (10). It did not, however have an effect on circulating glutathione activity or subsequent inflammatory markers. More recently, a study

examining the effects of $FeSO_4$ and iron polymaltose complex in a DSS model of IBD reported elevated inflammatory markers, disease activity, severity and further histological damage as a result of $FeSO_4$ (22). On the contrary, we did not observe increased disease activity in our DSS model supplemented with $FeSO_4$ and ULT; rather, we concluded a protective element of both iron supplements on the disease severity. Several observations can be identified by our contradicting results. Firstly, we administered a ~60 mg human dose equivalent of iron – which is a standard iron dose for those with iron deficiency; whereas the published study (22) employed a 300 mg human dose equivalent. Furthermore, studies have relied on iron delivery via gavage or *ad libitum* food intake. In our study we gave a standard iron dosage via supplementation, as we were limited by gavage due to the insoluble nature of our koji iron compound. These variations may have influenced the vast differences observed in gastrointestinal related side effects between these studies.

The DSS model has been studied in a number of applications. Wirtz and colleagues reported that the upper lethal dose of DSS is 5%, whereby rodents experience a marked reduction in weight, blood volume and goblet cells (33). Furthermore, high death rates in chemical induced IBD models are often a result of severe colon perforation and bacterial infections. Despite these observations, we reported protective characteristics as a result of both $FeSO_4$ and ULT iron supplements on disease activity and post-mortem disease severity. Given the short duration of our combined method of DSS and iron supplementation, we were not surprised by the diminished disease outcomes. Hypoferremia is a common symptom of this IBD model (34), and in this study, it was observed that iron supplements prevented the depletion of both hemoglobin and hematocrit when compared against the healthy control rats. We hypothesized that the disease activity protection conferred by the iron supplementation may in part, be due to the support of

hemoglobin production. A study examining the role of heme-injected IBD mice reported that systemic heme supplementation greatly remedied DSS-induced colitis in mice (35). They proposed that the mechanism mediating this attenuation was the ability for heme repletion therapy to maintain gut and epithelial regeneration via heme oxygenase-1, which plays a major role in IBD-related intestinal inflammation (36). Although inflammation and bacterial infections are of large concern with highly bioavailable iron compounds, perhaps the mitigation in lack of iron stores and anemia outweighed the previously reported deleterious effects of iron on gastrointestinal integrity.

Despite a significant decrease in disease activity, gross disease scores, and mitigation of iron depletion, there was a significant rise in cytokines, IL-17A and IL-1α as a result of $FeSO_4$ supplementation. IL-17A is an important regulator in the promotion of intestinal fibrosis, by its role in stimulating upstream inflammatory cascades (37). Therefore, a rise in IL-17A in circulation may indicate increased tissue fibrosis, although it is inconclusive whether the observed elevated IL-17A in IBD rats supplemented with $FeSO_4$ was directly related to colonic fibrosis. There have been several studies reporting the pathophysiological role of IL-17A in IBD. For instance, Chae and colleagues reported the mitigation of epithelial fibrosis and bowel obstruction in an IL-17A global knockout mouse (38). Despite these reports, clinical studies employing anti-IL17A drugs have not demonstrated the clinical benefits in patients with Crohn's disease (39). Interestingly, neutrophil gelatinase-associated lipocalin (NGAL) is an innate immune response protein that is directly stimulated by a rise in IL-17A, and its function is to scavange and sequester iron from bacterial phagocytosis (40). Therefore, NGAL has been identified to protect against bacteria growth by preventing iron acquisition, as evidenced by a NGAL knockout mouse model which resulted in bacterial infections from iron uptake (41).

Because of the probable unabsorbed labile iron in the colon, we postulate that IL-17A in the DSS, $FeSO_4$ group may have induced the production of NGAL, preventing readily available iron for bacterial overgrowth in the colon and further exacerbation of histological damage and disease risk. In further exploratory studies, it would be important to examine the production of IL-17A and NGAL in the colonic tissue upon the administration of iron supplementation.

In our study, we primarily demonstrated that low doses of oral iron supplementation during the progression of a chemically-induced acute rodent model of IBD may have a protective measure against the disease severity, potentially attributed to hemoglobin regeneration and increased epithelial turnover. Ultimately, we concluded that more gentle forms of iron supplements, such as ULT might be more beneficial in reducing the prevalence of IBD-specific intestinal inflammation as evidenced by calprotectin concentrations and interleukin mediators. Furthermore, based on our previous work with ULT, there may be potential benefit from ULT supplementation in chronic ailments like IBD, due to its effectiveness in improving iron stores and lack of NTBI generation. These findings should be supported in a clinical study comparing the efficacy of low-dose iron supplementation in different forms to prevent and improve the severity of IBD.

Acknowledgements

We would like to acknowledge and thank Jennifer Groeltz-Thrush with the Iowa State University Veterinary Diagnostic Laboratory in assisting with preparing tissues, slides, and training with immunohistochemistry. Authors contributions are as follows - A.E.B drafted the original version of this manuscript. A.E.B performed all aspects of animal maintenance, intervention, and iron related laboratory experiments. R.J.D. performed all of the colonic excising, scoring, as well as histological grade assessment and scoring. A.E.B., R.J.D., P.C.,

J.L.W., O.M., C.J., and T.F. assisted in end-point procedures. A.E.B, M.J.R., and M.B.R. assisted in the study design. All authors read and approved the final version of the manuscript.

References

1. Dahlhamer JM, Zammitti EP, Ward BW, Wheaton AG, Croft JB. Prevalence of Inflammatory Bowel Disease Among Adults Aged ≥18 Years — United States, 2015. *MMWR Morb Mortal Wkly Rep*. 2016; 65:1166–9.

2. Colombel J-F, Mahadevan U. Inflammatory Bowel Disease 2017: Innovations and Changing Paradigms. *Gastroenterology*. 2017; 152:309–12.

3. Nielsen O, Soendergaard C, Vikner M, Weiss G, Nielsen OH, Soendergaard C, Vikner ME, Weiss G. Rational Management of Iron-Deficiency Anaemia in Inflammatory Bowel Disease. *Nutrients*. 2018; 10:82.

4. Stein J, Dignass AU. Management of iron deficiency anemia in inflammatory bowel disease - a practical approach. *Ann Gastroenterol*. 2013; 26:104–13.

5. Nielsen OH, Ainsworth M, Coskun M, Weiss G. Management of Iron-Deficiency Anemia in Inflammatory Bowel Disease. *Medicine*. 2015; 94:e963.

6. Lomer MCE, Cook WB, Jan-Mohamed HJB, Hutchinson C, Liu DY, Hider RC, Powell JJ. Iron requirements based upon iron absorption tests are poorly predicted by haematological indices in patients with inactive inflammatory bowel disease. *Br J Nutr*. 2012; 107:1806–11.

7. Parkkinen J, von Bonsdorff L, Peltonen S, Grönhagen□Riska C, Rosenlöf K. Catalytically active iron and bacterial growth in serum of haemodialysis patients after i.v. iron–saccharate administration. *Nephrol Dial Transplant*. 2000; 15:1827–34.

8. Constante M, Fragoso G, Lupien-Meilleur J, Calvé A, Santos MM. Iron Supplements Modulate Colon Microbiota Composition and Potentiate the Protective Effects of Probiotics in Dextran Sodium Sulfate-induced Colitis. *Inflamm Bowel Dis*. 2017; 5:753-66.

9. Motta JP, Allain T, Green-Harrison LE, Groves RA, Feener T, Ramay H, Beck PL, Lewis IA, Wallace JL, Buret AG. Iron sequestration in microbiota biofilms as a novel strategy for treating inflammatory bowel disease. *Inflamm Bowel Dis*. 2018; 24:1493–502.

10. Mahalhal A, Williams JM, Johnson S, Ellaby N, Duckworth CA, Burkitt MD, Liu X, Hold GL, Campbell BJ, Pritchard DM, et al. Oral iron exacerbates colitis and influences the intestinal microbiome. *PLoS One*. 2018; 13:e0202460.

11. Lee T, Clavel T, Smirnov K, Schmidt A, Lagkouvardos I, Walker A, Lucio M, Michalke B, Schmitt-Kopplin P, Fedorak R, et al. Oral versus intravenous iron replacement therapy distinctly alters the gut microbiota and metabolome in patients with IBD. *Gut*. 2016; 66:863–71.

12. Reddy MB, Armah SM. Impact of Iron-Enriched *Aspergillus oryzae* on Iron Bioavailability, Safety, and Gut Microbiota in Rats. *J Agric Food Chem*. 2018; 66:6213–8.

13. Bries AE, Wang C, Agbemafle I, Wels B, Reddy MB. Assessment of Acute Serum, Non-Transferrin Bound Iron and Gastrointestinal Symptoms with 3-Week Consumption with Iron-Enriched Aspergillus Oryzae Compared to Ferrous Sulfate. *Curr Dev Nutr*. 2019; 12:nzz127.

14. Bries AE, Hurrell RF, Reddy MB. Iron Absorption from Bouillon Fortified with Iron-Enriched Aspergillus oryzae Is Higher Than That Fortified with Ferric Pyrophosphate in Young Women. *J Nutr*. 2020; 150:1109–15.

15. Nair A, Jacob S. A simple practice guide for dose conversion between animals and human. *J Basic Clin Pharm*. 2016; .

16. Buchowski MS, Mahoney AW, Kalpalathika MPV. Nonheme iron absorption, apparent iron absorption and hemoglobin regeneration efficiency in anemic and normal rats fed with dietary heme and nonheme iron at various levels. *Nutr Res*. 1989; 773-83.

17. Park YW, Mahoney AW, Cornforth DP, Collinge SK, Hendricks DG. Bioavailability to Anemic Rats of Iron from Fresh, Cooked or Nitrosylated Hemoglobin and Myoglobin. *J Nutr*. 1983; 113:680–7.

18. Swain JH, Newman SM, Hunt JR. Bioavailability of elemental iron powders to rats is less than bakery-grade ferrous sulfate and predicted by iron solubility and particle surface area. *J Nutr*. 2003; 133:3546–52.

19. Swain JH, Newman SM, Hunt JR. Nutrient Requirements Bioavailability of Elemental Iron Powders to Rats Is Less than Bakery-Grade Ferrous Sulfate and Predicted by Iron Solubility and Particle Surface Area. 2003.

20. Appleyard CB, Wallace JL. Reactivation of hapten-induced colitis and its prevention by anti- inflammatory drugs. *Am J Physiol - Gastrointest Liver Physiol*. 1995; 269.

21. Koetzner L, Grover G, Boulet J, Jacoby HI. Plant-derived polysaccharide supplements inhibit dextran sulfate sodium-induced colitis in the rat. *Dig Dis Sci*. 2010; 55:1278–85.

22. Toblli JE, Cao G, Angerosa M. Ferrous sulfate, but not iron polymaltose complex, aggravates local and systemic inflammation and oxidative stress in dextran sodium sulfate-induced colitis in rats. *Drug Des Devel Ther*. 2015; 9:2585–97.

23. Swain JH, Tabatabai LB, Reddy MB. Nutrient Interactions and Toxicity Histidine Content of Low-Molecular-Weight Beef Proteins Influences Nonheme Iron Bioavailability in Caco-2 Cells 1,2. *J Nutr*. 2002; 132:245–51.

24. Billett H. Hemoglobin and Hematocrit. *Histor, Physic, Laborat Examin.* 1990.

25. Fraenkel PG. Anemia of Inflammation: A Review. *Medical Clinics of North America.* 2017; 285–96.

26. Wang CY, Babitt JL. Hepcidin regulation in the anemia of inflammation. *Curr Opin Hemat*. 2016. p. 189–97.

27. Begum S, Latunde-Dada GO. Anemia of inflammation with an emphasis on chronic kidney disease. *Nutrients*. 2019.

28. Reddy MB, Armah SM, Stewart JW, Brien KOO. Iron Absorption from Iron-Enriched Aspergillus oryzae Is Similar to Ferrous Sulfate in Healthy Female Subjects. *Curr Devel Nutr.* 2018; 1–8.

29. Dothel G, Vasina V, Barbara G, De Ponti F. Animal models of chemically induced intestinal inflammation: Predictivity and ethical issues. *Pharmacol Therap*. 2013.

30. Zimmermann MB, Hurrell RF. Nutritional iron deficiency. *Lancet.* 2007.

31. Chua ACG, Klopcic BRS, Ho DS, Fu SK, Forrest CH, Croft KD, Olynyk JK, Lawrance IC, Trinder D. Dietary iron enhances colonic inflammation and IL-6/IL-11-Stat3 signaling promoting colonic tumor development in Mice. *PLoS One*. 2013; 8.

32. Toblli JE, Cao G, Angerosa M. Ferrous sulfate, but not iron polymaltose complex, aggravates local and systemic inflammation and oxidative stress in dextran sodium sulfate-induced colitis in rats. *Drug Des Devel Ther*. 2015; .

33. Wirtz S, Neufert C, Weigmann B, Neurath MF. Chemically induced mouse models of intestinal inflammation. *Nat Protoc*. 2007; 2:541–6.

34. Kaitha S, Bashir M, Ali T. Iron deficiency anemia in inflammatory bowel disease. *World J Gastrointest Pathophysiol*. 2015; 6:62.

35. Kayama H, Kohyama M, Okuzaki D, Motooka D, Barman S, Okumura R, Muneta M, Hoshino K, Sasaki I, Ise W, et al. Heme ameliorates dextran sodium sulfate-induced colitis through providing intestinal macrophages with noninflammatory profiles. *Proc Natl Acad Sci U S A*. 2018; 115:8418–23.

36. Sebastián VP, Salazar GA, Coronado-Arrázola I, Schultz BM, Vallejos OP, Berkowitz L, Álvarez-Lobos MM, Riedel CA, Kalergis AM, Bueno SM. Heme oxygenase-1 as a modulator of intestinal inflammation development and progression. *Frontier Immunol.* 2018.

37. Creyns B, Cremer J, Hoshino T, Geboes K, de Hertogh G, Ferrante M, Vermeire S, Ceuppens JL, Van Assche G, Breynaert C. Fibrogenesis in Chronic DSS Colitis is Not Influenced by Neutralisation of Regulatory T Cells, of Major T Helper Cytokines or Absence of IL-13. *Sci Rep*. 2019; 9:1–14.

38. Chae WJ, Gibson TF, Zelterman D, Hao L, Henegariu O, Bothwell ALM. Ablation of IL-17A abrogates progression of spontaneous intestinal tumorigenesis. *Proc Natl Acad Sci U S A*. 2010; 107:5540–4.

39. Hueber W, Sands BE, Lewitzky S, Vandemeulebroecke M, Reinisch W, Higgins PDR, Wehkamp J, Feagan BG, Yao MD, Karczewski M, et al. Secukinumab, a human anti-IL-17A monoclonal antibody, for moderate to severe Crohn's disease: Unexpected results of a randomised, double-blindplacebo- controlled trial. *Gut*. 2012; 61:1693–700.

40. Ferreira MC, Whibley N, Mamo AJ, Siebenlist U, Chan YR, Gaffen SL. Interleukin-17-induced protein lipocalin 2 is dispensable for immunity to oral candidiasis. *Infect Immun*. 2014; 82:1030–5.

41. Flo TH, Smith KD, Sato S, Rodriguez DJ, Holmes MA, Strong RK, Akira S, Aderem A. Lipocalin 2 mediates an innate immune response to bacterial infection by sequestrating iron. *Nature*. 2004; 432:917–21.

Tables and Figures

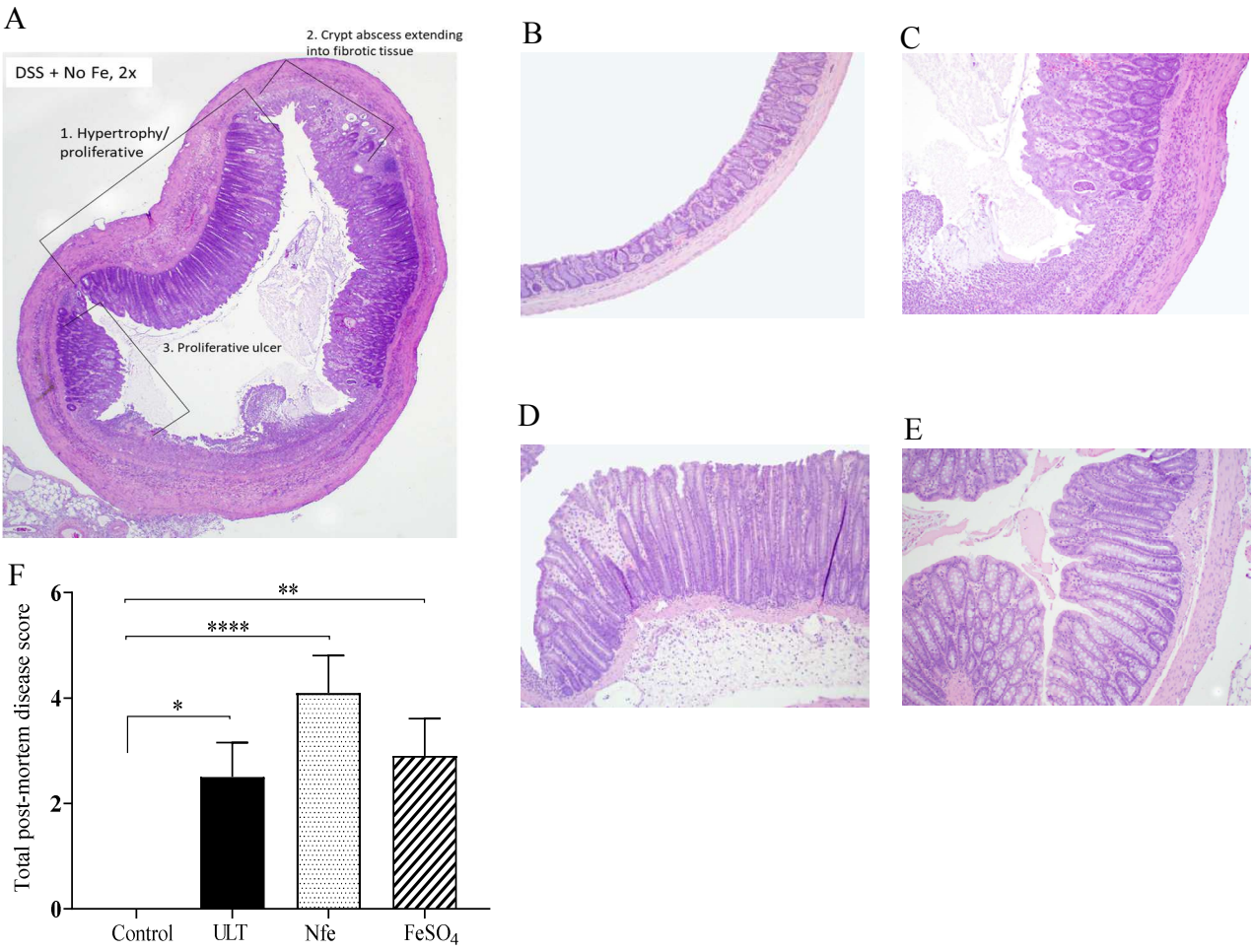

Figure D-1. Effects of 3.5% dextran sulfate sodium on colonic lesion score, inflammation and grade of affected area determined by histopathology of a colonic cross section from IBD-induced Sprague Dawley rats supplemented with and without iron. Hemotoxylin and eosin staining of colonic tissue sections were analyzed for histopathology parameters in Table 1. Image was representative of examples of grade and affected area in the control rats (A), in addition to the representative histology (H&E staining; magnification, 10X) of colonic-sample sections to demonstrate differences in proliferation in control (B), NFe (C), ULT (D), $FeSO_4$ (E). Post-mortem colon injury scores were determined (F). Data are presented as mean ± SEM, $n = 10$. Bars are expressed as *P <0.05, ** <0.01, *** <0.001. Abbreviations used: ULT, ultimine; FeSO4, ferrous sulfate; and NFe, no iron.

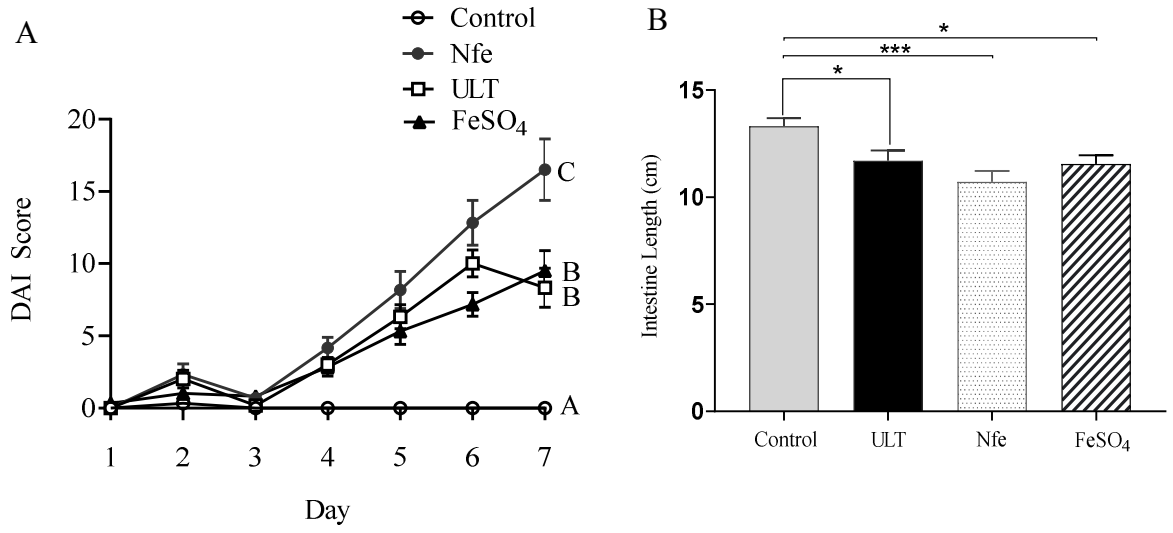

Figure D-2. DAI scores over one week (A) and post-mortem intestinal length (B) for control; NFe; ULT; and $FeSO_4$ using one-way ANOVA with Dunnett multiple comparisons. Data are means ± SEMs; $n = 10$. Mean values without a common letter, are significantly different ($P < 0.05$); whereas bars are expressed as *$P < 0.05$, ** < 0.01, *** < 0.001. Abbreviations used: ULT, ultimine; $FeSO_4$, ferrous sulfate; and NFe, no iron.

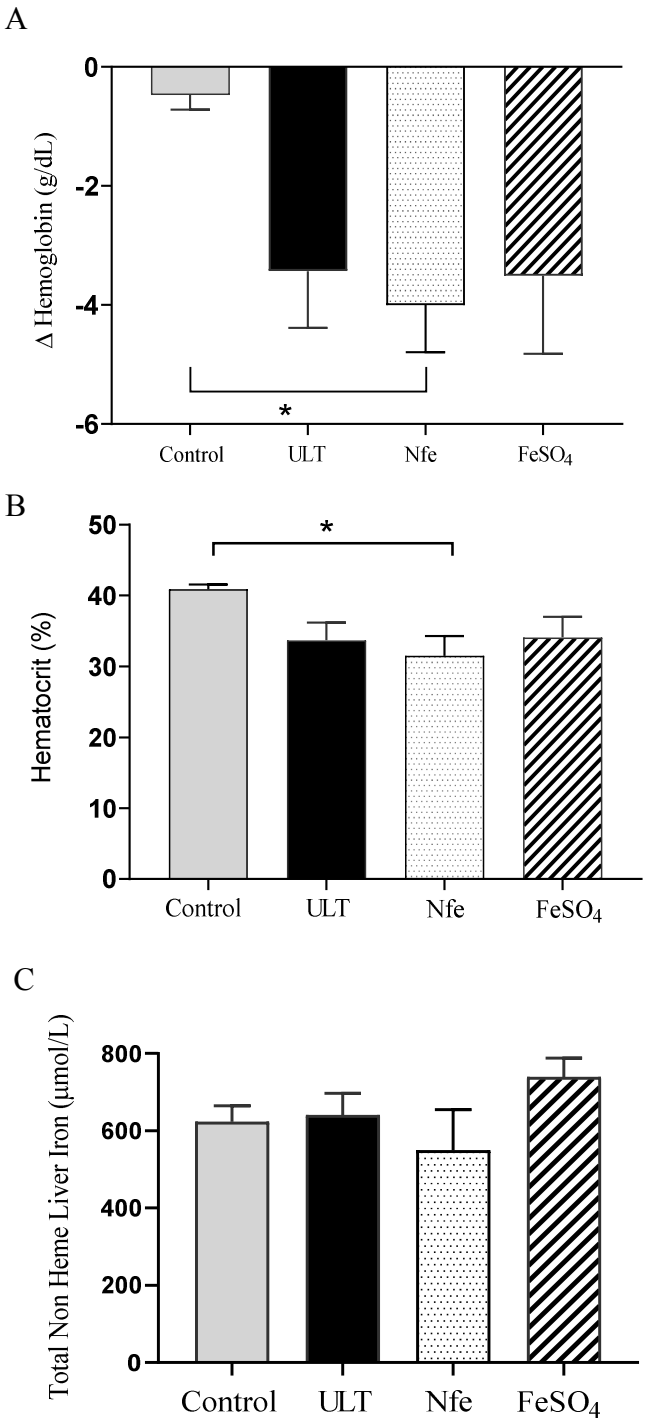

Figure D-3. Change in hemoglobin from baseline to end of life (A) final hematocrit (B) and total non-heme liver iron (C) for control; NFe; ULT; and $FeSO_4$ using one-way ANOVA with Dunnett multiple comparisons. Data are means ± SEMs; $n = 10$. Bars are expressed as $^*P < 0.05$, ** <0.01, *** <0.001. Abbreviations used: ULT, ultimine; $FeSO_4$, ferrous sulfate; and NFe, no iron.

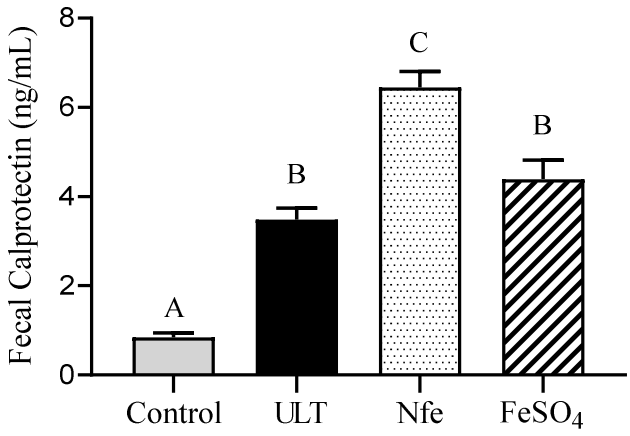

Figure D-4. Fecal calprotectin for control; NFe; ULT; and $FeSO_4$ using one-way ANOVA with Dunnett multiple comparisons. Data are means ± SEMs; $n = 10$. Mean values without a common letter, are significantly different ($P < 0.05$). Abbreviations used: ULT, ultimine; $FeSO_4$, ferrous sulfate; and NFe, no iron.

Table D-1. Histological scoring for gross anatomy of the colon in control and 3.5% DSS-induced Sprague Dawley rats for 8 consecutive days[1].

Colonic Lesion Score	**Colonic Inflammation**	**Grade of affected area**
0= Intact crypt	0= normal	0= 0%
1= 1/3 crypt loss	1= lamina propria	1= 1%–25%
2= 2/3 crypt loss	2= inflammation + gland dropout	2= 26%–50%
3= complete crypt loss, intact surface	3= complete abscess	3= 51%–75%
4= crypt loss + ulceration		4= 76%–100%

[1] Post-mortem disease scoring index is calculated by taking the sum of the lesion score, inflammation, and grade of colonic section affected. All scoring was performed in a blinded fashion by a Veterinary Pathologist.

Table D-2. Histological scoring for crypt lesion, inflammation, and hypertrophy of distal colon of control and IBD-induced Sprague Dawley rats[1].

Parameter	**No DSS**	**DSS + NFe**	**DSS + ULT**	**DSS + $FeSO_4$**
		Mean ± SEM		
Crypt	0 ± 0^{A}	3.5 ± 0.4^{B}	3.4 ± 0.4^{B}	3.4 ± 0.4^{B}
Grade	0 ± 0^{A}	1.7 ± 0.42^{B}	1.4 ± 0.34^{B}	1.2 ± 0.15^{B}
Inflammation	0 ± 0^{A}	2.1 ± 0.28^{B}	2.1 ± 0.23^{B}	1.6 ± 0.34^{B}
Grade	0 ± 0^{A}	2.0 ± 0.42^{B}	1.5 ± 0.31^{B}	2.9 ± 0.71^{B}
Total histological disease	0 ± 0^{A}	9.3 ± 1.3^{B}	8.4 ± 0.93^{B}	8.2 ± 0.73^{B}
Distal colon thickness	168.4 ± 29.7^{A}	518.8 ± 52.3^{B}	521.9 ± 55.2^{B}	449.8 ± 35.6^{B}

[1] Data are means ± SEMs; $n = 10$. Data within the same row without a common letter differ ($P < 0.05$). Abbreviations used: DSS, dextran sulfate sodium; IBD, inflammatory bowel disease; Fe, iron; $FeSO_4$, ferrous sulfate; and ULT, ultimine.

Table D-3. Circulating cytokine and chemokine indicators for control and IBD-induced Sprague Dawley rats[1].

Inflammatory marker	**No DSS**	**DSS + NFe**	**DSS + ULT**	**DSS + $FeSO_4$**
IL-1 alpha	0 ± 0^{A}	0 ± 0^{A}	0.97 ± 0.7^{AB}	1.9 ± 0.6^{B}
IL-1 beta	4.34 ± 0.7^{A}	11.26 ± 8.4^{A}	11.55 ± 6.2^{A}	22.5 ± 5.2^{A}
IL-2	27.5 ± 4.7^{A}	28.63 ± 7.1^{A}	43.3 ± 16.8^{A}	26.7 ± 15.2^{A}
IL-6	0 ± 0^{A}	0 ± 0^{A}	3.84 ± 3.04^{A}	0.18 ± 0.2^{A}
IL-10	6.26 ± 2.2^{A}	1.96 ± 1.4^{A}	14.7 ± 7.9^{A}	2.3 ± 2.3^{A}
IFN-gamma	0 ± 0^{A}	4.76 ± 4.8^{A}	10.48 ± 4.5^{A}	10.3 ± 2.4^{A}
IL-17A	9.88 ± 1.9^{A}	14.7 ± 2.5^{A}	21.9 ± 6.1^{A}	39.5 ± 5.0^{B}
IL-18	57.35 ± 10^{A}	52.0 ± 9.4^{A}	197.9 ± 87.3^{A}	45.72 ± 21.8^{A}

[1] Data are means $\pm$ SEMs; $n = 10$. Data within the same row without a common letter differ ($P < 0.05$). Abbreviations used: DSS, dextran sulfate sodium; IBD, inflammatory bowel disease; IL, interleukin; IFN, interferon; Fe, iron; $FeSO_4$, ferrous sulfate; and ULT, ultimine.